Proceedings of the 11th Brazilian Congress of Thermal Sciences and Engineering -- ENCIT 2006
Braz. Soc. of Mechanical Sciences and Engineering -- ABCM, Curitiba, Brazil, Dec. 5=8, 2006

Paper CIT06-0916

HEAT TRANSFER IN SYNOVIAL JOINTS DURING THE PROCESS OF THE HEATING ARTICULAR: A PILOT STUDY

Angélica Rodrigues de Araújo
Federal University of Minas Gerais. Av. Antônio Carlos, 6627 - Pampulha - 31.270-901 - Belo Horizonte / MG
angelica@bios.srv.br

Marcos Pinotti Barbosa
Federal University of Minas Gerais. Av. Antônio Carlos, 6627 - Pampulha - 31.270-901 - Belo Horizonte / MG
pinotti@ufmg.br

Márcio Fonte Boa Cortez
Federal University of Minas Gerais. Av. Antônio Carlos, 6627 - Pampulha - 31.270-901 - Belo Horizonte / MG
fonteboa@demec.ufmg.br

Alexandre Gonçalves Teixeira
Bios Eletrônica e Informática. R. Castelo de Lisboa, 301C - Castelo - 31.330.340 - Belo Horizonte / MG
alexandre@bios.srv.br

Abstract: This study aims to measure superficial and deep tissue layers temperature variations in a dog´s knee to carry through a first analyze of the heating transfer process in synovial joint. The joint heating was done with two hidrocollator packs, applied during 30 minutes over skin surface of the knee joint involving it completely. Before and during all the heating process, the rectal temperature and the surface layers were monitored by a mercury thermometer and by thermocouples. The registry of the surface thermic field was done before and immediately after the use of the hidrocollator packs using a thermocamera. The inicial and terminal temperature values comparation were used to evaluate the effects of the hidrocollator packs over the temperature of each one of the tissue layer. The behavioral analysis of the temperature during the heating process was made based on temperature graphics in function of the time for each one of the regions in study. The mean variation temperature of the joint were of 5,7ºC ± 2,2ºC. The magnitude of the variation and the behavior of the temperature were, although, different for each one of the evaluated layers. Decreasing exponential equations of the first and second orders represented well the profiles of the temperature for the heating process and allowed the development of a relation between the temperature of the skin surface with the temperature intra-articular.

Keywords: Tissue heating, bioheating transfer, synovial articulation, temperature measurement

1. Introduction

The muscle and joint heating has been considered an effective method for the treatment of various human pathological conditions (Abramson *et al.*, 1964; Castor and Yaron, 1976; Borell *et al.*, 1980; Chen *et al*., 1997; Lessard *et al.*, 1997; Sluka *et al*., 1999; Starkey, 2001; Bel and Prentice, 2004). The benefits of this therapy depend, however, of the temperature that the biological tissues will reach during the heating process. In accordance with the literature, to occur therapeutic effects of the tissue heating it is needed that the temperature of the target treated structure varies within a certain average amplitude (Lehmann *et al.*, 1970; Harris and McCroskery, 1974; Weinberger and Lev, 1991). Alterations beyond this threshold will induce to placebo treatment, with no clinical effectiveness, and also the excess variations might damage the tissues (Lehmann *et al.*, 1966; Liu *et al.*, 1999; Greenhalgh *et al.*, 2004).

Currently, various method and techniques are available for the promotion of the heating of the corporal structures. Hidrocollator packs, ultra-sound devices, short-wave and micro-wave are among the most frequently used, mainly in physiotherapist applications (Fadilah *et al.*, 1997; Drapper *et al.*, 1999; Drapper *et al.*, 2002; Robertson *et al.*, 2005). These resources generate differentiated standards of tecidual heating which will influence as much in the magnitude as in the depth in witch the temperature modifications may occur (Lehmann *et al.*, 1966; Weinberger *et al.*, 1989; Liu *et al.*, 1999; Jiang *et al.*, 2002). Therefore, understand how the temperature of the different tissue alters in responds to the application of a certain thermal modalities is a important step to fundament the clinical effectiveness and safety of the thermotherapy treatments.

The studies about the temperature behavior of the biological systems during the heating process have been focused, in most of the cases, in the evaluation of the temperature behavior during the heating processes in a single tissue layer (Garret *et al.*, 2000; Deng and Liu, 2002). Rare are the literature works that evaluate the process of heating transfer considering the jointly as several tissue layers. Such fact has been contributing for the decision of the professionals about the use of the thermo therapy's modalities were made based more in the professional experience and less in the scientific evidences.

The present work comes, however, to add it to the existent research about the heating transfer in living tissue, using innovative approach a first analyze of the temperature behavior in the different tissue layer of the animal articulation. It aims, specifically, to measure superficial and deep tissue layers temperature variations in a dog´s knee to determine a mathematical model witch relate the temperature of the intra-articular with the temperature of the skin surface of the synovial joints *in vivo*.

2. Material and Method

For the realization of this study it was used an adult dog (*Canis familiaris*), with no defined race, with male genre, with corporal mass of 21,0 kg. The experimental protocol used was approved by the *Comitê de Ética em Experimentação Animal – CETEA* from University Federal of Minas Gerais and was conducted obeying to the ethical principles from the *Colégio Brasileiro de Experimentação Animal – COBEA* (Cobea, 2001).

The experiment was carried through in the surgical block in the Veterinarian Hospital of the University Federal of Minas Gerais, to the temperature of 22,9°C and air relative humidity of 41%. All the procedures were carried through in the right knee, with the animal positioned in left lateral decubitus, over a surgical table adequately lined. Before the beginning of the procedures, the animal was pre-medicated with xilazina 2% (1,0 mg/kg, intravenous) and right after submitted the general anesthesia. This was inducted with pentobarbital 3% (12,5 mg/kg, intravenous) and kept with additional doses of the same fármaco, in such way that the animal continued during the whole experimental period in the third plane of the third anesthetic level.

After tricotomia and anti-sepsia of the skin surface of the knee D with PVPI® and iodate alcohol, were positioned, in an aseptic way, thermocouples type K special class (0,25 mm of tickness and error limit of ±1,1°C or ±0,4%) in the areas which it was desired to monitor the joint temperature: externally, in the skin surface, one medially and another laterally to the joint and, internally, in the subcutaneous, pericapsular and intra-articular regions. These last ones were implemented and positioned in their respective places with the help from cannulas which served as guide to the passage of the thermocouples. Before being positioned in their respective places, all the thermocouples were previously sterilized. The perception of the tissue sensation during the insertion of the thermocouples helped in the localization of the subcutaneous and periscapsular. The confirmation of the thermocouples in the intra-articular region was made by the previous aspiration of the synovial liquid through the cannula. All the thermocouples (external and internal) were fixed in their respective places by simple sutures.

To help the analysis and to check if the methodology used for the application of the thermal resources were effective in promoting uniform skin heating, and consequently of the layer close to them, the thermal field of the skin surface was also monitored immediately before and after the heating application using a thermo camera *Thermovision AGEMA*-P20 (*FLIR SYSTEM*™). For the realization of these measurements the considered emissivities for the skin was 0,95 and the equipment were positioned with 0,60 m of distance from the target, focused over the anterior aspect of the knee. The images captured by the thermocamera were transferred for a computer and processed using the ThermaCAM™ Researcher 2001 (*FLIR SYSTEM*™) program.

The rectal temperature was also monitored during the whole experimental period using, initially, a glass mercury thermometer *BD* Thermoflat®, with 0,1ºC resolution, in which later add it a thermocouples type K, with the same already described characteristics. The thermometer reading was made each ten minutes, until the positioning time of the thermocouple in the rectal mucosa and, later, each half hour for the clinical evaluation of the animal. The initial readings of the mercury thermometer were used to calculate the mean values of the rectal anesthesia pré-sedation/induction and the ones of the thermocouples to evaluate the behavior of the corporal temperature during the application of the thermotherapy resource.

The system for data acquisition DATAPAC©1990-2005, *Klin Tracker for Windows v3.04*, was used for acquisition and storage of the data. This acquisition started after the thermocouples were positioned and fixed in their respective places and extended continuously until the ending of the experiment, with the data register each two seconds. At the end of the experimental period, the data were transferred to a micro-computer (Pentium® M45-S355, TOSHIBA) to be processed and analyzed.

As source of heating it was used two hidrocollator packs (*MERCUR Body Care*®), weighting 1,0 kg, previously warm in water at the mean temperature of 80,2°C ± 0,1°C during half an hour. The hidrocollator packs were applied at an mean temperature of 76,7°C ± 0,1°C, for a period of 30 minutes, one medially and the other laterally to the knee, in such a way that the joint became completely involved. Before being applied, the hidrocollator packs were wrapped in a towel, in such way that existed two layers of towel between the skin and the compresses. Crepom bands were used for the fixation of the packs and to keep an adequate contact between the thermo therapy resource and the joint surface. The thermal isolation of the system was made with the help of three other towels positioned over the hidrocollator packs, in order to involve the group completely. The application of the thermal resource followed the recommendations of the *Australian Physiotherapy Association* (*APA*) (Robertson *et al.,* 2001). During the process, the leg of the target joint remained elevated (approximately 30º abduction), in order to avoid interference in the thermal exchanges due to the contact between the physical agent and the surgical table.

The hidrocollator packs were also monitored during the while period of joint heating by thermocouples type K, identical to the ones used for the temperature measurement of the joint, positioned inside each ones of the hidrocollator packs. The acquisition and storage of these data were carried through the DATAPAC©1990-2005 system.

By the end of the experimental period, the animal was submitted to euthanasia and the dissection of the knee joint was carried through for confirmation of the thermocouples positioning in each one of the tissue layers of interests.

2.1 Methods for the analyze of the temperature data

The physical model to simulate the knee of the animal was to consider an unique cylinder (Fig. 1), compound by for annealing concentric layers, each one representing a different kind of tissue: the skin, the subcutaneous, the periscapular and intra-articular regions. The mean of the initial (T_i) and terminal (T_f) temperatures, the maximum (T_{max}) and minimum (T_{min}) temperature and the differences between the maximum and minimum temperatures ($\Delta T_{max-min}$) and between the terminal and initial temperatures (ΔT_{f-i}) for each one of the regions were used to evaluate the effect in the thermal resource over the temperature of each one of the tissue layers.

The behavior analysis of the temperature during the heating process of the joint were made based on the temperature graphics T (°C) in function of the time t (s) obtained for each one of the regions in study. Basing of the aspect of the obtained curves, exponential decreasing equations [Eq. (1)] were selected to do the mathematical adjust of data. These were carried through using the programs ORIGIN v 6.0 e MATLAB v 6.5.1.

$$T = T_0 + \Delta T \cdot e^{-t/\tau} \tag{1}$$

Where: T is the temperature (°C) in the time t
t is the time (s)
T_0 is the temperature (°C) in the time $t = \infty$
ΔT is the difference between the initial and terminal temperature Ti (°C) e T_0
τ is the time constant of the system(s)

The time constants τ obtained were compared between them and, based in this comparison, it was looked determine the existence of relations between the temperature behavior of the evaluated areas, with emphasis in the relation of the skin as the intra-articular region. The time (t_e) from which the temperature variation in the advance of time was smaller than ± 0,5% of the terminal value of the temperature was also determined for each one of the evaluated layers and using as criteria for the definition of the system stability.

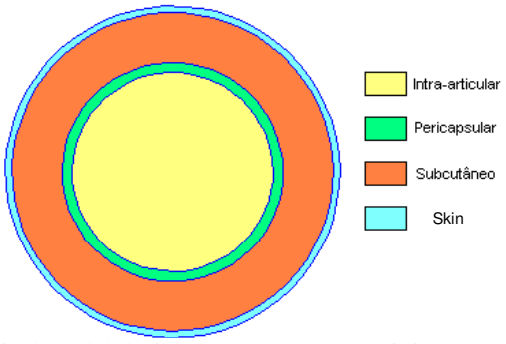

Figure 1. Physical model designed to represent the joint knee of a dog.

3. Results and Discussion

The mean of the rectal temperature before the animal be sedated and anesthetized was of 37,8°C ± 0,1°C and changed to 35,9°C ± 0,2°C at the end of the experiment. According to literature (Giacobini, 1990), the corporal temperature for a healthy dog it varies in normal situations, between 37,5°C a 39,9°C. The lower values of the corporal temperature found at the end of the experimental period may be consequence of the depressive effect of the drugs used to sedate and anesthesia the dog. According to Muir and Hubbel (1995), Prado *et al.* (1997) e Maria *et al.* (2004), the xilazina and the pentobarbital, due the reduction of the conduction of the stimulation of the brain cortex, may cause undesired pharmacological effects, such as cardio-respiratory depression, decrease in the corporal temperature, salivation and vomit.

The acquired data in the preceding time of the application of the thermal resource shown that the temperature of the evaluated layer are different among themselves and are lower than the rectal temperature (Tab. 1). This founds are in agree with Pardasani and Adlakha (1995) that say that the temperature is not equal a will not either be equally sustained in the different parts of the body. In the most central part, it tends to be a in a higher level and precisely controlled, in

contrast to the most superficial layers, which are commonly lower and varies more, according with the external conditions.

Can be observed that as much as there is a thermal gradient between the corporal temperature and the temperature of the skin, there exist also between the mean temperature of the skin ($31,9^oC \pm 1,9^oC$) and the temperature intra-articular ($33,1^oC \pm 0,4^oC$). According to Low and Reed (2001), this difference may be kept thanks to the low thermal conductivity of the interpostos tissues between the skin and the most central region (Bowman *et al.*, 1975) and to the organization of the vascular net and distribution of the blood flow in these tissues (Chen and Holmes, 1980; Pardasani and Adlakha, 1995). This organization could also explain the differences found between the temperature of the skin regions, a time that the main vases responsible for the irrigation of the lower members are concentrated in the internal side of the legs (Pennes, 1948; Chato, 1980; Weinbaum and Jiji, 1985; Qinghong *et al.,* 2003).

Table 1. Rectal and articular temperature before the application of the thermical resources (mean ± standard deviation).

Situation	**Temperature (^oC)**					
	Rect	**Skin (medium region)**	**Skin (lateral region)**	**Subcutaneo**	**Pericapsular**	**Intra-articular**
Pré-thermotherapy	36,3 ± 0,2	33,7 ± 0,1	29,8 ± 0,3	30,5 ± 0,1	29,5 ± 0,1	33,4 ± 0,1

3.1 Joint heating

The hidrocollator packs, at the mean temperature of $76,7^oC \pm 0,1^oC$, applied by 30 minutes over the skin surface of the knee, were effective in raising the temperature of all the studied regions (Tab. 2). This found is in agreement with the majority of the thermo therapy works, which mention the increase of the tissue temperature in reply to the superficial heating (Abramson *et al.,* 1964; Mainardi *et al.,* 1979; Weinberger *et al.,* 1989; Draper *et al.,* 2004). In mean. The temperature of the join had suffered an elevation of $5,7^oC \pm 2,2^oC$, with peak in the temperature occurring after 30 minutes of heating.

Table 2. Temperature of the skin and the subcutaneous, pericapsular and intra-articular regions for the process of heating articular (mean ± standard deviation).

Temperature (^oC)	**Regions**				
	Skin (medium region)	**Skin (lateral region)**	**Subcutaneo**	**Pericapsular**	**Intra-articular**
Ti	33,9 ± 0,3	30,4 ± 0,6	30,6 ± 0,1	29,4 ± 0,1	33,5 ± 0,1
Tf	39,2 ± 0,1	36,2 ± 0,1	37,3 ± 0,0	38,6 ± 0,1	36,8 ± 0,0
Tf – Ti	5,3 ± 0,2	5,8 ± 0,6	6,6 ± 0,1	9,1 ± 0,2	3,3 ± 0,1
Tmax	39,4 ± 0,2	36,3 ± 0,1	37,4 ± 0,2	39,2 ± 0,2	36,9 ± 0,1
Tmax – Ti	5,5 ± 0,2	5,0 ± 0,1	$6,6^o$ ± 0,1	9,8 ± 0,2	3,4 ± 0,2

The behavior of the temperature in the hidrocollator packs, of the skin and of the intra-articular region during the heating process can be visualized in the Fig. 2. It is possible to observe that the temperature elevation of the tissue does no follow the temperature reduction of the hidrocollator packs. This keeps falling until the end of the heating process ($t_{e(pack)}$ = 1718 seconds) to the step that the intra-articular region and specially from the skin tend to stabilize quicker ($t_{e(intra\text{-}artic)}$ = 1408 seconds e $t_{e(skin\ \ surface)}$ = 1128 seconds, respectively). According to Low and Reed (2001), this happened because the heating added in one single part of the body is dispersed by conduction and by convection until become lost in other surfaces and, consequently, the temperature increase in a specific place will be the equilibrium between the gain and dispersion of the heating. Keller and Seiler (1971) e Vanhoutte *et al.* (2002) tell that the body hability in alter the blood flow which circulate through the vascular plexus and by the tissue anastomoses arterio-venosas is one of the main elements of the control of the temperature of the tissue.

At the and of the heating process, the hidrocollator packs presented the mean temperature of $63,3^oC \pm 1,10^oC$, the skin of $37,2^oC \pm 1,5^oC$ and the intra-articular region of $36,8^oC \pm 1,1^oC$. The analise of the images refering to the thermical field of the skin surface in the pos-heating (Fig. 3B) had shown that the used technique for the application of the hidrocollator packs was adequate to promote homogenous heating of the skin, once that this presented itself relatively uniform. Such fact is important in the interpretation of the results once that the temperature of each one of the tissue layers was measured in only one point and an non-uniform distribution of the heating could result in mistaken interpretation of the data.

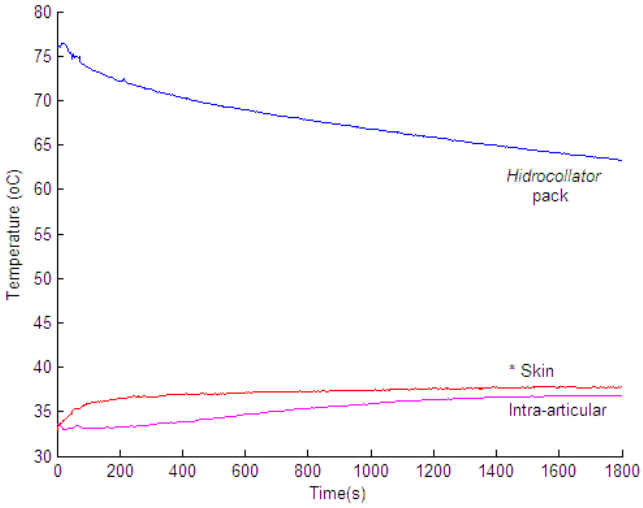

Figure 2. Behavior of the temperature in the hidrocollator packs, of the skin surface and of the intra-articular region during the heating period.
*Skin represents the mean temperature between the medium and lateral region of the skin of the knee.

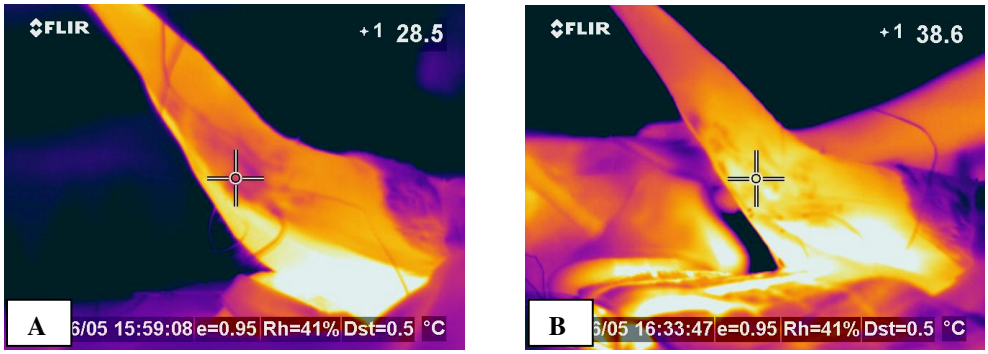

Figure 3. Thermal field of the skin surface in the joint knee of the dog. A: pre-thermotherapy image; B: image after themotherapy.

The temperature profile during the time for the heating process of the joint can be viewed in the Fig. 4. It can be observed that in all the tissue layers, the temperature layers presents the exponential behavior in the time and, with the exception of the periscapular region, all of them tend to steady state at the end of the experiment.

As general rule, the time in which the tissue will respond to a determine gradient of temperature will depend on its thermal capacity C (J/°C), in other words, of it mass (ρV) and of is specific heat (c_p). Any increase in C will make the thermal system responds more slowly to the variations in their thermal environment and will increase the needed time for the thermal equilibrium be reached. This time can be interpretaded as the thermal time constant τ (s) of the system (Incropera and Dewitt, 2003). The time constants for each one of the layers of the model and of the joint of the knee of the dog are represented in Tab. 3. It can be observed that, with exception of the medium skin and of the intra-articular regions the time constants of the layers are relatively close.

Lehmann *et al.* (1966) tell that the distribution and the temperature behavior of the tissue layer can be marcadely modified by the cooling effect produced by the increase in the blood flow in the skin region. This one intends to avoid that the tissue temperature exceeds the limits of the thermal safety, transferring the excess of energy for out of the system (Draper *et al.,* 2004).

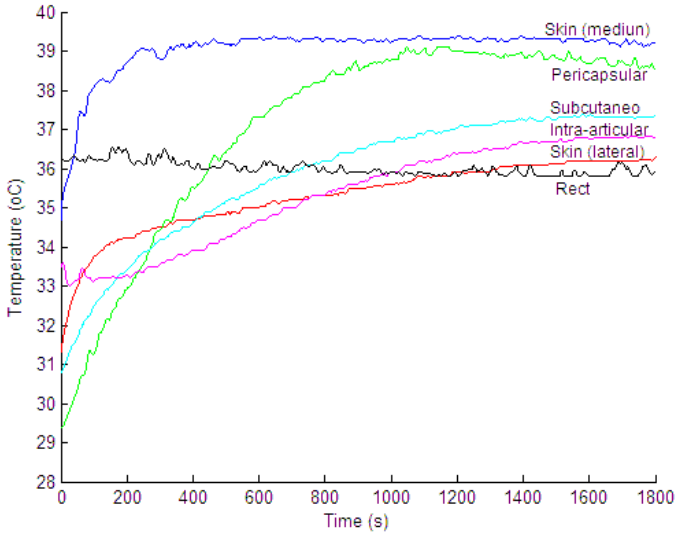

Figure 4. Behavior of the rectal temperature, of the skin (medium and lateral side) and of the subcutaneous, periscapsular and intra-articular regions during the heating process of the knee of the dog.

Table 3. Time constants of the regions that constitutes the joint model for the heating process.

Joint layers	**Time constant (s)***
Skin (lateral region)	562,6
Skin (medium region)	91,4
Subcutaneo	509,2
Pericapsular	361,0
Intra-articular	1510,0

*Note: time constants considering the tissue behavior as being represented by a decreasing exponential function of the first order.

Among the evaluated tissue layers, can be observed that the temperature of the intra-articular region presents a different behavior compared to the other in the initial time of the heating, keeping practically stable until the time t = 200 s ("dead time"). Only after this interval is that this one began to rise. Horvath and Hollander (1949) described, in their study, a bahevaior similar to this. According to the author, the skin temperature increased marcadly in reply to application of hot compresses in the skin surface, while the temperature of the deeper tissues reduces slightly ou reamined stable. This phenomenom was called "reflex cooling" and rarely has been described in the literature. According to Horvath and Hollander (1949), the increase of the temperature of the surface causes the blood to be directed to the most superficial tissue layers, inductind to a momentaneous fall in the temperature of the deep tissues or avoinding for some times that the same varies in reply to the applied heating source. Weinberger and Levi (1991) tell also that when the tissue heating be carried through conduction, the fact that the thermal conductivity differ from a tissue to other limits, in certain way, the time needed for variations of the temperature in the most deep tissue layers.

3.2 Analise of the behavior of the temperature during the process of joint heating

The analise of the regression curves of the temperature for the layers from the articular model shown that the thermic behavior of the tissues can be well represented by exponential decreasing equations of the first and second order ($Chi^2 = 0,02$; $R^2 = 0,99$). The inclusion of another term, as provided by the exponential function of the third order, does not provided improved in the aproximation. This sugests that the heating transfer in the living tissues during the heating process, although a complex phenomenon , occurs by two main mechanisms, the conduction and convection, depending of the physiological characteristics of the tissues, sometimes one predominating the other and, in other moments, complement themselves.

As a general rule, the results of the regression for the temperature of the medium region of the skin, for the subcutaneous tissue and for the periscapular region does not differed in a significant way while using the exponential equations of the first, second of third order, show that in these tissues, the behavior of the temperature can be represented by a exponential function of the first order (Fig. 5 a Fig 7). Such fact sugests that the heating transfer in this regions has string dependencies with one of the mechanisms of heating transfer. The physiological characteristics in this regions (tissue of greater perfusion relating to the lateral skin and the intra-articular regions) indicate that this mechanism is probably conection.

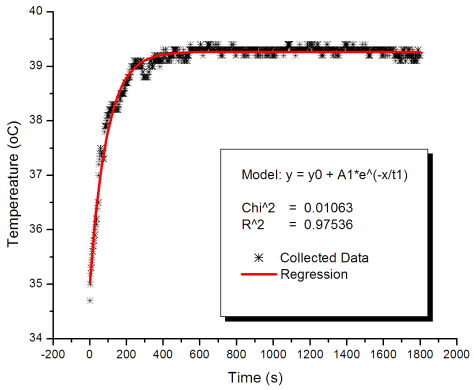

Figure 5. Result of the data regression for the temperature for the medium region of the skin (T_{pm}) using the exponential function of the first order, where: $T_{pm} = 39{,}3 - 4{,}2 \cdot e^{-t/91{,}4}$

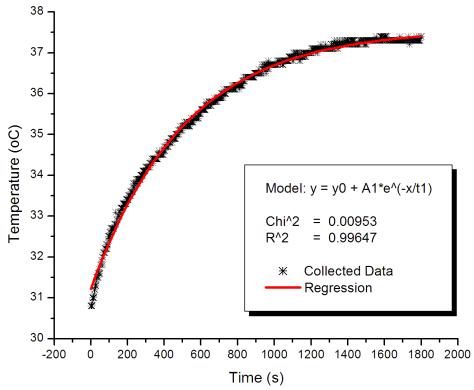

Figure 6. Result of the data regression for the temperature subcutaneo tissue (T_{sc}), using the exponential function of the first order, where: $T_{sc} = 37{,}6 - 6{,}4 \cdot e^{-t/509{,}2}$

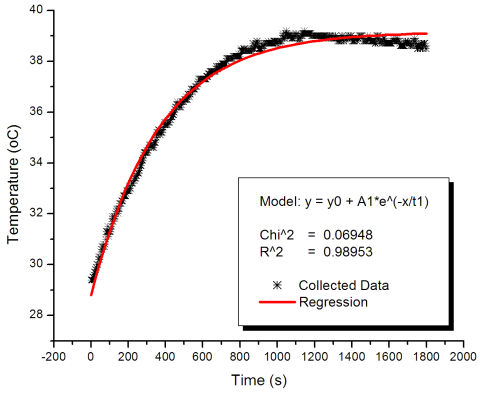

Figure 7. Result of the data regression for the temperature of the periscapular region (T_{pc}), using the exponential function of the first order where: $T_{pc} = 39{,}2 - 10{,}4 \cdot e^{-t/361{,}0}$

On the other way, the temperature behavior of the lateral region of the skin and the intra-articular region are well represented by exponential functions of the first order (Fig. 8 e Fig. 9), indicating that in this regions the heating transfer by thermal difusion and by convection are both responsable by the heating transfer that occur in this tissues.

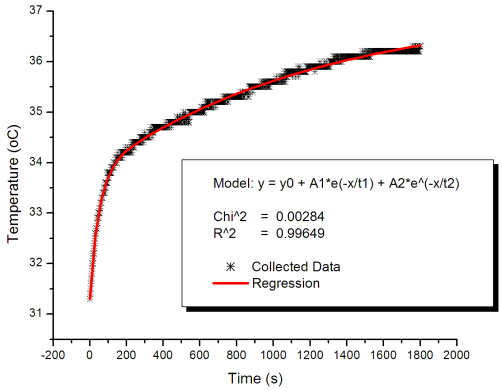

Figure 8. Results of the data regression for the temperature of the lateral region of the skin (T_{pl}), using exponential function of the second order, where: $T_{pl} = 37{,}1 - 2{,}5 \cdot e^{-t/48{,}3} - 3{,}3 \cdot e^{-t/1223{,}2}$

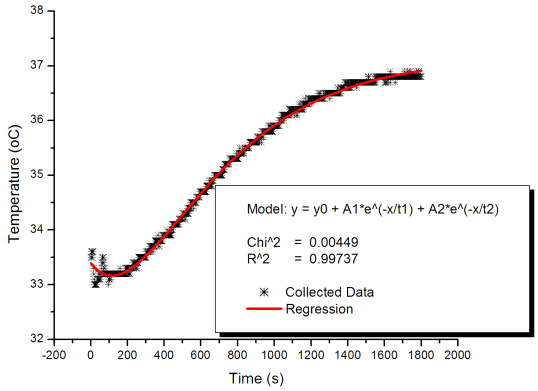

Figure 9. Result of the data regression for temperature of the intra-joint medium (T_{ia}) using the exponential function of the second order, where: $T_{ia} = 37{,}2 - 21{,}5 \cdot e^{-t/422{,}7} + 17{,}8 \cdot e^{-t/320{,}0}$

The analises carried through, together with the results of the regression, show that the lateral region of the skin and the intra-articular region has some similar physiological characteristics and that with the exception of the dead time period, the thermal behavior of this two regions tends to follow a similar profile (both dont hit the equilibrium state). Bases in that information, we executaded a new data regression of the temperature of the intra-articular region in which the "dead time" (200 seconds) was rejected. The new obtained time constant for the intra-articular region was compared with the time constant of the lateral region of the skin in order to determine if the temperature in this two regions could be related by some equation. The resulting equation of the new data regression of the temperature data for the intra-articular region, obtained using an exponential equaton of the first order was:

$$T_{ia} = 37{,}1 - 6{,}0 \cdot e^{-t/639{,}2} \tag{2}$$

In this equation can be verified that the time found constant ($\tau = 639{,}2$ seconds) is close to the time constant of the regression of the skine curve (lateral region), when this one was obtained also by a decreasing exponential function of the first order ($\tau = 560$ segundos).

Calculating then the difference (*Dif*) among the equation of the lateral region of the skin (Fig.8) and of the intra-articular region (Fig. 9), obtained after the "dead time" being rejected, and considering that both posses the same time constant τ, it can be concluded that:

$$Dif = T_{ia} - T_{pl} = (37{,}17 - 6{,}0 \cdot e^{-t/\tau}) - (36{,}6 + 3{,}4 \cdot e^{-t/\tau}) \tag{3}$$

In order to express *Dif* in function of the temperature of the lateral region of the skin T_{pl} and in that way relate the temperature of the intra-articular region T_{ia}, it added and subtracted the number 27,7 in the Eq. (3), obtaining:

$$Dif = 0{,}76 \cdot T_{pl} - 26{,}8 \tag{4}$$

Therefore:

$$T_{ia} = 1{,}76 \cdot T_{pl} - 26{,}8 \qquad (t > 200 \text{ s}) \tag{5}$$

The curve correspondent to the Eq. 5, can be vistualized in the Fig.10. The same represents a good aproximation for the colected data, since it disdain the initial time of the heating process (t < 200 seconds). The erros relative to the different times in which the intra-articular temperature begins to be stimated are represented in the Tab. 4.

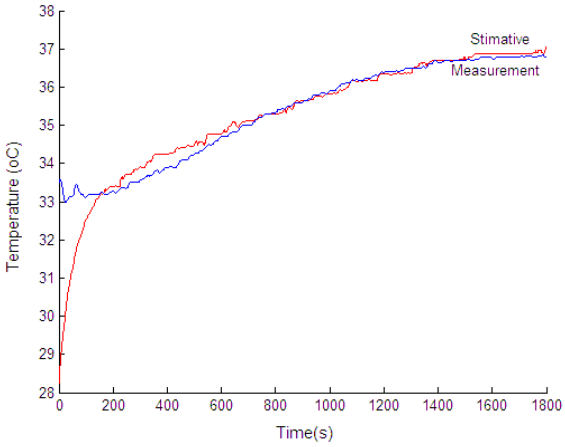

Figure 10. Profile of the temperature for the intra-articular region during the heating process. Blue curve (measurement): represent the values of the temperature for the intra-articular region of the knee of the dog, colected during the experimental period; Red curve (stimative): represents the values of the temperature stimated based in the equation $T_{ia} = 1{,}76 \cdot T_{pl} - 26{,}8$

Table 4- Maximum error for the equation related to the time in which the temprature is estimated.

Inicial time (s)	**Maximum error (%)**
200	1,42%
400	1,42%
800	0,70%
1200	0,70%
1500	0,70%

7. Conclusions

The pilot carried through evidentiated that the joint knee of a dog is a good model for the study of the tissue temperature during the processes of heating and cooling, once the the changes of the temperature inducted in the skin, in the subcutaneous tissue, in the periscapular region and in the intra-articular region by the application of the themotherapy resource could be evaluated.

The analyze of the colecter data and the obtained curves with this pilot had shown that the process of heating transfer in the synovial joint is a complex phenomenon due to involve physical and physiological aspects that, beyond being particular to each tissue, interact between themselves, during even more complex the study of the heating transfer in the biological systems.

Even though, a mathematical model realting the temperature of the ost internal tissue layers and of the skin surface could have been stabilished based in the regression, indicating that the temperature heating of the intra-articular region can be estimated based on the temperature of the lateral region during the heating process.

8. References

Abramson, D. I. *et al.*, 1967, "Comparison of wet and dry heat in raising temperature of tissues", Archives of Physical Medicine & Rehabilitation, Vol. 48, n. 12, pp. 654-661.

Bel, G. W. and Prentice, W., 2004, "Modalidades infravermelhas", In: Prentice, W. E., Modalidades terapêuticas para fisioterapeutas, 2. ed. Porto Alegre: Artmed Editora, Cap. 9, pp. 185-213.

Borell, R. M. *et al.*, 1980, "Comparison *in vivo* temperatures produced by hydrotherapy, paraffin wax treatment and fluidotherapy", Physical Therapy, n. 60, pp. 1273.

Bowman, H. F., Carvalho, E. G. and Woods, M., 1975, "Theory, measurement, and application of thermal properties of biomaterials", Annual Review of Biophysics and Bioengineering, Vol. 4, n. 00, pp. 43-80.

Castor, C. W. and Yaron, M., 1976, "Connective tissue activation: the effects of temperature studied in vitro", Archives of Physical Medicine & Rehabilitation, Vol. 57, pp. 5-9.

Chato, J, 1980, "Heat transfer to blood vessels", ASME Journal of Biomechanical Engineering, Vol. 102, pp. 110-118.

Chen, M. M. and Holmes, K. R., 1980, "Microvascular contributions in tissue heat transfer", Annals of the New York Academy of Sciences, Vol. 335, pp. 137-150.

Chen, S. S.; Wright, N. T. and Humphrey, J. D., 1997, "Heat-induced changes in the mechanics of a collagenous tissue: isothermal free shrinkage", Journal of Biomechanical Engineering, Vol. 119, n. 4, pp. 372-378.

Colégio Brasileiro de Experimentação Animal (COBEA), 2001, "Princípios éticos na experimentação animal", São Paulo: COBEA.

Deng, Z. S. and Liu, J., 2002, "Analytical Study on bioheat transfer problemas with spatial or transiente heating on skin surface or inside biological bodies", Journal of Biomechanical Engineering, Vol. 124, pp. 638-649.

Draper, D. O. *et al.*, 2004, "Shortware diathermy and prolonged stretching increase hamstring flexibility more than prolonged stretching alone", Journal of Orthopaedic & Sports Physical Therapy, Vol. 34, n. 1, pp. 13-20.

_____, 1999, "Temperature change in human muscle during and after pulsed short-wave diathermy", Journal of Orthopaedic & Sports Physical Therapy, Vol. 29, n. 1, pp. 13-22.

_____, 2002, "The carry-over effects of diathermy and stretching in developing hamstring flexibility", Journal of Orthopaedic & Sports Physical Therapy, Vol. 37, pp. 37-42.

Fadilah, R.; Pinkas, J. and Weinberger, A., 1987, "Heating rabbit joint by microwave applicator". Archives of Physical Medicine & Rehabilitation, Vol. 68, pp. 710-712.

Garrett, C. *et al.*, 2000, "Heat distribuition in the lower leg from pulsed shortwave diathermy and ultrasound treatments", Journal of Atletic Training, Vol. 35, pp. 50-55.

Giacobini, P., 1990,"Guia do seu cão", São Paulo: Ed. Abril. (Médico Veterinário).

Greenhalgh, D. G. *et al.*, 2004, "Temperature threshold for burn injury: an oximeter safety study", Journal of Burn Care & Rehabilitation, Vol. 25, n. 5, pp. 411-415.

Harris Jr, E. D. and McCroskery, P. A., 1974, "The influence of temperature and fibril stability on degradation of cartilage collagen by rheumatoid synovial collagenase", The New England Journal of medicine, Vol. 290, n. 1, pp. 1-6.

Hollander, J. L. and Horvath, S. M., 1949, "Changes in joint temperature produced by diseases and by physical therapy; preliminary report", Archives of Physical Medicine in Rehabilitatio, Vol. 30, pp. 437.

Incropera, F. and Dewitt, D. P., 2003, "Fundamentos de transferência de calor e massa", 5. ed. Rio de Janeiro: LTC Editora, 698 p.

Jiang, S. C. *et al.*, 2002, "Effects os thermal properties and geometrical dimensions on skin burn injuries", Burns, Vol. 28, pp. 713-717.

Keller, K. H. and Seiller L. J., 1971, "An analysis of peripheral heat transfer in man", Journal of Applied Physiology, Vol. 30, n. 5, pp. 779-786.

Lehmann, J. F. *et al.*, 1970, "Effect of therapeutic temperatures on tendon extensibility", Archives of Physical Medicine & Rehabilitation, pp. 481-487.

_____, 1966, "Temperaure distributions in the human thigh, produced by infrared, hot pack and microware applications", Archives of Physical Medicine & Rehabilitation, pp. 291-299.

Liu, J. *et al*., 1999, "New thermal wave aspects on burn evaluation of skin subjected to instantaneous heating", IEEE Transactions on Biomedical Engineering, Vol. 46, n. 4, pp. 420-428.

Low, J. and Reed, A, 2001, "Eletroterapia explicada: princípios e prática". 3. ed. São Paulo: Manole.

Mainardi, C. L. *et al.*, 1979, "Rheumatoid arthritis: failure of daily heat therapy to affect its progression", Archives of Physical Medicine & Rehabilitation, Vol. 60, pp. 390-392.

Maria, P. P. *et al.*, 2004, "Polyurethane resins derived from castor oil (Ricinus communis) for tibial crest deviation in dogs", Ciencia Rural, Vol. 34, n. 3, pp. 821-827.

Muir, W. W. and Hubbel, J. A. E., 1995, "Handbook of veterinary anesthesia", 2nd ed. Missouri: Mosby, 510 p.

Pardasani, K. R. and Adlakha, N., 1995, "Coaxial circular sector elements to study two dimensional heat distribuition problem in dermal gegions of humam limbs", Mathematical and Computer Modelling, Vol. 22, n. 9, pp. 127-140.

Pennes, H. H., 1948, "Analysis of tissue and arterial blood temperatures in the resting human forearm", Journal of Applied Physiology, Vol. 1, n. 2, pp. 93-122.

Prado Filho, O. R. *et al.*, 2000, "Xylazine as a pre-medicant for thiopental sodium anaesthesia in the dog", Acta Cirúrgica Brasileira, Vol. 15, n. 2.

Qinghong, H. E.; Liang, Z. and Sheldon, W., 2003, "Effect of Blood Flow on Thermal Equilibration and Venous Rewarming", Annals of Biomedical Engineering, Vol. 31, pp. 659-666.

Robertson, V. J. *et al*, 2001, "Guidelines for the clinical use of electrophysical agents" Australian Physiotherapy Association, pp.1-21. Disponível em:<http://apa.advsol.com.au/static content/staticpages/guidelines/epags.pdf>. Acesso em: 12 fev. 2005.

Robertson, V. J.; Ward, A. R. and Jung, P., 2005, "The effect of heat on tissue extensibility: a comparison of deep and superficial heating", Archives of Physical Medicine & Rehabilitation, Vol. 86, pp. 819-825.

Sluka, K. A. *et al.*, 1999, "Reduction of pain-related behaviors with either cold or heat treatment in an animal model of acute arthritis", Archives of Physical Medicine & Rehabilitation, Vol. 80, pp. 313-317.

Starkey, C., 2001, "Agentes Térmicos", In: Modalidades terapêuticas em fisioterapia, São Paulo: Manole, Cap. 4: pp. 114-172.

Vanhoutte, G. *et al.*, 2002, "*In vivo* non invasive study of the thermoregulatory function of the blood vessels in the rat tail using magnetic resonance angiography". NMR in Biomedicine, Vol. 15, pp. 263-269.

Weinbaum, S. and Jiji, L. M., 1985, "A new simplified bioheat equation for the effect of blood flow on local average tissue temperature", ASME Journal of Biomechanical Engineering, Vol. 107, n.2, pp. 131-139.

Weinberger, A. *et al.*, 1989, "Intra-articular temperature measurements after superficial heating", Scandinavian Journal of Medicine & Science in Sports, Vol. 21, pp. 55-57.

Weinberger, A. and Lev, A., 1991, "Temperature elevation of connective tissue by physical madalities", Critical Reviews in Physical and Rehabilitation Medicine, Vol. 3, n. 2, pp. 121-146.

Proceedings of the 11th Brazilian Congress of Thermal Sciences and Engineering -- ENCIT 2006
Braz. Soc. of Mechanical Sciences and Engineering -- ABCM, Curitiba, Brazil, Dec. 5=8, 2006

Paper CIT06-0289

AVALIAÇÃO DA PRESENÇA DE GORDURA EM TECIDO MUSCULAR USANDO DTA E TG

Karen Cristina Laurenti
Universidade de São Paulo – USP - Avenida do Trabalhador São Carlense, 400 – Centro – São Carlos – SP – CEP: 13566-590
e-mail: karen_laurenti@yahoo.com.br

Carlos Dias Maciel
Universidade de São Paulo – USP - Avenida do Trabalhador São Carlense, 400 – Centro – São Carlos – SP – CEP: 13566-590
e-mail: maciel@sel.eesc.usp.br

Paula Manoel Crnkovic
Núcleo de Engenharia Térmica e Fluidos, Escola de Engenharia de São Carlos, Universidade de São Paulo - Av. Trabalhador São-carlense, no. 400, 13566-590, São Carlos - SP, Brasil.
e-mail: paulam@sc.usp.br

Ivonete Ávila
Núcleo de Engenharia Térmica e Fluidos, Escola de Engenharia de São Carlos, Universidade de São Paulo - Av. Trabalhador São-carlense, no. 400, 13566-590, São Carlos - SP, Brasil.
e-mail: iavila@sc.usp.br

Resumo. *A carne é vista como a maior fonte de gordura na dieta humana, especialmente de ácidos gordurosos saturados e, quando associados com doenças da vida moderna acarretam em vários tipos de cânceres e doenças coronarianas. Este trabalho tem por objetivo avaliar e quantificar a presença de gordura entre as fibras musculares empregando-se a Análise Térmica. Os testess foram feitos utilizando técnicas TG (Termogravimetria) e DTA (Análise Térmica Diferencial). As amostras analisadas foram músculo e gordura bovina. Com a aplicação da termogravimetria (TG) determinou-se duas regiões de perda de massa que foram associadas à degradação de gorduras e de fibras musculares, e nas condições estudadas, os resultados mostraram-se promissores para a para a determinação quantitativa de gordura em fibras musculares. Complementarmente, as análises DTA permitiram observar picos endotérmicos referentes à fusão gordura presente nas amostras.*

Palavras chave: Termogravimetria, Análise Térmica Diferencial, Tecido Gorduroso.

1. Introdução

Recentemente, muitas pesquisas têm sido feitas sobre avaliação da composição de gordura na carne. A carne é vista como a maior fonte de gordura na dieta humana, especialmente de ácidos gordurosos saturados e, quando associados com doenças da vida moderna acarretam em vários tipos de cânceres e doenças coronarianas. A gordura consumida está associada com ácidos graxos e está diretamente relacionado com a saúde humana (Moran Jr, 1996). Por outro lado, esses componentes influenciam diretamente na firmeza do tecido gorduroso, tempo de cozimento, sabor, maciez e suculência (Lebas, 1979; Wood, 2003). O tecido gorduroso é um tipo especial de tecido conjuntivo, que foi modificado para permitir o armazenamento de gordura neutra. É encontrado em uma camada abaixo da pele, entre os músculos, nos espaços entre diversos órgãos e em quase todos os espaços do corpo que não são cheios (Guyton, 1988).

Para se avaliar a presença de gordura entre as fibras musculares, as técnicas analíticas empregadas neste estudo foram a Termogravimetria (TG) e Análise Térmica Diferencial (DTA). O método termogravimétrico é basicamente um método de natureza quantitativa na qual a mudança na massa da amostra pode ser determinada com precisão. Entretanto, as faixas de temperatura na qual a variação de massa ocorre são qualitativas e dependem do equipamento utilizado e das características da amostra (Stabursvik e Martens, 1980). A TG é largamente utilizada em quase todas as áreas da química e áreas correlatas, sendo definida como: a técnica na qual a massa de uma substância é medida em função da temperatura, enquanto a substância é submetida a uma programação controlada de temperatura (Tornberg, 2004; Moran Jr, 1996).

A DTA é uma técnica térmica em que se mede a diferença de temperatura entre a amostra e uma substância inerte durante o processo de aquecimento/resfriamento (Bernal *et al*, 2002; Wendlandt, 1985). Mudanças da temperatura da amostra são ocasionadas pelas transições ou reações entálpicas (endotérmica ou exotérmica). Geralmente, efeitos

endotérmicos são produzidos por transições de fase, desidratações, reduções e algumas reações de decomposição (Wendlandt, 1985).

Este trabalho tem por objetivo propor um método rápido para quantificar a presença de gordura entre as fibras musculares empregando-se a Análise Térmica. Será empregada a técnica TG para se determinar as regiões de perda de massa associadas à degradação de gorduras e fibras musculares. Complementarmente, serão feitas análises em DTA para observar transições entálpicas relacionadas aos fenômenos de degradação de amostras de músculo e gordura bovina.

2. Materiais e Métodos

2.1. Materiais

Utilizaram-se amostras de músculo e gordura bovina comercial, sendo analisadas sem receber qualquer tratamento prévio, isto é, os ensaios foram realizados em base úmida. As amostras foram pesadas na balança marca Mettler Toledo, modelo AG 245. As massas das amostras variaram de 27,8 a 57,7 mg, conforme mostradas na Tab. 1.

Tabela 1: Massa das amostras utilizadas nos experimentos TG e DTA

Amostras	TG (mg)	DTA (mg)
Gordura	45,4	51,0
Músculo	36,3	27,8
Músculo + Gordura	(28 + 28,1)	(29 + 28,7)

2.1. Ensaios em TG

Os experimentos TG foram realizados em uma Balança Termogravimetria (TG) Shimadzu – TGA-51H. Utilizaram-se amostras de músculo e gordura bovina comercial e suporte de amostra (cadinho) de alumínio (6 Ø x 5 mm). O gás de arraste empregado foi nitrogênio (atmosfera inerte) com vazão de 50 mL min^{-1} e razão de aquecimento de 10 $^oC\ min^{-1}$ até a temperatura de 600^{o}C.

A Figura 1 mostra o esquema do módulo termogravimétrico, sistema de aquisição de dados e trajeto do gás até o forno da balança TG. Através do sistema da balança flui apenas o gás de arraste controlado por um rotâmetro interno da balança TG. A amostra é submetida a um gradiente de temperatura dentro do forno e a variação da massa da amostra devido à degradação ou vlatilização é detectado pelo sistema da balança.

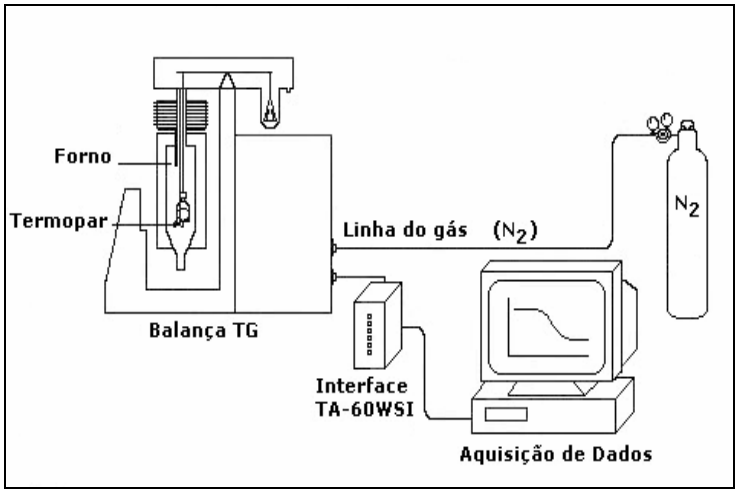

Figura 1: Sistema Termogravimétrico: linhas do gás de arraste e sistema de aquisição.

A Fig. 2 mostra uma curva típica em um ensaio TG em tecidos musculares. São mostrados os perfis TG (linha contínua) e DTG (linha pontilhada). Os indicadores (1) e (2) sobre a curva TG indicam os eventos de perda de massa observada em um ensaio utilizando-se uma amostra de músculo mais gordura bovina. O critério de corte para se definir as regiões (1) e (2) foram feitas com base na curva DTG, isto é, o final da etapa (1) corresponde ao ponto no qual a inflexão retorna ao ponto máximo. Todos os ensaios TG foram avaliados num intervalo de tempo de 0 a 3500 s que correspondem à temperatura de 25 a 600 ^{o}C.

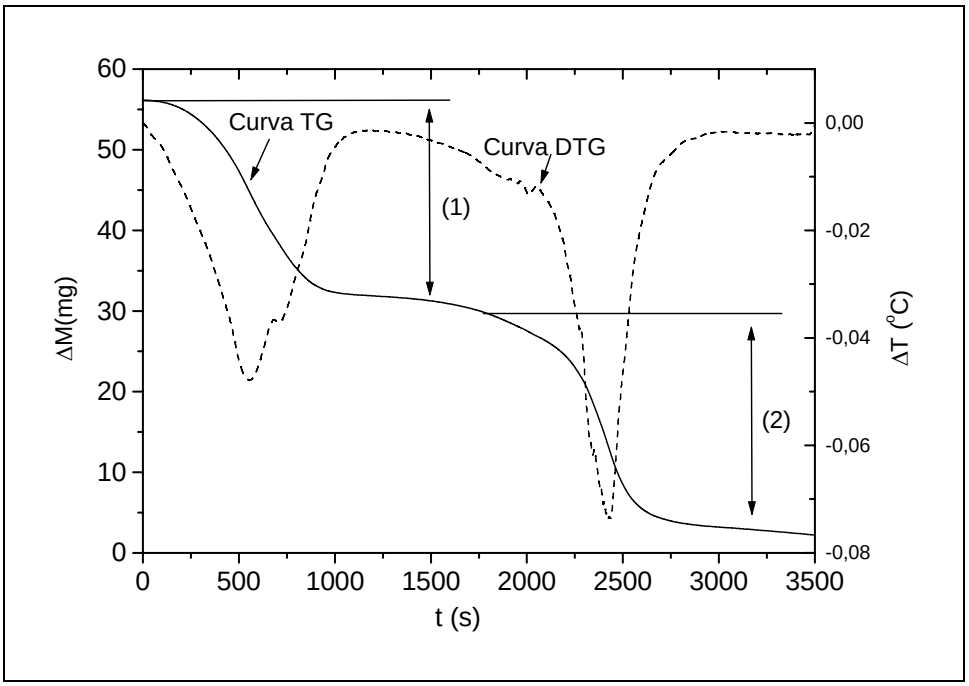

Figura 2. Curvas de variação de massa (ΔM ou Curva TG) e razão de aquecimento (ΔT) em função do tempo (t) para um dos ensaios TG.

A temperatura de 600 ^{o}C foi adotada para os testes, pois atende aos propósitos deste trabalho que é avaliar a presença de gordura no músculo. Além disso, nota-se que a amostra está praticamente decomposta nesta temperatura.

Os ensaios DTA foram feitos em um aparelho DTA da marca Shimadzu, modelo DTA-50. Os testes foram feitos nas mesmas condições experimentais daqueles descritos para os testes TG, porém como referência utilizou-se o cadinho de alumínio vazio.

3. Resultados e Discussão

As Fig. 3 e 4 apresentam as curvas TG e DTA respectivamente, obtidas em ensaios para as amostra de gordura bovina. Na curva TG observa-se claramente os dois eventos de perda de massa. O primeiro evento (1) ocorreu entre as temperaturas de 63 e 175 ^{o}C e pode ser atribuído à perda de água da amostra de gordura. O segundo evento (2) ocorreu entre as temperaturas de 175 a 500 ^{o}C, sendo atribuído a degradação da gordura. Nota-se também que praticamente toda a amostra foi degradada, restando aproximadamente 2 % de resíduo (inorgânicos).

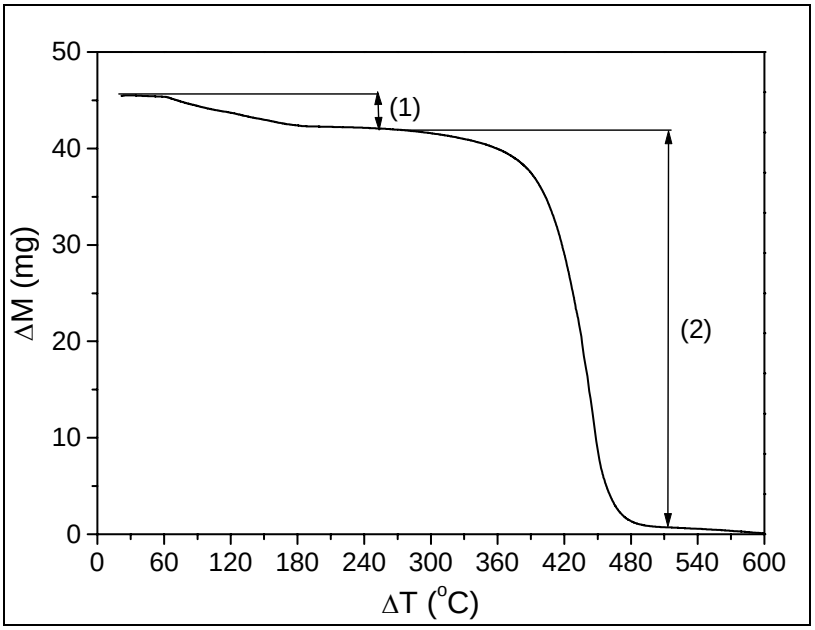

Figura 3: Curva de variação de massa (ΔM) em função da temperatura (ΔT) para amostra de gordura bovina.

Na curva DTA (Fig. 4), nota-se um pico (1) característico de fusão de gordura em torno de 147 ^{o}C, atribuído à fusão de gordura, porém nesta região de temperatura estão presentes outros picos indefinidos sobrepostos, assim há impossibilidade de se definir a linha base e consequentemente há dificuldade de se quantificar, com base na região de fusão, a gordura separadamente. Nesta curva DTA observa-se também outros picos endotérmicos em torno de 430 ^{o}C (2), isto é, região correspondente ao segundo evento de perda de massa da curva TG. Estes eventos são atribuídos à degradação da gordura presente, da mesma forma, por impossibilidade da definição da linha base e caracterização dos eventos com distinção, esta técnica apresenta-se qualitativa para os propósitos deste trabalho.

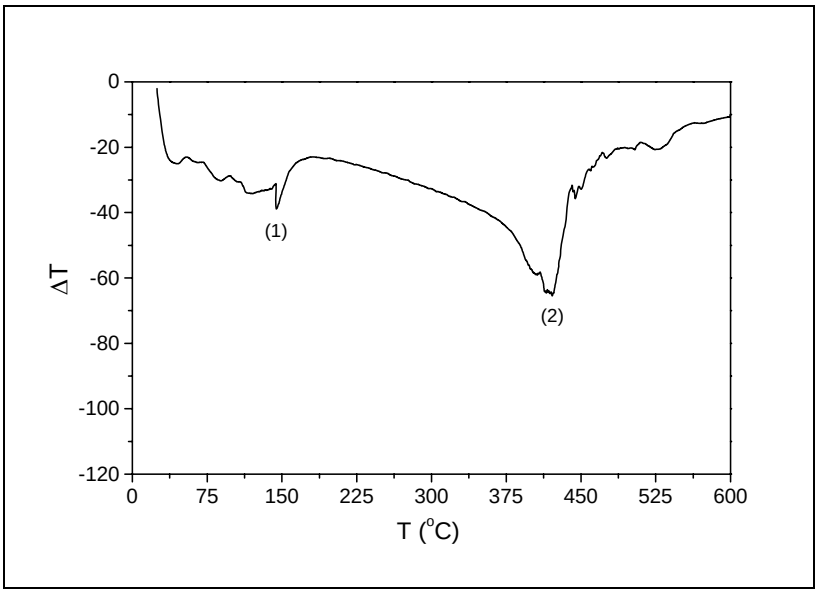

Figura 4: Curva de DTA em função da temperatura (T) para amostra de gordura bovina

Assim como na Curva TG para a amostra de gordura bovina (Fig.3), também para a amostra de músculo bovino observa-se claramente dois eventos de perda de massa. As Fig. 5 e 6 apresentam as curvas obtidas em ensaio TG e DTA para os testes utilizando-se as amostra de músculo bovino. Na curva TG, o primeiro evento (1) ocorreu entre as temperaturas de 23 e 220^{o}C que também pode ser atribuído à perda de água da amostra. O segundo evento indicado entre as temperaturas de 220 e 480 ^{o}C (2), ocorreu devido à degradação da fibra muscular. Ao final do experimento obteve-se um resíduo de aproximadamente de 3 % da massa da amostra inicial.

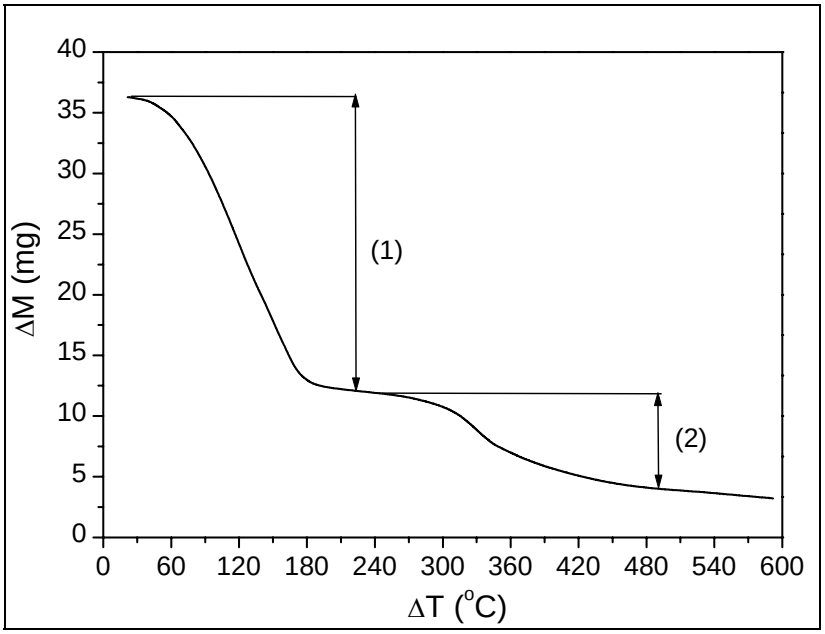

Figura 5: Curva de variação de massa (ΔM) em função da temperatura (ΔT) para amostra de músculo bovino.

Na curva DTA (Fig. 6) da amostra de músculo bovino não foi possível observar o pico de fusão da gordura (próximo a 147°C como observado na Fig.4), mas sim um pico endotérmico intenso próximo a 100º C e este pico foi atribuído à perda de água. Foram observados picos endotérmicos menores entre 300 e 400º e estes ocorreram devido à degradação da fibra muscular.

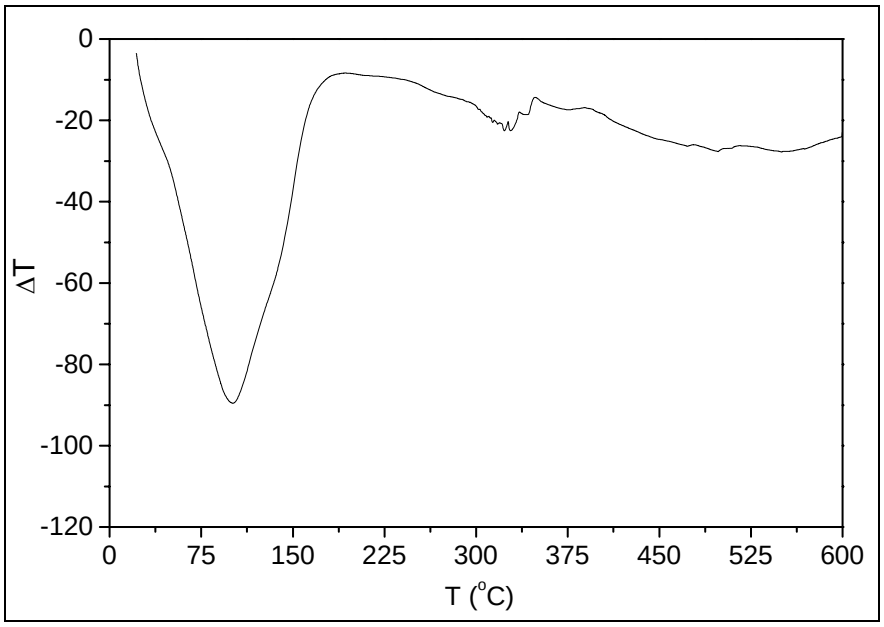

Figura 6: Curva DTA em função da temperatura (T) para amostra de músculo bovino.

Para o terceiro ensaio, utilizando-se uma amosta contendo uma mistura de músculo mais gordura bovina (Fig.7), observou-se o evento de perda de água (1) no intervalo de temperatura de 26 a 200 °C. A degradação da amostra (2) foi observada no intervalo de temperatura entre 200 e 480 °C.

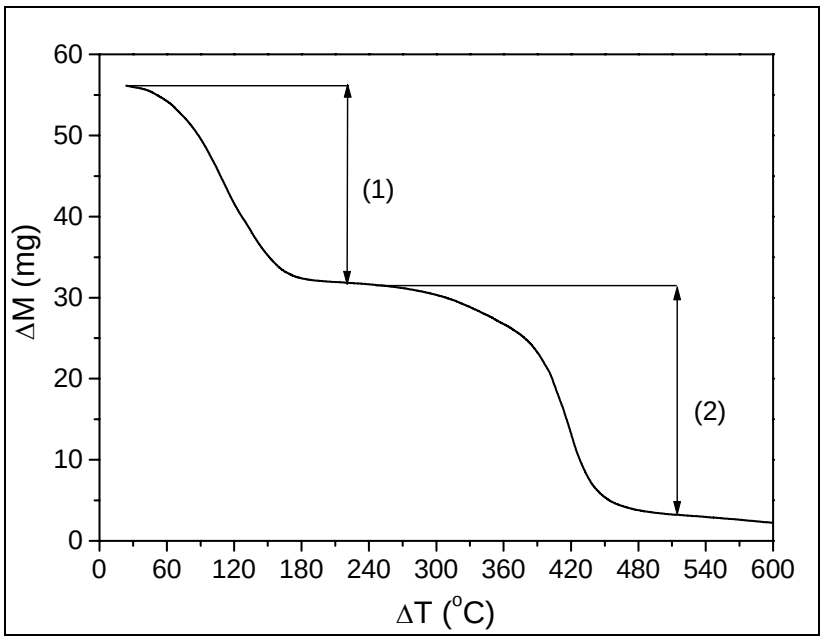

Figura 7: Curva de variação de massa (ΔM) em função da temperatura (ΔT) para amostra de gordura e músculo bovino.

Na Fig. 8 observa-se que a DTA da amostra de tecido muscular com gordura apresentou-se como a combinação dos gráficos de DTA anteriores (Fig. 4 e Fig. 6).

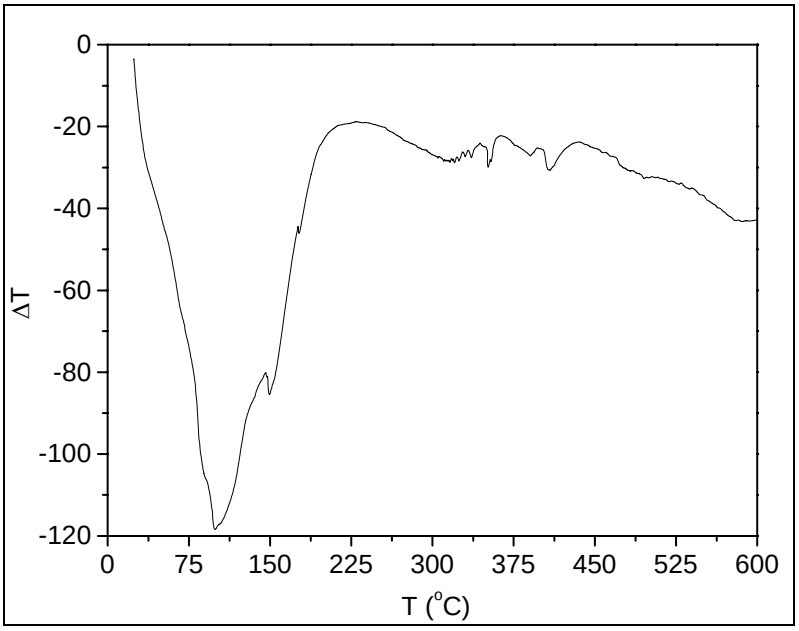

Figura 8: Curva DTA em função da temperatura (T) para gordura e músculo bovino.

Com o propósito de se comparar o comportamento de degradação térmica das três amostras, a Fig. 9 apresenta as três curvas TG simultaneamente, para isto a variação de massa é apresentada na forma percentual.

Comparando-se os resultados de perda de massa para cada uma das amostras, nota-se que na região referente à degradação da gordura, os valores estão coerentes com a característica de cada uma das amostras, isto é, para gordura pura, o valor é de 91% enquanto que para a mistura gordura mais músculo, a perda de massa é de aproximadamente 50%.

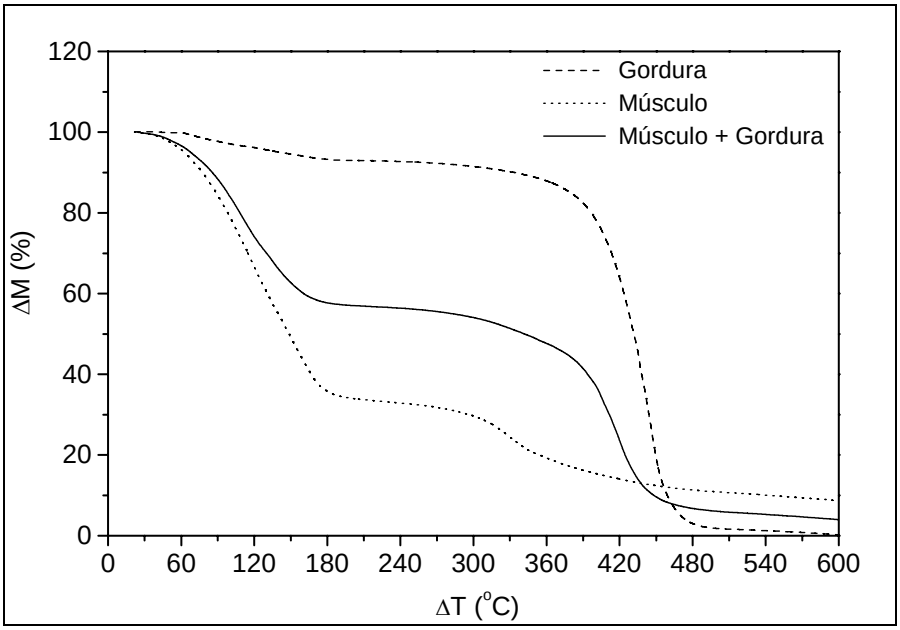

Figura 9: Curvas de variação de massa percentual (ΔM) em função da temperatura (ΔT) para todas as amostras.

A Tab.2 mostra os resultados obtidos dos ensaios TG para as três amostras analisadas os valores percentuais de perdas de massa ocorridos nos eventos observados.

Tabela 2: Massa das amostras utilizadas nos experimentos TG e DTA

Amostras		Gordura	Músculo	Gordura mais Músculo
Perda de Água	T (°C)	63 a 175	23 a 220	26 a 200
	Massa (%)	7	70	45
Degradação da Amostra	T (°C)	175 a 500	220 a 480	200 a 500
	Massa (%)	91	27	53
Resíduo	T (°C)	500 a 600	480 a 600	500 a 600
	Massa (%)	2	3	2

4. Conclusões

Os testes TG possibilitaram determinar e quantificar gordura nas amostras estudadas (músculo e gordura bovina). Os testes com DTA apresentaram-se como uma técnica promissora para se determinar a presença de gorduras, além de se apresentar como uma técnica complementar à TG por indicar picos endotérmicos entre 200 e 480°C.

A termogravimetria apresentou-se eficiente por permitir distinguir duas regiões: perda de água e degradação de gordura. Os cálculos de perda de massa para ambas as regiões foram feitos para as 3 amostras (músculo, gordura e gordura+ músculo) e estão apresentados na Tabela 2. Complementarmente, os testes feitos em DTA indicaram as transições entálpicas por meio de picos endotérmicos nos respectivos intervalos de temperatura.

Embora outros autores tenham empregado técnicas termo analíticas (tais como DSC) para o estudo de gorduras animais (Benedito *et al.*, 2001; Tomberg, 2005) estes trabalhos mostraram transições referentes à desnaturação de proteínas presentes nas amostras, portanto as temperaturas empregadas foram até 200°C. No presente estudo foi possível quantificar a gordura presente nos tecidos musculares por empregar temperaturas mais altas, até 600°C. Portanto, tanto a técnica que mostra as transições entálpicas (DTA) quanto a técnica termogravimétrica apresentaram-se eficientes nos propósitos deste trabalho.

5. Agradecimentos

À médica veterinária Dra. Karina Pontieri.

Ao Núcleo de Engenharia Térmica e Fluidos (NETeF) da Escola de Engenharia de São Carlos (USP/EESC) pela disponibilidade dos equipamentos para os ensaios TG e DTA.

Ao CNPq, CAPES e FAPESP pelo suporte financeiro.

6. Referências

Benedito, J., Carcel, J.A., Rossello, C. e Mullet, A. (2001). Composition assessment of raw meat mixtures using ultrasonics. *Meat Science*, 57, 365-370.

Bernal, C., Couto, A. B. , Breviglieri, S. T., Cavalheiro, E.T.G.(2002). Influência de alguns paramêtros experimentais nos resultados de análises calorimétricas diferenciais – DSC. *Quim. Nova*, Vol. 25, No. 5, 849 – 855.

Guyton, A.C., Fisiologia Humana, 6a. edição, Editora Guanabara Koogan, Rio de Janeiro, 1988.

Lebas, F. *Cuniculture*, 1979, 6, 159.

Martens, H., Vold, E. (1976). DSC studies of muscle protein denaturation. In *Proceedings of the 22nd European meeting of meat research workers*, Malmö, Sweeden (p. J 9.3).

Mitruka, B.M. e Rawnsley, H.M. (1977) Clinical Biochemical and Hematological Reference Values in Normal Experimental Animal. *New York: Masson Publishing*

Moran Jr, E.T. (1996). Fat modification of animal products for human consumption. Poultry Science Departament, Auburn University. USA

Mothé, C.G. Azevedo, A. D., in: Análise Térmica de Materiais, Capítulo 4, pág. 115.

Stabursvik, E., e Martens, H. (1980) Thermal desnaturation of protein in post rigor muscle tissue as studies by differential scanning calorimetry. *Journal of Science Food and Agriculture*, 31, 1034 – 1042.

Tornberg, E. (2005). Effects of heat on meat proteins – Implications on structure and quality of meat products. *Meat Science* 70, 493-508.

Wendlandt, W.W., Thermal Analysis, 3rd ed., Wiley: New York, 1985, p. 213 - 460.

Wood, J.D., Richardson, R.I., Nute, G.R., Fisher, A.V., Campo, M.M., Kasapidou, E., Sheard, P.R., Enser, M. (2003). Effects of fatty acids on meat quality: a review. *Meat Science* 66, 21-32.

Wrigt, D.J., Leach, I. B., and Wilding, P. (1977). Differential sanning calorimetric studies of muscle and its constituents. *Journal of Science Food Agriculture*, 28, 557.

EVALUATION OF THE PRESENCE OF MUSCULAR FAT IN TISSUE USING DTA AND TG

Karen Cristina Laurenti
Program of Interunidades in Bioengineering - School of Engineering of São Carlos, University of São Paulo, Av. Trabalhador São-carlense 400, 13566-590, São Carlos - SP, Brazil.
e-mail: karen_laurenti@yahoo.com.br

Carlos Dias Maciel
Department Electrical Engineering, School of Engineering of São Carlos, University of São Paulo, Av. Trabalhador São-carlense 400, 13566-590, São Carlos - SP, Brazil.
e-mail: maciel@sel.eesc.usp.br

Paula Manoel Crnkovic
Group and Thermal and Fluids Engineering, School of Engineering of São Carlos, University of São Paulo, Av. Trabalhador São-carlense 400, 13566-590, São Carlos - SP, Brazil.
e-mail: paulam@sc.usp.br

Ivonete Ávila
Group and Thermal and Fluids Engineering, School of Engineering of São Carlos, University of São Paulo, Av. Trabalhador São-carlense 400, 13566-590, São Carlos - SP, Brazil.
e-mail: iavila@sc.usp.br

Abstract: The meat is a major source of fat in human alimentation, especially in saturated fat and, when combined with the stree in modern life, people may be suffering from many kind of cancer or coronary diseases.*This work has an objective to quantify the fat presence of the fat in muscular fibres using it Thermal Analysis. The analyses had been made by Termogravimety and Differential Thermal Analysis and for the preliminary tests it has using bovine muscle and fat. In Termogravimetry the loss of mass muscular associated with the degradation of fats and fibres have been determined. From the studied conditions, the results of the experiment found in the tests made in Termogravimetry had revealed viable quantitative determination of fat in muscular fibres. The Termogravimetry tests has quantified the present of fat in the samples. The Differential Thermal Analyss had complemented this work, where it was observed decurrent peaks of fusing of the fat presence.*

keywords: Termogravimetry, DifferentialThermal Analysis, Fat Tissue.

Proceedings of the 11th Brazilian Congress of Thermal Sciences and Engineering -- ENCIT 2006
Braz. Soc. of Mechanical Sciences and Engineering -- ABCM, Curitiba, Brazil, Dec. 5-8, 2006

Paper CIT06-0310

MODELO MECÂNICO PARA SILMULAÇÃO DO CONDICIONAMENTO PULMONAR DO AR RESPIRADO

Dr. Nelson Bergonse Neto
Pontifícia Universidade Católica do Paraná – Rua Padre Agostinho, 227 (Ap. 11) – Mercês – Curitiba/PR – CEP: 80.410-020
e-mail: bergonsent@terra.com.br

Prof. Dr. Luís Mauro Moura
Pontifícia Universidade Católica do Paraná – Rua Imaculada Conceição, 1155 – Prado Velho – Curitiba/PR – CEP: 80.215-901
e-mail: Encit2006@pucpr.br

Prof. Dr. Luiz Carlos Von Bahten
Pontifícia Universidade Católica do Paraná – Rua Candido de Abreu, 140 (cj. 801-802) – Centro Cívico – Curitiba/PR – CEP: 80.530-901
e-mail: vonbahten@yahoo.com.br

Prof. Dr. Marlos de Souza Coelho
Pontifícia Universidade Católica do Paraná – Rua Comendador Franco, 2429 – Guabirotuba – Curitiba/PR – CEP: 81.520-000
e-mail: clinicadotorax@marloscoelho.com.br

Dr. Wilson de Souza Stori Junior
Pontifícia Universidade Católica do Paraná – Rua Batista Pessini, 654 (casa 01) – Vista Alegre – Curitiba/PR – CEP: 80.820-000
e-mail: wstori@uol.com.br

Dr. Gilberto da Fontoura Rey Bergonse
Hospital de Reabilitação de Anomalias Crânio-faciais – USP/SP – Rua Octavio Pinheiro Brisolla, 7-12 (ap. 62) – Vila Universitária – Bauru/SP – CEP: 17.012-059
e-mail: gilbertobergonse@ibest.com.br

Resumo. *Este trabalho apresenta de um modelo mecânico desenvolvido para condicionar o ar inspirado e expirado em valores normais de temperatura (37,0+/-0,6ºC), pressão (0 a 20 cmH_2O) e umidade relativa (100%) que um homem jovem (25 anos) hígido de 80 kg condicionaria sob ventilação mecânica. Utilizaram-se diversos tipos de materiais, como plástico, metal, madeira, vidro e eletro-eletrônicos, construiu-se um aparelho que foi regulado com capacidade vital de 5000 ml, volume corrente de 800 ml, pressão inspiratória máxima de 20 cmH_2O, PEEP de 2 cmH_2O e temperatura do gás dentro do sistema de 37,0+/-0,6ºC. O aparelho foi submetido à ventilação mecânica com volume corrente de 800 ml, pressão inspiratória máxima de 20 cmH_2O, fluxo inspiratório de 40 l/min, PEEP de 2 cmH_2O, freqüência respiratória de 17 rpm, F_iO_2 de 0,21 e temperatura do gás igual à do meio ambiente por um período de 29,8 minutos. A cada dois segundos, foram registradas as alterações de temperatura do ar circulado no sistema. Mediante análise estatística dos dados coletados observou-se que o aparelho foi eficiente no condicionamento do ar aproximadamente nos moldes do ser humano (temperatura 37,3ºC; pressão máxima de 20 cmH_2O e umidade relativa de aproximadamente 100%). Conseguiu-se desenvolver um aparelho que pode simular o condicionamento do ar nos mesmos moldes que o aparelho respiratório normal. Este mesmo aparelho pode ainda simular o condicionamento pulmonar do ar de humanos com diferentes biótipos, tornando-se um instrumento útil em estudos que envolvam os processos de transferência de calor e massa na ventilação pulmonar.*

Palavras chave: Termodinâmica, Respiração artificial, Hipotermia.

1. INTRODUÇÃO

O ser humano, como qualquer animal homeotérmico, apresenta um complexo metabolismo corporal mediado por sistemas enzimáticos, quase todos temperatura dependentes. Sendo assim, é de vital importância que a temperatura corpórea central permaneça constante (37,0+/-0,6ºC) para o perfeito funcionamento do organismo. O controle dessa temperatura está sob a responsabilidade do hipotálamo e é atingido mediante o equilíbrio entre a produção e a perda de calor (Guyton, 1991).

Durante procedimentos cirúrgicos o paciente fica a mercê de um ambiente cirúrgico não controlado e sem o funcionamento perfeito dos mecanismos termoreguladores do organismo, que são totalmente ou em parte bloqueados pela anestesia, evoluindo para algum grau de hipotermia (Bahten, 2001; Goldberg, 1992; Margarido, 1997; Morris, 1971 e Schechter, 1992).

A hipotermia causa efeitos deletérios ao organismo como alterações no metabolismo basal, no transporte de oxigênio e gás carbônico, nas concentrações de íons hidrogênio no sangue e mudanças hidroeletrolíticas e hormonais (Bahten, 2001; Biem, 2003; Guyton, 1991; Morcom, 2003 e Prandini, 2002).

O aparelho respiratório, entre outras funções, é responsável pelo condicionamento do ar respirado, de vital importância tanto para o processo da respiração como para a manutenção da homeotermia. Através deste ocorre 25% da perda calórica do organismo (Guyton, 1991).

As reações térmicas da árvore traqueobrônquica são dependentes principalmente da temperatura e da umidade relativa do ar inspirado. A temperatura do ar inalado é o principal fator envolvido na troca de energia térmica do aparelho respiratório, uma vez que a temperatura deste ar pode ser muito variável e a perda ou o ganho de calor pelo organismo está diretamente relacionada à diferença de temperatura entre o ar inalado e a superfície mucosa do aparelho respiratório (Good, 1957 e Mather, 1953). Outros fatores também importantes para as reações térmicas da árvore traqueobrônquica são a taxa de ventilação por minuto, a temperatura da parede das vias aéreas, alterações vasomotoras e alterações na membrana da mucosa (Cramer, 1957; Hanna, 1986; McFadden, 1982 e Webb, 1951).

Durante a inspiração, o ar é aquecido por meio do calor da mucosa das vias aéreas, que reflete a temperatura do fluxo sangüíneo. Na maior parte das vias aéreas, a troca de calor está na dependência da circulação brônquica, mas a partir dos bronquíolos terminais essa função é assumida pela circulação pulmonar, que garante o condicionamento total do ar quando este chega ao alvéolo (Dery, 1973 e Hanna, 1986).

Existem duas regiões maiores de condicionamento do ar. A primeira é constituída das cavidades nasal e oral, que funcionam como a principal região condicionadora em que o ar atinge quase o máximo de condicionamento. A segunda é a árvore traqueobrônquica, que desempenha um papel secundário, sendo que em direção da periferia do pulmão as trocas de calor e umidade se tornam menos eficientes (Hanna, 1986; Ingelstedt, 1956; McFadden, 1982 e McFadden, 1983).

Acredita-se que até os brônquios de 7ª ordem a tarefa de condicionamento do ar já esteja completa, sendo que o ar chega aos bronquíolos respiratórios e aos alvéolos em condições corporais (temperatura de 37,0ºC e umidade relativa de 100%) (Hanna, 1986 e Ingelstedt, 1956).

Alguns estudos mostram a eficiência do processo de umidificação do ar, por demonstrar que, mesmo em pacientes intubados em que a umidade relativa do ar que chega a traquéia é de aproximadamente 51% e essa umidade aumenta para aproximadamente 100% na divisão dos brônquios lobares (Cramer, 1957 e Dery, 1973).

Para efeito de estudo de troca térmica entre o ar e o aparelho respiratório, existem variáveis de volume e pressão com importância fundamental que são: a pressão do ar dentro do aparelho respiratório, o volume de ar que circula dentro do aparelho respiratório na unidade de tempo e o volume de ar que permanece dentro do sistema respiratório no final da expiração (Ratto, 1997).

A pressão do ar dentro do aparelho respiratório não é constante em nenhum momento e é bastante variável. Em indivíduos hígidos, varia de 2 a 5 cmH_2O até 20 a 30 cmH_2O (Guyton, 1991).

O volume de ar que circula dentro do aparelho respiratório na unidade de tempo, também chamado de fluxo aéreo, é o produto entre o volume corrente (VC), e a freqüência respiratória (FR) (Ratto, 1997).

O volume de ar que permanece dentro do sistema respiratório no final da expiração normal é chamado de Capacidade Residual Funcional (CRF) e torna-se importante uma vez que este, invariavelmente, é maior que o volume corrente e que, a cada ciclo respiratório, ele é trocado apenas parcialmente, interferindo nas alterações de temperatura e de umidade do ar inspirado.

Mediante fórmulas já consagradas pela literatura médica, é possível estimar os valores normais da capacidade pulmonar total (CPT), capacidade vital (CV), volume corrente (VC) e volume residual (VR); mas é sempre importante lembrar que estes valores estimados podem sofrer uma variação de 15 a 20% e ainda ser considerados dentro da faixa de normalidade (Ratto, 1997). A capacidade vital é calculada para homens maiores de 15 anos por intermédio das Fórmulas de Baldwin, Cournand e Richards Jr. (CV em ml = 27,63 – (0,112 X idade) X altura em cm) (Ratto, 1997). A capacidade pulmonar total também é calculada através das Fórmulas de Baldwin, Cournand e Richards Jr. (CPT em ml = CV / 0,80, para pessoas entre 15 e 34 anos) (Ratto, 1997). O volume corrente (VC) é de 5 a 10 ml/kg para indivíduos hígidos (Guyton, 1991). O volume de reserva expiratória, assim como a capacidade residual funcional, não pode ser estimada por fórmulas, mas apenas medido por meio de exame complementar (prova de função pulmonar) (Ratto, 1997).

É de fundamental importância salientar que, todos os cálculos de ventilação pulmonar que utilizam a massa corporal como uma das variáveis, esta deve ser a massa corporal ideal, baseada em um índice de massa corporal de 20 a 25.

Vários estudos já foram realizados para determinar a perda de energia térmica e de umidade através das vias aéreas tanto em animais quanto em humanos, mas nenhum em procedimentos cirúrgicos com intubação orotraqueal (Good, 1957; Hanna, 1986; Mather, 1953; McFadden, 1982; McFadden, 1983 e Webb, 1951).

Este estudo procurou criar e construir um modelo mecânico que pudesse ser regulado conforme a necessidade de pesquisadores, para simular o condicionamento do ar inspirado e expirado a valores normais de temperatura, pressão e umidade relativa de um ser humano hígido. Sua finalidade é servir de base para outros estudos que envolvam termorregulação e ventilação mecânica, sem a necessidade de experimentação inicial em animais.

2. MÉTODOS

Esta pesquisa foi realizada no Laboratório de Termodinâmica do Centro de Ciências Exatas e Tecnológicas da Pontifícia Universidade Católica do Paraná. Por se tratar de um modelo experimental e não utilizar normas de experimentação animal, não houve necessidade de aprovação por comissão de ética.

Os materiais utilizados foram divididos em: plásticos, metálicos, madeira, vidraçaria, eletro-eletrônicos, fixação e vedação, isolamento térmico e acabamento. A maioria destes materiais necessitou modificações para este trabalho.

Os materiais plásticos utilizados foram: uma placa de PVC rígido, canos e conexões de PVC rígido (TIGRE®), dois registros plásticos de 3 vias com válvula unidirecional (OXIGEL®), mangueiras plásticas, folhas de transparências A4, filme plástico de poliestireno, tecido sintético de poliéster, cesto de lixo cilíndrico de 6 l e uma cânula orotraqueal de 8,0 mm (RUSH®).

Os materiais metálicos utilizados foram de ferro galvanizado, latão, bronze, chumbo e cobre, em forma de: parafusos, arruelas, porcas, hastes, registros, conexões em T, bicos adaptadores, chumbo granulado e telas.

A madeira utilizada foi: *pinus* e fórmica.

Os componentes elétricos utilizados foram: fio elétrico de cobre, *plugs* de tomada, bocais para lâmpada, lâmpadas incandescente e fluorescente, aquecedor para aquário (BW®), chaves de luz intermediárias, mangueira luminosa branca, filtro de linha, *cooler* de computador, termostatos eletrônicos (MW®), microcomputador com processador Pentium 3, 450 MHz e 128 MB de memória RAM, *software* Agilent Banchlink versão 1.4 (Agilet®), termopares tipo T de cobre e constantan, sistema de aquisição e controle de sinais do tipo Agilent 34970A com placa de multiplexação 34901A de 20 canais (Agilet®) e um ventilador mecânico marca TAKAOKA® modelo MONTEREY 3.

A fixação e a vedação dos componentes foram feitos através de: abraçadeiras, cola de silicone, cola de PVC, cola de éster de cianoacrilato, cola *spray* para espuma e isopor Nº77 (3M®), espuma expansiva de poliuretano, fita adesiva transparente e fita isolante (3M®).

O isolamento térmico baseou-se em placas de papelão e isopor.

O acabamento foi feito com folhas de papel Contact® branca e transparente.

Utilizou-se ainda dois tubos de vidro.

Dividiu-se o presente trabalho em construção, montagem, regulagem e experimentação.

2.1. Construção

Para a realização do experimento, fez-se necessária a construção individual de cada uma das partes do aparelho que foram: a Válvula de PEEP, a Válvula de Segurança, o Cilindro Principal, o Fole, os Lastros de Pressão, o Umidificador, os Manômetros, o Painel de Controle, o Porão, a Caixa de Armazenamento e o Distribuidor de Ar.

A válvula de pressão pulmonar expiratória final (Válvula de PEEP) teve por finalidade a simulação da pressão pulmonar expiratória final (PEEP). Foi desenvolvida para manter uma pressão mínima no sistema que poderia variar de 0 a 30 cmH_2O. A construção desta válvula utilizou como base um cano de 45 cm de comprimento e 75 mm de diâmetro. O funcionamento desta válvula foi baseado em um mecanismo de coluna d`água para o controle da pressão.

A Válvula de segurança teve por finalidade o controle da pressão máxima dentro do sistema (40 cmH_2O). A construção desta válvula utilizou como base um cano de 55 cm de comprimento e 75 mm de diâmetro. O funcionamento desta válvula foi baseado em um mecanismo de coluna d`água para o controle da pressão.

O Cilindro Principal foi a peça mais importante na construção do aparelho e teve como função o controle do volume de ar, da umidade relativa do ar e da temperatura dentro do sistema. Teve como base um cesto de lixo cilíndrico de 6 l. À este cilindro adaptou-se: um registro plástico de três vias com válvula unidirecional para controle de entrada e saída do ar, a válvula de segurança, um manômetro, dois sensores de temperatura do tipo Termopar (um para água e um para o ar), um sensor de temperatura do termostato e um aquecedor de aquário. Ainda na tampa superior deste cilindro foi feito um orifício de 150 mm para adaptação do Fole que será descrito na seqüência. Este cilindro apresentava uma escala variando de 700 ml (mínimo) a 5200 ml (máximo). De baixo para cima, um lado da escala mostrava em ordem crescente o volume de água, enquanto o outro lado mostrava em ordem decrescente o volume de ar.

O Fole foi criado visando à simulação do volume corrente no aparelho, foi desenvolvido um Fole que usou como base um cano com 20 cm de altura e 150 mm de diâmetro que foi acoplado na extremidade superior do cilindro principal. Este apresentava um mecanismo regulador de volume que variava de 0 a 2000 ml e um compartimento superior para a colocação dos lastros de pressão.

Os Lastros de Pressão foram confeccionados com chumbo e criados para obter-se a pressão desejada no sistema, esta teve que ser calculada com base na área da tampa superior do fole que transmitiria a pressão para o ar que entrava e saía do sistema e o ar que permanecia neste. Como o diâmetro da tampa superior do fole era 142 mm, calculou-se uma área de 15.863,755 mm^2 (Ab = 3,14159 X 142^2 / 4). Como 1 cmH_2O = 0,01 gf/mm^2, para obter-se uma pressão de 1 cmH_2O no sistema determinou-se que era preciso uma força de 158,36755 gf (0,01 gf/mm^2 = F / 15.836,755 mm^2) ou uma massa de 158,36755 g aplicada sobre a tampa superior do fole. Assim, estabeleceu-se que uma massa de 158,36755 g, aplicada sobre o sistema, acarretaria em uma pressão de 1cmH_2O e criaram-se lastros de 10, 5, 2 e 1 cmH_2O. Estes lastros seriam colocados no recipiente próprio sobre a tampa do fole, conforme a necessidade.

O Umidificador foi criado tendo em vista que o ar que entraria no sistema não era saturado e tinha uma temperatura inferior a 37,0ºC, este, ao ser aquecido, absorveria água e isto constituiria um risco de diminuição nos níveis líquidos de calibragem do cilindro principal e das válvulas. A sua construção utilizou como base um cano com 10 cm de altura e 100 mm de diâmetro, que para a umidificação do ar utilizava um principio de borbulhamento do ar em água , através de cálcuos, definira-se que 1600 orifícios de 0,5 mm de diâmetro, seriam suficientes para a umidificação sem sobrecarca de pressão no aparelho.

Os Manômetros foram construídos em número de dois: um para medir a pressão no interior da caixa de armazenamento e o outro, a pressão do cilindro principal. Ambos apresentavam uma escala em centímetros que variava de -5, na sua parte inferior, até +40, na superior.

O Painel de Controle foi construído sobre uma placa de PVC de 40 cm X 40 cm e foi dividido verticalmente, da esquerda para a direita, em quatro partes iguais, sendo cada uma destinada a um tipo de controle: Temperatura (um termostato de controle da temperatura da água do cilindro principal e um do ar da caixa de armazenamento), Pressão (um manômetro para a aferição da pressão do cilindro principal e um da caixa de armazenamento), Chaves de Comando (interruptores para ativação dos termostatos, ventilador e luzes) e Força Elétrica (filtro de linha com fusíveis para proteção do equipamento).

Como anexo à base da caixa de armazenamento, foi construído um sistema de escoamento, por gravidade, para esvaziar os recipientes do interior da caixa e permitir a saída do respiro da Válvula de Segurança. Este sistema e escoamento foi denominado Porão e utilizou mangueiras e registros para sua confecção.

A Caixa de Armazenamento teve como propósito o isolamento térmico e foi construída a partir de uma caixa de papelão simples de 3 mm de espessura e dimensões de 62 cm X 36,5 cm X 65 cm, com o seu interior revestido por placas de isopor de 30 mm de espessura.

O Distribuidor de Ar foi construído com o intuito de controlar a entrada e saída do ar no sistema e teve como base um registro plástico de 3 vias com válvula unidirecional. Esta peça apresentava ainda um limitador que permitia que a cânula de intubação só progredisse até o nível de seu anel identificador do balonete quando fosse conectada no pulmão artificial.

2.2. Montagem

A montagem do sistema foi feita dentro da Caixa de Armazenamento através da fixação do Cilindro Principal, da Válvula de PEEP, da Válvula de Segurança e do Umidificador ao fundo da caixa com cola de silicone. Todas as peças apresentavam sob si um orifício de escoamento. Num segundo, momento foram fixados ao assoalho da caixa: um ventilador (homogeneização da temperatura), uma lâmpada fluorescente (para iluminação), uma lâmpada incandescente (para aquecimento).

Um orifício de 20 mm foi feito na parede lateral direita da caixa, para a fixação do Distribuidor de Ar.

Após a fixação de todas as estruturas acima descritas, no interior da caixa, procedeu-se à conexão entre elas através de mangueiras obedecendo a seguinte seqüência: via de entrada do Distribuidor de Ar, Umidificador, Cilindro Principal (registro unidirecional de 3 vias), Válvula de PEEP e saída de ar do Distribuidor de Ar. Ainda ao Cilindro Principal conectou-se Válvula de Segurança. Houve ainda as conexões do respiro da Válvula de Segurança e dos manômetros.

Toda a fiação elétrica foi devidamente conectada entre si e ao Painel de Controle.

Por um orifício na parede lateral esquerda da caixa entraram oito sensores de temperatura (Termopar), ligados a um sistema computadorizado de coleta e analise de dados térmicos. Estes sensores foram posicionados em pontos estratégicos para a coleta de dados da seguinte maneira: A) entrada de ar do distribuidor (entrada do ar no sistema), B) entrada de ar do cilindro principal (entrada do ar no centro do aparelho), C) dentro do cilindro principal (água do cilindro principal), D) dentro do cilindro principal (ar do cilindro principal), E) saída de ar do cilindro principal (saída do ar do centro do pulmão), F) saída de ar do distribuidor (saída do ar do sistema), G) interior da caixa de armazenamento (interior do aparelho), H) exterior da caixa de armazenamento (Ambiente externo) e I) interior da cânula de intubação (ar inspirado e expirado).

Por último, foi fixado o Painel de Controle à face externa da parede anterior da caixa na altura exata para a calibragem dos manômetros.

Todos os orifícios que comunicavam o interior da Caixa de Armazenamento com o meio externo foram vedados com espuma expansiva (Figs. 1, 2 e 3).

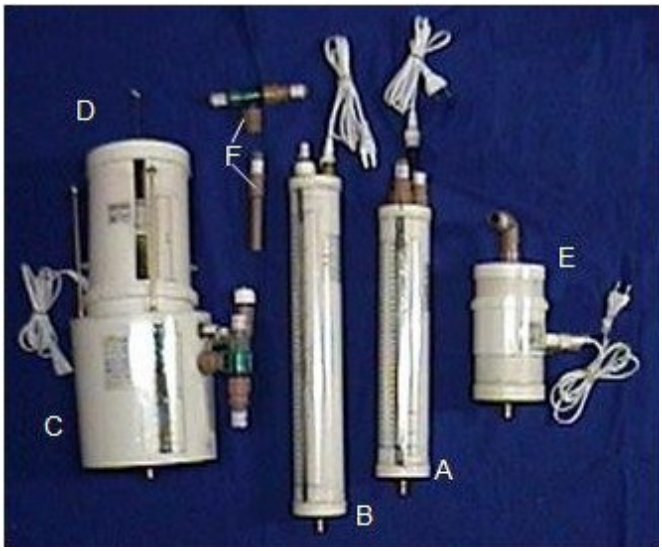

Figura 1. Peças principais do aparelho isoladas: A) Válvula de PEEP, B) Válvula de Segurança, C) Cilindro Principal, D) Fole, E) Umidificador e F) Distribuidor de Ar.

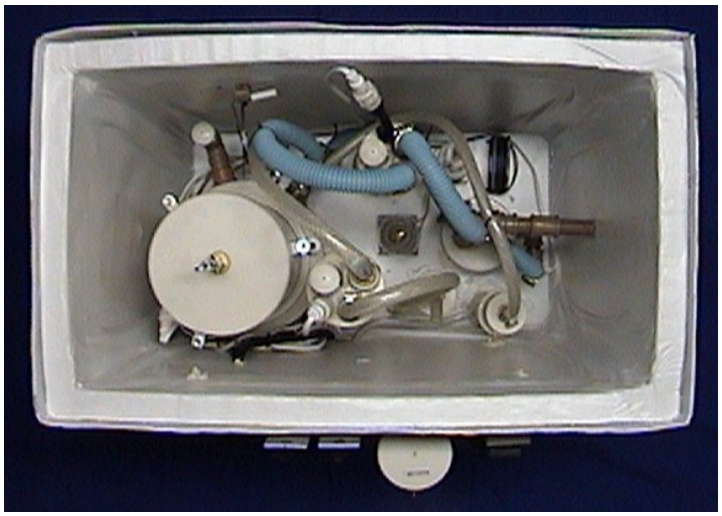

Figura 2. Vista interna do aparelho montado: Peças acomodadas dentro da Caixa de Armazenamento e suas conexões.

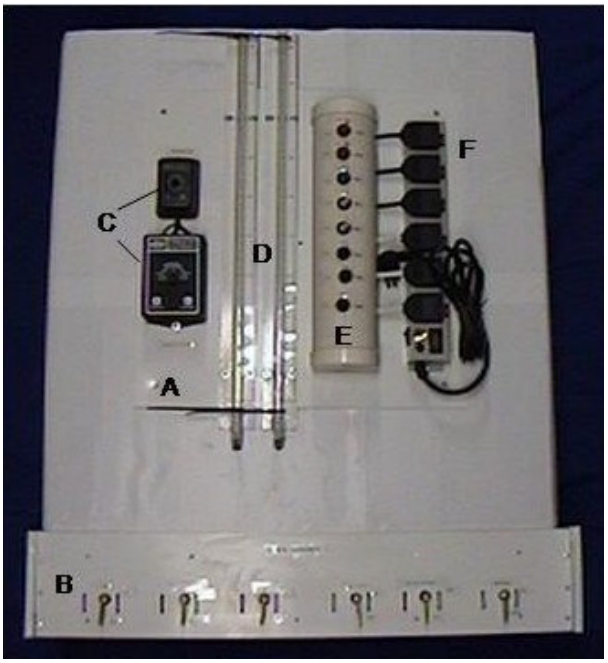

Figura 3. Vista anterior do aparelho montado: A) Painel de Controle, B) Porão, C) Termostatos, D) Manômetros, E) Chaves de Comando e F) Força Elétrica.

2.3. Regulagem

Tanto o aparelho quanto o ventilador mecânico foram regulados tendo em vista dados específicos para um adulto jovem (25 anos) hígido de 80 kg com 1,88 m de altura do sexo masculino.

Para a calibragem do aparelho, foi utilizada uma solução de água destilada e azul de metileno a 0,0005% (as propriedades físico-químicas e termodinâmicas desta solução foram idênticas às da água destilada) (Ruiz, 1954).

O aparelho foi regulado com os seguintes parâmetros: capacidade vital de aproximadamente 5000 ml, mediante a colocação de 1600 ml de solução no Cilindro Principal, volume corrente de 800 ml por meio do ajuste do mecanismo limitador de volume do Fole, pressão no início da expiração e final da inspiração 20 cmH_2O mediante a colocação de 3.167,34 g de lastro sobre a tampa do Fole, pressão no final da expiração e início da inspiração 2 cmH_2O (PEEP fisiológico) com a colocação de 260 ml de solução dentro da Válvula de PEEP e temperatura do gás dentro do sistema de 37,0^{O}C (Good, 1957; Mather, 1953; McFadden, 1982 e McFadden, 1982). Ajustou-se ainda a Válvula de Segurança em 40 cmH_2O, que é pressão fisiológica máxima admitida nas vias aéreas (Guyton, 1991), mediante a colocação de 1818 ml de solução dentro desta válvula.

O Ventilador Mecânico foi regulado para fornecer ao Pulmão Artificial gás com as seguintes características: volume corrente 800 ml, pressão inspiratória máxima 20 cmH_2O, fluxo inspiratório 40 l/min, PEEP 2 cmH_2O (fisiológico), freqüência respiratória 17 resp/min, F_iO_2 0,21 (ar ambiente) e temperatura do gás igual à do meio externo (LoCicero, 2000).

2.4. Experimentação

O aparelho foi ativado e mantido em repouso para que houvesse equilíbrio térmico dentro do sistema à 37,0ºC. Conectou-se a cânula orotraqueal ao aparelho e ao conjunto de ventilação mecânica e então iniciou-se a ventilação, que foi mantida até que fosse atingido novamente o equilíbrio térmico dentro do sistema (Fig. 4).

As variações térmicas no sistema foram registradas a cada dois segundos e analisadas.

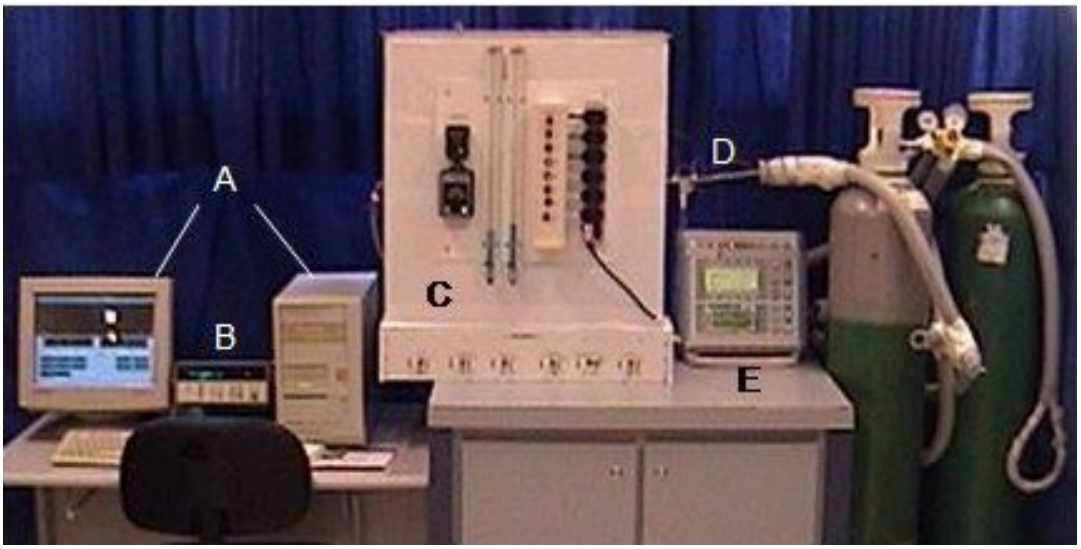

Figura 4. Aparelho ativado sob ventilação mecânica e com coleta computadorizada de dados: A) Microcomputador com *software* Agilent Banchlink versão 1.4 (Agilet®), B) Sistema de aquisição e controle de sinais do tipo Agilent 34970A (Agilet®), C) Aparelho de condicionamento, D) Termostatos do painel de controle, E) Manômetros do painel de controle, F) Chave de comando do painel de controle, G) Força elétrica do painel de controle, H) Porão, I) Cânula orotraqueal de 8,0 mm e J) Ventilador mecânico.

3. RESULTADOS

No início do experimento, a temperatura registrada nos sensores térmicos era de: A = 21,4ºC, B = 21,4ºC, C = 21,7ºC, D = 21,6ºC, E = 21,6ºC, F = 21,8ºC, G = 21,8ºC e H = 21,2ºC. Nesta fase do experimento, o sensor I foi desconsiderado. O aparelho foi ativado e mantido em repouso sendo as variações de temperatura captadas pelos sensores e registradas a cada dois segundos, até que o equilíbrio térmico à 37,0+/-0,6ºC foi atingido com 3978 segundos (Tab. 1 e Fig. 5).

Tabela 1. Valores de equilíbrio térmico do aparelho em repouso e sob Ventilação Mecânica

SENSORES	TEMPERATURA (°C.)						TEMPO DE EQUILÍBREO	
	REPOUSO			VENTILAÇÃO			(seg.)	
	Mín.	Máx.	Méd.	Mín.	Máx.	Méd.	REPOUSO	VENTILAÇÃO
Ar Inspirado	-	-	-	22,4	23,0	22,9	-	0
Entrada de Ar Aparelho	37,3	38,8	38,2	31,5	31,7	33,9	3416	366
Entrada de Ar Cilindro Principal	38,5	39,6	39,1	35,7	38,5	37,3	3450	366
Água Cilindro Principal	37,5	37,8	37,6	37,2	37,6	37,4	3308	0
Ar Cilindro Principal	37,8	38,0	37,9	36,9	37,7	37,3	3978	360
Saída de Ar Cilindro Principal	37,6	38,7	38,1	35,6	36,6	36,1	3430	370
Saída de Ar Aparelho	36,8	37,6	37,2	36,7	37,7	37,3	3406	0
Interior Caixa de Armazenamento	36,2	37,2	36,8	36,2	37,2	36,7	3416	0
Ambiente Externo	21,0	22,2	21,8	22,2	22,9	22,6	0	0
TEMPO TOTAL PARA EQUILÍBRIO TÉRMICO							3978	370

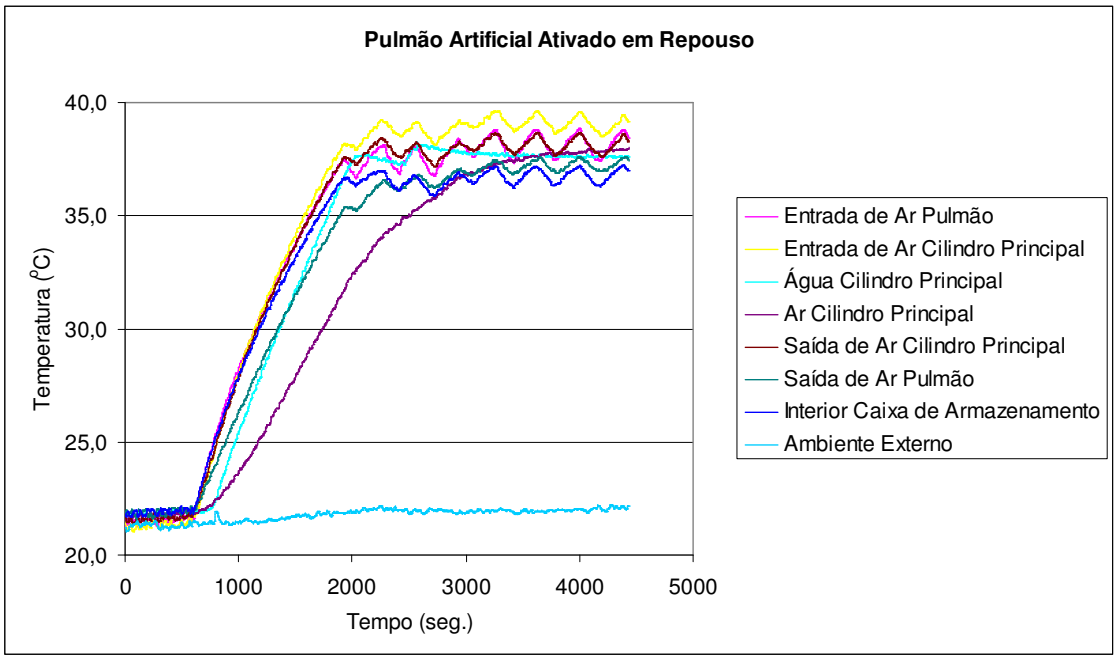

Figura 5. Curva térmica do aparelho durante o período em que permaneceu ativado em repouso

Após ter sido atingido o equilíbrio térmico com o aparelho em repouso, procedeu-se à ventilação mecânica. Iniciando-se a ventilação mecânica, houve uma rápida e discreta queda nas temperaturas registradas pelos sensores na faixa de 0,9ºC, mas que, devido ao funcionamento eficaz dos termostatos, foi recuperada rapidamente, atingindo-se novamente o equilíbrio térmico a 37,0+/-0,6ºC em 370 segundos (Tabela 1 e Figura 6).

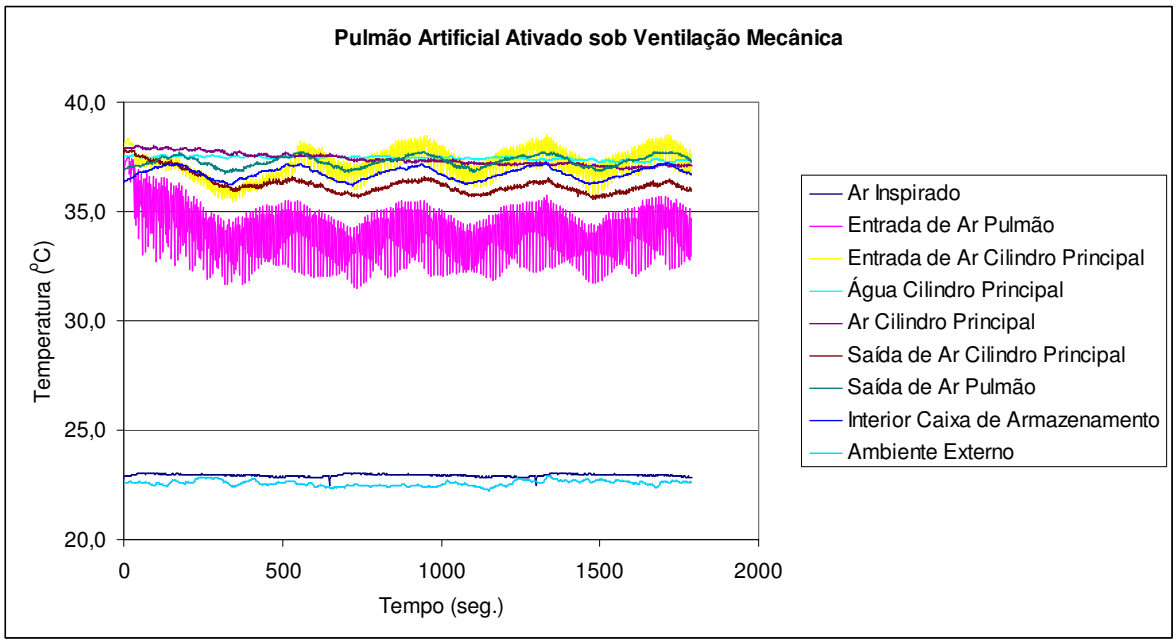

Figura 6. Curva térmica do aparelho durante o período em que permaneceu ativado sob Ventilação Mecânica

A pressão dentro da Caixa de Armazenamento, medida por um dos manômetros, manteve-se em 0 cmH_2O durante todo o experimento e a pressão no interior do Cilindro Principal, medida pelo outro manômetro, esteve oscilando entre 2 cmH_2O (no final da expiração) e 20 cmH_2O (no final da inspiração).

Ao final de 1788 segundos de ventilação mecânica, foram desligados o Ventilador Mecânico e o aparelho; abriu-se a Caixa de Armazenamento e verificou-se o nível de líquido que calibrava cada uma das peças, constatando-se que todos os níveis não tinham sofrido alteração, exceto o do Umidificador, que tinha baixado de 4 para 2,8 cmH_2O (perda de 129 ml de água).

4. DISCUSSÃO

Vários estudos já foram realizados para determinar a perda de energia térmica e de umidade através das vias aéreas, tanto em animais quanto em humanos, mas nenhum em procedimentos cirúrgicos com intubação orotraqueal. (Hanna, 1986; Mather, 1953; McFadden, 1982; McFadden, 1983 e Webb, 1951).

Cogita-se, mas ainda sem embasamento científico suficiente, a possibilidade de controlar a perda de calor e umidade que ocorre pelas vias aéreas. Espera-se, futuramente, através delas, fornecer calor e umidade ao organismo, tendo em vista o tratamento da hipotermia.

Este estudo procurou criar e construir um modelo mecânico que pudesse ser regulado conforme a necessidade de pesquisadores, para simular o condicionamento do ar inspirado e expirado por um ser humano hígido. Sua finalidade é servir de base para outros estudos que envolvam termoregulação e ventilação mecânica, sem a necessidade de experimentação inicial em animais.

Os materiais utilizados foram escolhidos segundo: a facilidade de aquisição, a facilidade de manuseio, o menor peso possível, o menor volume possível, a resistência, o custo, a capacidade de isolamento térmico, a capacidade de vedação e fixação e, em alguns casos, a transparência.

Cada um destes materiais apresenta um comportamento próprio quando se trata de troca térmica e este comportamento está diretamente relacionado com duas de suas características: o calor específico e a constante de difusão térmica (Ruiz, 1954). Visando contornar as complicações que estas características de cada material acarretariam ao experimento, minimizou-se a troca térmica que haveria pela parede destes materiais utilizando-se dois termostatos e dois aquecedores, um para o ar do sistema e outro para o ar da Caixa de Armazenamento, o que anulou quase totalmente o gradiente de temperatura entre os dois sistemas, minimizando em muito a troca de energia térmica entre eles.

A criação de um aparelho que simulasse um pulmão em termos de inspiração, expiração, pressão de gás, umidade relativa do gás, temperatura e volume de gás mostrou-nos que os valores de referência destes dados eram muito amplos e estavam relacionados com outros dados como: altura, peso, idade e sexo e que então era preciso construir um aparelho que fosse regulável conforme a necessidade do pesquisador. Para este trabalho, definiu-se que o padrão de referência seria um adulto jovem (25 anos) hígido de 80 kg com 1,88 m de altura do sexo masculino.

A idéia para regulagem de volume foi a criação de peças com um volume fixo e substituir em parte o seu volume de ar interno por outra matéria que permanece-se aprisionada nesta peça. Como a umidade era essencial no experimento, resolveu-se utilizar a água como meio redutor de volume de ar.

A regulagem de pressão foi feita baseada em duas válvulas e lastros de chumbo. As pressões que precisavam ser simuladas eram: pressão no início da expiração e no final da inspiração (Lastros de Chumbo); pressão no final da expiração e no início da inspiração (Válvula de PEEP); e pressão máxima admitida nas vias aéreas (Válvula de Segurança). As válvulas de pressão foram baseadas em sistemas de colunas de água devido à facilidade e ao menor custo.

Quanto à pressão no início da expiração e no final da inspiração, esta estava ligada diretamente à pressão dentro do Cilindro Principal, que dependia da pressão dentro do Fole. Calculou-se, baseado na área da tampa superior do Fole, o quanto de massa aplicada sobre ela seria necessário para gerar a pressão desejada dentro do sistema.

A temperatura do gás deveria ser mantida a 37,0+/-0,6ºC e, para isso, recorreu-se ao uso de termostatos eletrônicos específicos para aquários, que permitiam uma variação máxima de temperatura de 0,5ºC.

Neste experimento, havia a necessidade de sensores que monitorassem a temperatura rapidamente e com precisão, isto devido ao fato de que o ar dentro do sistema estava em movimento constante. Optou-se, então, pela utilização de termopares tipo T de cobre e constantan. Estes termopares têm como vantagens: ser pequenos (1 mm de diâmetro), responder rapidamente a pequenas alterações de temperatura e ter grande sensibilidade (Bahten, 2001).

Devido ao ar que entraria no sistema não ser saturado e ter uma temperatura menor de 37,0ºC, este ar, ao ser aquecido, absorveria água e isto constituiria um risco de diminuição nos níveis de calibragem do cilindro e das válvulas (Ruiz, 1954). Por isso, criou-se o Umidificador que saturaria este ar a 100% de umidade relativa quando da sua entrada no sistema. Apenas ao final do experimento é que se descobriu a eficiência do Umidificador, quando se constatou que não houve consumo da água nos outros compartimentos do aparelho.

A vedação térmica foi outro ponto importante no experimento, uma vez que o interior do aparelho deveria ser hermético e isolado termicamente. Durante o primeiro teste de vedação, vários pequenos vazamentos de ar e líquido foram identificados e prontamente corrigidos com cola de silicone.

A temperatura e a umidade relativa da sala de experiência não interferiram no experimento, visto que este consistia em um ambiente isolado termicamente.

Na calibragem do aparelho, foi utilizada a Capacidade Vital calculada pela fórmula de Baldwin, Cournand e Richards Jr. (Ratto,1997) visto que, apesar de o ideal ser a utilização da Capacidade Residual Funcional, esta não pode ser estimada por fórmulas.

Apesar de a Capacidade Vital ser maior do que a Capacidade Residual Funcional, isto não interferiu negativamente no experimento, pois a variável de interesse era o Volume Corrente. Aliás, o uso de um volume maior de ar dentro do Cilindro Principal possibilitou a maior diluição, dentro do sistema, do ar inspirado, assim como maior tempo de permanência deste e uma maior facilidade no seu condicionamento.

Os valores aferidos pelos manômetros nos mostraram que os cálculos dos Lastros de Pressão foram precisos, assim como o funcionamento da Válvula de PEEP.

Avaliando-se as temperaturas registradas pelos sensores durante todo o experimento, tem-se que o tempo de latência do aparelho (tempo da ativação até o equilíbrio térmico) foi de 3978 segundos e que a temperatura de saída do ar do sistema, que era o principal dado do experimento, foi de 37,3ºC.

5. CONCLUSÃO

Ao final deste estudo, conseguiu-se desenvolver um aparelho que pode simular o condicionamento do ar nos mesmos moldes que o aparelho respiratório normal condiciona. Este mesmo aparelho pode ainda simular o condicionamento pulmonar do ar de humanos com diferentes biotipos.

Espera-se que o sucesso obtido na criação deste aparelho possa servir como base e estímulo para outras pesquisas no campo da transferência de calor e massa no aparelho respiratório, visto que, conforme o tipo de estudo, ele pode facilitar o trabalho do pesquisador por dispensar a experimentação inicial em seres vivos.

6. BIBLIOGRAFIA

Bahten L. ; 2001, “Perda de calor determinada pela exposição das alças intestinais em ratos” [Doutorado]. Campinas: Universidade estadual de campinas.

Biem J, Koehncke N, Classen D, Dosman, 2003, “Out of the cold: management of hypothermia and frostbite”. Cmaj;168(3):305-11.

Cramer, II., 1957, “Heat and moisture exchange of respiratory mucous membrane”. Ann Otol Rhinol Laryngol;66(2):327-43.

Dery R. The evolution of heat and moisture in the respiratory tract during anaesthesia with a non-rebreathing system. Can Anaesth Soc J 1973; 20(3):296-309.

Goldberg ME, Epstein R, Rosenblum F, Larijani GE, Marr A, Lessin J, et al. Do heated humidifiers and heat and moisture exchangers prevent temperature drop during lower abdominal surgery? J Clin Anesth 1992;4(1):16-20.

Good AL, Sellers AF., 1957, “Temperature changes in the blood of the pulmonary artery and left atrium of dogs during exposure to extreme cold”. Am J Physiol;188(3):447-50.

Guyton A. Ventilação pulmonar. ; 1991, “In: Esbérard C, editor. Tratado de fisiologia médica”. 8 ed. Rio de Janeiro: Guanabara Koogan S.A.. p. 351-62.

Guyton A.; 1991, “Temperatura corporal, Regulação térmica e febre”. In: Esbérard C, editor. Tratado de fisiologia médica. 8 ed. Rio de Janeiro: Guanabara Koogan S.A.. p. 699-710.

Hanna LM, Scherer PW.,1986, “Regional control of local airway heat and water vapor losses”. J Appl Physiol;61(2):624-32.

Ingelstedt S., 1956, “Studies on the conditioning of air in the respiratory tract”. Acta Otolaryngol;56(Suppl 131):1-80.

LoCicero JIZ, J. B.; 2000, “Ventilatory support of postoperative surgical patients”. In: Shields TW, editor. General Thoracic Surgery. Philadelphia: Lippincott Williams and Wilkins. p. 517-34.

Margarido N.; 1997, “Ambiente cirurgico-sala cirúrgica”. In: Goffi F, editor. Técnica cirurgica: bases anatômicas, fisiopatológicas e técnicas da cirurgia. 4 ed. São Paulo: Editora Ateneu. p. 12-27.

Margarido N.; 1997, “Agressão cirurgica”. In: Goffi F, editor. Técnica cirurgica: bases anatômicas, fisiopatológicas e técnicas da cirurgia. 4 ed. São Paulo: Editora Ateneu. p. 92-9.

Mather GW, Nahas GG, Hemingway A., 1953, “Temperature changes of pulmonary blood during exposure to cold”. Am J Physiol; 173(3):390-2.

McFadden ER, Jr., Denison DM, Waller JF, Assoufi B, Peacock A, Sopwith T., 1982, “Direct recordings of the temperatures in the tracheobronchial tree in normal man”. J Clin Invest;69(3):700-5.

McFadden ER, Jr., 1983, “Respiratory heat and water exchange: physiological and clinical implications”. J Appl Physiol;54(2):331-6.

Morcom F., 2003, “Chill out: therapeutic hypothermia improves survival”. Emerg Nurse; 11(4):24-8.

Morris RH., 1971, “Influence of ambient temperature on patient temperature during intraabdominal surgery”. Ann Surg; 173(2):230-3.

Morris RH., 1971, “Operating room temperature and the anesthetized, paralyzed patient”. Arch Surg;102(2):95-7.

Prandini ML, SN; Valente, PR; Stavale, JN., 2002, “Regional mild hypothermia in the protection of the ischemic brain”. Acta Cirúrgica Brasileira;17(4):232-5.

Ratto OJ, JRB., 1997, "Diagnóstico funcional. In: Tarantino A, editor. Doenças pulmonares". 4 ed. Rio de Janeiro: Editora Guanabara Koogan S.A.;. p. 147-160.
Ruiz LAF.; 1954, "Curso de Termodinâmica.", 2 ed. Buenos Aires: Libreria Y editorial Alsina.
Schechter RJ., 1951, "Appropriate temperature control is essential in the operating room environment". Retina 1992;12(1):74-5.
Webb P. "Air temperatures in respiratory tracts of resing subjects in cold". J Appl Physiol;4(5):378-82.

MECHANICAL MODEL FOR SIMULATION OF LUNGS CONDITIONING OF THE BREATHED AIR

Dr. Nelson Bergonse Neto
Pontifícia Universidade Católica do Paraná – Rua Padre Agostinho, 227 (Ap. 11) – Mercês – Curitiba/PR – CEP: 80.410-020
e-mail: bergonsent@terra.com.br

Prof. Dr. Luís Mauro Moura
Pontifícia Universidade Católica do Paraná – Rua Imaculada Conceição, 1155 – Prado Velho – Curitiba/PR – CEP: 80.215-901
e-mail: Encit2006@pucpr.br

Prof. Dr. Luiz Carlos Von Bahten
Pontifícia Universidade Católica do Paraná – Rua Candido de Abreu, 140 (cj. 801-802) – Centro Cívico – Curitiba/PR – CEP: 80.530-901
e-mail: vonbahten@yahoo.com.br

Prof. Dr. Marlos de Souza Coelho
Pontifícia Universidade Católica do Paraná – Rua Comendador Franco, 2429 – Guabirotuba – Curitiba/PR – CEP: 81.520-000
e-mail: clinicadotorax@marloscoelho.com.br

Dr. Wilson de Souza Stori Junior
Pontifícia Universidade Católica do Paraná – Rua Batista Pessini, 654 (casa 01) – Vista Alegre – Curitiba/PR – CEP: 80.820-000
e-mail: wstori@uol.com.br

Dr. Gilberto da Fontoura Rey Bergonse
Hospital de Reabilitação de Anomalias Crânio-faciais – USP/SP – Rua Octavio Pinheiro Brisolla, 7-12 (ap. 62) – Vila Universitária – Bauru/SP – CEP: 17.012-059
e-mail: gilbertobergonse@ibest.com.br

Abstract
This research aimed at creating an mechanical model to condition the air being breathed in and out to normal temperature values (37.0+/-0.6ºC), pressure (0 to 20 cmH_2O) and relative humidity (100%) such as that of a healthy, 175-pound (80 kg), young (25 years) male under mechanical ventilation. Using several kinds of material such as plastic, metal, wood, glass and electronic components, a device was assembled, set to 5,000 ml of vital capacity, 800 ml of flow rate, maximum intake pressure of 20 cmH_2O, PEEP of 2 cmH_2O and internal system gas temperature of 37.0+/-0.6ºC. Mechanical ventilation was applied to the model with a flow rate of 800 ml, maximum intake pressure of 20 cmH_2O, intake respiratory rate of 40 l/min, PEEP of 2 cmH_2O, respiratory rate of 17 rpm, F_iO_2 of 0.21 and gas temperature equal to room temperature for a period of 29.8 minutes. The changes in the temperature of the air flowing in the system were recorded every two seconds. It was observed through statistical analysis that the device was effective in conditioning the air near human standards (37.3ºC temperature; 20 cmH_2O maximum pressure and 100% relative humidity approximately). At the end of this research a device that simulates the air conditioning in the same way that the repiratory tract does has been developed. This same device is still able to simulate the lungs air conditioning of different human biotypes becoming a useful tool in studies of thermodynamics and lung ventilation.

Keywords: Thermodynamics, Artificial Respiration, Hypothermia

Proceedings of the 11th Brazilian Congress of Thermal Sciences and Engineering -- ENCIT 2006
Braz. Soc. of Mechanical Sciences and Engineering -- ABCM, Curitiba, Brazil, Dec. 5-8, 2006

Paper CIT06-0343

SIMULAÇÃO NUMÉRICA DE PROCESSOS DE SOLIDIFICAÇÃO EM SISTEMAS BINÁRIOS APLICADOS À CRIOPRESERVAÇÃO DE CÉLULAS

Cristiano V. da Silva
Departamento de Engenharia Mecânica – Universidade Federal do Rio Grande do Sul – UFRGS.
Rua Sarmento Leite, 425, 90050-170 - Porto Alegre, RS, Brasil.
E-mail: cristiano@mecanica.ufrgs.br

Marcus V. A. Bianchi
Johns Manville Technical Center, Littleton, CO 80127 – USA.
E-mail: marcus_bianchi@yahoo.com

Resumo. *A preservação e o armazenamento de células e tecidos têm sido largamente utilizados em pesquisa científica e aplicações clínicas. A compreensão do processo de solidificação de soluções salinas é fundamental para o desenvolvimento de novos protocolos de criopreservação. No presente estudo, o congelamento de uma solução de cloreto de sódio a 1% em massa é simulado. As equações de conservação de massa, quantidade de movimento, energia, e espécies químicas foram discretizadas e resolvidas numericamente utilizando-se o Método dos Volumes Finitos para um domínio bidimensional que contém a parede da bolsa plástica e a solução salina. A perda de água da célula foi calculada a partir da história de temperatura e concentração durante o processo de solidificação e verificou-se que, dependendo da posição inicial da célula na bolsa, a célula tem probabilidades de sobrevivência diferentes durante o processo.*

Palavras chave*: Solidificação, Criopreservação, Método dos Volumes Finitos, Células, Desidratação.*

1. Introdução

Processos de solidificação são bastante estudados nas mais variadas áreas de pesquisa. Estes processos podem acontecer tanto artificialmente como naturalmente, e possuem uma grande variedade de aplicações. Na indústria siderúrgica, por exemplo, o processo de solidificação de metais é de fundamental importância, pois controla a qualidade e as características dos produtos. Além disso, uma série de processos naturais incluem solidificação, tais como a formação de icebergs, rochas vulcânicas, granizo entre outros.

A preservação e o armazenamento de células biológicas (hemáceas e espermatozóides, por exemplo) vêm sendo muito usados em pesquisa científica e clínica. No entanto há uma contradição entre o conceito de preservação e as conclusões de resultados experimentais, que mostram que materiais criopreservados podem ser danificados durante o próprio processo de preservação. Quando as células são resfriadas a aproximadamente –5 °C, tanto a célula quanto o material extracelular permanecem líquidos e super resfriados. Entre –5 °C e –15 °C gelo se forma fora da célula, mas seu interior permanece super resfriado, provavelmente porque a membrana da célula bloqueia o crescimento de cristais de gelo no citoplasma (Lunardini, 1981). A água super resfriada no interior da célula tem, por definição, um potencial químico maior do que o da água na solução extracelular parcialmente congelada: assim a água que difunde da célula osmoticamente congela externamente à mesma. O que acontece depois depende da taxa de resfriamento da célula. Se a célula é resfriada muito rapidamente, a água intracelular não difunde tão rapidamente para o meio externo de forma a manter o equilíbrio; a célula se torna cada vez mais super resfriada e, eventualmente, gelo intracelular se forma ocasionando a morte da célula. Se por outro lado a célula é resfriada muito lentamente, a contração (devida à desidratação) e a exposição da célula por longo período de tempo a altas concentrações de eletrólitos (devidas à precipitação de gelo externo) antes que a concentração eutética seja atingida também pode danificar a célula (Mazur, 1984).

A maioria dos trabalhos disponíveis em processos de solidificação aplicados em criopreservação de tecidos, assumem a existência de uma taxa de resfriamento constante incidindo sobre as células, não resolvendo o processo de solidificação da solução, de modo que a validação da modelagem proposta para este trabalho se torna difícil. Entretanto, a validação para a fluido dinâmica e de transferência de calor do processo foi realizada através da simulação de casos bem conhecidos na literatura, obtendo-se bons resultados. A validação da modelagem de solidificação foi feita através da simulação de um caso semelhante ao resolvido por Bianchi e Viskanta (1994), também obtendo boa concordância. Viskanta et al. (1997) mostraram que mesmo considerando uma taxa de resfriamento constante externa à bolsa, a taxa de resfriamento local não é a mesma para todo o domínio, e que células em diferentes posições na bolsa sofrem diferentes variações de volume celular. Os autores apresentaram uma simulação de processos de solidificação de uma solução de cloreto de sódio em água a 1 % em massa, colocados em uma bolsa plástica de parede plana. Com a obtenção dos resultados de temperatura e concentração de sal, utilizam o modelo desenvolvido por Mazur (1963) para calcular a cinética de transporte de água predizendo o comportamento do volume celular. A resolução deste problema

foi feita sobre um domínio unidirecional, incluindo a bolsa, desprezando efeitos de convecção natural para diferentes taxas de resfriamento.

Diversos trabalhos desenvolveram modelos de perda de água das células a baixas temperaturas (Mazur, 1963; Mazur, 1990; Toner et al., 1990; Karlsson e Toner, 1996). Mazur and Koshimoto (2002) apresentam um estudo numérico sobre a cinética da perda de água em espermatozoides de ratos quando estes sofrem um processo de resfriamento com taxas de 250ºC/min a 2000ºC/mim. Neste estudo eles obtiveram curvas de variação de volume celular de uma célula isolada, e submetida a variações de concentração e temperatura prescritas, não resolvendo o processo de solidificação da solução salina. Estas curvas, juntamente com dados experimentais, estimam a temperatura na qual ocorre o início da nucleação de cristais de gelo no interior de células super resfriadas, que por sua vez fornecem dados estatísticos para o início da formação destes cristais como uma função das taxas de resfriamento. Estes dados foram comparados com dados experimentais obtidos a partir de taxas de resfriamento onde sabidamente ocorre a formação de gelo intracelular e apresentaram boa concordância.

Low et al. (2003) realizaram a simulação numérica do processo de resfriamento de uma liga ternária contendo água, cloreto de sódio, agente crioprotetor e células em suspensão, no interior de uma bolsa plástica. O modelo "continuum" foi considerado. A história de temperaturas durante a mudança de fase, a perda de água intracelular e a variação volumétrica das células em diferentes posições são calculadas. Os resultados deste trabalho mostram que mesmo com taxas constantes de resfriamento impostas sobre a parede da bolsa, os células no interior da bolsa em diferentes posições sofrem diferentes taxas de resfriamento, confirmando o que foi dito por Viskanta et al. (1997). As maiores taxas de resfriamento ocorrem em regiões mais internas da bolsa, de modo que a variação do volume celular é dependente da posição na bolsa. Neste trabalho não foi resolvido o campo de concentrações no interior da bolsa.

Em outro trabalho, Mazur et al. (2005-a) realizaram um estudo experimental sobre as causas da formação de gelo intracelular em óvulos de ratos e de sapos, quando estes são submetidos a processos de criopreservação, relacionados à temperatura na qual este gelo começa a se formar. Dando continuação a este trabalho, Mazur et al. (2005-b) apresentaram um estudo experimental sobre o processo de criopreservação de óvulos de ratos em suspensão numa solução salina contendo 1 %e 1,5 % em massa de crioprotetor (etileno glicol). A solução é submetida a uma taxa de resfriamento de -50ºC/min até atingir a temperatura de –70ºC no final do processo. Eles verificaram que a temperatura na qual ocorre a formação de cristais de gelo extratracelular, quando a solução é submetida a estas taxas de resfriamento, é dependente da concentração do crioprotetor. Além disso eles também verificaram que o início e fim da formação destes cristais ocorre em diferentes intervalos de tempo quando diferentes concentrações de crioprotetor são usadas. Nestes trabalhos não foram resolvidos os campos de temperaturas e de concentrações. Uma célula isolada foi analisada, não sendo resolvido o processo de solidificação da solução. Também foi considerado que a taxa de resfriamento imposta na parede da bolsa é a mesma que incide sobre as células dentro da solução.

O presente trabalho tem o objetivo de simular processos de solidificação de soluções salinas para um domínio bidimensional resolvendo as equações de energia, espécies químicas e quantidade de movimento. Os resultados obtidos são aplicados em processos de criopreservação de células, enfocando o problema que surge devido ao fluxo de soluto que ocorre através da membrana celular durante o resfriamento. Não é considerada a formação de gelo intracelular.

2. Formulação do modelo

Assumindo coordenadas cartesianas, as equações do modelo "continuum" de mistura compostas pelas equações de conservação de massa, de quantidade de movimento nas direções horizontal (x) e vertical (y), conservação de energia e de espécies químicas para um sistema de mudança de fase foram previamente desenvolvidas por Bennon e Incropera (1987) e, nestas coordenadas podem ser expressas da seguinte forma:

2.1. Conservação de massa

$$\frac{D}{Dt}\left(\rho_l\right) = 0 \tag{1}$$

onde ρ_l é a densidade da fase líquida, t é o tempo e D é a derivada material da densidade.

2.2. Conservação da quantidade de movimento

Para a direção horizontal,

$$\rho_l \frac{D\vec{V}}{Dt} = \vec{\nabla}\cdot\left(\mu_l \vec{\nabla} u\right) - \frac{\mu_l}{K_x}\left(u\right) - \frac{\partial P}{\partial x} \tag{2}$$

onde μ_l é a viscosidade da fase líquida, K_x é a permeabilidade na região bifásica ("mushy region") na sua respectiva direção, P é a pressão, $\vec{\nabla}$ é o operador vetorial, x é a coordenada espacial na direção horizontal e u é a velocidade nesta direção.

Para a direção vertical

$$\rho_l \frac{D\vec{V}}{Dt} = \vec{\nabla}\cdot\left(\mu_l \vec{\nabla} v\right) - \frac{\mu_l}{K_y}(v) - \frac{\partial P}{\partial y} - \rho g\left[\beta_T\left(T - T_{in}\right) + \beta_S\left(C_l - C_{in}\right)\right] \tag{3}$$

onde T_{in} e C_{in} são a temperatura e concentração inicial, $\vec{V}$ é o vetor velocidade, T é a própria temperatura, C_l é a concentração de sal no líquido e C a concentração de mistura. β_T e β_S são os coeficientes de expansão térmica e de concentração de soluto, respectivamente. Aqui a permeabilidade da "mushy region" na direção vertical é definida por K_y, y é a coordenada espacial na direção vertical e v é a velocidade nesta direção.

2.3. Conservação de energia

$$\begin{aligned}\rho_l c_\alpha \frac{DT}{Dt} = {} & \vec{\nabla}\cdot\left(\kappa_{ef}\vec{\nabla}T\right) - \vec{\nabla}\cdot\left[\varepsilon_l\rho_l\left(c_l - c_\alpha\right)\vec{V}T\right] - \vec{\nabla}\cdot\left[\varepsilon_e\rho_l\left(c_e - c_\alpha\right)\vec{V}T\right] - \vec{\nabla}\cdot\left[\varepsilon_\alpha\rho_l\left(h_l - h_\alpha\right)\left(\vec{V} - \vec{V}_\alpha\right)\right] \\ & - \rho_l\Delta h_{l\to\alpha}\frac{\partial\varepsilon_l}{\partial t} - \rho_l\Delta h_{e\to\alpha}\frac{\partial\varepsilon_e}{\partial t} - \frac{\partial}{\partial t}\left[\varepsilon_l\rho_l\left(c_l - c_\alpha\right)T\right] - \frac{\partial}{\partial t}\left[\varepsilon_e\rho_l\left(c_e - c_\alpha\right)T\right]\end{aligned} \tag{4}$$

onde c é o calor específico, ε é a fração volumétrica, h é a entalpia, $\Delta h_{l\to\alpha}$ é a variação de entalpia do líquido para o sólido primário α e $\Delta h_{e\to\alpha}$ é a variação de entalpia do sólido eutético para o sólido primário (α). A condutividade térmica da mistura é definida como κ_{ef}. Os subíndices l, α e e representam as fases líquida, e sólidas alpha-α e eutética.

2.4. Conservação de espécies químicas

$$\rho_l c_\alpha \frac{DT}{Dt} = \vec{\nabla}\cdot\left(\varepsilon_l\rho_l D_l\vec{\nabla}C\right) - \vec{\nabla}\cdot\left[\varepsilon_l\rho_l D_l\left(C_l - C\right)\right] - \vec{\nabla}\cdot\left[\varepsilon_\alpha\rho_l\left(C_l - C_\alpha\right)\left(\vec{V} - \vec{V}_\alpha\right)\right] \tag{5}$$

onde D_l é a difusividade do sal no líquido.

A permeabilidade da "*mushy region*" que aparece nas equações de momento em x e y são baseadas na equação de Kozeny-Carman (Asai e Muchi, 1978).

Considerações inerentes ao modelo de equações apresentado acima: (i) propriedades termofísicas de cada fase constantes, (ii) escoamento laminar, (iii) comportamento newtoniano da fase líquida, (iv) escoamento na região bifásica seguindo a lei de Darcy, (v) permeabilidade isotrópica, (vi) aproximação de Boussinesq para o termo de empuxo, (vii) equilíbrio termodinâmico local, (viii) condutividade térmica efetiva calculada pelo modelo de resistências em paralelo, (ix) difusão de espécies desprezível na fase sólida, (x) coeficiente de partição da mistura igual a zero, (xi) densidade constante e igual a do líquido para evitar problemas de dilatação e contração durante o processo de solidificação. A condição de equilíbrio termodinâmico local permite o uso do diagrama de fase para fornecer a mistura e composições das fases, enquanto que a consideração de densidade constante durante o congelamento implica em desprezar efeitos de deformação das fases.

A equação da cinética da perda de água sofrida pelas células no resfriamento foi derivada em função da temperatura e da concentração do meio, e está defina da seguinte forma (Mazur, 1990):

$$\frac{d\mathrm{V}}{dt} = L_p A\overline{R}T\left[\left(1 - C_{l,i}\right) - \left(1 - C_{e,i}\right)\right] \tag{6}$$

onde a concentração de soluto intracelular $C_{l,i}$ pode ser considerada constante para cada tipo de célula, e a concentração de soluto extracelular $C_{e,i}$ é conseqüência dos fenômenos físicos que ocorrem no meio externo. No presente trabalho esta concentração é determinada pelo processo de solidificação. Na equação acima a variável A representa a área superficial de uma célula esférica, $\overline{R}$ é a constante molar dos gases ideais, V é o volume de água intracelular, e L_p a permeabilidade hidráulica da membrana celular que é definida como:

$$L_P = L_P^g \exp\left[\frac{-E^*}{\bar{R}}\left(\frac{1}{T}-\frac{1}{T_g}\right)\right] \tag{7}$$

onde L_p^g é o coeficiente de permeabilidade hidráulica na temperatura de referência T_g, e E^* é a energia de ativação da penetração de água.

As equações diferenciais referentes ao modelo de mistura são discretizadas através do Método dos Volumes Finitos (Patankar, 1980). Deste modo as equações de conservação de espécies e de energia são acopladas com o modelo de mudança de fase (Bianchi, 1997), e a equação de energia acoplada também com as equações de quantidade de movimento, através dos termos de empuxo. A resolução do algoritmo para os valores nodais das frações volumétricas também necessita ser desenvolvida. Os valores dos fatores de relaxações usados na resolução das equações de energia, espécies e quantidade de movimento foram de 0,5, 0,7, e 0,5 respectivamente. Foi utilizado um coeficiente de subrelaxação para a correção da pressão de 0,8. O sistema de equações algébricas em volumes finitos obtido pelo procedimento de discretização foi resolvido usando o TDMA – "Tri-Diagonal Matrix Algorithm", linha por linha, fazendo ainda uso da técnica de correção em bloco (Patankar, 1980; Maliska, 2003). O acoplamento pressão-velocidade foi resolvido pelo algoritmo SIMPLE – "*Semi-Implicit Metod for Pressure Linked Equations*" também apresentado por Patankar (1980). A discretização dos termos de fonte da equação de conservação de espécies químicas foi baseada no trabalho de Prakash e Voller (1989). Já para as equações de energia e quantidade de movimento os termos de fonte foram discretizados em diferenças finitas, segundo Patankar (1980).

Para a resolução deste problema, após realizados testes de independência de malha, utilizou-se uma malha 100 volumes na direção horizontal por 90 volumes na direção vertical. O problema é resolvido de forma transiente, e os resultados de temperatura, velocidade, e concentração de espécies químicas são usados para o cálculo da cinética da perda de água das células através da Eq. (6). Esta equação foi resolvida através de integração utilizando-se a Regra do Trapézio (Hoffman, 1992).

Considera-se uma bolsa plástica retangular, na qual se encontra uma solução de cloreto de sódio em água, contendo células em suspensão. A fim de preservar as células presentes na solução, a bolsa é resfriada externamente com uma taxa de resfriamento controlada. O processo de solidificação se inicia, desprezando-se efeitos de não-equilíbrio, e eventualmente toda a solução já completamente solidificada, incluindo as células presentes na bolsa, atingem temperaturas baixas o suficiente para que virtualmente não haja reações químicas.

O foco do presente trabalho é o processo de solidificação e as conseqüências deste na sobrevivência das células. O problema então é, dada a geometria da bolsa, calcular a distribuição de temperaturas e de concentrações, e também campo de velocidades para se saber a posição das células a cada instante, para poder determinar a taxa de perda de água das células, e com isso o nível de sobrevivência das mesmas dentro da bolsa. Então idealiza-se a bolsa plástica, onde estão depositadas as células, como sendo uma cavidade bidimensional simétrica na direção horizontal, de largura $2X_L$ e altura Y_L,como está mostrado na Fig. 1. e_L é a espessura da bolsa plástica.

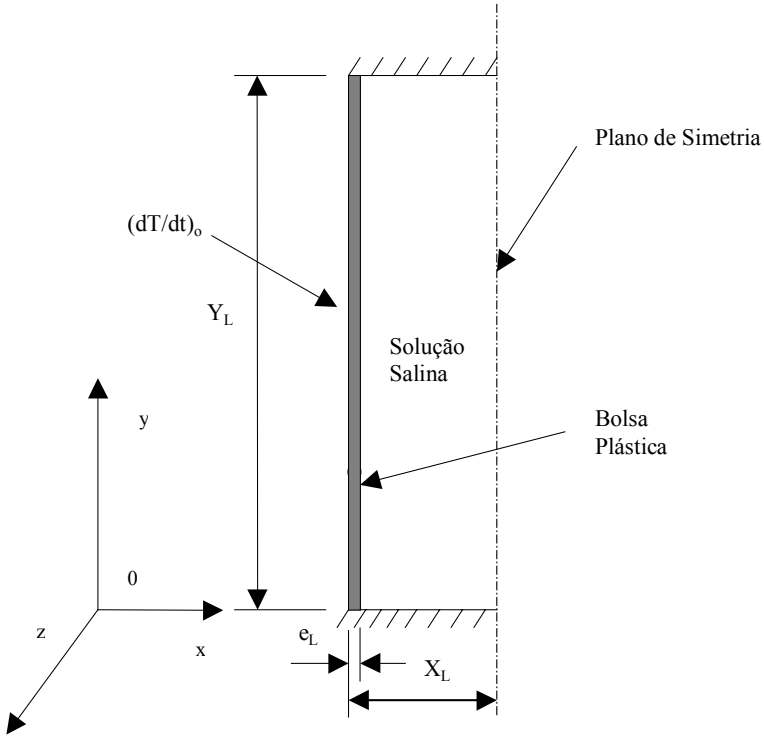

Figure 1. Bolsa plástica utilizada no processo de resfriamento (Meio domínio, contendo parede da bolsa).

As simulações foram desenvolvidas para dois casos, em ambos considerando-se a simetria do problema. Para estes dois casos a concentração de sal da solução é de 1% em massa. Para o caso I utiliza-se uma taxa de resfriamento constante de –10ºC/min aplicada sobre a parede externa da bolsa, sendo a temperatura da solução salina igual a 2ºC. Para o caso II utiliza-se a mesma taxa de resfriamento constante de -10ºC/min aplicada sobre a bolsa, sendo a temperatura da solução salina alterada para 20ºC.

As propriedades termofísicas de soluções salinas, e demais grandezas usadas na resolução do problema foram retiradas de várias fontes (Bianchi e Viskanta, 1994; Mazur, 1963; Gebhart at al., 1988; Zaytsev e Aseyev, 1992), e estão compiladas nas Tabs. 1 e 2.

Tabela 1. Propriedades termofísicas das fases sólida, líquida e eutética.

Propriedades	Fase líquida (l)	Fase Sólida (α)	Fase Sólida (Eutética - e)
c [kJ/kgK]	3911	1945	1690
ρ [kg/m^3]	1007	1530	1530
k [W/mK]	0,562	2,285	1,910
D [m^2/s]	1,611x10^{-9}	-	-
μ [Pa/s]	1,814x10^{-3}	-	-

Tabela 2. Propriedades termofísicas e grandezas usadas na resolução do problema.

Propriedades	Magnitude	Propriedades	Magnitude
X_L [m]	9,5x10^{-3}	$\Delta h_{l\to\alpha}$ [J/kg]	333,7x10^2
Y_L [m]	0,1	$\Delta h_{e\to\alpha}$ [J/kg]	333,4x10^2
e_L [m]	5x10^{-4}	k_{eff} [W/m K]	62,9
β_T [1/K]	1,968x10^{-5}	$\overline{R}$ [μm^3 Pa/mol K]	83,144x10^{-5}
β_S [-]	7,968x10^{-3}	A [μm^2]	3,04
K_0 [m^2]	5x10^{-11}	E^* [J/mol]	58,61
g [m/s^2]	9,81	V [μm^3]	2,775
T_{eut} [ºC]	-21,1	L_p^g [μm/s Pa]	1,095x10^{-7}
T_{in} [ºC]	2 ou 20	T_g [K]	273,15
C_{eut} [%]	23,3	C_{in} [%]	1

3. Resultados

Para todos os casos é de fundamental importância verificar o posicionamento das células a cada instante de tempo, pois uma determinada célula pode percorrer um determinado caminho dentro da bolsa, e outra célula um caminho diferente, e com isso passar por histórias de temperaturas e concentrações também diferentes e terem logicamente, níveis de desidratação diferenciados.

A Fig. 2 mostra qualitativamente a situação para o tempo de solidificação de 250 segundos. Note que neste momento já existe fase eutética precipitada, uma vez que a linha "solidus" já percorreu parte do domínio, como pode ser visto na Fig. 2-d. Como a fase líquida, fora da região bifásica, tem uma espessura muito reduzida, as velocidades começam a ficar menores devido a presença da "mushy region". É possível verificar que a recirculação envolve a "mushy region", que tem uma permeabilidade menor, de forma a também diminuir a magnitude das velocidades. Como seria de esperar, o problema é unidirecional, ou seja, as linhas "liquidus" e "solidus" são planas. Embora a temperatura da parede –23ºC já seja inferior à temperatura do eutético -21,1ºC, a espessura de plástico funciona como um isolante térmico, causando um forte gradiente de temperatura no polietileno. É possível notar que na maior parte do domínio as velocidades são verticais, de forma que a linha "liquidus" se mantém plana, como pode ser visto na Fig. 2-d. Apenas próximo às paredes horizontais há componentes não verticais da velocidade. As isotermas e as isoconcentrações são verticais e acopladas entre si, uma vez que a difusividade de espécies químicas é pequena se comparada à difusividade térmica.

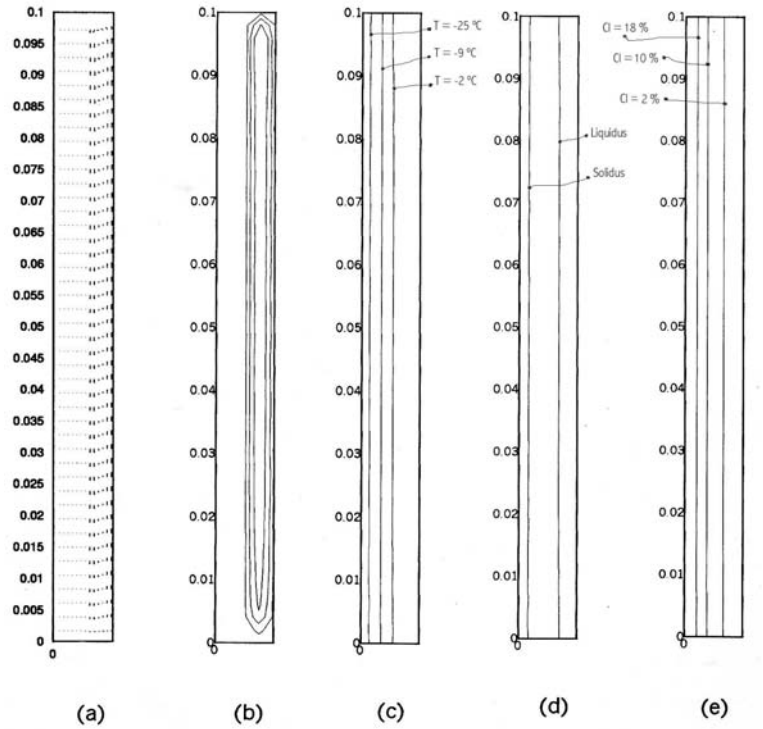

Figura 2 - Comportamento do processo de solidificação em t = 250 s para o caso I: (a) Vetores velocidade, (b) Função de corrente, (c) Isotermas, (d) Posição da região bifásica, (e) Isoconcentrações.

A Fig. 3 mostra qualitativamente o comportamento do processo de solidificação para o tempo de 150 segundos.

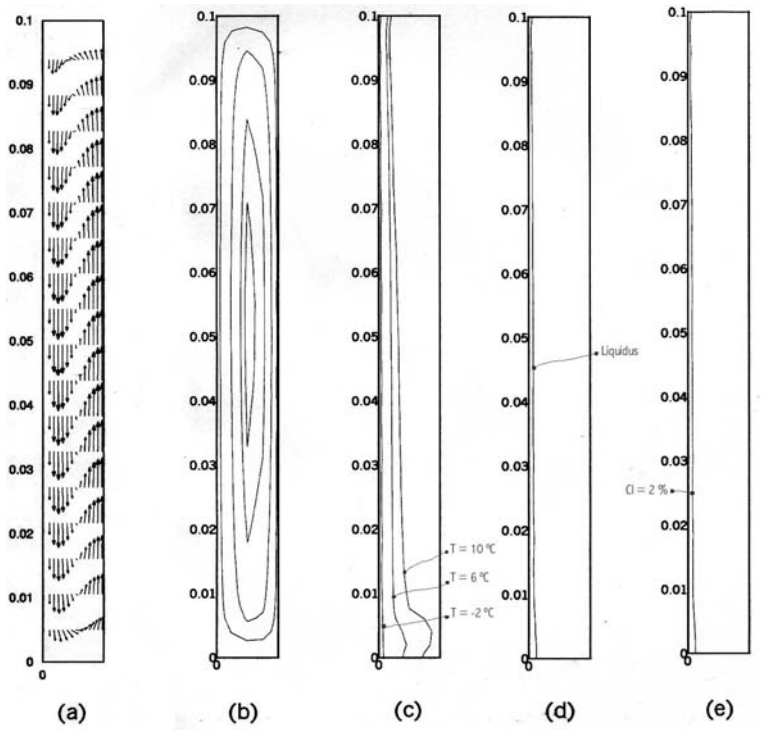

Figura 3 - Comportamento do processo de solidificação em t = 150 s para o caso II: (a) Vetores velocidade, (b) Função de corrente, (c) Isotermas, (d) Posição da região bifásica, (e) Isoconcentrações.

Embora pareçam verticais na maior parte do domínio, as velocidades junto ao polietileno tem um componente horizontal na direção positiva de u . Observe também que os perfis de velocidade são diferentes dependendo da altura no domínio (Fig. 3-a). Como a advecção se torna importante devido à maior diferença de temperatura, note que para

este caso começam a aparecer deformações nas isotermas e linha "liquidus" (Fig. 3-c, e Fig. 3-d). A inclinação que aparece nestas figuras, é resultado da ação dos termos de empuxo. Devido à interação de líquido mais quente com a região bifásica no alto do domínio, a espessura desta região é menor naquela localidade do que seria se não houvesse escoamento. Note que na Fig. 3-c as duas isotermas mais à direita estão ainda na região líquida, uma vez que a temperatura "liquidus" é de -0,63ºC. É evidente, então, que há um resfriamento local nesta região devido ao escoamento que vem da região bifásica, que se encontra mais fria do que o líquido. É possível verificar que este mesmo escoamento altera o perfil de concentrações na Fig. 3-d.

As Figs. 4-a e 4-b mostram as trajetórias de algumas células depositadas na bolsa para os casos I e II, respectivamente, com referência à posição vertical inicial y/Y_L = 0,32. Pode-se observar que existe uma variação considerável da posição das células na direção y a partir da posição inicial. Já na direção x tem-se para a célula (42,30) que eqüivale as posições adimensionais (x/X_L = 0,18; y/Y_L = 0,31) um deslocamento quase despercebido com relação à variação de deslocamento na direção y, enquanto que para as demais células analisadas nesta figura não existe variação de posicionamento no sentido horizontal da bolsa. Note que as células (22,30), (42,30) e (62,30) que possuem posições adimensionais (0,18;0,31), (0,38;0,31), e (0,59;0,31), respectivamente, possuem uma trajetória descendente, enquanto que a célula (82,30) que eqüivale a (0,79;0,31) possui uma trajetória inversa. As células mais distantes da parede fria têm um movimento ascendente, enquanto as mais próximas têm um movimento descendente na maior parte do tempo de solidificação. No caso II pode-se melhor verificar a influência da convecção natural no processo de resfriamento.

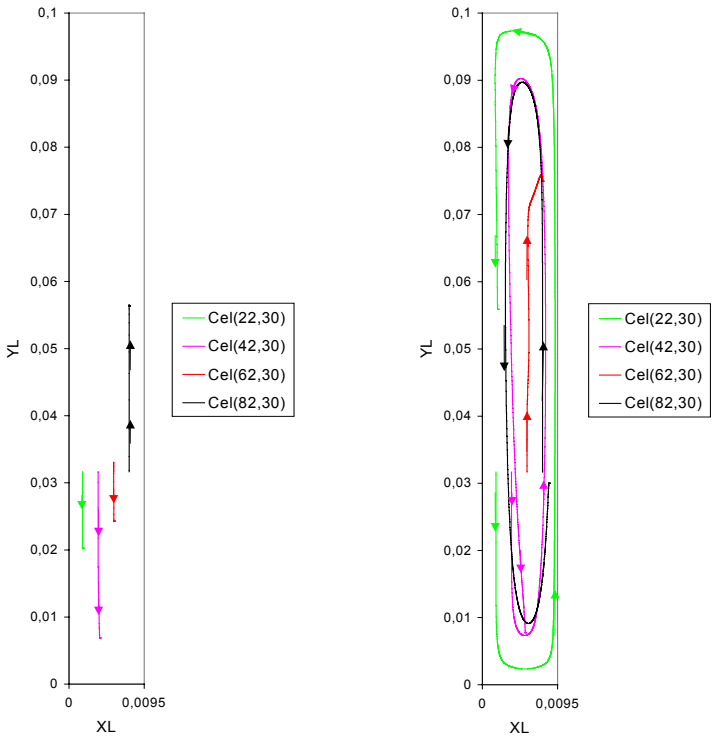

Figura 4 - Trajetória das células sobre o domínio durante o processo de resfriamento referente à posição inicial y/Y_L = 0,32: (a) Caso I, (b) Caso II.

Como um resultado final do processo de criopreservação de células pode-se observar nas Figs. 5-a e 5-b como foi o comportamento geral das células em relação a variação do volume intracelular devido a perda de água sofrida durante o processo para os casos I e II, respectivamente. Esta figura apresenta o volume final das células com relação à posição inicial destas células. Pode-se verificar na Fig. 5-a que a variação de volume celular não é homogênea para as diferentes posições iniciais das células. É possível notar que para valores de y/Y_L entre 0,2 e 0,7, as variações no perfil de variação de volume são muito pequenas, como se mostrou na Fig. 5-a. Por outro lado, fora deste intervalo vertical, nas partes inferiores e superiores a ele há diferenças maiores. É para estas células que os efeitos de advecção causada pela convecção natural são mais significativos. Na parte inferior, as células tendem a passar mais tempo por regiões de baixa

concentração de sal, uma vez que elas acompanham o escoamento, primeiramente mais horizontal até fazer o contorno e subir ao longo do eixo de simetria. Esta região demora mais a solidificar. Assim, as perdas de água são menores, como pode ser visto pela maior região de tonalidade vermelha. Na parte superior, por outro lado, acontece o oposto, uma vez que as células que ali se encontram percorrem o domínio na direção da frente de solidificação. Como ali as concentrações são maiores, há uma maior perda de água, ocasionando na maior diminuição de volume, como pode ser constatado pela região mais azulada no alto à esquerda.

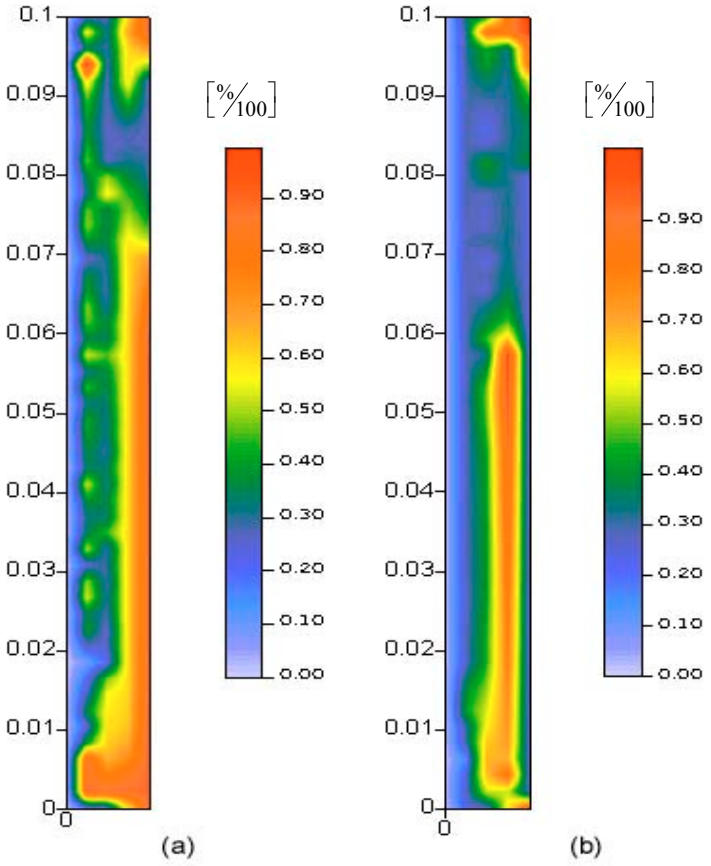

Figura 5 - Variação de volume celular dentro da bolsa, relacionadas as suas posições iniciais, ao final do processo de resfriamento: (a) Para o caso I, (b) Para o caso II.

Na Figura 5-b está ilustrada a variação do volume celular para o caso II na posição inicial das células na bolsa. Embora haja semelhanças com a figura correspondente do caso I (Fig. 5-a), há diferenças evidentes. Note primeiramente a região vermelha completamente envolvida por regiões onde a variação de volume foi maior, que se estende entre $0< y/Y_L <0{,}6$. Este volume de líquido teve uma variação de concentrações menor do que o restante do domínio, de forma que as taxas de perda de água foram consequentemente menores. Uma outra região na parte superior direita da bolsa também apresenta menores taxas de perda de água.

4. Conclusões

Baseado nas investigações do processo de solidificação, as seguintes conclusões podem ser apresentadas:

1. Para uma temperatura inicial de 2ºC e taxa de resfriamento considerada, -10ºC/min, os efeitos das forças de empuxo são praticamente inexistentes e o problema pode ser considerado como unidirecional.
2. A distribuição de concentração também é afetada pela taxa de resfriamento, pois esta é fortemente dependente da temperatura. Quanto se tem um menor gradiente de temperatura, tem-se uma maior região ocupada com solução salina de concentração diferente e maior que a inicial.
3. As forças de empuxo passam a ter alguma influência nas distribuições de temperatura e concentração quando a temperatura inicial é elevada para 20ºC. Neste caso, as linhas "liquidus" e "solidus" deixam de ser verticais e há um acúmulo de líquido frio com maior concentração de sal na parte inferior do domínio. Uma solução considerando o domínio unidimensional levaria a resultados questionáveis.

O problema de encolhimento por desidratação (crenação), que acontece devido ao fluxo de água através da membrana celular durante o processo de criopreservação de células foi estudado neste trabalho para os dois casos previamente descritos.

Baseado nos resultados obtidos pode-se escrever as seguintes conclusões:

1- Mesmo quando a advecção é desprezível, a variação do volume celular não é a mesma para todas as posições da bolsa. A taxa de resfriamento local varia para cada posição e é diferente da taxa de resfriamento imposta sobre a parede externa da bolsa seja constante.
2- Quanto maior for a taxa de resfriamento menor é a variação do volume celular, e pode-se dizer que maior é o nível de sobrevivência das células na bolsa. Para ambos os casos as células mais ao centro da bolsa obtiveram uma menor perda de água.
3- Quando a advecção é importante, o escoamento leva as células a regiões com diferentes temperaturas e concentrações. Assim, a perda de água da célula depende fortemente da posição inicial da célula no domínio.

5. Referências

Asai, S. e I. Muchi (1978), Theoretical analysis and model experiments on the formation mechanism of channel-type segregation, Transactions ISIJ 18, pp.90–98.

Bennon, W. D. e F. P. Incropera (1987), A continuum model for momentum, heat and species transport in binary solid-liquid phase change systems - I. model formulation, International Journal of Heat and Mass Transfer 30, pp. 2161–2170.

Bianchi, M. V. A. (1997), Crystal Morphology and Gas Evolution during Solidification Processes, PhD thesis, Purdue University, West Lafayette, Indiana.

Bianchi, M. V. A. e R. Viskanta (1994), On the morphology of ice crystals grown from ammonium chloride solutions, in Proceedings of the ASME International Mechanical Engineering Congress and Exposition, Vol. HTD 284, ASME, New York, pp. 323–331.

Gebhart, B., Y. Jaluria, R. L. Mahajan e B. Sammakia (1988), Buoyancy-Induced Flows and Transport, Hemisphere, Washington.

Hoffman, J. D. (1992), Numerical methods for engineers and scientists, McGraw-Hill, Inc.

Karlsson, J. O. M. e M. Toner (1996), Long-term storage of tissues by cryopreservation: critical issues, Biomaterials 17 (3), pp. 243–256.

Low, D. W., L. Q. He, S. X. Cheng, J. P. Yu, e D.Y. Gao (2003). A numerical Study of cell behaviour in a ternary solution during the freezing process. *Cryoletters* 24 (3), pp. 161-170**.**

Lunardini, V. J. (1981), Heat Transfer in Cold Climates, Liton, New York.

Maliska, C. R. (2003), Transferência de Calor e Mecânica dos Fluidos Computacional, 2nd ed, Livros Técnicos e Científicos Editora S.A., Rio de Janeiro, Brasil.

Mazur, P. (1963), Kinetics of water loss from cells at subzero temperatures and the likelihood of intracellular freezing, J. Gen. Physiol. 47, pp. 347–369.

Mazur, P. (1984), Freezing of living cells: Mechanisms and implications', Cell Biophysics 17, 53–92.

Mazur, P. (1990), Equilibrium, quasi-equilibrium, and non-equilibrium freezing of mammalian embryos, Am. J. Physiology. 16, pp.125–142.

Mazur, P. e C. Koshimoto (2002). Is Intracellular Ice Formation the Cause of Death of Mouse Sperm Frozen at High Cooling Rates? Biology of Reproduction, 66, pp. 1485–1490.

Mazur, P., S. Shinsuke, L. P. Irina, F.W. Kleinhans e E. Keisuke (2005-a). Extra- and intracellular ice formation in mouse oocytes. *Crypbiology* 51, pp. 29-53.

Mazur, P., L. P. Irina, S. Shinsuke, F.W. Kleinhans e E. Keisuke (2005-b). Effects of hold time after extracellular ice formation on intracellular freezing of mouse oocytes. *Crypbiology* 51, pp. 235-239.

Patankar, S. V. (1980), Numerical Heat Transfer and Fluid Flow, Hemisphere, New York.

Prakash, C. e V. Voller (1989), On the numerical solution of continuum mixture model equations describing binary solid-liquid phase change, Numerical Heat Transfer 15, pp. 171–189.

Toner, M., E. G. Cravalho e M. Karel (1990), Thermodynamics and kinetics of intracellular ice formation during freezing of biological cells', J. Appl. Phys. 67(3), pp. 1582–1593.

Viskanta, R., M. V. A. Bianchi, J. K. Critser e D. Gao (1997), Solidification processes of solutions, Cryobiology 34, pp. 348–362.

Zaytsev, I. D. e G. G. Aseyev, (1992), Properties of Aqueous Solutions of Electrolytes, CRC Press, Boca Raton.

NUMERICAL SIMULATION OF THE SOLIDIFICATION OF BINARY SOLUTIONS APPLIED TO CRYOPRESERVATION OF BIOLOGICAL MATERIAL

Cristiano V. da Silva
Department of Mechanical Engineering – UFRGS. Rua Sarmento Leite, 425, 90050-170
Porto Alegre, RS, Brazil.
E-mail: cristiano@mecanica.ufrgs.br

Marcus V. A. Bianchi
Johns Manville Technical Center, Littleton, CO 80127 – USA.
E-mail: marcus_bianchi@yahoo.com

Abstract. Cryopreservation and banking of biological cells and tissue have been widely utilized in scientific research and clinical applications. Understanding of the solidification process of salt solutions is crucial to develop successful cryopreservation protocols. In the present study, freezing of a sodium chloride solution (1%) in a flat bag is simulated. Mass, momentum, energy, and species conservation equations were numerically solved using the Control Volume Method in a two-dimensional domain. Then, using the temperature and salt concentration data calculated, the kinetics of water loss from a model cell is predicted. The results show that, depending on the initial position of the cell in the bag, the history of water loss varies, and so does the cell preservation.

Keywords: Solidification, Cryopreservation, Control Volume Method, Cell, Mushy Region.

Paper CIT06-0473

MEDIÇÃO DA DIFUSIVIDADE TÉRMICA DA DENTINA HUMANA UTILIZANDO O MÉTODO DO FLASH DE LASER

Manoelita Figueiredo de Magalhães
Departamento de Engenharia Mecânica da Universidade Federal de Minas Gerais – DEMEC-UFMG
Avenida Antônio Carlos, 6627 - Campus Pampulha
CEP: 31270-901 - Belo Horizonte – MG - Brasil
Fone: (31) 3499-5145 – Fax: (31) 3443- 3783
manoelita@uai.com.br

Ricardo Alberto Neto Ferreira
Centro de Desenvolvimento da Tecnologia Nuclear – CDTN-CNEN
Cidade Universitária, Pampulha
CEP: 30123-970 - Belo Horizonte - Minas Gerais - Brasil
Fone: (31) 3499-3150 – Fax: (31) 3499- 33390
ranf@cdtn.br

Pablo Andrade Grossi
Centro de Desenvolvimento da Tecnologia Nuclear – CDTN-CNEN
Cidade Universitária, Pampulha
CEP: 30123-970 - Belo Horizonte - Minas Gerais - Brasil
Fone: (31) 3499-3248 – Fax: (31) 3499- 3311
pabloag@cdtn.br

Roberto Márcio de Andrade
Departamento de Engenharia Mecânica da Universidade Federal de Minas Gerais – DEMEC-UFMG
Avenida Antônio Carlos, 6627 - Campus Pampulha
CEP: 31270-901 - Belo Horizonte – MG - Brasil
Fone: (31) 3499-5145 - Fax: (31) 3443 3783
roberto@demec.ufmg.br

Resumo: *Atualmente, a remoção do tecido cariado em Odontologia pode ser realizada tanto com instrumentos rotatórios (brocas convencionais) como por meio do laser em alta intensidade. Ambos os processos provocam aquecimento da estrutura dental podendo exercer um efeito altamente nocivo sobre a polpa viva. É necessário prevenir estes efeitos térmicos quando se prepara ou irradia tecidos duros, evitando danos indesejáveis aos tecidos adjacentes. Torna-se de fundamental importância conhecer o comportamento da variação de temperatura produzida durante os processos de tratamento dentário que produzem calor. Uma revisão na literatura, a respeito de medições das propriedades termofísicas da dentina humana, revelou uma grande dispersão nos valores obtidos pelos diferentes autores. Em nenhum destes trabalhos se fez medição direta de difusividade térmica da dentina humana, mas os valores reportados são valores apenas calculados a partir de dados de medições de condutividade, densidade e calor específico. O objetivo deste trabalho foi realizar no CDTN medições de difusividade térmica na dentina humana através do método do flash de laser. Os valores de difusividade térmica de cinco amostras de dentina humana, medidos através deste método, situaram-se entre*
0,199x10^{-6}m^2/s e 0,265x10^{-6}m^2/s, muito próximos dos valores calculados por Braden (1964) e por Brown, Dewey, Jacobs (1970).

Palavras chaves: dentina humana, difusividade térmica, medição, método flash laser.

1. Introdução

Os diversos recursos utilizados para o tratamento e diagnóstico no tratamento dentário interagem com os tecidos biológicos e podem provocar efeitos térmicos altamente nocivos com graves conseqüências.

Zach e Cohen (1965) realizaram um estudo sobre a resposta pulpar à aplicação externa de calor e avaliaram histologicamente as respostas pulpares a várias técnicas operatórias a fim de se estabelecerem padrões de segurança. A produção de calor foi a principal responsável pelas alterações pulpares quando os dentes foram preparados. Os resultados dos estudos demonstraram que as polpas saudáveis não se recuperaram de um aumento de temperatura acima de 5,5°C. O acúmulo de evidências que indicam que a polpa dental é um tecido mais sensível do que anteriormente se acreditava contribuiu para a expansão, particularmente na década passada, de técnicas operatórias e de instrumentação. Os resultados deste estudo indicaram que polpas saudáveis, no mínimo nas espécies testadas, não se recuperaram de um aumento de temperatura intrapulpar de 20°F (-6,6°C) em cerca de 60% dos casos. Quinze por cento dos dentes aquecidos a 10°F não se recuperaram. Aumentos de temperatura, abaixo deste nível crítico, produziram reações severas relacionadas com o grau de calor - quase invariavelmente levaram à recuperação da polpa, mas deixaram seqüelas histológicas. Aumentos de temperatura acima de 20°F quase invariavelmente destruíram a polpa. De acordo com este

estudo, a temperatura pulpar não deve ultrapassar 5,5ºC para não danificar a polpa, órgão responsável pela vitalidade dental, daí a importância em se ter o controle de temperatura durante os procedimentos que provocam calor na realização do tratamento dentário (por exemplo, o uso de brocas de alta rotação ou de laser em alta intensidade para preparo cavitário ou remoção de tecido cariado do dente), a fim de se manter a temperatura pulpar abaixo deste valor crítico citado.

Para explicar esta interação entre os tecidos biológicos e os processos físicos é necessária uma abordagem multidisciplinar com a integração de áreas distintas como a Engenharia e a Odontologia no conhecimento das propriedades termofísicas do dente.

A difusividade térmica é a propriedade que diz quão rápido um material pode transmitir calor. É diretamente proporcional à condutividade térmica, e inversamente proporcional à densidade e ao calor específico do material, conforme a Eq. (1) a seguir:

$$\alpha = \frac{k}{\rho c_p} \qquad \text{Eq. (1)}$$

onde:
α = difusividade térmica (m^2/s),
k = condutividade térmica (W/m.K),
ρ = densidade (Kg/m^3),
c_p = calor específico (J/kg.K).

A difusividade térmica mede a relação entre a capacidade de o material conduzir energia térmica e a sua capacidade em acumular energia térmica. Os materiais com α grande respondem rapidamente às variações do ambiente térmico, enquanto materiais com α pequeno respondem mais lentamente, e levam mais tempo para atingir novas condições de equilíbrio (Incropera e DeWitt, 1992).

Um importante agente injuriante à polpa é o preparo cavitário, que exerce elevada agressão sobre a polpa dentária, sendo o calor o responsável pela injúria mais severa. Fatores representativos desta injúria estão associados à extensão do preparo cavitário e à sua profundidade. Atualmente, com o surgimento dos equipamentos de laser para uso odontológico, além dos preparos de cavidades em dente utilizando-se brocas, pode-se usar também lasers em alta intensidade para ablação do tecido dental. Existem vários estudos mostrando a interação dos lasers com a dentina e procurando determinar parâmetros seguros para uso clínico, devido à preocupação em impedir que o calor provocado durante o processo ablativo danifique a polpa.

A interação térmica com o tecido a ser tratado é uma conseqüência inevitável quando se aplica o laser. Por conseguinte, a temperatura que se desenvolve na polpa é um fator muito importante quando se procura avaliar a indicação do laser no tratamento de dente vitalizado (Gutknecht e Eduardo, 2004).

Zezell *et al.* (1996) usaram o laser de Ho:YLF para estudar as alterações de temperatura dental "*in vitro"*. Um protótipo de laser Ho:YLF emitindo em 2,065μm; 1,25J; com largura de pulso de 250μs foi desenvolvido para aplicações biomédicas. As alterações de temperatura foram medidas com a energia de 500mJ/pulso, 30pulsos na mesma posição com densidade de energia de $2079J/cm^2$/ pulso. Dois grupos de dentes foram usados; o grupo I com câmara pulpar vazia e o grupo II com a câmara pulpar preenchida com pasta térmica. Em ambos os casos, não houve aumento de temperatura acima de 3,8°C.

Os autores relataram, ainda, que a incidência da luz laser, com alta densidade de energia, aumenta a temperatura na área do foco e sua vizinhança. É desejável minimizar o fluxo de calor para diminuir as injúrias térmicas, fornecendo energia suficiente em menos tempo que a difusão do calor pelos tecidos por condução (a relaxação térmica é inversamente proporcional ao quadrado do volume irradiado). Os tecidos duros dentais são pobres condutores de calor, isto é, agem como verdadeiros isolantes (Brown, Dewey e Jacobs, 1970; Sagi *et al.*, 1992). O aumento de temperatura na polpa é diretamente proporcional à quantidade de energia aplicada e, conseqüentemente, o tempo de exposição é de fundamental importância. Altas densidades de energia em curtos períodos de tempo causam menos danos à polpa. Jeffrey *et al.* (1990a, b), White *et al.* (1991) e Paghdiwala, Vaidyanathan e Padhdiwala (1993) afirmaram que a espessura de dentina deve ser considerada e que dentes com menor remanescente de dentina apresentaram maior elevação de temperatura.

Zezell *et al.* (1996) relataram, também, que o aumento de temperatura esperado *"in vivo*" pode ser menor que nas experiências "*in vitro*", devido ao tecido mole que contorna o dente e ao fluxo de sangue através do tecido pulpar nos dentes.

Para estimar o dano pulpar, o aumento de temperatura decorrente da radiação laser precisa ser mensurado. Assim, usando termopares e imagem térmica, Hibst e Keller (1990) observaram o efeito térmico de um único pulso do laser de Er:YAG que é pequeno e limitado às vizinhanças do impacto. A energia e o calor são adicionados a cada pulso adicional. A distribuição de temperatura depende não somente da energia radiante, como também do número de pulsos e da taxa de repetição. As condições de irradiação podem provocar danos irreversíveis à polpa direta ou indiretamente. As observações experimentais podem ser explicadas qualitativamente por um simples processo de ablação. As

temperaturas foram maiores para ablacionar esmalte do que para a remoção de dentina e não somente o fundo da cratera se aquece, mas também a área total da parede das crateras. A temperatura aumenta com o aumento da energia radiante e com o aumento da taxa de repetição dos pulsos. A escolha apropriada dos parâmetros laser, como a energia radiante, a taxa de repetição e o perfil do feixe, pode evitar danos mesmo quando focalizado diretamente na polpa.

De acordo com o estudo de Lizarelli (2000) sobre lasers de Nd:YAG nos regimes de nano e picossegundos em esmalte e em dentina, vários experimentos têm demonstrado que pulsos ultracurtos no domínio de subpicossegundos promovem uma combinação de efeitos termomecânicos que superam algumas das objeções ao uso de um laser como instrumento removedor. Usando os parâmetros apropriados de operação, lasers com pulsos ultracurtos podem se comportar melhor do que instrumentos convencionais, incluindo alguns dos lasers pulsados comercialmente já disponíveis na Odontologia. A exploração e otimização nos parâmetros dos lasers disponíveis podem promover a remoção de certas objeções ao amplo uso dos lasers. O uso de lasers de pulsos ultracurtos para ablação de tecido dentário previne o superaquecimento e é uma alternativa para a remoção mecânica de material, além de minimizar o volume deste material removido.

Torna-se de fundamental importância conhecer o comportamento da variação de temperatura produzida durante os processos de tratamento ou de preparo cavitário do dente que produzem calor. A literatura apresenta uma grande dispersão de resultados das propriedades termofísicas da dentina humana entre as diversas técnicas pesquisadas, e a maioria dos trabalhos não é recente, tendo sido realizados anteriormente ao uso clínico do laser em Odontologia, que nos dias atuais é usado em diferentes comprimentos de onda. Também não foram encontrados estudos reportando medições de difusividade térmica em dentina através do método do flash de laser que é o método de referência do INMETRO.

O presente estudo teve por objetivo medir a difusividade térmica de dentina humana através do método do flash de laser e comparar com os resultados obtidos por outros autores através de outros métodos, enriquecendo a escassa literatura existente, e preenchendo uma lacuna, já que não se encontrou na literatura resultados de medições diretas de difusividade térmica de dentina humana, mas apenas valores calculados. Com estes resultados será possível avaliar melhor a coerência entre os procedimentos clínicos que provocam calor e o comportamento biológico, de forma a prevenir resultados danosos ao dente, tornando-os menos empíricos. As medições foram realizadas no Laboratório de Medição de Propriedades Termofísicas de Combustíveis Nucleares e Materiais do CDTN.

2. Revisão da Literatura

Para a análise da transferência de calor é necessário usar muitas propriedades dos materiais denominadas propriedades termofísicas que incluem duas categorias distintas: as propriedades de transporte e as propriedades termodinâmicas. As propriedades de transporte incluem os coeficientes da taxa de difusão, como k, a condutividade térmica (no caso da transferência de calor), e ν, a viscosidade cinemática (no caso da transferência de momento). Por outro lado, as propriedades termodinâmicas referem-se a estados de equilíbrio do sistema. A densidade (ρ) e o calor específico (c_p) são duas destas propriedades que se usam extensamente na análise termodinâmica (Incropera e DeWitt, 1992). A seguir são apresentados alguns dos trabalhos encontrados na literatura sobre medições de propriedades físicas, como densidade (massa específica), e térmicas, como condutividade, calor específico e difusividade térmica de dentes humanos.

Manly, Hodge e Ange (1939) verificaram que há uma variação considerável nos valores reportados na literatura para a densidade dos tecidos dentais duros, e não encontraram nenhum trabalho a respeito da distribuição da densidade nos tecidos. Mediram a densidade de dentina humana encontrando um valor médio de 2 140 Kg/m^3.

Lisanti e Zander (1950) iniciaram os primeiros estudos sobre a condutividade térmica da dentina e afirmaram não terem encontrado, anteriormente a esta data, referências na literatura sobre este assunto uma vez que os procedimentos, até então utilizados, necessitavam de amostras muito maiores que o tamanho de um dente humano. O valor médio encontrado por estes autores para a condutividade térmica da dentina humana foi 0,959 W/m.K.

Simeral (1951) mediu a condutividade térmica de dentina humana encontrando um valor de 0,984 W/m.K, bem próximo do valor de 0,959 W/m.K encontrado por Lisanti e Zander (1950).

Phillips, Johnson e Phillips (1956) encontraram para a condutividade térmica da dentina humana um valor de 0,108 W/m.K que é cerca de 10 vezes menor que os valores encontrados por Lisanti e Zander (1950) e Simeral (1951), respectivamente 0,959 W/m.K e 0,984 W/m.K.

Peyton e Simeral (1954) obtiveram um valor de 1172 J/Kg.K para o calor específico da dentina humana.

Soyenkoff e Okun (1958) procuraram desenvolver um método simples e rápido para medir a condutividade térmica de tecidos dentais, similar ao método usado por Lisanti e Zander (1950) e por Phillips, Johnson e Phillips (1956), mas usando pequenos termistores fornecidos pela Werstern Electric Company ao invés de termopares, evitando as complicações causadas pela apreciável capacidade térmica dos fios e perdas térmicas em amostras de pequeno tamanho devidas ao diâmetro relativamente grande dos termopares. Encontraram 0,402 W/m.K para uma amostra de dentina da raiz e 0,448 W/m.K para uma amostra de dentina da coroa, e além disso com um erro estimado em 20%.

Craig e Peyton (1961) utilizaram um equipamento semelhante ao utilizado por Lisanti e Zander (1950) e obtiveram os seguintes valores médios para a condutividade térmica de dentina humana: 0,582 W/m.K para fluxo de calor na direção perpendicular aos túbulos e 0,569 W/m.K na direção paralela, e afirmaram que estes dados mostram

que a direção dos túbulos não influencia a condutividade térmica da dentina. Estes autores também comentam sobre discrepâncias de até 10 vezes entre os valores reportados na literatura.

Braden (1964) realizou um experimento para medir a condução de calor em dentes humanos hígidos. Aplicou um estímulo térmico no dente e analisou teoricamente a mudança de temperatura nele, quando o estímulo de temperatura constante era aplicado sobre toda a superfície oclusal. Utilizando os valores de condutividade térmica, calor específico e de densidade encontrados na literatura, calculou curvas teóricas e as comparou com os seus resultados experimentais. Como houve uma boa concordância entre os seus resultados experimentais e as curvas teóricas, calculou a difusividade térmica a partir destes valores encontrados na literatura encontrando para a dentina humana uma difusividade térmica de 0,260 x 10^{-6} m^2/s.

Brown, Dewey e Jacobs (1970) mediram a densidade e o calor específico de dentina humana e, a partir dos valores de condutividade térmica medidos por Craig e Peyton (1961), nas direções perpendicular e paralela aos túbulos dentinários, calcularam os respectivos valores para a difusividade térmica encontrando os seguintes valores: 0,187 x 10^{-6} m^2/s (direção perpendicular), e 0,183 x 10^{-6} m^2/s (direção paralela). Também comentam sobre a inconsistência entre os dados de densidade, condutividade térmica, calor específico e difusividade térmica encontrados na literatura.

A Tab. 1 sintetiza os resultados encontrados na literatura a respeito de propriedades termofísicas de dentina humana. Os valores originais, apresentados no sistema c.g.s, foram convertidos para o sistema MKS. Em nenhum destes trabalhos encontrados na literatura foi feita uma medida direta da difusividade térmica de dentina humana. Os valores de difusividade apresentados nestes trabalhos são valores calculados a partir de valores medidos de condutividade, densidade e calor específico de dentina humana.

Tabela 1. Propriedades termofísicas da dentina humana.

Autor(es)	Densidade (Kg/m^3)	Calor específico (J/Kg.K}	Condutividade térmica (W/m.K)	Difusividade térmica ($x10^6 m^2/s$)
Manly, Hodge e Ange (1939)	2 140	-	-	-
Lisanti e Zander (1950)	-	-	0,959	-
Simeral (1951)	-	-	0,984	-
Phillips, Johnson e Phillips (1956)	-	-	0,108	-
Peyton e Simeral (1954)	-	1 172	-	-
Soyenkoff e Okun (1958)	- -	- -	0,402 (raiz //) 0,448 (coroa //)	- -
Craig e Peyton (1961)	- -	- -	0,582 ⊥ * 0,569 // **	- -
Braden (1964)	-	-	-	0,260
Brown, Dewey e Jacobs (1970)	1 960	1 591	- -	0,187 ⊥ * 0,183 // **

* fluxo de calor perpendicular aos túbulos dentinários.
** fluxo de calor paralelo aos túbulos dentinários.

3. Metodologia

3.1 Preparo das amostras de dentina

Esta pesquisa foi submetida ao Comitê de Ética em Pesquisa da UFMG para aprovação, por haver necessidade de se utilizar dentes humanos extraídos, tendo sido aprovado pelo parecer número 454/05.

As amostras foram preparadas em terceiros molares extraídos de pacientes de ambos os gêneros, na faixa etária de 18 a 26 anos. Estes dentes tiveram extração indicada, devido à impossibilidade de erupção por falta de espaço (dentes inclusos) e foram cedidos pelo Instituto de Previdência dos Servidores do Estado de Minas Gerais. Estes dentes foram lavados e mantidos em soro fisiológico até a realização dos ensaios, para não sofrerem desidratação e se aproximar da condição fisiológica, onde, na boca, os dentes ficam hidratados pela saliva. Selecionou-se molares com coroas mais volumosas e com menores câmaras pulpares com o objetivo de confeccionar discos inteiramente em dentina, tendo 8mm de diâmetro e 2 a 3mm de espessura. Desgastou-se as incisais dos dentes até a remoção total da camada de esmalte incisal, para expor toda a dentina e também obter uma superfície plana para posicioná-los adequadamente na base da fôrma de embutimento. Embutiu-se todos os dentes assim preparados utilizando-se a resina acrílica Durofix-2 transparente de cura a frio da firma Struers®. Após o tempo de cura de 24 horas, foram feitas marcas com caneta de retro-projetor nos blocos com os dentes embutidos, no nível do teto da câmara pulpar, para orientar os cortes a serem feitos e obter amostras cilíndricas com superfície plana e regular e toda em dentina. Utilizando-se uma serra de disco adiamantado, foram feitos cortes para se retirar fatias de dentina com 2 a 3mm de espessura. Algumas fatias foram cortadas no sentido axial do dente, para se ter amostras em que o fluxo de calor durante o ensaio ocorra aproximadamente na direção perpendicular à direção dos túbulos dentinários. Outras foram cortadas paralelamente à

superfície plana de dentina já isenta de esmalte, para se ter amostras em que o fluxo de calor ocorra paralelamente à direção dos túbulos. A finalidade destes dois tipos de amostras objetivou verificar se a direção dos túbulos dentinários influencia nos resultados das medições. Este procedimento de preparo das amostras foi realizado no Laboratório de Metalografia do Departamento de Engenharia Metalúrgica da UFMG.

Como a amostra necessita ser cilíndrica e com um diâmetro de 8mm, que é o diâmetro do porta-amostra e do feixe de laser de CO_2 utilizado nas medições, a camada externa das amostras foi removida para obter-se amostras cilíndricas e com este diâmetro. Inicialmente, utilizou-se uma serra copo (trefina) de 8mm de diâmetro, mas este procedimento foi logo abandonado porque a serra copo perdia o corte com muita facilidade. Optou-se, então, por desgastar a camada externa das amostras em baixa rotação com esmeril de uso odontológico de carbeto de silício da firma Carborundum, até obter-se a forma circular com 8mm de diâmetro. O diâmetro dos discos foi medido com um paquímetro com resolução de 0,05mm, e a espessura com um micrômetro com resolução de 0,001mm. As amostras foram colocadas individualmente em frascos numerados, preenchidos com soro fisiológico, para não desidratarem, aproximando-se da situação existente "*in vivo"* até a realização do experimento.

3.2 Método do flash de laser

O método do flash para medir as propriedades térmicas de materiais sólidos foi proposto em 1960 por Parker *et al.* (1961) do U.S. Navy Radiological Defense Laboratory. Eles mediram a difusividade térmica de metais usando uma lâmpada de flash a xenônio. Posteriormente, Deem e Wood (1962) utilizaram um laser a rubi no lugar do flash de xenônio e demonstraram sua adequabilidade como fonte de energia.

Na técnica original, um flash intenso e curto de energia radiante é aplicado uniformemente sobre a face de uma amostra homogênea com a forma de um disco (geralmente do tamanho de uma pequena moeda), durante um período de tempo desprezível, e o pulso de calor difunde unidirecionalmente para a face oposta, obtendo-se um registro do histórico de temperatura resultante nesta face oposta, através de um termopar ou de um sensor infravermelho (Fig. 1).

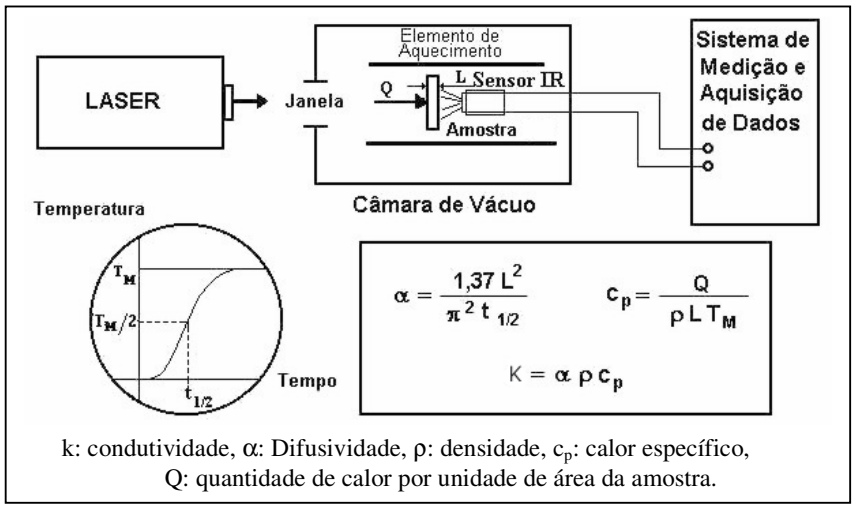

Figura 1 – Princípio do método do flash de laser para medição de propriedades termofísicas de materiais
Fonte: Ferreira, R. A. N. *et al.*, 2002.

A fonte de energia radiante é usualmente um laser ou uma lâmpada de flash de xenônio e os tempos de irradiação são da ordem de um milisegundo ou menos. A difusividade é calculada a partir da espessura L da amostra e do tempo requerido para a temperatura da face oposta atingir um dado percentual do seu valor máximo (usualmente o tempo chamado $t_{1/2}$ correspondente a 50% da excursão). O calor específico c_p é calculado a partir da densidade ρ e da espessura L da amostra, da temperatura máxima T_M atingida na sua face oposta, e da quantidade Q de calor entregue a ela. A condutividade térmica k é então calculada pelo produto da difusividade a pelo calor específico c_p e pela sua densidade ρ ($k = \alpha.\rho.c_p$). Um método de adimensionalização do histórico de temperatura resultante na face oposta pode ser aplicado, de modo que a curva experimental de aumento da temperatura possa ser comparada com a curva teórica e assim desvios em relação às condições ideais podem ser facilmente detectados.

Desde então o método flash laser vem sendo cada vez mais reconhecido como sendo uma poderosa ferramenta para medições de propriedades térmicas dos mais diversos materiais, já que este método apresenta muitas vantagens, tais como:

a. curto tempo requerido para as medições;
b. efeito relativamente pequeno de perda de calor pela amostra;

c. requer amostras de pequeno tamanho;
d. com um único método mede-se tanto a difusividade térmica quanto o calor específico da amostra.

O método tem sido estendido a fluxo bidimensional de calor de modo que amostras grandes podem ser medidas e as difusividades em ambas as direções, axial e radial, em materiais anisotrópicos podem ser obtidas. Tem sido usado para medir materiais cujas difusividades térmicas variam de $0{,}1 \times 10^{-6}$ a $1\,000 \times 10^{-6}$ m^2/s (uma faixa de 10^4) e a temperaturas entre de 80 e 3.000 K, utilizando amostras pequenas e facilmente fabricáveis e os resultados podem ser obtidos em segundos (Taylor, 1978). Tem sido empregado para medir a difusividade térmica de materiais e combustíveis nucleares, metais, ligas, cerâmicos, semicondutores, compósitos, metais líquidos, fibras de carbono, materiais reforçados com fibras, camadas individuais ou compósitos em camadas, condutância de contato térmico em interfaces, e compósitos dispersos, além das medições mais rotineiras (Taylor, 1978).

Tem sido demonstrado que, usando-se um sistema de aquisição de dados, e modelos matemáticos adequados a situações em que as condições experimentais reais não correspondam exatamente às condições de contorno idealizadas na teoria do método, pode-se reduzir os erros de medição abaixo de 0,5% (Taylor, 1978).

Ferreira *et al.* (2002) apresentaram de forma detalhada a aplicação da técnica flash laser no Laboratório de Medições de Propriedades Termofísicas (LMPT) do Centro de Desenvolvimento da Tecnologia Nuclear (CDTN), onde foram realizadas as medições deste trabalho. Grossi (2003) realizou uma análise dos principais problemas encontrados durante as medições experimentais. Grossi, Ferreira e Andrade (2005a, b) propuseram uma metodologia de análise das incertezas dinâmicas associadas a este sistema de medição. Uma solução da equação de difusão térmica, utilizando técnicas de formulação em volumes de controle foi apresentada por Grossi *et al.* (2002). Um novo modelo físico-matemático foi proposto por Grossi (2003) e Grossi, Ferreira e Andrade (2004) utilizando algoritmos de otimização por mínimos quadrados com o objetivo de obter a solução inversa do problema de difusão térmica aplicado ao método flash laser. A utilização do modelo físico-matemático permite incorporar todas as fontes de erro o que torna possível a minimização das incertezas do resultado de medição das propriedades termofísicas.

4. Resultados de medições de difusividade térmica de dentina humana através do método do flash de laser

A Tab. 2 apresenta os resultados de medições de difusidade térmica através do método do flash de laser realizadas em cinco amostras cilíndricas com 8mm de diâmetro. Foram feitas um total de dez medições em cada amostra. O cálculo da incerteza expandida das medições de difusividade térmica utilizou um intervalo de confiança (IC) de 95% e um fator de abrangência k.=.2,325. O valor máximo de incerteza nas medições foi de ±1,92%.

Tabela 2. Resultados de medições de difusividade térmica de dentina humana através do método do flash de laser.

Número da amostra	Direção do fluxo de calor em relação aos túbulos dentinários	Espessura da amostra (mm)	Difusividade térmica média ($x10^6 m^2/s$)	Desvio padrão ($x10^6 m^2/s$)	Incerteza expandida (IC 95%)
1	//	2,270	0,204	0,005	1,50%
2	⊥	1,950	0,199	0,006	1,92%
3	//	2,970	0,256	0,006	1,69%
4	//	2,421	0,224	0,004	1,30%
5	//	2,935	0,265	0,005	1,45%

A Fig. 2 apresenta um resultado típico de medição de difusividade térmica de dentina humana, e a Fig. 3 um gráfico dos resultados de difusividade térmica em função da temperatura efetiva.

PROTOCOLO
MEDIÇÃO DE PROPRIEDADES TERMOFÍSICAS
MÉTODO DO FLASH DE LASER

Número do Ensaio: AA387
Data: 13/04/2006

Dados da Amostra

Material: Dentina Amostra nº 2 (Perpendicular)	Densidade: - Kg/m^3
Espessura: 0,001950 m	Diâmetro: 0,008 m

Clientes: Diversos
Finalidade: Medição de Difusividade Térmica de Dentina Humana.

Dados do Ensaio	
Temperatura Ambiente ($T_{amb.}$):	23,88 °C
Temperatura Inicial da Amostra (T_i):	23,86 °C
Temperatura Final da Amostra (T_M):	27,91 °C
Temperatura Média ($T_M/2$):	25,89 °C
Temperatura Efetiva (T_{ef}):	30,34 °C
Tempo de meia excursão ($t_{1/2}$):	2,6050 s
Difusividade Térmica (α):	$0{,}203 \times 10^{-6}$ m²/s

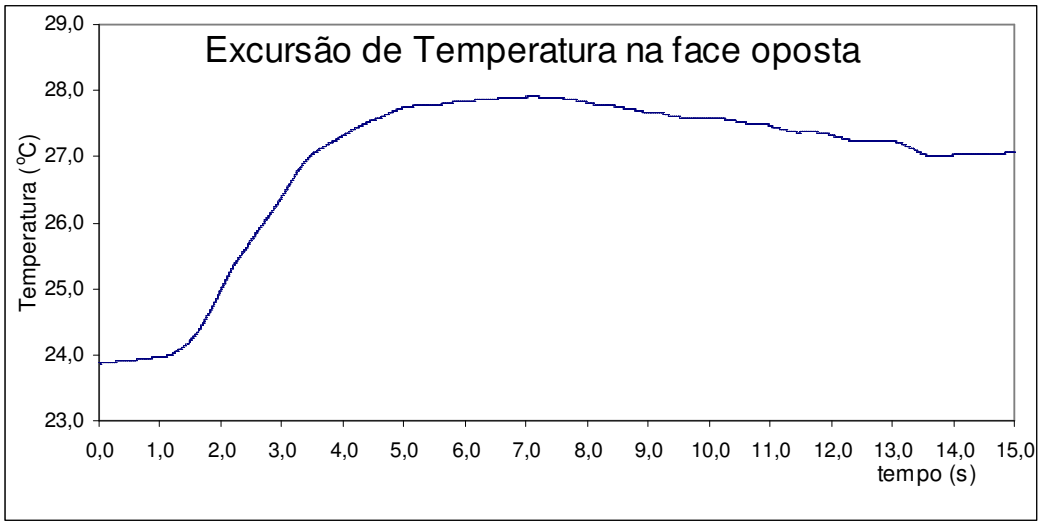

Figura 2. Registro típico de uma medição de difusividade térmica de dentina humana através do método do flash de laser.

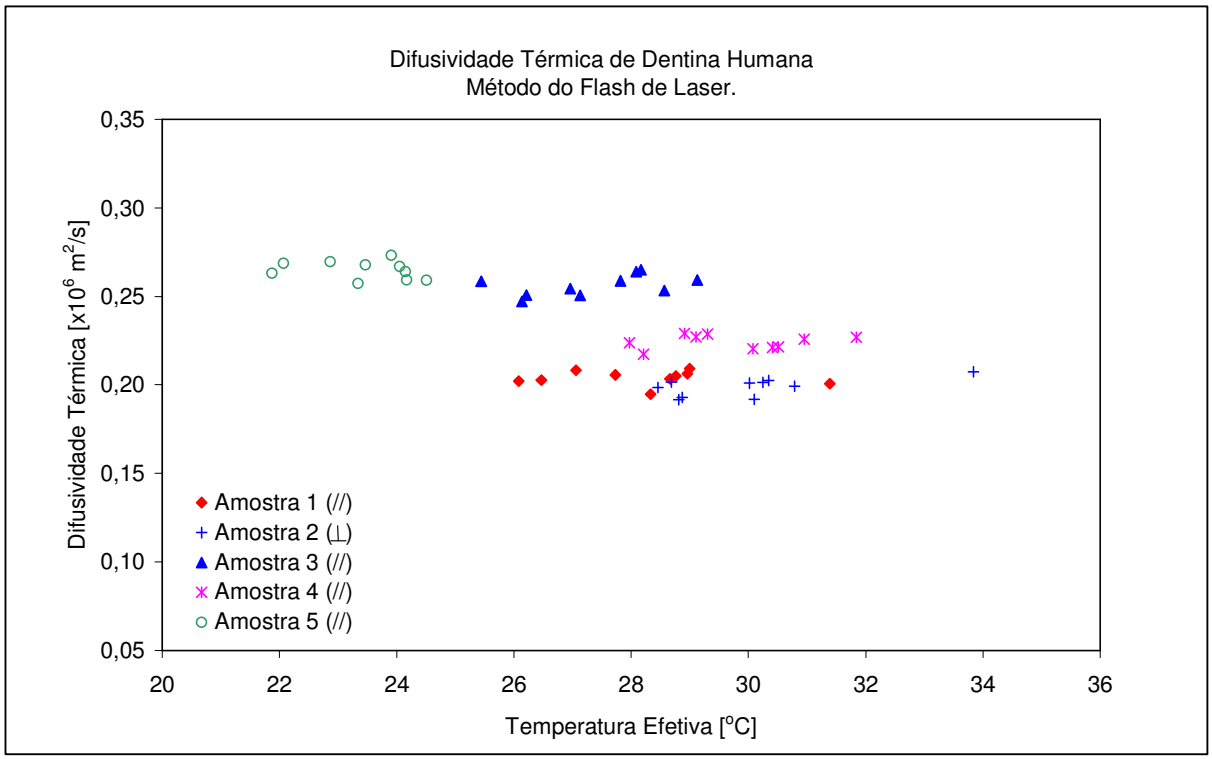

Figura 3. Difusividade térmica de dentina humana em função da temperatura efetiva.

Calculou-se valores para a condutividade térmica empregando-se a equação (1), os valores de difusividade térmica medidos no presente trabalho, e os valores de densidade e calor específico obtidos por Manly, Hodge e Ange (1939) e Peyton e Simeral (1954), respectivamente, obtendo-se os valores abaixo:

Amostra 1 (//): k = 0,204 .$10^{-6}$$m^2$/s . 2140 Kg/$m^3$. 1172 J/Kg.K = 0,514 W/m.K
Amostra 2 (⊥): k = 0,199 .$10^{-6}$$m^2$/s . 2140 Kg/$m^3$. 1172 J/Kg.K = 0,499 W/m.K
Amostra 3 (//): k = 0,256 .$10^{-6}$$m^2$/s . 2140 Kg/$m^3$. 1172 J/Kg.K = 0,643 W/m.K
Amostra 4 (//): k = 0,224 .$10^{-6}$$m^2$/s . 2140 Kg/$m^3$. 1172 J/Kg.K = 0,562 W/m.K
Amostra 5 (//): k = 0,265 .$10^{-6}$$m^2$/s . 2140 Kg/$m^3$. 1172 J/Kg.K = 0,664 W/m.K

Comparando-se com os valores encontrados na literatura, estes valores situam-se muito próximos dos valores obtidos por Soyenkoff e Okun (1958) e Craig e Peyton (1961).

5. Discussão

Apesar dos primeiros trabalhos sobre as propriedades termofísicas do dente humano situarem-se após o final da década de 30, encontrou-se poucos estudos específicos a respeito deste assunto.

Analisando os poucos trabalhos já realizados, percebeu-se que a metodologia, em alguns trabalhos, foi parcialmente descrita e executada de formas diversas e empregando-se diferentes metodologias pelos pesquisadores. Observou-se uma grande discrepância entre os resultados de condutividade térmica encontrados (diferenças de até cerca de dez vezes, ou seja, uma ordem de grandeza), a qual pode ser atribuída às variações de metodologia e também à falta de padronização das condições de trabalho. O valor de 0,108 W/m.K para a condutividade térmica de dentina humana encontrado por Phillips, Reinking e Phillips (1954) é cerca de 10 vezes menor que o valor de 0,984 W/m.K encontrado por Simeral (1951).

Verificou-se uma boa concordância entre os valores de difusividade térmica medidos no presente trabalho, utilizando-se o método do flash de laser, e os valores encontrados, através de cálculos, por Brown, Dewey e Jacobs (1970) e por Braden (1964). Além disso, verificou-se que a direção dos túbulos dentinários não influencia a difusividade térmica da dentina humana, confirmando conclusão de Craig e Peyton (1961).

6. Conclusão

Baseado nos estudos realizados pode-se concluir que:

a. os valores medidos de difusividade térmica da dentina humana, obtidos através do método do flash de laser, situaram-se na faixa de 0,199 x$10^{-6}$$m^2$/s a 0,265x$10^{-6}$$m^2$/s, muito próximos dos valores calculados por Braden (1964) (0,260x10^{-6} m^2/s) e por Brown, Dewey e Jacobs (1970) (⊥: 0,187x10^{-6} ; //: 0,183x10^{-6} m^2/s);

b. verificou-se que não há influência da direção dos túbulos dentinários na difusividade e condutividade térmica da dentina humana, confirmando-se a conclusão de Craig e Peyton (1961);

c. os valores calculados para a condutividade térmica utilizando-se os valores de difusividade térmica obtidos no presente trabalho e de densidade e calor específico obtidos por Manly, Hodge e Ange (1939) e Peyton e Simeral (1954), respectivamente, confirmam os valores de condutividade térmica obtidos por Soyenkoff e Okun (1958) e Craig e Peyton (1961);

d. a discrepância entre os resultados dos diferentes autores pode ser explicada pelas diferenças nas condições de trabalho;

e. é necessário padronizar as metodologias para a medição das propriedades termofísicas para que se consigam resultados mais próximos dos reais e eles possam ser usados de forma confiável em procedimentos clínicos que geram calor no dente;

f. é importante que a metodologia seja bem detalhada para que os procedimentos possam ser seguidos por outros pesquisadores e possam se obter resultados compatíveis.

Agradecimentos

Ao Centro de Desenvolvimento da Tecnologia Nuclear – CDTN-CNEN pela disponibilização do Laboratório de Medição de Propriedades Termofísicas de Combustíveis Nucleares e Materiais.

Referências

Braden, M., 1964, "Heat conduction in normal human teeth", Arch Oral Biol., vol.9, pp.479-486.

Brown, W. S.; Dewey, W. A. and Jacobs, H. R., 1970, "Thermal properties of teeth", J. Dent. Res., vol.49, no.4, pp.752-755.

Craig, R. G. and Peyton, F. A., 1961, "Thermal conductivity of tooth structure, dental cements and amalgam", J. Dent. Res., vol.40, no.3, pp.411-417.

Deem, H. W. and Wood, W. D., 1962, "Flash thermal-diffusivity measurements using a laser", Review Science Instruments, vol.33, pp.1107.

Ferreira, R. A.N.; Miranda, O.; Dutra Neto, A.; Grossi, P. A.; Martins, G. A.; Reis, S. C.; Alencar, D. A.; Soares Filho, J. G.; Lopes C. C. and Pinho, M. G., 2002, "Implantação no CDTN de Laboratório de Medição de Propriedades Termofísicas de Combustíveis Nucleares e Materiais através do Método flash laser", In: ENFIR.- Encontro Nacional de Física de Reatores, 13, 2002, Rio de Janeiro. Anais... Rio de Janeiro: ABEN.

Grossi, P. A., 2003, "Modelagem físico-matemática de sistemas de determinação de propriedades termofísicas com aplicação ao método flash laser", 2003. 107p. Dissertação (Mestrado em Engenharia Mecânica) - Escola de Engenharia, Universidade Federal de Minas Gerais, Belo Horizonte.

Grossi, P. A.; Andrade, R. M.; Ferreira, A. N.; Ziviani, M., 2002, "Solução da equação de difusão térmica, utilizando a técnica de volumes finitos, para otimização do método flash laser", In: Congresso Nacional de Engenharia Mecânica, 2, 2002, Paraíba. Anais... João Pessoa: CONEM.

Grossi, P. A.; Ferreira, A. N.; Andrade, R. M., 2004, "Review of the flash laser method", In: Brazilian Congress of Thermal Engineering and Sciences, 10, 2004. Anais... Rio de Janeiro: ENCIT.

Grossi, P. A.; Ferreira, A. N.; Andrade, R. M., 2005a, **"**Estimativa da incerteza na medição dinâmica de temperatura através da resposta dinâmica A sinais de teste", In: Congresso Ibero-Americano de Engenharia Mecânica, 2005. Anais... Cidade do México: 7 CIBIM.

Grossi, P. A.; Ferreira, A. N.; Andrade, R. M., 2005b, "Uncertainty estimate of the temperature dynamic Measurement by system identification", In: 18th International Congress OF Mechanical Engineering 2005. Anais... Ouro Preto: COBEM.

Gutknecht, N. and Eduardo, C. P., 2004, "A odontologia e o laser", Atuação do laser na especialidade odontológica, Ed. Quintessence, São Paulo, 320p.

Hibst, R. and Keller, U., 1990, "Heat effect of pulsed Er: YAG laser radiation. International Congress on Laser in Dentistry", II. Proceeding of Spie, v.1200. Laser surgery: advanced characterization, therapeutics, and system II. University of Ulm.

Incropera, F. P. and Dewitt, D. P., 1992, "Fundamentos de transferência de calor e de massa", Ed. LTC, Rio de Janeiro, Tradução de Horacio Macedo.

Jeffrey, I. W. M.; Lawrensen, B.; Longbottom, C.; Saunders, E. M., 1990a, "CO2 laser application to the mineralized dental tissues – the possibility of iatrogenic sequelae". J. Dent., vol.8, no.1, pp.24-36.

Jeffrey, I. W. M.; Lawrensen, B.; Saunders, E. M.; Longbottom, C., 1990b, "Dentinal temperature transients caused by exposure to Co2 laser irradiation and possible pulpal damage", J. Dent., vol.18, no.1, pp.31-36.

Lisanti, V. F. and Zander, H. A., 1950, "Thermal conductivity of dentin", J. Dent. Res., vol.29, no.4, pp.493-497.

Lizarelli, R. F. Z., 2000, "Lasers de Nd:YAG nos regimes de nano e de picossegundos em esmalte e em dentina: análises morfológica e química", Dissertação (Mestrado em Ciências e Engenharia de Materiais) - Instituto de Física de São Carlos, Universidade de São Paulo, São Paulo.

Manly, R. S.; Hodge, H. C. and Ange, L. E., 1939, "Density and refractive index studies of dental hard tissues", J. Dent. Res., vol.15, pp.203-211.

Paghdiwala, A. F.; Vaidyanathan, T. K. and Paghdiwala, M. F., 1993, "Evaluation of erbium:YAG laser radiation of hard dental tissues: analysis of temperature changes, depth cuts and structural effects", Scanning Microsc., vol.7, no.3, pp.989-997.

Parker, W. J.; Jenkins, R. J.; Butler, C. P. and Abbott, G. L., 1961, "Flash method of determining thermal diffusivity, heat capacity and thermal conductivity". J. Appl. Phys., vol.32, no.9, pp.1679-84, apud Grossi, P. A., 2003, "Modelagem físico-matemática de sistemas de determinação de propriedades termofísicas com aplicação ao método flash laser", Dissertação (Mestrado em Engenharia Mecânica) – Escola de Engenharia da Universidade Federal de Minas Gerais, Belo Horizonte.

Peyton, F. A. and Simeral, W. G., 1954, "Specific heat of tooth structure", Alumni Bulletin of the University of Michigan Dental School, vol.56, pp.33 apud Brown, W. S.; Dewey, W. A. and Jacobs, H. R., 1970, "Thermal properties of teeth", J. Dent. Res., vol.49, no.4, pp.752-755.

Phillps, R. W.; Johnson, R. J. and Philips, L. J., 1956, "Improved method for measuring the coefficient of thermal conductivity of dental cement", JADA, vol.53, pp.577 apud Soyenkoff, B. C. and Okun, J. H., 1958, "Thermal conductivity measurements of dental tissues with the aid of thermistors", J. Am. Dent. Assoc., vol.57, pp.23-30.

Phillps, R. W.; Reinking, R. H. and Philips, L. J., 1954, "Thermal conductivity of dental cement: a method and determinations for three commercial materials", J. Dent. Res., vol.33, no.4, pp.511-518 apud Soyenkoff, B. C. and Okun, J. H., 1958, "Thermal conductivity measurements of dental tissues with the aid of thermistors", J. Am. Dent. Assoc., vol.57, pp.23-30.

Sagi, A.; Shitzer, A.; Katzir, A. and Akselrod, S., 1992, "Heating of biological tissue by laser irradiation: theoretical model", Opt. Eng., vol.31, no.7, pp.1417-1424.

Simeral, W. G., 1951, "Thermal conductivity of dental materials, microfilm of papers presented at the annual IADR", Dental Materials Group Meeting, March, 1951, J. Dent. Res., vol.30, pp.499, apud Craig, R. G. and Peyton, F. A., 1961, "Thermal conductivity of tooth structure, dental cements and amalgam", J. Dent. Res., vol.40, no.3, pp.411-417.

Soyenkoff, B. C. and Okun, J. H., 1958, "Thermal conductivity measurements of dental tissues with the aid of thermistors", J. Am. Dent. Assoc., vol.57, pp.23-30.

Taylor, R. E., 1978, "Heat pulse thermal diffusivity measurements", School of Mechanical Engineering, Purdue University, West Lafayette, Indiana.

White, J. M.; Goodis, H. E.; Rose, C. M. and Daniels, T. E., 1991, "Effects of Nd:YAG laser on pulps of extracted human teeth", J. Dent. Res., vol.69, pp.300.

Zach, L. and Cohen, G., 1965, "Pulp response to externally applied heat", Oral Surg. Oral Med. Oral Pathol., vol.19, no.4, pp.515-530.

Zezell, D. M.; Cecchini, S. C. M.; Pinotti, M. and Eduardo, C. P., 1996, "Temperature changes under Ho:YLF irradiation". In: Wigdor, H. A.; Featherstone, J. D. B.; White, J. M. and Neev, J. Proceedings of lasers in dentistry II. San Jose: SPIE, p.34-39.

HUMAN DENTIN THERMAL DIFUSIVITY MEASUREMENT BY THE FLASH LASER METHOD

Manoelita Figueiredo de Magalhães
Mechanical Engineering Department - DEMEC
Federal University of Minas Gerais - UFMG
Antônio Carlos Avenue, 6.627 - University City, Pampulha - Zip Code: 31270-901
Belo Horizonte - MG, Brazil - Phone number (31) 3499 5145 - Fax (31) 3443 3783
manoelita@uai.com.br

Ricardo Alberto Neto Ferreira
Nuclear Technology Development Center - CDTN
Nuclear Energy National Commission - CNEN
University City, Pampulha - Zip Code: 30123-970 - Belo Horizonte - MG, Brazil
Phone number (31) 3499 3150 - Fax (31) 3499 3390
ranf@cdtn.br

Pablo Andrade Grossi
Nuclear Technology Development Center - CDTN
Nuclear Energy National Commission - CNEN
University City, Pampulha, Zip Code: 30123-970 - Belo Horizonte - MG, Brazil
Phone number (31) 3499 3150 - Fax (31) 3499 3311
pabloag@cdtn.br

Roberto Márcio de Andrade
Mechanical Engineering Department - DEMEC
Federal University of Minas Gerais - UFMG
Antônio Carlos Avenue, 6.627 - University City, Pampulha, Zip Code: 31270-901
Belo Horizonte - MG, Brazil - Phone number (31) 3499 5145 - Fax (31) 3443 3783
roberto@demec.ufmg.br

Summary

Nowadays, the cavity removal in dentistry can be performed with rotatory instruments (conventional burs) or high intensity laser. Both techniques can heat the tooth and harm the pulp. Avoiding those thermal effects is important for the preparation and irradiation of the hard tissue, in order to prevent undesirable harm of the adjacent tissue. It is important to study the temperature variation produced during dental treatments that cause heat. The literature review about the measurement of thermal properties conducted in human dentin revealed a great variation of the values obtained by several authors, and most of the studies are outdated. None of these studies have directly measured the thermal diffusivity of human dentin, and the reported values are only calculated values based on measures of conductivity, density and specific heat. The aim of the present study was to measure at CDTN the thermal diffusivity of human dentin using the laser flash technique. The obtained thermal diffusivity values of five human dentin samples measured by this method range from 0,199 $x10^{-6}m^2/s$ to $0,265x10^{-6}m^2/s$, very close to the values calculated by Braden (1964) and Brown, Dewey and Jacobs (1970).

Key-words: human dentin, thermal diffusivity, measurement, flash laser method.

Proceedings of the 11th Brazilian Congress of Thermal Sciences and Engineering -- ENCIT 2006
Braz. Soc. of Mechanical Sciences and Engineering -- ABCM, Curitiba, Brazil,- Dec. 5-8, 2006

Paper CIT06-0489

ANALYSIS OF SKIN BURN INJURY THROUGH INTEGRAL TRANSFORM TECHNIQUES

A. V. Presgrave
Instituto Militar de Engenharia - Seção de Engenharia Mecânica e de Materiais
Praça General Tibúrcio 80 - 22290-270 Rio de Janeiro, RJ, Brazil
amandapresgrave@gmail.com

R. O. C. Guedes
Instituto Militar de Engenharia - Seção de Engenharia Mecânica e de Materiais
Praça General Tibúrcio 80 - 22290-270 Rio de Janeiro, RJ, Brazil
guedes@ime.eb.br

F. Scofano Neto
Instituto Militar de Engenharia - Seção de Engenharia Mecânica e de Materiais
Praça General Tibúrcio 80 - 22290-270 Rio de Janeiro, RJ, Brazil
scofano@ime.eb.br

Abstract: *Skin burn injuries is one of the most common hazards encountered in daily life and in industrial environments such as petrochemical and plastic plants. These accidents are usually associated to contact with hot substances, gas leaks or intense heat fluxes associated to combustion processes. The main contribution of this work is to carefully assess the skin burn injury phenomenon by employing the well known Pennes bioheat equation. Here, the skin is taken as one layer medium subjected to a time varying heat flux boundary condition at its external surface. This model is handled analytically through means of integral transform techniques and the transient temperature field is studied in order to accurately predict the severity of the burn injury. The results are compared with previously reported data in the literature in order to discuss the relative merits of the mathematical model and the solution scheme presented in this contribution.*

Keywords. *Pennes equation, burn injury, integral transform.*

1. Introduction

Burn accidents are said to be one of most common and painful hazards a person may experience. Depending on the intensity of the burn, nerve endings may be severely damaged causing an intense distress and in some cases long-term hospitalization are required. Burn injuries can also affect muscles, bones, and blood vessels. Besides, a burn injury can impair the respiratory system and body temperature together with its thermal regulation.

Usually, burns are classified in two ways: the method of the burn and the degree of the burn, (Diller and Ryan; 1998). The most common causes of burn injuries related to the method are: thermal, chemical, electrical, light and radiation. As for the degree of the burn, the following assortment is found: first degree, second degree and third degree burns. A first degree burn is a superficial impairment that only affects the outer layer of the skin known as the epidermis. Usually this burn will heal on itself in a couple of days with minor or no scarring. In same cases, there may be peeling of the skin and some temporary discoloration. A second degree burn occurs when the injury affects the second layer of the skin - the dermal layer. The patient experiences deep intense pain and there may be some blisters together with some reddening of the skin. When treated with reasonable care, such burns will heal themselves in about three weeks time. A third degree burn is also referred as a full thickness burn since it affects all the layers of the human skin. Due to its nature, it is the most serious of all burns as it requires extensive medical care. Surprisingly, many third-degree burn patients do not report pain but this reaction is due to the fact that the nerve endings have been severely damaged.

A brief literature review suggests that the mathematical simulation of skin burns have received quite a lot of attention in the years following the end of the Second World War. More recent studies rely on the so-called Pennes' bioheat transfer equation. Pennes (1948) suggested that in order to account for the effect of the blood flow in a biological tissue, a source / sink term directly proportional to the difference between the temperature of the tissue and that of the arterial blood should be added in the standard heat diffusion equation. Torvi and Dale (1994) employed Pennes' bioheat transfer equation in order to predict skin temperatures and times for second and third degree burns under simulated flash fire conditions. Flash fires are hazards that are often encountered in petrochemical industries and are usually associated to intense heat fluxes of short duration, typically less than five seconds. By employing a finite element solution scheme in a three layered skin model, they performed a series of numerical investigations and compared their results with previously published results. Among their findings, they concluded that the wide variation of thermophysical properties mentioned by earlier investigators had minimum effect in the prediction of second degree burn and were found to be more relevant when a third degree injury was assessed. Also worth mentioning is the fact

that the blood perfusion term could be neglected in the determination of the transient temperature field. Liu et al (1999) also employed a one-dimensional analysis in a three layered skin by developing a thermal wave model of the bioheat transfer process. Since they were also interested in modeling flash fire situations, their main reason for utilizing this non-Fourier analysis was to estimate the deviations between the finite heat propagation velocity to that of the classical Pennes' model. They conducted a series of simulations in order to assess the role of the volumetric blood perfusion term and also found out that it could be neglected. They concluded that the mechanisms of wave like behavior of heat transfer in living tissues were complex and no generalization appeared to be possible at that point of their research. Their simulations suggested that only when an extremely high heat flux rate is present will the thermal wave effect dominate over the heat diffusion process. It appears that the main difficulty in established a conclusive idea relied on the fact that no well-established evaluation of the thermal relaxation time was available for biological tissues.

Ng and Chua (2002) studied the bioheat transfer equation for both the one-dimensional and two-dimensional situations by employing finite difference for the 1D case and a finite element package for the 2D simulation. A convective boundary condition and a constant temperature at the surface of the skin were utilized in order to simulate the heat source associated to the burn injury. They also attempted to estimate the effect the therapeutic efficacy of postburn cooling by simulating the immersion of the biological tissue in water at some selected temperatures once the heating period ended. Their main conclusion is that the one-dimensional model appeared to be quite accurate since the deviation for the estimates utilizing the 2D situation was quite small. Jian et al (2002) also employed a convective boundary condition at the outer layer of the human skin in order to predict the skin burn process. Their results suggest that the transient temperature field is significantly affected by the epidermis and dermis thicknesses while variations of the initial temperature and blood perfusion have little effect in temperature levels.

Mercer and Sidhu (2005) also utilized a one-dimensional multi-layer bioheat transfer model to study the effects of skin burn due to the deployment of automotive airbags. Again they found out that over the time scales of interest, typically around 0.5 to 2 seconds, the blood perfusion process had no major impact. Based on their numerical simulations, they concluded that a passenger may experience first and second degree burns due to venting of the airbags during deflation and also due to the direct contact with the fabric of the airbag.

2. Analysis

This section starts out by considering a generalized version of the heat transfer equation for a perfused organic tissue subjected to an external heat source in such a way in order to portray the skin burn injury problem. Here, we employ the well-known Pennes' equation model. As mentioned before, this model can be briefly described as a standard heat diffusion problem with an extra term that accounts for the blood flow in the organic tissue being analyzed. Therefore, the transient bioheat transfer problem is written as (Hartnett and Irvine, 1992):

$$\rho C \frac{\partial T}{\partial t} = \nabla \bullet (k \nabla T) + q_{met} + q_{ext} + q_{per} \tag{1}$$

The first term on the right hand side of Eq.(1) is immediately recognized as the heat diffusion term throughout the tissue. The next term, q_{met}, is the metabolic heat transfer rate per unit volume of tissue while q_{ext} represents the influence of an external heat source which, for example, can be relevant in the cases of hyperthemia treatment in cancerous tissues (Azevedo, 2004). The last term, q_{per}, is the heat transfer rate per unit volume of tissue due to blood perfusion. Based on his own experimental evidence, Pennes (1948) stated that the thermal impact of the blood flow could be characterized by introducing an energy sink term. This blood flow effect is assumed to be proportional to the volumetric perfusion level, ω, and to the difference between the local tissue temperature and that of the arterial blood, $(T - T_b)$ in such a way that:

$$q_{per} = -\rho_b C_b \varpi (T - T_b) \tag{2}$$

Therefore, by considering the skin as a single layer, the transient one-dimensional heat transfer equation becomes (Presgrave, 2005; Presgrave et al. 2005):

$$\rho C \frac{\partial T(x,t)}{\partial t} = k \frac{\partial^2 T(x,t)}{\partial x^2} - \omega \rho_b c_b (T(x,t) - T_b) + q_{met}, \; 0 < x < l \; , \; t > 0 \tag{3}$$

$$T(x,0) = T_b \quad 0 \le x \le 1 \tag{4}$$

$$q_0 \, e^{-dt} + k \frac{\partial T(0,t)}{\partial x} = 0 \quad t > 0 \tag{5}$$

$$T(l,t) = T_b \quad t > 0 \tag{6}$$

An analysis of the above formulation shows that the skin is initially at the body core temperature, T_b 37 °C, when suddenly an exponentially decaying heat flux is applied at the skin surface where d is the regression factor. Consistent with previous contributions, for example, Torvi and Dale (1994), it is also assumed that this heat flux basically affects the immediate vicinity of the skin surface and, consequently, the innermost layers remain at the body core temperature, Eq. (6), whose value is considered to be the same of that of the arterial blood.

The relations represented by Eqs. (3) to (6) can be written in a dimensionless form by employing the following variables.

$$\chi = \frac{x}{l} \tag{7}$$

$$\tau = \frac{k}{\rho C}\frac{t}{l^2} \tag{8}$$

$$\theta = \frac{T - T_b}{\frac{q_0 l}{k}} \tag{9}$$

Thus, it is a simple matter to show that the dimensionless version of the mathematical formulation being analyzed is expressed by:

$$\frac{\partial\theta(\chi,\tau)}{\partial\tau} = \frac{\partial^2\theta(\chi,\tau)}{\partial\chi^2} - P_f\theta(\chi,\tau) + Q \quad 0 < \chi < 1, \quad \tau > 0 \tag{10}$$

$$\theta(\chi,0) = 0 \quad 0 \le \chi \le 1 \tag{11}$$

$$e^{-\beta\tau} + \frac{\partial\theta(0,\tau)}{\partial\chi} = 0 \quad \tau > 0 \tag{12}$$

$$\theta(1,\tau) = 0, \quad \tau > 0 \tag{13}$$

where Q, P_f and β are the dimensionless metabolic rate, perfusion coefficient and rate of decay of the external heat source which causes the burn injury. These quantities are expressed as follows:

$$Q = \frac{q_{met}\, l}{q_0} \tag{14}$$

$$P_f = \frac{\omega\, \rho_b\, C_b\, l^2}{k} \tag{15}$$

$$\beta = \frac{d\, \rho\, C\, l^2}{k} \tag{16}$$

A common assumption in burn injury studies, (Torvi and Dale, 1994; Liu et al, 1999, Jiang et al, 2002; Mercer and Sidhu, 2005), is to admit that both the perfusion and metabolic effects can be disregarded in the analysis since their contribution to the heat balance is usually much smaller than that of the external heat source. Pursuing this same idea, we seek the solution of problem (10) - (13) in terms of the following eigenfunction expansion:

$$\theta(\chi,\tau) = \sum_{i=1}^{\infty} A_i(\tau)\psi_i(\chi) \tag{17}$$

where the eigenfunctions $\psi_i(\chi)$ are related to the Sturm-Liouville system described below:

$$\frac{d^2\psi_i(\chi)}{d\chi^2} + \mu_i^2\,\psi_i(\chi) = 0 \quad 0 < \chi < 1 \tag{18}$$

$$\frac{d\,\psi_i(0)}{d\,\chi} = 0 \tag{19}$$

$$\psi_i(1) = 0 \tag{20}$$

Due to the simplicity of the above problem, its eigenfunctions are immediately recognized as $\psi_i(\chi) = \cos(\mu_i\,\chi)$ and the norms are found to be $N_i = \frac{1}{2}$.

By employing the orthogonality property of the chosen eigenproblem, we conclude that:

$$A_i(\tau) = \frac{1}{N_i}\int_0^1 \theta(\chi,\tau)\psi_i(\chi)d\chi \tag{21}$$

and thus the integral-transform pair is found to be (Cotta; 1993, Cotta; 1998):

$$\bar{\theta}_i(\tau) = \frac{1}{N_i^{1/2}}\int_0^1 \theta(\chi,\tau)\psi_i(\chi)d\chi \quad \text{transform relation} \tag{22}$$

$$\theta(\chi,\tau) = \sum_{i=1}^{\infty}\frac{1}{N_i^{1/2}}\psi_i(\chi)\bar{\theta}_i(\tau) \quad \text{inverse relation} \tag{23}$$

The next step is to rewrite the original problem formulation in terms of the transformed variable $\bar{\theta}_i(\tau)$. This task is accomplished through a series of mathematical steps which are well-documented in Mikhailov and Ozisik (1984). The resulting decoupled system of ordinary differential equations that govern $\bar{\theta}_i(\tau)$ is:

$$\frac{d\,\bar{\theta}_i(\tau)}{d\,\tau} + \mu_i^2\,\bar{\theta}_i(\tau) = \frac{1}{N_i^{1/2}}\psi_i(0)e^{-\beta\tau} \tag{24}$$

while its initial conditions is determined by employing the integral transform, Eq. (22), in relation (11) to yield:

$$\bar{\theta}_i(0) = 0 \tag{25}$$

System (24) is solved analytically to obtain:

$$\bar{\theta}_i(\tau) = \frac{1}{N_i^{1/2}}\frac{\psi_i(0)}{\mu_i^2 - \beta}\left(e^{-\beta\tau} - e^{-\mu_i^2\tau}\right) \tag{26}$$

and by inserting this result in the inverse relation, Eq. (23), the dimensionless temperature field is expressed as:

$$\theta(\chi,\tau) = 2\sum_{i=1}^{\infty}\frac{\cos(\mu_i\,\chi)}{\mu_i^2 - \beta} + 2\sum_{i=1}^{\infty}\frac{\cos(\mu_i\,\chi)}{\beta - \mu_i^2}e^{-\mu_i^2\tau} \tag{27}$$

While Eq, (27) is indeed a closed form solution for the burn injury formulation here analyzed, the convergence characteristics of its first term are expected to be poor since the chosen eigenvalue problem does not account for the non-homogeneous term associated to the external heat flux. Thus, we seek an alternative solution based on the "split-

up" solution procedure similar to those discussed in Mikhailov and Ozisik (1984). The basic idea is to consider the temperature field as the sum of two contributions which are expressed by an auxiliary problem, $\theta_{aux}(\chi)$, and a homogeneous problem $\theta_h(\chi,\tau)$ in such a way that:

$$\theta(\chi,\tau)=\theta_{aux}(\chi)e^{-\beta\tau}+\theta_h(\chi,\tau) \tag{28}$$

where the problem for $\theta_{aux}(\chi)$ is given by:

$$\frac{d^2\theta_{aux}(\chi)}{d\chi^2}+\beta\,\theta_{aux}(\chi)=0 \quad 0<\chi<1 \tag{29}$$

$$\frac{d\,\theta_{aux}(0)}{d\,\chi}+1=0 \tag{30}$$

$$\theta_{aux}(1)=0 \tag{31}$$

By inserting Eq. (28) in relations (10) - (13) and with the aid of problem (29) - (31), we find that $\theta_h(\chi,\tau)$ is governed by:

$$\frac{\partial\theta_h(\chi,\tau)}{\partial\tau}=\frac{\partial^2\theta_h(\chi,\tau)}{\partial\chi^2} \quad 0<\chi<1,\tau>0 \tag{32}$$

$$\theta_h(\chi,0)=-\theta_{aux}(\chi) \quad 0\le\chi\le1 \tag{33}$$

$$\frac{\partial\theta_h(0,\tau)}{\partial\chi}=0 \quad \tau>0 \tag{34}$$

$$\theta_h(1,\tau)=0 \quad \tau>0 \tag{35}$$

The above problem can be readily solved by the same eigenfunction expansion procedure described earlier and consequently the transient temperature field is:

$$\theta_h(\chi,\tau)=-\sum_{i=1}^{\infty}\left\{\frac{1}{N_i}\int_0^1\theta_{aux}(\chi)\psi_i(\chi)\,d\chi\right\}\psi_i(\chi)e^{-\mu_i^2\tau} \tag{36}$$

where the solution for the $\theta_{aux}(\chi)$ problem is given by:

$$\theta_{aux}(\chi)=\frac{\tan\left(\sqrt{\beta}\right)}{\sqrt{\beta}}\cos\left(\sqrt{\beta}\,\chi\right)-\frac{sin\left(\sqrt{\beta}\,\chi\right)}{\sqrt{\beta}} \tag{37}$$

Accordingly, an alternative expression for the dimensionless skin burn injury problem formulation with enhanced convergence characteristics is :

$$\theta(\chi,\tau)=\frac{e^{-\beta\tau}}{\sqrt{\beta}}\left\{\tan\left(\sqrt{\beta}\right)\cos\left(\sqrt{\beta}\,\chi\right)-sin\left(\sqrt{\beta}\,\chi\right)\right\}+2\sum_{i=1}^{\infty}\frac{\cos(\mu_i\chi)}{\beta-\mu_i^2}e^{-\mu_i^2\tau} \tag{38}$$

where the eigenvalues μ_i are determined from:

$$\mu_i=\frac{(2i-1)\pi}{2} \tag{39}$$

3. Results and Discussion

Having established two analytical solutions for the skin burn injury problem, Eq. (27) and (38), we are now in a position to evaluate the relative merits of the procedures outlined in the previous section and also to establish some insight into the physical problem in question. However, it seems naturally reasonable to initially address the role of both the perfusion and the metabolic heat effects in the heat transfer process.

Table 1 - Geometry and Properties of the Skin

	Specific Heat $C\left[\frac{J}{kg\ ^\circ C}\right]$	**Blood Perfusion Rate** $\varpi\left[\frac{m_b^3/s}{m^3}\right]$	**Thermal Conductivity** $K\left[\frac{W}{m\ ^\circ C}\right]$	**Thickness** $l[m]$	**Density** $\rho\left[\frac{kg}{m^3}\right]$
Epidermis	3578 - 3600	0	0.21 - 0.26	80 X 10^{-6}	1200
Dermis	3200 - 3400	0.00125	0.37 - 0.52	0.00200	1200
Sub-Cutaneous	2288 - 3060	0.00125	0.16 - 0.21	0.01000	1000
Blood	3770	------	------	------	1060
Single-Layer (in-vivo)	3600	0.00125	0.48 - 2.80	0.01208	1200
Single-Layer (in-vitro)	3600	0.00125	0.21 - 0.41	0.01208	1200

Table 1 shows some relevant thermophysical properties of the three layers of the human skin, namely the epidermis, the dermis and the sub-cutaneous tissues. Also presented are the properties for the single layer human skin collected from both in-vivo and in-vitro experiments (Torvi and Dale, 1994). The rate of metabolic energy production is usually between 100 and 300 W/m^2. Although many scenarios for the burn injury problem can be envisioned, here we are basically interested in the so-called "flash-fire" accident. These situations are associated to high heat fluxes, typically in the range of 24 to 84 kW/m^2 with an exposure time of about 3 to 5 seconds. For these specific cases, the regression coefficient d is around unity since the ratio $\frac{q}{q_0}$ is less than 1% at the end of a 5 second exposure. Therefore, characteristic values of the dimensionless metabolic heat source, perfusion coefficient and regression coefficient are found to be around 1.5 X 10^{-4}, 4.5 and 3900. Clearly, it seems reasonable to assume that the contribution of the external source is the most dominant effect in the heat transfer process. Of course, care should be taken in this conclusion since this source is only active for about 5 seconds and there might be some speculation about the role of both the perfusion process and metabolic heat once the heat source extinguishes. As mentioned before, the literature review suggests that these effects are only relevant in situations where a low heat flux is applied over a reasonably long exposure time. Moreover, it takes about 20 seconds for the skin to react to the thermal load by increasing blood flow in the affected areas (Torvi and Dale, 1994) and in the presence of high fluxes, second and third degree burns are much likely to develop before 20 seconds. In addition to this reasoning, numerical multi-layered skin simulations such as those of Liu et al. (1999), corroborate the fact that blood perfusion effects and metabolic heat production have minimum importance in the simulation of the transient temperature distributions.

Another important issue is the convergence rate of both the classical integral transform solution, Eq. (27), and of the split-up solution, Eq. (38). In general terms, it was found that a truncation order of N=100 is adequate enough to warrant graphical convergence for the split-up solution at times greater than 10^{-2} seconds. As previously anticipated, numerical simulations revealed that the direct application of the integral transform procedure to the skin burn formulation resulted in very poor convergence patterns. Perhaps, this conclusion is better envision by inspecting figures 1 and 2 which present the transient temperature field for both the two solution schemes for the case of an initial incident flux of $q_0 = 54\frac{kW}{m^2}$ and an exposure time of 5 seconds. The transient temperature distribution study for the skin surface (fig. 1) and the basal layer (fig. 2), which marks the transitional point between the epidermis and the dermis, show that a 500 expansion term for direct approach presents a strong deviation from the more accurate solution based on the split-up procedure, during the heating phase which lasts for about 1 second. As time progresses, both figures 1 and 2 indicate that the two solution schemes yield identical results. As a matter of fact, this trend can be

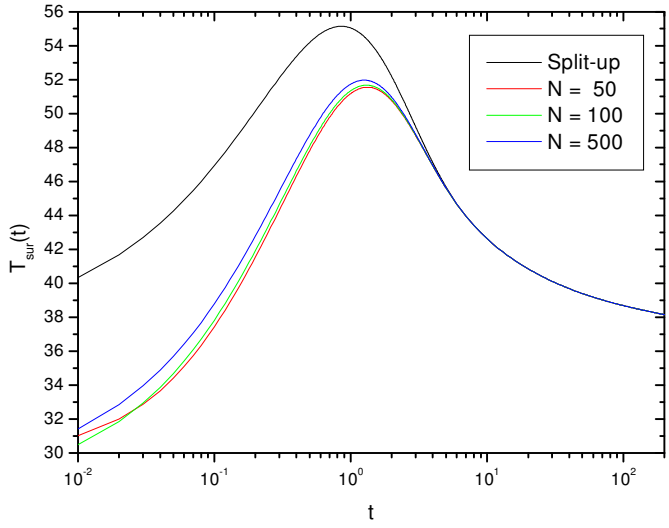

Figure 1. Converged Split-up Solution versus Direct Solution $k = 0.764\ W/m^{\circ}C$, $q_0 = 54\,kW/m^2$, $d = 1(1/s)$

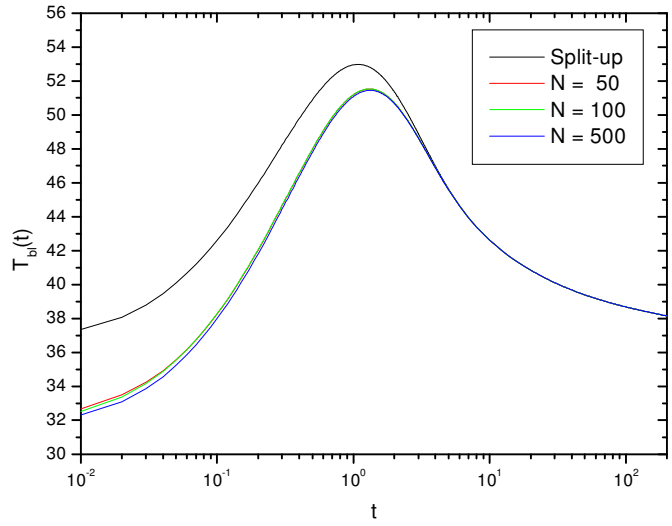

Figure 2. Converged Split-up Solution versus Direct Solution $k = 0.764\ W/m^{\circ}C$, $q_0 = 54\,kW/m^2$, $d = 1(1/s)$

explained upon an inspection of the chosen eigenvalue problem, Eq. (18) – (20). The boundary condition of the Sturm-Liouville problem at the skin surface, Eq. (19), cannot take into account the influence of external heat source and therefore, it is no surprise to find a significant deviation between the two solutions during the early transient stages. On the other hand, as time increases, the external heat source rapidly decays due to its exponential nature and consequently relation (19) becomes a more accurate representation of the physical problem which is expressed by a match of the two solution schemes. Our findings suggest that the direct approach only yields good quality results for the latter part of the transient process and does not capture adequately the more important heating phase. As a general rule, solution (27) should be discarded in favor of the split up procedure and accordingly the next simulations are based only through the evaluation of Eq. (38).

Figure 3 presents the transient temperature field at three selected locations, namely the skin surface $(x = 0\mu m)$, the basal layer $(x = 80\mu m)$ and at the mid plane of the epidermis $(x = 40\mu m)$. An examination of these results shows that, during the heating phase, the skin surface reaches a peak temperature of about 55 °C while the basal layer seems to be 2°C colder. Throughout the cooling phase, the temperature fields at all the three positions rapidly collapses and decay at the same rate since the external heat source is no longer in action. Precise evaluations of the transient temperature field,

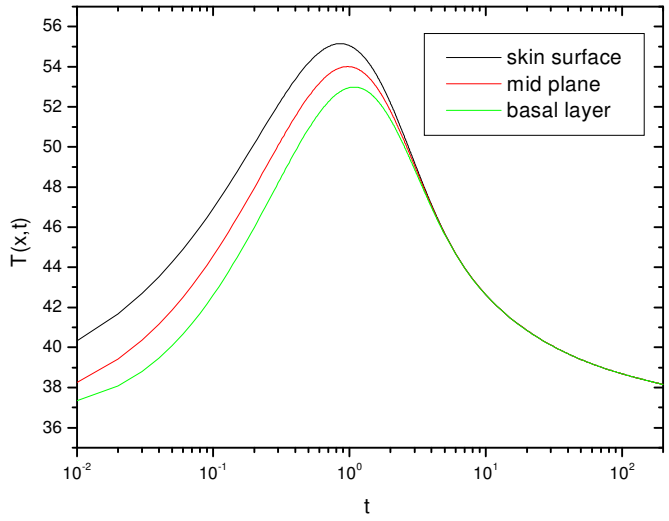

Figure 3. Transient Temperature Distributions $k = 0.764\ W/m^{\circ}C, q_0 = 54\,kW/m^2$, $d = 1(1/s)$

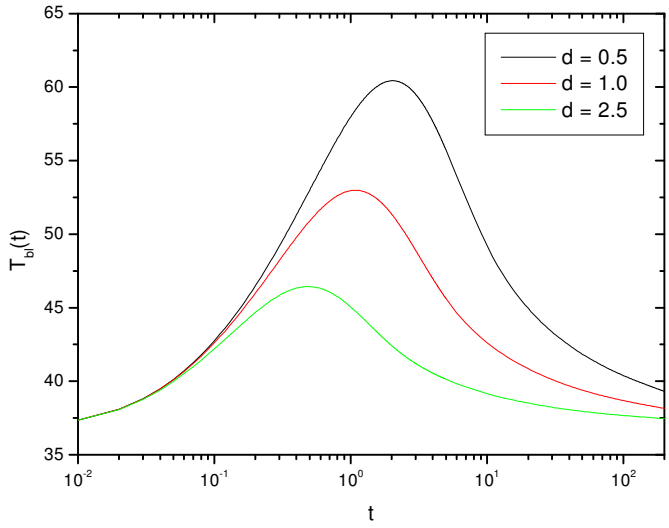

Figure 4. Basal Layer Temperature Distributions $k = 0.764\ W/m^{\circ}C, q_0 = 54\,kW/m^2$

especially at the basal layer, are important since thermal damage occurs once the skin temperature reaches 44°C (Torvi and Dale, 1994). This particular simulation, related to a five second exposure time for an initial heat flux of $q_0 = 54\frac{kW}{m^2}$, shows that the basal layer is above 44°C during approximately 10 seconds and thus some thermal damage, probably a first or even a second degree burn, is expected.

Figures 4 and 5 study the influence of the exposure time in the transient temperature field for both the skin surface and the basal layer considering a fixed initial heat flux of $q_0 = 54\frac{kW}{m^2}$. As expected, long exposure times such 10 and 5 seconds (*d = 0.5* and *1.0*, respectively) will result in high peaks of temperatures as displayed in figs. 4 and 5. The curve associated to *d = 2.5* (exposure time of 2 seconds) is an application related to a possible thermal injure on a driver's hands due to the venting of hot gases from airbag depletion in car accidents. An inspection of both figures 4 and 5 to

this particular case shows that minimum thermal damage is expected since the temperatures levels are slightly above the 44°C threshold and for a short time of less than one second. This observation is consistent with the findings of Mercer and Sidhu (2005) whose simulations predicted that first degree burn injuries will only develop under extreme conditions.

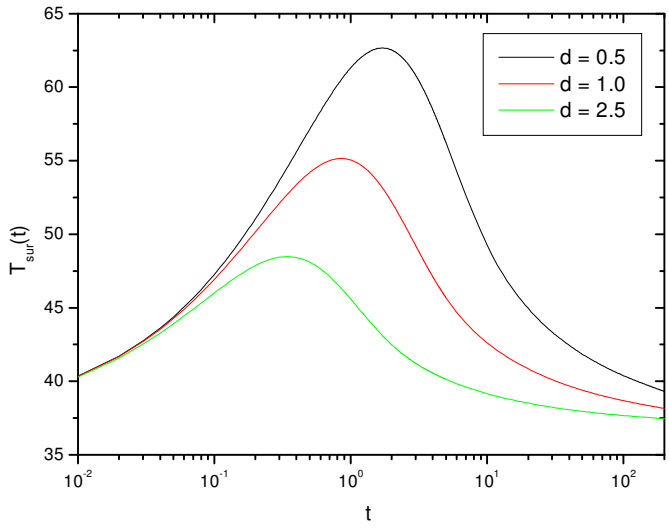

Figure 5. Skin Surface Temperature Distributions $k = 0.764\ W/m^{\circ}C, q_0 = 54\,kW/m^2$

Finally, the variations of the initial heat flux are assessed in figs. 6 and 7 for a fixed exposure time of 5 seconds. The case related to the case of $q_0 = 84\frac{kW}{m^2}$ is of particular interest since it corresponds to a typical exposure of propane gas flash fire on nude skin (Torvi and Dale, 1994). The simulations in fig. 7 reveal that the temperature at the basal layer reaches a peak of about 60 °C at approximately one second after the initial exposure. Also, this layer remains above the 44°C threshold for about 10 seconds suggesting that a severe burn injury will most likely occur. On the other hand, the other two cases might represent the heat flux incident on skin from such a fire when covered with a protective garment. It is interesting to notice that in the situation related to $q_0 = 24\frac{kW}{m^2}$ no thermal damage is expected since the temperature levels are below 44°C.

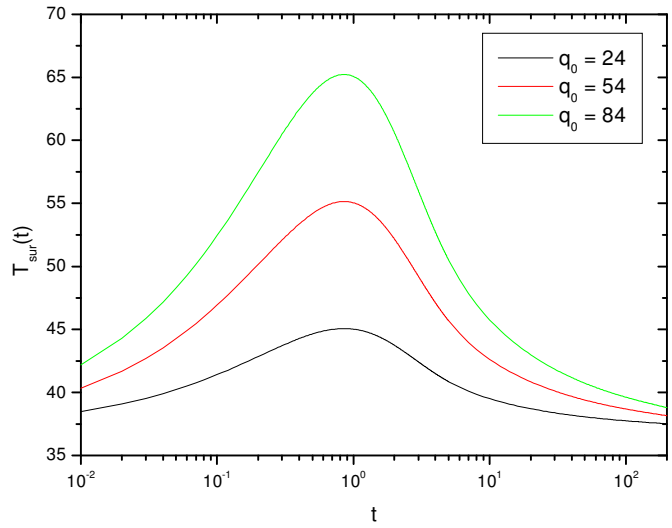

Figure 6. Skin Surface Temperature Distributions $k = 0.764\ W/m^{\circ}C, d = 1(1/s)$

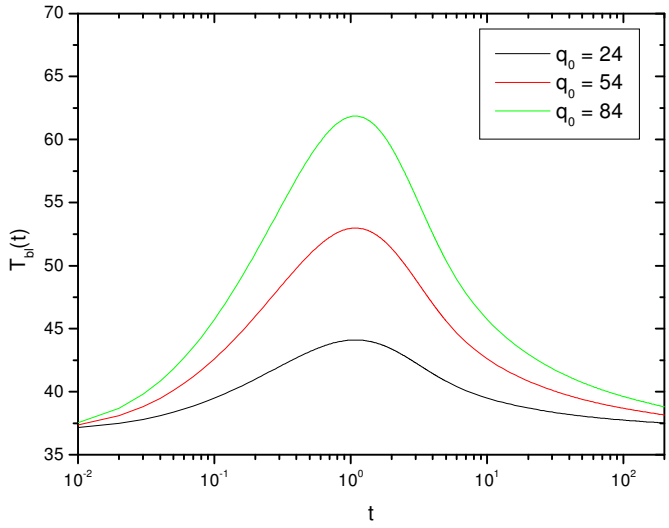

Figure 7. Basal Layer Temperature Distributions $k = 0.764\ W/m^{\circ}C, d = 1(1/s)$

4. Conclusion

This contribution advanced two solution schemes based on integral transform techniques in order to address the skin burn injury problem modeled by the bioheat transfer equation. Based on our simulations, the direct application of the integral transform technique yielded poor convergence characteristics during the heating phase and did not prove to be a good solution procedure to the problem. On the other hand, the split-up procedure provided fast convergence rates and is recommended in the simulations of thermal damages on human skin due to an external heat source. The simulations also revealed that the transient temperature fields are quite sensible to variations of exposure time and to the intensity of the surface heat flux. Our current research aims at characterizing the burn injury in a more precise way by employing the cumulative integral rate of tissue damage and by considering the simultaneous effects of all the three skin layers.

5. References

Azevedo, M. D. B., 2004, "Analytical Numerical Simulation of the Bioheat Transfer in Organic Tissues" (in Portuguese), M.Sc. Dissertation, IME, Rio de Janeiro, Brazil, 252 p.

Cotta, R. M., 1993, "Integral Transforms in Computational Heat and Fluid Flow", CRC Press, Florida, 340 p.

Cotta, R. M. (ed.), 1998, "The Integral Transform Method in Thermal and Fluids Science and Engineering", Begell House, New York, 430 p.

Diller, K., R. and Ryan, T. P., 1998, "Heat Transfer in Living Systems: Current Opportunities", Journal of Heat Transfer, Vol. 120, pp. 810-829.

Hartnett, J.P. and Irvine, T.F. (eds.), 1992, "Advances in Heat Transfer", Academic press, Vol. 22, 586 p.

Jiang, S. C., Ma, N. and Zhang, X. X., 2002, " Effects of Thermal Properties and Geometrical Dimensions on Skin Burn Injuries", Burns, Vol. 28, pp. 713-717.

Liu, J., Chen, X. and Xu, L.X., 1999, "New Thermal Wave Aspects on Burn Evaluation of Skin Subjected to Instanteneous Heating", IEEE Transactions on Biomedical Engineering, Vol. 46, No. 4, pp. 420-428.

Mercer, G. N. and Sidhu, H.S., 2005, " Modeling Thermal Burns due to Airbag Deployment", Burns, Vol. 31, pp. 977-980.

Mikhailov, M. D. and Özisik, M. N., 1984, "Unified Analysis and Solutions of Heat and Mass Diffusion", Dover Publications, New York, 458 p.

Ng, E.Y.K. and Chua, L.T., 2002, "Comparison of one- and two-dimensional Programmes for Predicting the State of Skin Burns", Burns, Vol. 28, pp. 27-34.

Pennes, H.H., 1948, "Analysis of Tissue and Arterial Blood Temperatures in the Resting Human Forearm", Journal of Applied Physiology, Vol. 1, pp. 93-122.

Presgrave, A. V., 2005, "Modelling and Simulation of Blood Perfusion Effects in Bioheat Transfer Problems" (in Portuguese), M.Sc. Dissertation, IME, Rio de Janeiro, Brazil, 205 p.

Presgrave, A. V., Guedes, R. O. C. and Scofano Neto, F., 2005, " Hybrid Analytical Numerical Solution to the Bioheat Transfer Equation" , Proceedings of the 18th International Congress of Mechanical Engineering, Ouro Preto, Brazil.

Torvi, D. A. and Dale, J. D., 1994, "A Finite Element Model of Skin Subjected to a Flash Fire", Journal of Biomedical Engineering, Vol. 116, pp. 250-255.

6. Copyright Notice

Proceedings of the 11th Brazilian Congress of Thermal Sciences and Engineering -- ENCIT 2006
Braz. Soc. of Mechanical Sciences and Engineering -- ABCM, Curitiba, Brazil,- Dec. 5-8, 2006

Paper CIT06-0497

THERMAL COMFORT AND SECOND-LAW ANALYSIS OF THERMOREGULATION MECHANISMS: PRELIMINARY CONSIDERATIONS AND PROSPECTIVE EXTENSIONS

José Antonio Rabi
Faculty of Aninal Science and Food Engineering, University of São Paulo
Av. Duque de Caxias Norte, 225, Pirassununga, SP, 13635-900, Brazil
jrabi@fzea.usp.br

Cecilia Elizabeth Saavedra Fresia
Faculty of Exact Sciences and Technology, National University of Tucumán
Av. Independencia, 1800, Tucumán, 4000, Argentina
cfresia@gmail.com

Graciela Benzal
Faculty of Biochemistry, Chemistry and Pharmacy, National University of Tucumán
Ayacucho 491, Tucumán, 4000, Argentina
gbenzal@fbqf.unt.edu.ar

Abstract. *Mathematical modeling has played important role regarding the definition of parameters to assess and quantify biological or physiological phenomena. Of particular interest, second-law analysis can provide useful information about thermal and chemical processes as it identifies irreversible phenomena bringing about entropy generation and, hence, exergy losses. Accordingly, the so-called objective thermal comfort index (OTCI) has been recently defined in terms of entropy generation related to human thermoregulation in response to changes in ambient conditions. Alternatively, the present paper discusses a prospective definition of a thermal comfort or heat (cold) stress index based on the exergetic analysis of human thermoregulatory mechanisms. Inasmuch as irreversibilities reduce process effectiveness, additional metabolic exergy loss (beyond a "comfort" level) could in principle lead a living organism to experience discomfort of some kind. Bearing in mind that exergy is evaluated based on thermodynamic state parameters related to the ocupant (system) as well as to the corresponding ambient (surroundings), this paper suggests preliminary connections between thermal comfort and exergy losses in line with the so-called heat balance equation for the human body. Potential extensions of such exergetic analysis are also discussed upon.*

Keywords*. mathematical modeling, thermal comfort, thermoregulation, second-law analysis, exergy*

1. Introduction

Several parameters have been defined so as to assess human thermal comfort as well as heat or cold stress. Among those one may list: resultant temperature, equivalent temperature, effective temperature (new and standard), predicted mean vote and predicted percentage dissatisfied, heat stress index, index of thermal stress, required sweat rate, predicted four-hour sweat rate, heart rate prediction, wet bulb and wet globe temperature index, wind-chill index, equivalent still air temperature, shade temperature (equivalent or still) and required clothing insulation index (Parsons, 1993). They are referred to as direct parameters if based on data read from instruments used to mimic human body responses, empirical parameters if obtained by means of numerical regression of human physiological responses as subjects undergo distinct ambient conditions or rational parameters when based on theoretical reasoning.

The aforesaid parameters are helpful to bioclimatic and energy-efficient building design – a notable effort towards energy saving. For that reason, occupants' thermal comfort analysis should be based on indices depicting physiological responses to ambient as reliably as possible. Likewise, there are issues concerning Food Engineering workplaces (e.g. refrigeration chambers, food processing areas or food storage rooms) for which thermodynamic modeling may help defining specific working and/or production practices, precautions or standards for occupants (workers).

Mathematical modeling has been playing a role of rising importance to many fields. In particular, its association to life sciences is mutually interesting with regards to understanding and analyzing biological systems. On one hand, new and wide research horizons become available to Physics and Engineering. Natural phenomena have indeed served as inspiration to technological advances and innovation (Mammana, 1981), which should not be surprising if one considers that existing biological systems have already undergone natural (and rigorous) selection. On the other hand, Medicine and Biology have progressively benefited from the utilization of calculus apparatus and information technology. Such (should one say symbiotic?) cooperation enables not only the design of multipurpose equipment but also the inference of assessment methodologies for biological or physiological phenomena.

As far as thermal comfort and/or heat (cold) stress are concerned, rational parameters can be defined based on an energy balance applied to the human body, accounting for concurrent effects from the ambient such as air temperature

and humidity, radiant temperature and air speed, in conjunction with behavioral (human) factors like activity-related metabolism and clothing. In other words, rational parameters evoke the first law of thermodynamics. Yet, in terms of energy consumption (or conversely, energy saving), second-law analysis can improve process efficiency by identifying irreversible phenomena bringing about exergy losses. Taking into account both ambient conditions and the process itself, exergy is a physical property that can be properly introduced in the analysis in order to enhance our grasp on process thermodynamic efficiency (Szargut *et al.*, 1988).

Boregowda *et al.* (2001) used second-law analysis to quantify thermal comfort. As a result, the so-called objective thermal comfort index (OTCI) was put forward as a function of entropy generation, combining both human thermal responses and environmental variables. More recently, Prek (2004) evoked the exergy concept in order to predict those human physiological responses in steady-state, based on the so-called two-compartment (or two-node) model for the human body as well as having in mind the need for such sort of thermodynamic analysis in line with current exergetic research in the building sector (e.g. low-exergy HVAC systems).

Accordingly, the present paper outlines some preliminary exergetic concepts based on the energy balance equation applied to the human body, as an attempt to set groundwork to define a thermal comfort (or heat / cold stress) parameter based on human thermoregulatory mechanisms. Ultimately, the paper prospects potential correlations between exergy losses due to distinct heat and/or mass transfers in response to changes in ambient thermodynamic conditions.

2. Human thermoregulation and thermodyncamic analysis: basic concepts

In order to sustain its own life, organisms continuously burn some sort of "fuel" (i.e., food) so as to liberate energy to meet its metabolic requirements. The designation bradymetabolism applies to those life forms whose metabolic heat release rate is insufficient to maintain an appreciable thermal gradient between its core and the surroundings (Bligh, 1985). On the contrary, tachymetabolism refers to those organisms presenting fast fuel consumption and heat release rates. On body temperature basis, species can be classified as poikilotherms or homeotherms whether such temperature fluctuates or is kept somewhat constant over a range of environmental conditions, respectively. Moreover, endothermic species are able to derive most of their energy needs from internal metabolism whereas ectothermic species are able to control heat uptake from the environment.

Human normal temperature ranges from 36^{o}C to 37.5^{o}C so that average figures should be generally found between 36.7^{o}C and 37^{o}C as measured in the mouth (oral temperature) while rectal temperature is about 0.6^{o}C higher (Guyton, 1995). It is important to mention that positive or negative deviations of more than a few degrees from those mean values bring about serious health disorders or even life threats. The fact that humans (and all other mammals) are homeotherms implies that energy interactions take place between body and environment.

The first law of thermodynamics should be evoked for the analysis of such energy transfers. Yet, this law makes no quantitative distinction between energy interactions so that work and heat, for example, are treated as equivalent forms of energy in transit. Assuming that body processes follow a spontaneous path, one could in principle go beyond and question whether the body is sensitive to energy quality. In order words, one could ask about the body "preference" to exchange a given quantity of an energy form rather than transferring the same amount of another form so as to fulfill its homeostasis. In this sense, second-law analysis could play an important role to set energy quality differences among distinct thermoregulatory mechanisms.

Initially, assumptions should be made about some basic issues concerning the thermodynamic analysis of human thermoregulation. Among those, it is possible to point to the following:

- *System definition*: Depending on the level of comprehensiveness, the body can be treated either as a closed system (control mass) or as an open system (control volume). If heat losses from evapotranspiration or from respiration are accounted for, water is transferred to ambient as sweat / water vapor from the skin or as exhaled air moisture from lungs. Conversely, water and food intakes play the counterpart role. In both cases, the body rigorously behaves as an open system (control region). Yet, the amount of transferred matter (e.g. lost water) might be small enough so that the body can be seen as a closed system (at least for short time periods).
- *Process classification*: From thermal comfort (or discomfort) dynamics standpoint, one could argue to what extent thermoregulation entails quasi-equilibrium or non-equilibrium processes and whether such mechanisms complete a cycle or constitute some sort of steady-state "operation". As cited by Parsons (1993), ASHRAE / ISO 7730 define thermal comfort as 'that condition of mind which expresses satisfaction with the thermal environment'. In steady-state, Parsons (1993) simply regards it as a lack of discomfort but also acknowledges that thermal sensations (e.g. thermal pleasure) are transient in nature and thus cannot be experienced in steady-state conditions.
- *Irreversibility nature*: Fully reversible process is a well-known idealization and two basic groups of irreversibilities are found in real processes, namely, spontaneous non-equilibrium processes and dissipative phenomena. The latter refer to direct dissipation of work into internal energy whereas the former reflect the natural tendency of systems to achieve equilibrium state with its surroundings (e.g. temperature equalization). As far as human body is concerned, metabolic energy production is deeply related to occupant's activity. Energy for mechanical (muscular) work varies from approximately zero up to 25% of total metabolic rate (Parsons, 1993) and the excess is released as heat to the ambient, mostly over a finite temperature difference with respect to body (fairly constant) temperature.

- *Ambient characterization*: According to its usual definition, everything outside the system boundary comprises the surroundings. In the present analysis, the later could correspond to the indoor ambient whereas the former refers to the occupant. Clearly, the occupant (system) is not isolated as there are at least heat interactions with the ambient (surroundings). In the light of such energy transfers, the ambient could be thought as a thermal energy reservoir (TER). Similar rationale could be applied with respect to mass (sweat, water vapor, moisture) transfers so that the ambient could also be modeled as an inlet matter reservoir (IMR). Mechanical energy reservoir (MER) concepts are evoked for muscular work, if any. It is worth noting that, despite the ambient thermodynamic state may undergo variations, they are not caused by interactions with the occupant but they are responses to prevailing meteorological (external) conditions. Therefore, for a given short time period, stable equilibrium can be assumed to the ambient.

2.1. Thermoregulation and first-law analysis: energy balance

The first law of thermodynamics deals with energy interactions concerning the energy content variation of a system (open or closed). Expressed by means of an energy balance, such conservation principle has basically a quantitative nature as it accounts for all energy forms and interactions equivalently, regardless of its potential to be converted into useful work. Accordingly, by involving heat transfers between human body and its neighboring environment, one may assess the corresponding body energy balance in line with (Bligh, 1985), namely:

$$\frac{\mathrm{d}E_{\mathrm{body}}}{\mathrm{d}t} = \left(\dot{Q}_{\mathrm{met}} - \dot{W}_{\mathrm{musc}}\right) - \left(\dot{Q}_{\mathrm{evap}} + \dot{Q}_{\mathrm{conv}} + \dot{Q}_{\mathrm{cond}} + \dot{Q}_{\mathrm{rad}}\right) \tag{1}$$

Each term in the above equation has dimension of energy × time^{-1} and, along with its sign convention, such equation is also in line with that presented by ASHRAE (2001), where $\mathrm{d}E_{\mathrm{body}}/\mathrm{d}t$ is identified to the so-called (total) heat storage. It is implicitly assumed that $\mathrm{d}E_{\mathrm{body}}/\mathrm{d}t$ lumps the heat storage rates in both core and skin (shell) compartments.

Alternatively, Prek (2004) split up those compartments, thus ascribing a heat balance equation for each one. Even so, such equations were coupled to one another by a common heat transfer rate comprising both heat conduction (passive exchange due to direct contact) and heat transfer through blood flow. Thermoregulation tries to keep core temperature as steady as possible (around $T_{\mathrm{core}} \cong 37^{\mathrm{o}}\mathrm{C}$) while skin temperature varies. The later is often assessed as an average skin temperature T_{skin} so that mean body temperature T_{body} can be evaluated as the following weighted sum:

$$T_{\mathrm{body}} = \alpha T_{\mathrm{skin}} + (1-\alpha) T_{\mathrm{core}} \tag{2}$$

The weighting factor α varies from 0.1 to 0.3 for vasodilated and vasoconstricted skin, respectively (Parsons, 1993).

The difference $(\dot{Q}_{\mathrm{met}} - \dot{W}_{\mathrm{musc}})$ in the first pair of brackets in Eq. (1) is referred to as net heat production (i.e., heat release) rate and it is always positive because $\dot{Q}_{\mathrm{met}} > \dot{W}_{\mathrm{musc}}$. It corresponds to the remaining energy released from total metabolic heat production rate $\dot{Q}_{\mathrm{met}}$ (which might include shivering) as external mechanical (muscular) power $\dot{W}_{\mathrm{musc}}$ is discounted. The second pair of brackets comprises the sum of four heat transfer rates $\left(\dot{Q}_{\mathrm{evap}} + \dot{Q}_{\mathrm{conv}} + \dot{Q}_{\mathrm{cond}} + \dot{Q}_{\mathrm{rad}}\right)$, respectively due to sweat or moisture evaporation, convection, conduction and thermal radiation. According to the sign convention introduced in Eq. (1), positive values for $\dot{Q}_{\mathrm{evap}}$, $\dot{Q}_{\mathrm{conv}}$, $\dot{Q}_{\mathrm{cond}}$ and $\dot{Q}_{\mathrm{rad}}$ correspond to heat losses to the environment through the skin surface and respiratory tract (ASHRAE, 2001).

When the abovementioned energy interaction rates are combined as indicated by Eq. (1), $\mathrm{d}E_{\mathrm{body}}/\mathrm{d}t$ assesses the energy content variation within the occupant's body. In view of that, a temperature rise is related to $\mathrm{d}E_{\mathrm{body}}/\mathrm{d}t > 0$ while a temperature drop refers to $\mathrm{d}E_{\mathrm{body}}/\mathrm{d}t < 0$. If steady-state is then assumed, $\mathrm{d}E_{\mathrm{body}}/\mathrm{d}t = 0$ should be introduced in Eq. (1), leading to the so-called conceptual heat balance equation (Parsons, 1993):

$$0 = \left(\dot{Q}_{\mathrm{met}} - \dot{W}_{\mathrm{musc}}\right) - \left(\dot{Q}_{\mathrm{evap}} + \dot{Q}_{\mathrm{conv}} + \dot{Q}_{\mathrm{cond}} + \dot{Q}_{\mathrm{rad}}\right) \;\Rightarrow\; \dot{Q}_{\mathrm{met}} - \dot{W}_{\mathrm{musc}} = \dot{Q}_{\mathrm{evap}} + \dot{Q}_{\mathrm{conv}} + \dot{Q}_{\mathrm{cond}} + \dot{Q}_{\mathrm{rad}} \tag{3}$$

It is useful to normalize the previous energy balance over different body sizes by considering heat transfer rates on a per unit-area basis, specifically, per unit of body surface area $\dot{q} = \dot{Q} / A_{\mathrm{body}}$ (= energy flux = energy × time^{-1} × area^{-1}), so that the conceptual heat balance equation under steady-state conditions can be expressed as:

$$\dot{q}_{\mathrm{met}} - \dot{w}_{\mathrm{musc}} = \dot{q}_{\mathrm{evap}} + \dot{q}_{\mathrm{conv}} + \dot{q}_{\mathrm{cond}} + \dot{q}_{\mathrm{rad}} \tag{4}$$

One may also conceive a net heat transfer taking place from inner cells to body surface (system boundary) so that heat is eventually transferred to the ambient from the skin and lungs (through respiration). Considering heat transfer

mechanisms on the right-hand side of Eq. (3), it is thus convenient to identify and group those taking place through the skin $\dot{q}_{\text{skin}}$ and those related to respiration $\dot{q}_{\text{resp}}$. Consequently, Eq. (3) can be conveniently cast into:

$$\dot{q}_{\text{met}} - \dot{w}_{\text{musc}} = \dot{q}_{\text{skin}} + \dot{q}_{\text{resp}} \tag{5}$$

As implicitly assumed in the above equation, conductive heat transfer $\dot{q}_{\text{cond}}$ is usually neglected for typical situations (Parsons, 1993). Although $\dot{w}_{\text{musc}}$ may comprise voluntary (e.g. walking and typewriting) and involuntary motions (e.g. heart beating and peristalsis), the later are likely to be already accounted for depending on the way the metabolic heat release $\dot{q}_{\text{met}}$ is experimentally measured as based on the rate of respiratory O_2 consumption and CO_2 production. As presented in ASHRAE (2001), an empirical equation for $\dot{q}_{\text{met}}$ has been suggested by Nishi (1981).

2.2. Thermoregulation and second-law analysis: entropy generation

Due to its quantitative nature, the first law of thermodynamics is not able to point to imperfections of thermal and chemical processes. Conversely, opting for the capacity for doing work as a measure of energy quality, the second law imposes restrictions to energy conversions. In other words, it introduces a qualitative character to distinct energy forms and interactions depending on its equivalent potential to be converted into useful work. This law grants thorough and spontaneous transformation of a "noble" (organized) energy form (e.g. potential energy) into a "poor" (chaotic) form (e.g. internal energy) but the opposite conversion cannot be fully accomplished.

The second law can be expressed in terms of entropy variation ΔS. When applied to an isolated system, which in the present analysis comprises the human body and its surrounding ambient, it states that:

$$\Delta S_{\text{isol}} = \Delta S_{\text{body}} + \Delta S_{\text{surr}} \geq 0 \tag{6}$$

where the equality sign (i.e., entropy conservation) refers to idealized reversible process. Real processes are intrinsically irreversible so that the second law predicts $\Delta S_{\text{isol}} > 0$. Such entropy increase within an isolated system can be directly identified to an entropy generation term S_{gen} (Kotas, 1995). The more irreversible a process is, the greater the value resulting for the entropy generation, which can also be expressed as a rate term $\dot{S}_{\text{gen}}$ (= entropy × time^{-1}).

Combining human thermal physiological responses and thermal environmental variables into an entropy generation term, Boregowda *et al.* (2001) introduced the so-called objective thermal comfort index (OTCI). According to their formulation, OTCI is evaluated as 'the percentage deviation in the value of entropy generation from the comfort or equilibrium condition', which it is assumed to provide 'a measure of the level of satisfaction expressed by the mind with thermal environment'. The OTCI is mathematically defined as:

$$\text{OTCI}(\%) = H\left[1 - \frac{(S_{\text{gen}})_{\text{act}}}{(S_{\text{gen}})_{\text{com}}}\right] \times 100 \tag{7}$$

where subscripts 'act' and 'com' refer to actual and comfort values of the entropy generation term, respectively. The later is presumed to be a function of both environmental variables and human thermal responses, namely:

$$S_{\text{gen}} = S_{\text{gen}}\left(T_{\text{skin}}, T_{\text{core}}, Q_{\text{evap,skin}}, Q_{\text{conv,skin}}, Q_{\text{rad,skin}}, Q_{\text{evap,resp}}, Q_{\text{conv,resp}}, Q_{\text{met}}, I_{\text{cl}}, T_{\text{air}}, \phi\right) \tag{8}$$

Apart from previously defined quantities, I_{cl} is the thermal insulation (resistance) of the clothing worn by the occupant whereas T_{air} and ϕ are air temperature and relative humidity, respectively.

At this point, it is worth commenting the dimensionless coefficient H introduced by the OTCI definition. Referred to as human coefficient, H accounts for the variation in individual responses to thermal environment and it depends on age, sex, race and other related factors. In view of that, one could point out that H is an attempt to bridge physiological and psychological responses, in line with ASHRAE / ISO 7730 standard definition for thermal comfort. For pilot OTCI calculations, Boregowda *et al.* (2001) assumed $H = 1$ under the assumption of a 'standard human'.

2.3. Thermoregulation and second-law analysis: exergy loss

The first and second laws of thermodynamics can be suitably combined to assess the maximum work available from a given energy form (interaction) or to assess the required work to restore the system back to its initial condition after carrying out an irreversible process (Kotas, 1995). Either way, exergy is a thermodynamic property introduced to allow process inspection with regard to the most efficient (hypothetically reversible) way by which it could be achieved.

Exergetic analysis may help identifying thermal processes inefficiencies by evaluating thermodynamic imperfections. It is worth noting that exergy is a function of state parameters related to the system under investigation (= occupant) as well as to the surroundings (= ambient).

By reasoning that exergy of a given system increases as it presents any parameter (e.g. temperature, pressure and chemical potential) that differs from its counterpart in the environment, one might suppose that thermal discomfort (or stress) could originate from an exergy loss excess as occupant's body departs from some comfort set point. Exergetic analysis may then lead to the concept of a thermal comfort (or stress) index for humans (or perhaps animals, from the Animal Science perspective) as thermoregulatory mechanisms attempt to bring the body back to a "comfortable" (i.e., minimum) exergy loss rate or level with reference to the ambient.

In order to propose such "comfortable" exergy loss rate (level), one should ascertain a set of environmental factors (air temperature and humidity, radiant temperature and air speed) as well as behavioral factors (activity and clothing) that in conjunction best meet occupant's satisfaction feeling. As total exergy loss equals the sum of exergy losses from single components (Szargut *et al.*, 1988), losses due to physical and chemical processes related to each physiological thermoregulatory mechanism should be accounted for in principle.

Occupant's total exergy can be divided into four components: kinetic, potential, physical and chemical. While the first two are related the high-grade energy (i.e. organized, fully convertible to work), the last two concern to low-grade energy (i.e., disorganized, partially convertible) and depend on both temperature and pressure of the prevailing ambient (Kotas, 1995). Hence, it seems plausible that these last two exergy components (physical and chemical) should suffice for a preliminary whole-body comfort exergetic analysis.

Just like entropy, exergy is exempt from a conservation law and an exergy loss term is thus introduced in order to close the exergy balance for the system under investigation. Exergy loss is consistent with the degraded useful energy due to process irreversibilities and it is worth recalling that Gouy-Stodola law (Szargut *et al.*, 1988; Kotas, 1995) relates exergy loss $\Delta\Xi$ (= irreversibility I) to entropy generation of an isolated system ΔS_{isol} according to:

$$\Delta\Xi = I = T_0 \, \Delta S_{\text{isol}} \tag{9}$$

where T_0 is the temperature of the surroundings.

Two sorts of irreversibility can arise in real processes, namely, intrinsic and avoidable. The former has to do with minimum irreversibilities imposed by constraints (e.g. uncontrolled chemical reactions and heat capacities mismatch) whereas the later is simply evaluated from the difference between actual (total) and intrinsic irreversibilities (Kotas, 1995). Thus, intrinsic irreversibility and its corresponding exergy loss could then be identified to basal metabolism or, rather, to some comfort zone, which would help defining the proposed comfort exergy loss rate (level).

Bearing in mind that humans do have the ability to acclimatize or acclimate (i.e. to naturally or artificially acquire physiological response changes after prolonged exposure to heat), an issue that remains and deserves to be studied is a prospective connection between the ambient temperature and the dimensionless human coefficient H introduced in the OTCI definition (Boregowda *et al.*, 2001), as previously discussed. For instance, it is well known that beyond a critical head temperature (set-point) a sharp shift occurs from heat loss through insensible evaporation to heat loss through sweating (Guyton, 1995). There is also a similar set point shift from the basal heat release to the shivering-induced heat release. It is interesting to observe that both set points are skin-temperature dependent.

3. Thermal comfort as a steady-state condition: preliminary model

As already cited, in steady-state Parsons (1993) simply regards thermal comfort as a lack of discomfort. In view of that and as a preliminary approach, the present work assumes that the occupant is an open system undergoing a steady flow process (e.g. a short-time exposure to a given ambient).

Human responses to thermal environments have been traditionally attributed to body interactions with four ambient parameters – air temperature and humidity, radiant temperature and air speed – combined to two personal parameters – human metabolism and clothing. These factors are then claimed to provide the six basic parameters defining human thermal environments (Fanger, 1970; Parsons, 1993) and, from the thermodynamic viewpoint, they refer to measurable physical quantities employed in the corresponding energy interactions calculations.

As suggested by Eq. (5), for practical purposes thermal interactions are grouped into heat losses due to respiration, heat losses occurring at the skin, metabolic heat production and mechanical (muscular) work. As a result, the right-hand side of Eq. (5) is rewritten as.

$$\dot{q}_{\text{met}} - \dot{w}_{\text{musc}} = \left(\dot{q}_{\text{evap,skin}} + \dot{q}_{\text{conv,skin}} + \dot{q}_{\text{rad,skin}}\right) + \left(\dot{q}_{\text{evap,resp}} + \dot{q}_{\text{conv,resp}}\right) \tag{10}$$

As implicitly assumed, conductive heat transfer is neglected for typical situations (Parsons, 1993) while radiative heat transfer has virtually no contribution to the respiration term since air is presumably transparent to thermal radiation.

It is worth recalling that evaporative heat losses $\dot{q}_{\text{evap,resp}}$ and $\dot{q}_{\text{evap,skin}}$ are inherently based on mass transfers to the ambient, which then behaves like an EMR. One could argue that an IMR should be attributed to water intake (as well as

food). Nonetheless, it seems reasonable to assume that it is precisely an excessive water loss as sweat, water vapor or moisture that helps to build up and/or enhance (thermal) discomfort.

As far as heat transfers are concerned, a TER is referred to each convective term $\dot{q}_{\text{conv,resp}}$ and $\dot{q}_{\text{conv,skin}}$. The later may "lump" the TER for thermal radiation $\dot{q}_{\text{rad,skin}}$ as corresponding heat losses from the skin are sometimes modeled into a single term. By the same token, an additional TER is assigned to the metabolic heat source term $\dot{q}_{\text{met}}$ whereas a MER is ascribed to the muscular power term $\dot{w}_{\text{musc}}$.

The proposed model framework is sketched in Fig. (1). As $\dot{q}_{\text{met}}$ is strictly positive, the direction of the associated heat flow is indicated by the arrow in Fig. (1). On the other hand, heat flow direction can be opposite with respect to the other two TER's depending on the temperature difference between ambient and occupant's (control mass) skin and core temperature. Furthermore, it is here assumed that the ambient and the occupant form an isolated system.

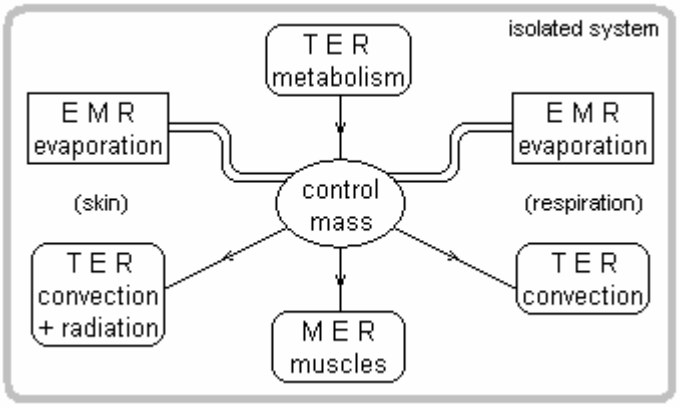

Figure 1. Thermodynamic model framework based on the heat balance equation for thermal comfort.

A classical approach for Eq. (10) has been proposed by Fanger (1970), also adopted by ASHRAE / ISO 7730, based on the following conditions: (*i*) the body is heat balance (i.e., body temperature is steady so that $dE_{\text{body}}/dt = 0$), (*ii*) sweat rate and (*iii*) mean skin temperature are within comfort limits. Employing the six fundamental parameters, the proposed equation for thermal comfort assessment is somewhat changed to:

$$\dot{q}_{\text{met}} - \dot{w}_{\text{musc}} = \dot{q}_{\text{vap,skin}} + \dot{q}_{\text{sw,skin}} + \dot{q}_{\text{conv,cl}} + \dot{q}_{\text{rad,cl}} + \dot{q}_{\text{evap,resp}} + \dot{q}_{\text{conv,resp}} \tag{11}$$

It is observed that heat transfers by convection or thermal radiation now include clothing interference while $\dot{q}_{\text{evap,resp}}$ was split into $\dot{q}_{\text{vap,skin}}$ = heat loss by water vapor diffusion through skin and $\dot{q}_{\text{sw,skin}}$ = heat loss by sweat evaporation from skin surface. Provided that units for all terms in Eq. (11) are W·m^{-2}, empirical correlations suggest that:

$$\begin{aligned}
\dot{q}_{\text{vap,skin}} &= 3.05[5.733 - 0.00699(\dot{q}_{\text{met}} - \dot{w}_{\text{musc}}) - P_{\text{sat,air}}] \\
\dot{q}_{\text{sw,skin}} &= 0.42[(\dot{q}_{\text{met}} - \dot{w}_{\text{musc}}) - 58.15] \\
\dot{q}_{\text{conv,cl}} &= f_{\text{cl}}\, h_{\text{conv}}\, (T_{\text{cl}} - T_{\text{air}}) \\
\dot{q}_{\text{rad,cl}} &= 3.96\times10^{-8}\, f_{\text{cl}}\, [(T_{\text{cl}} + 273)^4 - (T_{\text{rad}} + 273)^4] \\
\dot{q}_{\text{evap,resp}} &= 0.00173\, \dot{q}_{\text{met}}\, (5.867 - P_{\text{sat,air}}) \\
\dot{q}_{\text{conv,resp}} &= 0.0014\, \dot{q}_{\text{met}}\, (34 - T_{\text{air}})
\end{aligned} \tag{12}$$

In all previous equations, the sign convention follows the one adopted in Eqs. (1), in line with ASHRAE (2001), so that positive values correspond to heat losses from body to the environment. In those equations, $P_{\text{sat,air}}$ is water vapor partial pressure (kPa) at prevailing ambient air conditions while T_{air}, T_{rad} and T_{cl} are air, radiant and the so-called clothed-body surface temperatures (°C), respectively. The later depends, for example, on clothing insulation I_{cl} (in Clo units, 1 Clo = 0.155 m^2 K·W^{-1}) and it can be given by a quite lengthy expression:

$$T_{\text{cl}} = 35.7 - 0.0275\,(\dot{q}_{\text{met}} - \dot{w}_{\text{musc}}) - 0.155\, I_{\text{cl}}\, \{3.96\times10^{-8}\, f_{\text{cl}}[(T_{\text{cl}} + 273)^4 - (T_{\text{rad}} + 273)^4] + f_{\text{cl}} h_{\text{conv}}\, (T_{\text{cl}} - T_{\text{air}})\} \tag{13}$$

Convective heat transfer coefficient h_{conv} (W·m^{-2} K^{-1}) is given by:

$$h_{\text{conv}} = \max[2.38\,(T_{\text{cl}} - T_{\text{air}})^{0.25}\,, 12.1\sqrt{v}\,] \tag{14}$$

where v is air speed (m·s^{-1}). For a seated person, there are the following correlations, adapted from (Parsons, 1993):

$$h_{\text{conv}} = \begin{cases} 8.3\,v^{0.6} & , \quad 0.2 < v < 4.0 \\ 3.1 & , \quad 0 < v < 0.2 \end{cases} \tag{15}$$

Finally, the so-called clothing dimensionless area factor f_{cl} is given by:

$$f_{\text{cl}} = \begin{cases} 1.00 + 0.2\,I_{\text{cl}} & , \quad I_{\text{cl}} < 0.5 \text{ clo} \\ 1.05 + 0.1\,I_{\text{cl}} & , \quad I_{\text{cl}} > 0.5 \text{ clo} \end{cases} \tag{16}$$

while Parsons (1993) presents the following correlation

$$f_{\text{cl}} = 1 + 0.31\,I_{\text{cl}} \quad (I_{\text{cl}} \text{ in Clo units}) \quad \text{or} \quad f_{\text{cl}} = 1 + \frac{0.31}{0.155}\,I_{\text{cl}} \quad (I_{\text{cl}} \text{ in m}^2\,\text{K}\cdot\text{W}^{-1}) \tag{17}$$

Based on the prior heat balance equation, Eq. (11), its auxiliary empirical correlations, Eq. (12), and the proposed model framework, Fig. (1), irreversibilities (total exergy losses) related to human thermoregulation mechanisms can be assessed. Thus, applying Gouy-Stodola relation, Eq. (9), for an open system (occupant) undergoing a steady flow process, irreversibility rate can be generally assessed as (Kotas, 1985):

$$\dot{I} = T_0 \left[\sum_{\text{EMR}} \dot{m}_{\text{out}}\, s_{\text{out}} - \sum_{\text{IMR}} \dot{m}_{\text{in}}\, s_{\text{in}} - \sum_{\text{TER}} \frac{\dot{Q}}{T} \right] \tag{18}$$

where T_0 is the environment temperature (K), $\dot{m}$ and s stand respectively for mass flow (kg·s^{-1}) and specific entropy (J·K^{-1} kg^{-1}) of the related matter stream and $\dot{Q}$ is the thermal energy transferred through heat interaction with a given TER at temperature T. It is worth remembering that the above equation should be normalized to the total body surface area and also that no IMR is considered in the present analysis.

As previously mentioned, convective and radiative heat transfer from skin can be "lumped" into a single term. In order to do so, the later is linearized as follows:

$$\dot{q}_{\text{rad,cl}} = f_{\text{cl}}\, h_{\text{rad}}\, (T_{\text{cl}} - T_{\text{rad}}) \tag{19}$$

so that:

$$\dot{q}_{\text{conv,cl}} + \dot{q}_{\text{rad,cl}} = \dot{q}_{\text{c+r,cl}} = f_{\text{cl}}\, h_{\text{c+r}}\, (T_{\text{cl}} - T_{\text{ref}}) \quad , \quad h_{\text{c+r}} = h_{\text{conv}} + h_{\text{rad}} \quad \text{and} \quad T_{\text{ref}} = \frac{h_{\text{conv}} T_{\text{air}} + h_{\text{rad}} T_{\text{rad}}}{h_{\text{conv}} + h_{\text{rad}}} \tag{20}$$

For 'most typical indoor conditions', ASHRAE (2001) recommended value for the radiative heat transfer coefficient is $h_{\text{rad}} = 4.7$ W·m^{-2} K^{-1}.

In addition, two approaches could be followed for the irreversibility due to heat loss by mass transfer. One is to strictly use an EMR for all water losses through skin and lungs. In this case, one should be able to infer mass flows from Eqs. (11) and (12), using values from steam tables, i.e., vaporization enthalpy h_{fg} at the related skin and lung condition to be used with $\dot{q}_{\text{vap,skin}}$ and $\dot{q}_{\text{evap,resp}}$, respectively, and vapor enthalpy h_{f} for the skin-diffusion term $\dot{q}_{\text{sw,skin}}$. On the other hand, for the benefit of simplicity, one could ascribe a TER (at a suitable temperature T) for each aforementioned heat loss in order to be included into the last summation on the right-hand side of Eq (18). If the first approach is adopted along with the proposed linearization for the thermal radiation term, surface-normalized Eq (18) then results to:

$$\dot{I} = T_0 \left[\left(\dot{m}_{\text{vapor,skin}}\; s_{\text{g,skin}} + \dot{m}_{\text{sweat,skin}}\; s_{\text{f,skin}} + \dot{m}_{\text{moist,resp}}\; s_{\text{f,resp}} \right) - \left(\frac{\dot{q}_{\text{met}}}{T_{\text{core}}} - \frac{\dot{q}_{\text{c+r,cl}}}{T_{\text{rad}}} - \frac{\dot{q}_{\text{conv,resp}}}{T_{\text{air}}} \right) \right] \tag{21}$$

where the mass flows for water vapor, sweat (both from skin) and moisture (from lungs) are estimated as:

$$\dot{m}_{\text{vapor,skin}} = \frac{\dot{q}_{\text{vap,skin}}}{h_{\text{g,skin}}} \quad , \quad \dot{m}_{\text{sweat,skin}} = \frac{\dot{q}_{\text{sw,skin}}}{h_{\text{fg,skin}}} \quad , \quad \dot{m}_{\text{moist,resp}} = \frac{\dot{q}_{\text{evap,resp}}}{h_{\text{fg,resp}}} \tag{22}$$

4. Thermal sensation during transient process: prospective mathematical model

Because they are transient in nature, Parsons (1993) claims that thermal sensations cannot be experienced in steady-state conditions. For that reason, this paper also puts forward a mathematical model for the dynamic behavior (i.e. transient process) of the entropy generation (like the function S_{gen} used in OCTI calculations) and exergy loss referring to an occupant in a given ambient.

The model proposed in this work is an autonomous dynamic system which is non-linear with respect to variables $S = \Delta S$ (entropy generation) and $I = \Delta\Xi$ (total irreversibility = total exergy loss). Auxiliary parameters are also introduced (aiming at dimensional consistency) so that the following rate equations are put forward:

$$\begin{cases} \dfrac{\mathrm{d}I}{\mathrm{d}t} = f\left(I, S, \tau_1, \alpha_1, \beta_1\right) \\ \dfrac{\mathrm{d}S}{\mathrm{d}t} = g\left(I, S, \tau_2, \alpha_2, \beta_2\right) \end{cases} \Rightarrow \quad \begin{cases} \tau_1 \dfrac{\mathrm{d}I}{\mathrm{d}t} = I(1-\alpha_1 I) + \beta_1 IS \\ \tau_2 \dfrac{\mathrm{d}S}{\mathrm{d}t} = S(1-\alpha_2 S) - \beta_2 SI \end{cases} \tag{23}$$

where the time parameters τ_i are here taken as $\tau_1 = \tau_2 = 1$ (in time units), for the sake of simplicity. For consistency purposes, proportionality parameters dimensions are $[\alpha_1]$ = (exergy flux)$^{-1}$ = (energy flux)$^{-1}$ and $[\alpha_2]$ = (entropy flux)$^{-1}$ = clothing insulation, respectively, while for the other parameters $[\beta_1]$ = (entropy flux)$^{-1}$ = clothing insulation and $[\beta_2]$ = (exergy flux)$^{-1}$ = (energy flux)$^{-1}$, respectively.

With respect to the equation system, Eqs. (23), dI/dt represents the irreversibility (= exergy loss) variation rate. The first term on the right-hand side of this equation stands for a logistic behavior, suggesting a limited increase for I. The second cross-term contributes for irreversibility enhancement due to the presence of both I and S. Similarly, in the dS/dt equation for the variation rate of the entropy generation, the first term on the right-hand side also represents a limited augment for S, while the second cross-term contributes to the entropy generation increase due to both I and S.

From a qualitative study, four critical or equilibrium points are found, all belonging to the first quadrant: $(0,0)$, $(I_c,0)$, $(0,S_c)$ and (I_c,S_c). The origin, the second and third points are unstable because the related eigenvalues of the Jacobian are real and of opposite sign. They are referred to as nodal source points and they behave like repulsion points for nearby trajectories. The last critical point $(I_c,S_c) = \left(f_1(\alpha_1,\beta_1,\alpha_2,\beta_2), f_2(\alpha_1,\beta_1,\alpha_2,\beta_2)\right)$ is asymptotically stable and it is referred to as a nodal sink point (Jacobian eigenvalues are real and negative). If this later equilibrium point is identified to the comfort condition, then S_c and I_c correspond to thermal comfort levels (rates) of entropy generation and irreversibility, respectively. It should be noted that such values depend on α_i and β_i parameters to be introduced.

The behavior of solution trajectories $\left(I(t), S(t)\right)$ for transient processes (i.e., thermal sensations) is sketched in the phase plane in Fig. (2) (obtained through MATLAB 6.0). In other words, trajectories shown in Fig. (2) represent the evolution of both entropy generation and irreversibility during the process. One observes that trajectories approach the equilibrium point (I_c,S_c), with the tendency to move away from saddle points.

Critical points were calculated by attributing usual values to parameters characterizing a occupant-ambient system (i.e., human and environmental parameters). The model thus attempts to represent the dynamics of thermal sensation experienced by such isolated system. Adopted numerical values include α_1 = 1/0.8 Met^{-1} and β_2 = 0.8 Met (based on data for a person lying down and 1 Met = 58.15 W·m^{-2}) as well as β_1 = 0.30 Clo and α_2 =1/0.30 Clo^{-1} (based on data for typical tropical clothing outfit and 1 Clo = 0.155 m^2 K·W^{-1}).

In order to analyze the behavior of obtained trajectories, the phase plane is divided into four regions so that an initial condition (I_0,S_0) is assigned to each of them as presented in Tab. (1). It is then assumed that the occupant-ambient system is already defined so that point (I_0,S_0) represents occupant's initial state with respect to the variables I and S as well as to model parameters. Starting from the initial condition (I_0,S_0), Fig. (2) shows that trajectories asymptotically approach the comfort state given by equilibrium point (I_c,S_c), with distinct velocities. In what follows, the process behavior of both I and S variables is analyzed for different regions.

Table 1. Initial condition assignment to distinct sub-regions within the $I \times S$ phase plane.

Region I	Region II	Region III	Region IV
$S_0 > S_c$; $I_0 < I_c$	$S_0 > S_c$; $I_0 > I_c$	$S_0 < S_c$; $I_0 > I_c$	$S_0 < S_c$; $I_0 < I_c$

For example, if (I_0, S_0) belongs to region I, one observes that S decreases very fast (while I keeps a small value) down to a minimum value near to the repulsion point $(0, S_c)$. From this state on, both I and S asymptotically increase up to the point (I_c, S_c). Similarly, if the initial condition (I_0, S_0) belongs to region III, one verifies that I reduces down to a minimum value close to the repulsion point $(I_c, 0)$. Thereafter, both I and S asymptotically augment up to the comfort state point (I_c, S_c).

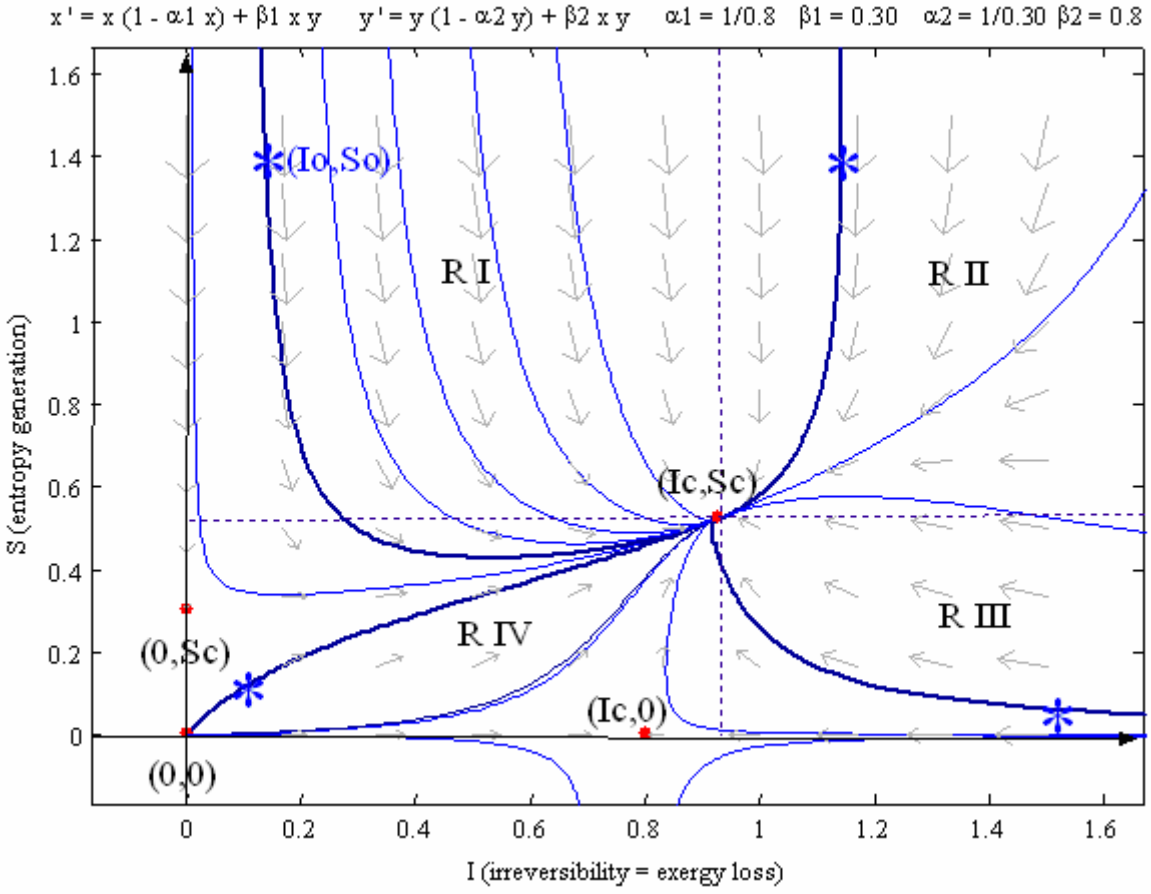

Figure 2. Trajectories in the phase plane obtained from the proposed model.

In region IV, it is worth discussing the distinct observed behavior. In this case, if the initial condition is close to the origin, then I and S have very small values. Trajectories show quite a uniform and asymptotic behaviour up to comfort point (I_c, S_c). It should be noted that in the proposed model both S and I never reach null values due to the repulsive nature related to the origin.

Mechanisms employing the model here proposed correspond to limited and symbiotic growth or decay. Behavior of entailed variables is of cooperative kind, i.e., the variation of one or another is such that both coexist along the time. Those variables undergo (process) variations so as to simultaneously reach a desired equilibrium state.

5. Closing remarks (towards future developments and model validation)

In order to survive, humans consume food, which is then converted into heat. As food seems to retain a higher level of organization (i.e., order) when compared to heat itself, one could claim that the human body has a low *mechanical* efficiency if heat should be considered a by-product from living cells. Such rationale can be misleading inasmuch as metabolically released heat is in fact crucial for life.

One could also postulate that natural selection applies to entropy-efficient or, alternatively, exergy-saving species. Irreversible phenomena do cause exergy losses, which in turn reduce process efficiency. As a consequence, there could be a shortfall of useful physiological effects or, rather, an increase of energy consumption (from whatever source such energy is derived) in order to have those biological effects suitably accomplished.

Energy balance for occupant's body is a necessary but not sufficient condition for thermal comfort as suggested, for example, by Fanger's predicted mean vote (PMV) definition. In addition, thermal feelings of hotness or coldness is a sensory experience (i.e. a psychological phenomenon), which is difficult to be defined on physical or physiological basis. Yet, it is recognized that environmental as well as personal conditions affect thermal sensation.

In thermoregulation, there has been some dispute about what is indeed the regulated variable and the list include all sort of temperatures (core, body, skin, brain), body energy content or heat outflow rate. As exergy function takes into account both ambient and occupant thermodynamic state parameters, it could be another promising "contender" in the above roll. At least, it has the ability to quite equally assess both extremes of thermal sensation and thermal comfort, namely, from uncomfortably cold up to uncomfortably hot.

The present work has presented and discussed concepts and directions which are believed to provide groundwork for the definition of a prospective exergy or irreversibility-based thermal comfort (or stress) index. The underlying question is whether or not the human body is sensible to irreversibilities (= exergy losses) as far as thermoregulatory mechanisms are concerned.

It is here presumed that steady-state thermal comfort could be probably identified to a minimum (= comfortable) irreversibility rate with respect to the prevailing ambient and occupant behavior. Means to validate (or not) all previous assumptions could include the comparison of results yielded from such exergetic analysis to those obtained based on well-established thermal comfort indexes as the PMV itself, which is in fact presently under way.

Concerning the transient model, depicted in Fig. (2), each solution trajectory can be attributed to thermodynamic state of the system, which evolves from an extreme (initial state) to another (steady-state), going through thermal comfort state. The later could eventually coincide with the final steady-state, as it occurs to most of trajectories in region II. On the other hand, trajectories in region I (for low *I* values) are observed to achieve a minimum point before reaching steady-state. In other instances, like trajectories in regions III and IV, thermal comfort state may correspond to the respective minimum point, which does not necessarily match with the steady-state for some trajectories.

6. References

ASHRAE – American Society of Heating, Refrigeration and Air-Conditioning Engineers, 2001, "Fundamentals Handbook", Chapter 8, Atlanta, USA.

Bligh, J., 1985, "Regulation of body temperature in man and other mammals", IN: Shitzer, A., Eberhart, R.C. (eds.), "Heat Transfer in Medicine and Biology", Plenum Press. New York, USA.

Boregowda, S.C., Tiwari, S.N., Chaturvedi, S.K., 2001, "Entropy generation method to quantify thermal comfort". Human Performance in Extreme Environments, vol. 6, n. 1, pp. 40-45.

Fanger, P.O., 1970, "Thermal Comfort", McGraw-Hill, New York, USA.

Guyton, A.C., 1995, "Textbook of Medical Physiology", W. B. Saunders, Philadelphia, USA.

Kotas, T.J., 1985, "The Exergy Method of Thermal Plant Analysis", Butterworths, London, UK.

Mammana, C.Z., 1981, "A filosofia natural da informação", Revista Brasileira de Tecnologia, vol. 12, n. 1, pp. 54-65.

Nishi, Y., 1981, Measurement of thermal balance of man, IN: Cena, K., Clark, J.A. (eds.), "Bioengineering thermal physiology and comfort", Elsevier, New York, USA.

Parsons, K.C., 1993, "Human Thermal Environments", Taylor & Francis, London, UK.

Prek, M., 2004, "Exergy analysis of thermal comfort", International Journal of Exergy, vol. 1, n. 3, pp. 303-315.

Szargut J., Morris, D.R., Steward, F.R., 1988, "Exergy Analysis of Thermal, Chemical and Metallurgical Process", Hemisphere, New York, USA.

7. Copyright Notice

Proceedings of the 11th Brazilian Congress of Thermal Sciences and Engineering -- ENCIT 2006
Braz. Soc. of Mechanical Sciences and Engineering -- ABCM, Curitiba, Brazil,- Dec. 5-8, 2006

Paper CIT06-596

OPTIMAL DESIGN OF NON-NEWTONIAN, MICRO-SCALE VISCOUS PUMPS FOR BIOMEDICAL DEVICES – PRELIMINARY RESULTS

Alexandre K. da Silva
Department of Mechanical Engineering, University of Hawaii – Manoa, 2540 Dole St., Holmes Hall 302, Honolulu, HI 96822, USA
e-mail: akds@hawaii.edu

Marcelo H. Kobayashi
Department of Mechanical Engineering, University of Hawaii – Manoa, 2540 Dole St., Holmes Hall 302, Honolulu, HI 96822, USA
e-mail: marcelok@hawaii.edu

Carlos F. M. Coimbra
Department of Mechanical Engineering, University of Hawaii – Manoa, 2540 Dole St., Holmes Hall 302, Honolulu, HI 96822, USA
School of Engineering, University of California, P.O. Box 2039, Merced, CA 95344, USA
e-mail: coimbra@hawaii.edu

Abstract. *The present paper addresses the numerical optimization of geometrical parameters of non-Newtonian micro-scale viscous pumps for biomedical devices. The objective is to maximize the mass flow rate per unit of shaft power consumed by the rotor when an external pressure load is applied along the channel that houses the rotor. Two geometric parameters are considered in the optimization process: (i) the height of the channel that houses the rotor (H) and (ii), the eccentricity (ε) of the rotor. Three different micro scale viscous pump configurations were tested: a straight housed pump (I-shaped housing) and two curved housed pumps (L- and U-shaped housings). The stress-strain constitutive law is modeled by a power-law relation. The results show that the geometric optimization of micro scale viscous pumps is critical since the mass flow rate propelled by the rotor is highly dependent on ε and H. Numerical simulations indicate that mass flow rate is maximized when $\varepsilon \sim 0$, namely when the rotor is placed at a distance of 0.05 radii from the lower wall. The results also show that micro scale viscous pumps with curved housing provide higher mass flow rate per unit of shaft power consumed when compared with straight housed pumps. The results are presented in terms optimized dimensions of all three configurations (i.e., H_{opt} and ε_{opt}) and for values of the power-law index varying between 0.5 (shear thinning fluids) and 1.5 (shear-thickening fluids).*

Keywords*. Micro-Scale Viscous Pumps, Optimal Design, MEMS, Biomedical Pumps, Non-Newtonian Flow.*

1. Introduction

Advances in the miniaturization of electro mechanical systems have enabled the fabrication of microsystems or microelectromechanical systems (MEMS), which offer several advantages over conventional devices. These advantages include superior resolution, precision and sensitivity, lower costs, and reliability due to redundancy. In biological applications there is also the possibility of incorporating sensing, processing, and actuation nearby or on the same substrate – see the recent reviews on MEMS Judy (2001) and Ziaie *et al.* (2004). Because of their physical and engineering significance as well as the relevance of their applications, micropumps have figured prominently among the development of MEMS.

Micropumps, broadly defined as having dimensions smaller than 100 μm, have a myriad of applications ranging from micro total analysis systems (μTAS) Reyes *et al.* (2002), Verpoorte (2002) and Auroux *et al.* (2002), to mass spectrometer systems and micro propulsion in space exploration Micci and Ketsdever (2000). Micro total analysis systems or "lab on a chip", whose primary research works aim at biological and life sciences, is expanding rapidly. Indeed, labs on a chip have been successfully used, for instance, in the culture and handling of cells, DNA separation and analysis, DNA sequencing, chiral separation of amino acids, antibody analysis, determination of active ingredients in a drug, determination of the presence of explosive compounds and polymerase chain reaction – see the reviews Reyes *et al.* (2002) and Verpoorte (2002). Common to all these devices is the need to pump fluid at flow rates of up to 1000 milliliter per minute through dimensions of the micro or nano scales.

Contrary to microelectronics, that succeeded in scaling down its transistors and systems to provide faster and cheaper devices, pumping does not, as a rule, benefit from miniaturization. Actually, ordinary inertia based devices, such as centrifugal pumps, do not work at the very low Reynolds number commonly associated with the micropumping requirements. Instead, effective micropumps have fallen in one of the following two main categories: the positive-displacement or reciprocating pumps and the dynamic or continuous flow pumps – see the recent reviews Nguyen (2002), Laser and Santiago (2004) and Woias (2004).

Typically, reciprocating micropumps use pulsating surface motion to displace the fluid by pressure work. By contrast, the physical-chemical and design principles involved in the continuous flow micropumps vary profusely. They include ultrasonic, electrohydrodynamic, electroosmotic, magnetohydrodynamic or electrochemical actuation. These

micropumps do function but require sophisticated fabrication processes and involves complex sealing problems – see the referred reviews for details. Sen *et al.* (1996) proposed a rotating micropump, where the relatively large viscous forces at these small scales are used to drive the fluid.

The viscous micropump combines the simplicity in design with effectiveness in pumping. Roughly speaking, the viscous micropump consists of a cylinder asymmetrically placed inside a micro-channel. The need for the rotor asymmetry can be understood, for instance, by considering an I-shaped micropump with no pressure load across the channel. If the rotor is located at the center of the channel, symmetry leads to zero net flow, regardless of the direction in which the rotor spins. However, if the symmetry is broken and the rotor is placed, say, closer to the top wall, as a clockwise rotor spins a net flow from the right to the left is generated. In this case, the symmetry break provides a preferential direction due to the increase in the shear between the fluid and the upper wall.

After its introduction in 1996, the viscous micropump has been the subject of a stream of publications including Sharatchandra *et al.* (1997), Sharatchandra *et al.* (1998), DeCourtye *et al.* (1998), Abdelgawad *et al.* (2004), Gad-el-Hak (1999), Abdelgawad *et al.* (2005) and da Silva *et al.* (2006). These authors examined various design features and fundamentals issues associated with such micropumps, including the effects of channel height, rotor eccentricity and angular velocity on the pump performance Sen *et al.* (1996), slip velocity Sharatchandra *et al.* (1997), thermal effects Sharatchandra *et al.* (1998), transient effects Abdelgawad *et al.* (2004), multistage configurations Abdelgawad *et al.* (2005) and power consumption and novel geometries da Silva *et al.* (2006). Although extensive and detailed, all previous reports have worked with Newtonian fluids.

In the face of the above, the main objectives of the present work are twofold: to determine the optimal geometrical parameters (i.e., channels thickness and rotor eccentricity) that result in maximum mass flow rate per unit of power shaft consumed, for non-Newtonian fluids, and to introduce and analyze the performance, again for non-Newtonian fluids, of our novel L- and U-shaped micropumps (da Silva *et al.* 2006) when compared with the traditional I-shaped design pioneered by Sen *et al.* (1996). Non-Newtonian fluids abound in Nature – the most notorious example in biomedical applications being blood. A simple non-Newtonian constitutive law is the so-called power-law model that postulates a power-law dependence of viscosity on the strain-rate. This model provides a good approximation of the stress-strain relationship for some biological fluids, including the whole human blood Walburn and Schneck (1976). In the present work we investigate the micro-pump design for blood flow as well as general bio-fluids that can be approximated by the power-law model.

The paper is organized as follows: in §2 we describe the micropump configuration and the numerical modeling. After that, in §3 we validate our numerical results by comparing our present results with the results reported by Sharatchandra *et al.* (1997) and Abdelgawad *et al.* (2004) for Newtonian fluids, and also with an analytical solution for a Non-Newtonian fluid. With the validated model we proceed with the definition of the figure of merit and optimization procedure: in §4 for blood flows and in §5 for general power-law fluids. In the last section §6 we sum up the main findings of this work.

2. Geometrical and Numerical Modeling

Consider the three micropump configurations shown in Fig. 1, where D represents the diameter of the rotor, L_u and L_d are the lengths of the upstream and downstream conduit channels and H is the height of the conduit channel. Due to viscous diffusion, the clockwise-turning rotor impels the fluid from left to right against an imposed pressure difference $\Delta P = P_H - P_L$.

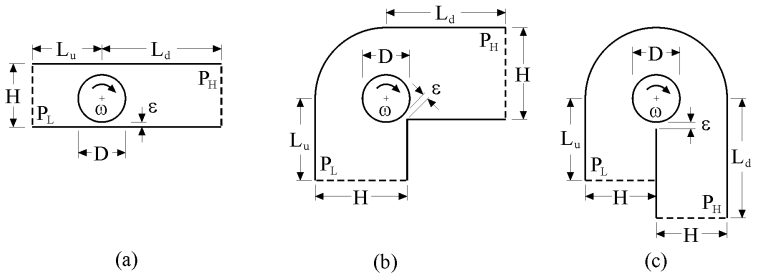

Figure 1. Numerical domain of a viscous micro pump: (a) I-shaped channel, L-shaped channel and U-shaped channel.

Because the effectiveness of a viscous micropump is associated with the eccentricity of the rotor with respect to the surrounding walls, we introduce a linear dimension ε that measures the distance between the lower wall and the rotor (see Fig. 1). For all three configurations, $\varepsilon = 0$ means that the rotor touches the lower wall not allowing any fluid flow between the lower wall and the rotor. If $\varepsilon > 0$, the rotor does not touch the lower wall and fluid is allowed to flow between the rotor and the adjacent surfaces. Finally, $\varepsilon < 0$ means that the rotor is partially embedded in the lower wall. Taking D as our length scale, the dimensionless geometrical parameters can be written as

$$(H, L_u, L_d, \varepsilon)^* = (H, L_u, L_d, \varepsilon)/D \tag{1}$$

The fluid is considered to be non-Newtonian, with a viscosity given by the power-law model

$$\eta = m\,\dot{\gamma}^{n-1} \tag{2}$$

where m and n are the consistency coefficient and the power law index respectively, and $\dot{\gamma}$ is the shear rate, which reads as

$$\dot{\gamma} = \nabla\vec{V} + \nabla\vec{V}^{T} \tag{3}$$

Because of the slow character for the flow, no instabilities are expected and the flow is assumed steady, laminar and incompressible. We define the following dimensionless variables

$$(u, v)^{*} = (u, v)/(\omega\, D/2),\ P^{*} = (P_H - P_L)/[m(\omega\, D/2D)^{n}) \tag{4}$$

and write the dimensionless governing equations as

$$\nabla\cdot\vec{V}^{*} = 0\,, \tag{5}$$

$$\mathrm{Re}_D\,(\vec{V}^{*}\cdot\nabla)\vec{V}^{*} = -\nabla P^{*} + \nabla\cdot\eta[\nabla\vec{V}^{*} + (\nabla\vec{V}^{*})^{T}]\,, \tag{6}$$

where $\mathrm{Re}_D = \rho(\omega\, D/2)^{2-n}\, D^{n}/m$ is the Reynolds number based on the rotor angular velocity and diameter.

Three different micro scale viscous pump configurations were considered: (i) a straight or I-shaped pump, (ii) a L-shaped pump and (iii), a U-shaped pump. The numerical domain is shown directly in Fig. 1 as the area surrounded by the dashed lines at the inlet and outlet, and the solid lines which guide the flow from the inlet to the outlet. The area of the rotor is not accounted for in the numerical simulations.

The flow boundary conditions are: $P^{*} = P_L{}^{*} = 0$ at the inlet and $P^{*} = P_H{}^{*}$ at the exit plane, where $P_H{}^{*} = \Delta P^{*} - P_L{}^{*}$. The pressure boundary condition at the inlet and outlet is implemented as $\mathbf{n}\cdot\mathbf{T} = -P_L$ at the inlet and $\mathbf{n}\cdot\mathbf{T} = -P_H$ at the outlet, where $\mathbf{T} = \sigma\mathbf{n}$ is the stress vector and σ is the Stokes stress tensor $\sigma = -p\mathbf{I} + \nu\,(\nabla\mathbf{u} + \nabla\mathbf{u}^{T})$. In addition, the tangential components of the velocities are set to zero (i.e., $\mathbf{t}\cdot\mathbf{u} = 0$) at the inlet and outlet of the micropump. Non-slip velocity conditions were used in all internal surfaces of the channel. The velocity of the rotor surface is maintained constant at $U = \omega\, D/2$ for each run. We adopted zero tangential velocities at the inlet and outlet after many numerical tests indicated that fully developed flow conditions at the inlet and outlet were obtained for values of L_u and L_d of the order of 4D when n = 1. However, due to the non-linear variation of the moment diffusion given by the power-law relation of Eq. (2), in all numerical simulations starting in Fig. 4, L_u and L_d were set equal to 4D and 12D respectively.

Our numerical simulations were performed using the Finite Elements Method toolbox COMSOL Multiphysics®, v. 3.2 from COMSOL, Inc. Second and first order Lagrange $\mathbf{P_2}$-$\mathbf{P_1}$ mixed finite-elements were used. The mesh density was exhaustively tested in order to guarantee that the results were mesh-independent (the mesh density accuracy test is omitted for brevity). For all three configurations of Fig. 1, the optimal number of elements is between 5000 and 10000 when the objective is to calculate the average flow velocity, which are distributed unevenly through the numerical domain (i.e., a denser mesh is applied to the surroundings of the rotor). When the computation of the group $W'^{*}/\mathrm{Re}_D{}^{2}$ is required, an even higher concentration of elements was used around the rotor, which increases the total number of elements to over 15000 on average, depending on the channel height.

The solution was obtained with a stationary non-linear solver based on a damped Newton's Method. The relative error convergence criterion is the weighted Euclidian norm defined as

$$\mathrm{err} = \left[\frac{1}{N}\sum_{i}\left(\frac{|E_i|}{W_i}\right)^{2}\right]^{1/2} \tag{7}$$

where N is the number of degrees of freedom, $\mathbf{E}_i$ is the estimated error of a current solution vector $\mathbf{U}_i$, defined as: $\mathbf{E}_i = -f(\mathbf{U}_i)/\,f'\,(\mathbf{U}_{i-1})$, and $W_i = \max(|\mathbf{U}_i|, \mathbf{S}_i)$ are the weighted factors. The $\mathbf{S}_i$ factor is defined as the product of a constant, in this case 0.1, times the average of all $|\mathbf{U}_j|$ for all the degrees of freedom named 'j'. The damping factor was set initially equal to 10^{-4} and the convergence criterion was set equal to 10^{-6}.

3. Validation of the Method

The validation of the numerical code started by setting the power-law index equal to the unit (i.e., n = 1) in order to compare the present data against previous results obtained by Sharatchandra *et al.* (1997) and Abdelgawad *et al.* (2004). The comparison evaluated the effect of the channel height on the average fluid velocity ($\bar{u}$) at the exit plane between

the present results and the results obtained by Sharatchandra *et al.* (1997), considering $Re_D = 1$, $\Delta P^*=1$, and $\varepsilon_{mod} = 0.25$, where the average fluid velocity is defined as

$$\bar{u}= H^{-1}\int_0^H u(y)dy, \tag{8}$$

and the modified eccentricity of the rotor (ε_{mod}) is defined as,

$$\varepsilon_{mod} = 0.5(H^* - 1) - \varepsilon^*, \tag{9}$$

where ε^* is the dimensionless eccentricity defined in Eq. (1). A comparison, which is omitted for brevity, shows an acceptable overall agreement between the present results and the results of Sharatchandra *et al.* (1997), where differences smaller than 2% on average is observed.

Figure 2 shows the direct comparison between the average flow velocity data obtained in present study and the results from Sharatchandra *et al.* (1997) and Abdelgawad *et al.* (2004) for an I-shaped viscous micropump versus the group $\varepsilon_{mod}/\varepsilon_{max}$, where ε_{max} represents the design where the rotor is placed at a distance of 0.05 radii from the lower wall. The Reynolds number (Re_D) and the pressure load (ΔP^*) were set equal to the unit. Two values of the channel thickness were considered: $H^* = 1.5$ and 2.5. According to Fig. 2, a nearly prefect agreement between our results and the results of Sharatchandra *et al.* (1997) is obtained throughout the whole of $\varepsilon_{mod}/\varepsilon_{max}$ considered.

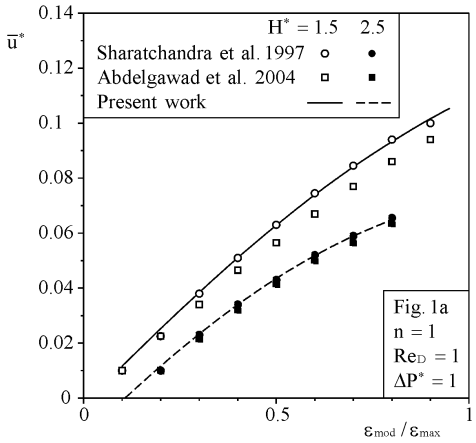

Figure 2. a) Validation of the numerical implementation for a Newtonian fluid.

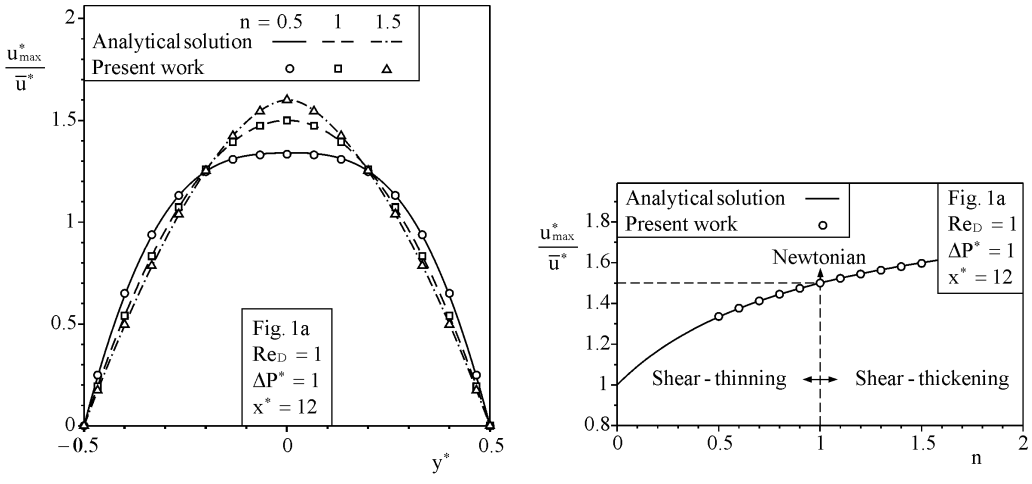

Figure 3. a) Validation of the channel flow fully developed velocity profile for three types of fluids: (a) shear thinning (n = 0.5), (b) Newtonian (n = 1) and (c) shear thickening (n = 1.5). (Left frame)
b) Comparison between the analytical and numerical ratio ($u^*_{max}/\bar{u}^*$) for $0.5 \le n \le 1.5$. (Right frame)

In the next step, Fig. 3a, we compare the effect of the power-law index on the fluid velocity profile for the micro pump shown in Fig.1a. The longitudinal location selected is located at 4D's of the channel exit plane (i.e., $x^* = 12$). The fully developed velocity profile reads as Bird *et al.* (2001)

$$\frac{u}{U_{mean}} = \frac{(1+2n)}{(1+n)}\left[1 - \left(\frac{y^*}{2}\right)^{1+1/n}\right], \tag{10}$$

where y^* indicates the dimensionless distance measured from the center of the channel. Figure 3a shows a perfect agreement between Eq. (10) and the numerical results for three values of n: 0.5, 1 and 1.5, which not only verifies that the flow is fully developed before the end of the channel, but also reinforces the zero tangential components of the velocities at the exit plane (i.e., $(\mathbf{t} \cdot \mathbf{u}) = 0$). Finally, we reach the code validation closure by comparing the ratio $u(y^* = 0)/U_{mean}$ between the numerical results and Eq. (10) for several values of n. Similarly to the comparison presented in Fig. 3a, Fig. 3b depicts a perfect agreement between analytical and numerical solution. One should note that, when n = 1 (i.e., Newtonian fluid), that ratio $u(y^* = 0)/U_{mean}$ returns the well-known value of 3/2 for a fully developed flow between parallel plates.

4. Blood Flow

As previously stated, the present study has two main objectives: (i) to determine the optimal geometrical parameters (i.e., channels thickness H^* and rotor eccentricity ε^*) that result in maximum mass flow rate ($\dot{m}^*$), and (ii), to study the performance of our newly proposed L and U-shaped micropumps when compared with the traditional I-shaped design pioneered by Sen *et al.* (1996) while working with non-Newtonian fluids. The mass flow rate per unit of length is defined as

$$\dot{m}^* = \bar{u}\, H^*. \tag{11}$$

In the first round of optimization (Figs. 4-6), no constraints were considered and the optimal geometric dimensions (i.e., channels thickness H^* and rotor eccentricity ε^*) were determined based on parameters such as Re_D and n. In this scenario, the optimization opportunity emerges from the fact that a micro scale viscous pump operates based on two main conditions: (i) the need of a certain level of confinement (i.e., a finite value for H^*) and (ii), the asymmetric placement of the rotor inside the channel.

The existence of the optimum geometry can be understood by noting that, in the limit of large channel height, the fluid average velocity tends to zero and consequently, the mass flow rate also approaches zero. In the other limit of 'small' values of the dimensionless channel thickness, it is clear that the flow is constricted between the rotor and the upper wall of the pump's channel, which also reduces the mass flow rate. Based on the above, an optimal value for the channel height such that the mass flow rate is maximized must exist; see da Silva *et al.* (2006). Moreover, changing the eccentricity and channel height strongly affects the power consumption of the micropump, leading to an optimum design constrained to power consumption.

4.1 Optimal Design of an I-Shaped micropump

The search for the optimal geometrical configuration started with the simplest design possible, Fig. 1a. The fluid is assumed non-Newtonian with a power-law index of n = 0.785, which according to Walburn and Schnech (1976), presents a good fit for human blood. In this case, we have two degrees of freedom, the channel thickness H^* and the eccentricity ε^*. Assuming fixed values for ε^*, Re_D and ΔP^*, we were able to find an optimal value for the channel height H^* that maximizes the average flow velocity ($\bar{u}$) and the mass flow rate ($\dot{m}^*$) just by varying H^*. Figure 4 shows that the channel thickness has a strong effect on $\bar{u}$ and $\dot{m}^*$, which strengthens the need for optimizing geometric parameters in a viscous micropump. Figure 4 also shows that different values of the optimal channel height (H^*_{opt}) are needed to maximize $\bar{u}$ and $\dot{m}^*$. Also interesting is the differentiated effect of non-optimal channel height on $\bar{u}$ and $\dot{m}^*$. According to Fig. 4, the selection of a channel height smaller than H^*_{opt} is much more detrimental to $\bar{u}$ and $\dot{m}^*$ when compared to a channel height in which $H^* > H^*_{opt}$.

Figure 5a shows the effect of the rotor eccentricity on the mass flow rate and average fluid velocity for an I-shaped pump with the following operating conditions: $Re_D = \Delta P^* = 1$. Each one of the open symbols shown in Fig. 5a represents the maximum value of $\dot{m}^*$ (squares) and $\bar{u}$ (circles) the can be obtained for a given value of ε^*. That is because, implicit in each symbol, is the optimization of $\dot{m}^*$ and $\bar{u}$ with respect to the channel thickness H^*, which is shown later in Fig. 5b. According to Fig. 5a, the maximum values of $\dot{m}^*$ and $\bar{u}$ are found around $\varepsilon^*_{opt} \sim 0$, which represent the maximum mass flow rate and average flow velocity optimized with respect to two degrees of freedom, ε^* and H^*. Furthermore, Fig. 5a also reveals that, differently from Fig. 4, where values of H^* smaller than H^*_{opt} were more detrimental to our two figures of merit (i.e., $\dot{m}^*$ and $\bar{u}$), in Fig. 5a, the eccentricity ε^* also plays a major role on $\dot{m}^*$ when $\varepsilon^* \neq \varepsilon^*_{opt}$, specially if $\varepsilon^* > \varepsilon^*_{opt}$. On the other hand, Fig. 5a shows that it maybe desirable to have $\varepsilon^* < \varepsilon^*_{opt}$ (i.e., the rotor partially embedded in the lower wall) due to the weak effect of the negative eccentricities on the average flow velocity.

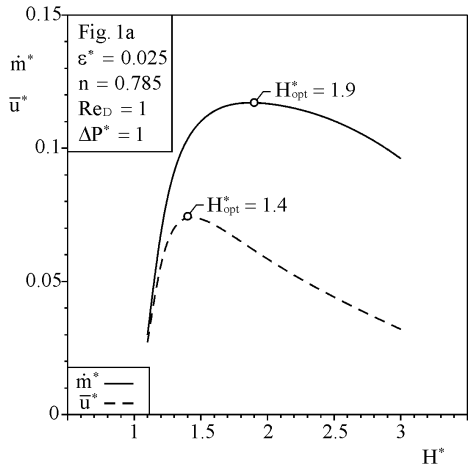

Figure 4. a) Effect of the of the channel height on the average fluid velocity and mass flow rate.

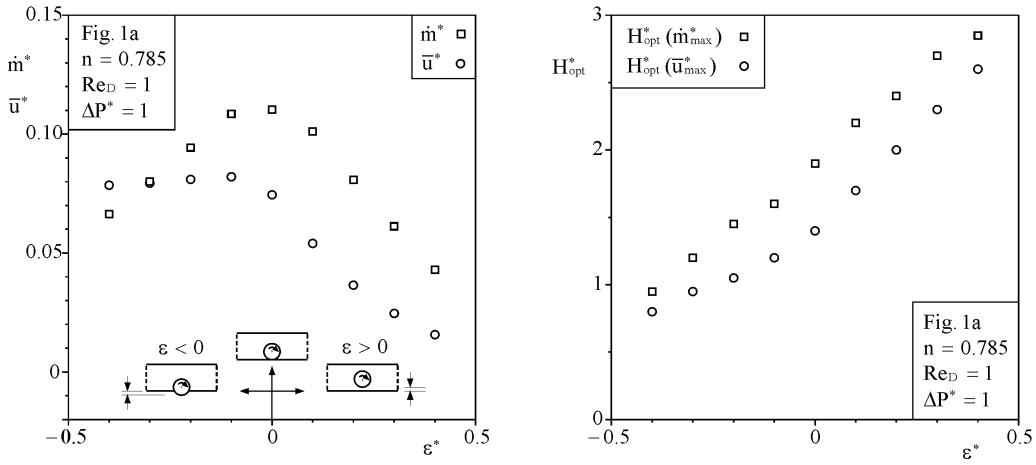

Figure 5. a) Effect of the rotor eccentricity on the maximized average fluid velocity and mass flow rate for the viscous micropumps given in Fig. 1a. (Left frame)
b) Effect of the rotor eccentricity on the optimal channel height for the viscous micropumps. (Right frame)

Figure 5b shows the effect of the eccentricity ε^* on the optimal channel height H^*_{opt}. According to Fig. 5b, H^*_{opt} increases monotonically with ε^*, which can be explained based on the required asymmetric placement of the rotor inside the channel (see §4). This means that any increment in ε^* is associated with an increment in H^*_{opt} so that a certain level of asymmetry can be sustained.

4.2 Curved Housed Micro Pumps

So far, we have demonstrated that significant improvement in terms of mass flow rate can be achieved with the correct selection of the channel height of an I—shaped pump. Next, we attempt to improve the already optimized micropump by aligning the housing of the pump with the rotor. As a results, two new micropump configurations are proposed: and L-shaped pump (Fig. 1b) and a U-shaped pump (Fig. 1c). The performances of the three configurations are presented not only in terms of maximum mass flow rate ($\dot{m}^*_{max}$) and optimal channel height (H^*_{opt}), but also in terms of the shaft power demanded by the rotor (W'^*). The relevance of the shaft power demanded by the rotor originates from the need to compare the performance of microscale pumps on similar basis (i.e., mass flow rate generated per unit of shaft power consumed). We start by defining the rotor's moment coefficient as

$$M = -\int_0^{2\pi} \tau \, d\theta \, . \tag{12}$$

Next, knowing that the torque per unit of length applied to rotor is $T' = M\, 2\pi\, R^2$ and that shaft power per unit of length is $W' = T\, \omega$, one can define the dimensionless shaft power per unit of length applied at the rotor as

$$W'^{*} = \frac{W'}{(m\,V^{n-1}/D^{n-1})^3/(\rho\,D)^2} = M^{*}\,Re_D^2\,. \tag{13}$$

In order to validate our numerical code, a preliminary data obtained for the dimensionless shaft power was compared against the numerical results obtained by Abdelgawada *et al.* (1997) in the steady state limit, since they performed a transient analysis of a Newtonian fluid. One should note that Abdelgawada *et al.* (1997) defined the rotor eccentricity as

$$\varepsilon_{mod,1} = 1 - 2\varepsilon^{*}/(H^{*} - 1)\,. \tag{14}$$

A comparison of the dimensionless shaft power per unit of length applied at the rotor, which is omitted for brevity, shows an acceptable overall agreement between the present results and the results of Sharatchandra *et al.* (1997), where differences smaller than 2% on average is observed.

Figure 6a depicts the effect of the shape of the micropump housing on the maximized figure of merit ($\dot{m}^{*}_{max}$), on the optimal channel height (H^{*}_{opt}) and on the shaft power requirement for a blood–like fluid (i.e., n = 0.785). According to Fig. 6a, the maximized mass flow rate, which is shown by the open bars, increases from left to the right. Furthermore, the shaft power demanded by the rotor decreases in the same direction, which indicates that the overall performance of micropumps (i.e., mass flow rate per unit of shaft power consumed) increases as the shape of housing approaches the shape of rotor. The draw back of micropump with curved housings (e.g., Fig. 1b and 1c) is that they require larger channel heights in order to operate optimally when compared with straight housed pumps (Fig. 1a). This can be observed in Fig. 6a by noticing that H^{*}_{opt} increases from the left (Fig. 1a) to the right (Fig. 1c).

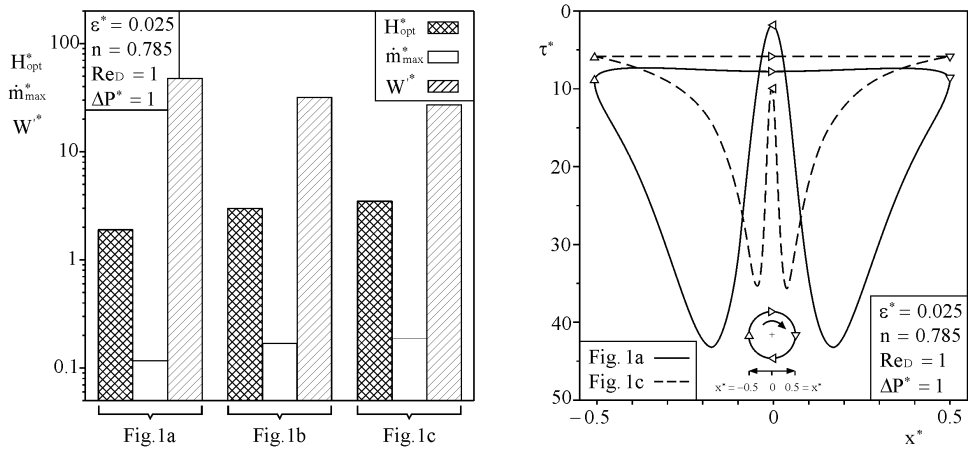

Figure 6. a) Effect of the shape of the micropump on the maximized mass flow rate, optimal channel height and shaft power demanded for a blood-like fluid (Left frame).
b) Effect of the shape of the micropump on the shear distribution over the rotor for a blood-like fluid (Right frame).

Figure 6b shows the shear distribution over the rotor's surface for an I-shaped pump (solid line) and a U-shaped pump (dashed line). One should notice that each one of the two curves is composed by four shear-distribution segments, which are separated by open triangles with different orientations. The triangle orientation coincides with the rotor's surface velocity vector as indicated in the rotor shown in the lower half of the figure. For instance, one can see that the shear distribution on the upper half on the rotor in mostly flat for and U-shaped micropump. Also, because the slow character of the flow, a symmetric shear distribution upstream and downstream can be seem around the rotor's center for both types of micropump. Furthermore, it is important to observe that the integral of the shear around the rotor's surface represents the shaft power required by the rotor divided by Re_D^2. This means that the difference in terms of shaft power demanded shown previously in Fig. 6a between the I-shaped and the U-shaped pumps is mostly due to the reduction of the shear around the lower half of the rotor. It is also note worthy that the alignment of the flow with the rotor provided by the U-shaped housing is also partially responsible for reducing the total required torque required by the rotor, since it brings the shear distribution of the upper half of rotor closer to the zero-shear ordinate when compared with an I-shaped housing as shown in Fig. 6b.

4.3 Optimal Design of U-Shaped Housing

In this section we search for even higher levels of performance of U-shaped pumps by studying the effect of the asymmetric placement of the rotor within micropump housing. As shown in Fig. 7a and 7b, the rotor now is free to

move vertically (ε_v^*) and horizontally (ε_h^*), where ε_v^* and ε_h^* represent respectively the vertical and horizontal distances between the center of the rotor and the center of the housing. These two variables can assume positive or negative values. For instance, Fig. 7a presents a configuration where both vertical and horizontal eccentricities are positive, and in Fig. 7b, both eccentricities are negative. Mixed combinations of positive eccentricities are also permitted. The objective is to analyze the effect of ε_v^* and ε_h^* on the mass flow rate. In order to reduce the number of degrees of freedom, the total channel height in constrained at $H_{tot}^* = 7$, which is twice as large as the optimized height of a U-shaped micropump shown previously in Fig. 6a for the same operating conditions ($Re_D = \Delta P^* = 1$ and $\varepsilon^* = 0.025$), where $\varepsilon_v^* = \varepsilon_h^* = 0$ (i.e., $H_{opt,in}^* = H_{opt,out}^* = H_{tot,opt}^*/2 = 3.5$). The fluid viscosity follow the power-law index suggested by Walburn and Schnech (1976), where n = 0.785.

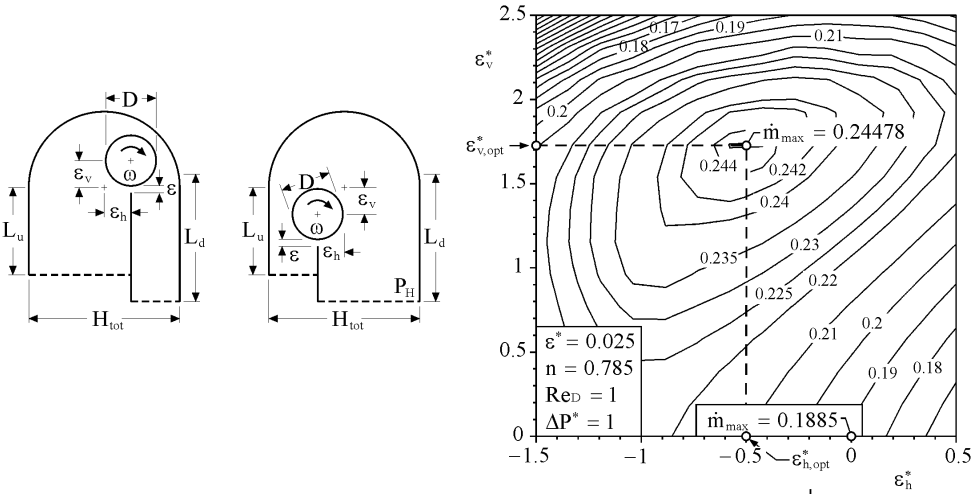

Figure 7. a) U-shaped viscous micropump with an asymmetric rotor, $\varepsilon_h > 0$ and $\varepsilon_v > 0$ (Left frame).
b) U-shaped viscous micropump with an asymmetric rotor, $\varepsilon_h < 0$ and $\varepsilon_v < 0$ (Middle frame).
c) Effect of the vertical and horizontal eccentricity on the mass flow rate (Right frame).

Figure 7c shows a contour plot that has as ε_v^* as ordinate and ε_h^* as abscissa. The curves represent constant mass flow rate designs given by a combination of the two degrees of freedom ε_v^* and ε_h^*. At a location $\varepsilon_v^* = \varepsilon_h^* = 0$, one can observe the maximum mass flow rate offered by a symmetrical configuration. The same value (i.e., $\dot{m}_{max}^* = 0.1885$) can be seen in Fig. 6a. Once ε_v^* and ε_h^* are added as degrees of freedom, the iso-mass flow rate curves show that higher levels of performance can be reached when the rotor is positioned at $\varepsilon_v^* \cong 1.72$ and $\varepsilon_h^* \cong -0.5$. The difference in performance between the two configurations is of the order of 30%. Also interesting is the fact that, because the total channel height is constrained ($H_{opt}^* = 7$), the maximum distance between the rotor's surface and the curved housing of the micropump is 3 dimensionless units, which happens when $\varepsilon_v^* = \varepsilon_h^* = 0$. For instance, if $\varepsilon_h^* = 0$, the rotor will touch the housing when $\varepsilon_v^* = 3$. This explains why the mass flow rate decreases when $|\varepsilon_v^*|$ or $|\varepsilon_h^*| \rightarrow 3.5$, as shown in the upper left corner of Fig. 7c.

5. Effect of the power-law on the optimal design

Figure 8a extrapolates the results presented in Fig. 6a for a wider range of the power law index, $0.5 \le n \le 1.5$. According to Fig. 8a, the trend observed previously in Fig. 6a holds throughout the whole range of the power law index considered. Micro scale viscous pumps with curved housing (i.e., L and U-shaped micropump) perform better (i.e., present higher values of $\dot{m}_{max}^*$) and at the same time, consume less shaft power than the I-shaped pump. As expected, Fig. 8a also shows that the power-law index has a strong effect on the dimensionless shaft power and maximized mass flow rate, since the shear rate is given by Eq. 3. Fluids with larger n have more ability to transfer momentum than a fluid with small n, which explains why $\dot{m}_{max}^*$ increases with n and at the same time why W'^* decreases with n. More important is the fact that the difference between the performances of the micro scale viscous pumps shown is Fig. 1 is sustained throughout the range on n considered proofing the superiority of micro scale pumps with curved housing when compared with an I-shaped pump.

Figure 8b shows the distribution of shear stress over the rotor's surface for a U-shaped pump operating with three different types of fluids (i.e., n = 0.5, 1 and 1.5). The symmetry of the shear distribution is due to the slow character of the flow. More interesting is the effect of the power-law index on the shear distribution. According to Fig. 8b, the overall shape of the shear distribution around the rotor is preserved for different values of the power-law index. However, the whole shear distribution curve, moves towards the zero-ordinate line as n increases. This behavior

explains the decrease in shaft power required by micro scale pumps operating with shear-thickening fluids as shown previously in Fig 8a when compared when pumps operating with shear-thinning fluids.

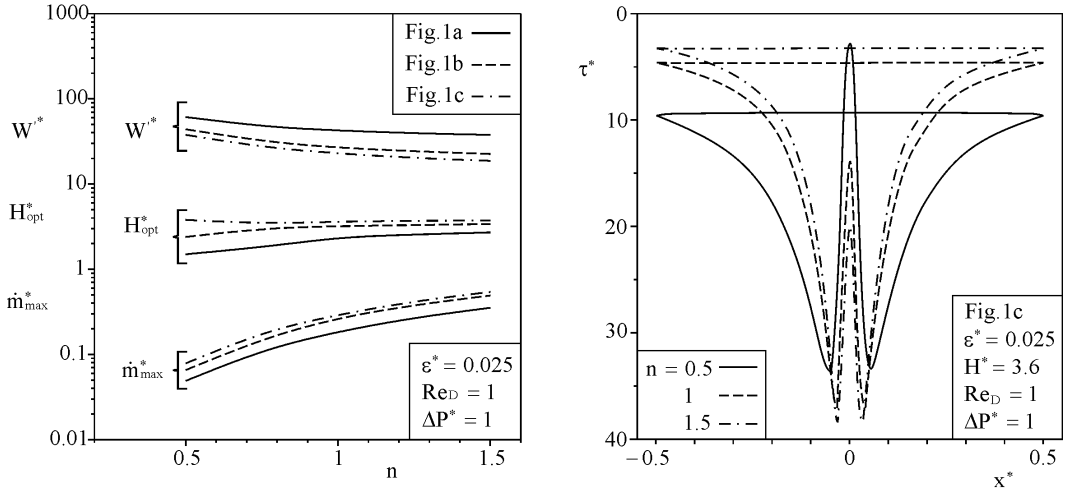

Figure 8. a) Effect of the power-law index on the optimal channel height, maximized mass flow rate and demanded shaft power. (Left frame)
b) Effect of the shape of the power-law index on the shear distribution over the rotor of a U-shaped micropump for a blood-like fluid (n = 0.785). (Right frame)

6. Conclusions

In this paper we presented and evaluated three different configurations of non-Newtonian micro scale viscous pumps for biomedical devices. The objective was to maximize the mass flow rate of a blood-like fluid per unit of shaft power consumed by the rotor, where the fluid shear-rate was given a power-law relation. The optimal geometrical design originated from certain geometrical conditions (§4) required to having an operational micro scale viscous pump. First, the channel housing for the micro scale viscous pump has to provide a certain level of confinement for the rotor. Secondly, the rotor has to be asymmetrically placed inside the channel.

The need for such requirements was verified by a preliminary parametric analysis on an I-shaped micro pump (§4.1), which showed that both conditions are crucial for the pump functionally, and more importantly, the channel height and the rotor eccentricity have a major effect on the mass flow rate. These finding clearly shows the relevance of the geometric optimization of the pump's housing. The numerical simulation also showed that slightly larger values for the optimized channel height (H_{opt}) are expected when the performance of the micro viscous pump is optimized based on the mass flow rate rather than average flow velocity. However, regardless the figure of merit (i.e., mass flow rate or average flow velocity) maximized results are expected as $\varepsilon \to 0$.

Next, in §4.2, two novel configurations of micro viscous pumps with curved housing (Figs. 1b and 1c) were proposed and numerically optimized for maximal mass flow rate while operating with a blood-like type of fluid. The results showed that pump configurations in which surrounding walls the are aligned with the rotor (i.e., Fig. 1b and 1c) provided larger mass flow rates and required less shaft power to operate when compared with straight housed pumps (Fig. 1a). This is an important finding that further supports the use of curved housed micro pumps in mobile or implanted medical devices, which have limited power resources.

In §4.3 we showed that the performance of and U-shaped micro scale viscous pump could be greatly improved by allowing the rotor to move vertically (ε^*_v) as well as horizontally (ε^*_h). More specifically, it was shown that, for a fixed value of the total channel thickness ($H^*_{tot,opt}/2 = 3.5$), the maximized mass flow rate can be increase by 30% if instead of having $\varepsilon^*_h = \varepsilon^*_v = 0$ (concentric configuration), we choose a non-concentric design where $\varepsilon^*_v \cong 1.72$ and $\varepsilon^*_h \cong -0.5$.

The numerical results presented in §5 also showed that, for a power-law index between $0.5 \le n \le 1.5$, micro scale viscous pumps with curved housing provide not only larger mass flow rates, but also require less shaft power when compared with an I-housed micro scale viscous pump.

Acknowledgement
A. K. da Silva thanks the College of Engineering of the University of Hawaii for a 2006 Seed-Grant Award.

Nomenclature

D rotor diameter, m
H channel height, m
L channel length, m

m consistency coefficient, Pa s^n
$\dot{m}$ mass flow rate, kg s^{-1}
M moment coefficient, N m^{-2}
n power-law index
P pressure, Pa
Re_D Reynolds number, ($Re_D = \omega D^2/2\nu$)
T torque, N m
$\bar{u}$ mean velocity, m s^{-1}
$\vec{V}$ velocity vector, m s^{-1}
W' rotor shaft power per unit of length, N s^{-1}

Greek Symbols

γ shear rate, s^{-1}
ε eccentricity, m
η viscosity, kg m^{-1} s^{-1}
ρ density, kg m^{-3}
ω rotor angular velocity, ($\omega = 2U/D$)

Subscripts

d downstream
max maximum
opt optimum
u upstream

Superscript

* dimensionless variables

References

Abdelgawad M, Hassan I, Esmail N. 2004. Transient behavior of the viscous micropump. Microscale Thermophysical Engineering 8:361-381.

Abdelgawad M, Hassan I, Esmail, N, Phutthavong P. 2005. Numerical investigation of multistage viscous micropump configurations. Journal of Fluids Engineering 127:734-742.

Auroux PA, Iossifidis D, Reyes DR, Manz A. 2002. Micro Total Analysis Systems. 2. Analytical standard operations and applications. Analytical Chemistry 74:2637-2652.

Bird RB, Stewart WE, Lightfoot EN. 2001. Transport Phenomena, New York: John Wiley & Sons.

COMSOL MultiPhysics Inc., (2005). User's Manual, Los Angeles, CA 90024.

da Silva AK, Kobayashi MH, Coimbra CFM. 2006. Optimal Theoretical Design of 2D Viscous Micro-Scale Pumps for Maximal Mass Flow Rate and Minimum Power Consumption. International Journal of Heat and Fluid Flow. (in press)

DeCourtye D, Sen M, Gad-el-Hak M. 1998. Analysis of Viscous Micropumps and Microturbines. International Journal of Computational Fluid Dynamics 10:13-25.

Gad-el-Hak M. 1999. The fluids mechanics of microdevices – The Freeman Scholar Lecture. Journal of Fluids Engineering 121:5-33.

Judy JW. 2001 Microelectromechanical systems (MEMS): fabrication, design and applications. Journal of Smart Materials and Structures 10:1115-1134.

Laser DJ, Santiago JG. 2004. A review of micropumps. Journal of Micromechanics and Microengineering 14:R35-R64.

Micci MM, Ketsdever AD. 2000. Micropropulsion for Small Spacecraft. American Institute of Aeronautics and Astronautics Inc. Reston, Va:399 – 422.

Nguyen NT, Huang X, Chuan, TK. 2002. MEMS-Micropumps: a review. Journal of Fluids Engineering 124:384-392.

Reyes DR, Iossifidis D. Auroux PA, Manz A. 2002. Micro Total Analysis Systems. 1. Introduction, theory, and technology. Analytical Chemistry 74:2623-2636.

Sen M, Wajerski D, Gad-el-Hak M. 1996. A novel pump for MEMS applications. Journal of Fluids Engineering 118: 624-627.

Sharatchandra MC, Sen M, Gad-el-Hak M. 1997. Navier-Stokes simulations of a novel viscous pump. Journal of Fluids Engineering 119:372-382.

Sharatchandra MC, Sen M, Gad-el-Hak M. 1998. Thermal aspects of a novel viscous pump. Journal of Heat Transfer 120:99-107.

Verpoorte E. 2002. Microfluidic chips for clinical and forensic analysis, Electrophoresis 23: 677-712.

Walburn FJ, Schneck DJ. 1976. A constitutive equation for the whole human blood, Biorheology 13:201-210.

Woias P. 2004. Micropumps – past, progress and future prospects. Sensors and Actuators B 105:28-38.

Ziaie B, Baldi A, Lei M, Gu Y, Siegel RA. 2004. Hard and soft micromachining for BioMEMS: review of techniques and examples of applications in microfluidics and drug delivery. Advanced Drug Delivery Reviews 56:145-172.

Proceedings of the 11th Brazilian Congress of Thermal Sciences and Engineering -- ENCIT 2006
Braz. Soc. of Mechanical Sciences and Engineering -- ABCM, Curitiba, Brazil,- Dec. 5-8, 2006

Paper CIT06-0605

ANALYTICAL SOLUTION TO THE TWO DIMENSIONAL TRANSIENT BIOHEAT EQUATION WITH CONVECTIVE BOUNDARY CONDITIONS

Mônica Debossam Barros de Azevedo
Instituto Militar de Engenharia, Seção de Engenharia Mecânica e de Materiais, Rio de Janeiro, Brazil.
mdebossam@yahoo.com.br

Rodrigo Otavio de Castro Guedes
Instituto Militar de Engenharia, Seção de Engenharia Mecânica e de Materiais, Rio de Janeiro, Brazil.
guedes@ime.eb.br

Francesco Scofano Neto
Instituto Militar de Engenharia, Seção de Engenharia Mecânica e de Materiais, Rio de Janeiro, Brazil.
scofano@ime.eb.br

Abstract. *In this paper, the classical integral transform technique is applied to solve the two dimensional Pennes bioheat transfer equation in Cartesian coordinates subjected to convective boundary conditions. A straightforward analytical solution is obtained allowing for benchmark results and furnishing a close insight of some relevant aspects of cancer treatment by hyperthermia.*

Keywords*. hyperthermia, Pennes equation, integral transform technique.*

1. Introduction

The success of the treatment of malignant tumors by hyperthermia calls for the knowledge of the temperature field for both healthy and cancerous tissues. This medical procedure consists in exposing malignant cells to temperatures in the range of 42 °C to 45 °C in order to retard, arrest or reverse the growth of tumors. Although susceptible to the increase in temperature, the normal cells do not exhibit the same degree of sensitivity as the malignant cells and therefore the potential of induced hyperthermia as a therapy for cancer has been long considered for both local and global treatments. For the case of local hyperthermia, it is important to predict and control the thermal fields generated by the external medical device responsible for increasing local temperature. However, the task of controlling both temperature levels and duration of the heating process cannot be satisfactory accomplished based solely on measurements because only a few localized temperature readings can be monitored during the therapy. Therefore, mathematical models commonly employed in engineering are often used in the simulation of heat transfer in living tissues, furnishing temperature profiles that may guide the physician before and after the treatment. One of these models is the bioheat transfer equation proposed by Pennes (1948) that consists in a heat diffusion equation together with an energy sink term that accounts for the effect of the temperature difference between the blood supply and the tissue. The source term of this equation carries the effects of both metabolic heat generation and the external heat source applied by the physician.

Previous investigations on this matter have relied on pure numerical methods such as finite differences (O'Brien and Mekkaoui, 1993; Rawnsley et al., 1994) and boundary elements (Chan, 1992) or on approximate and exact analytical solutions (Chato, 1980; Huang et al., 1994). Analytical solutions allow conditions that occur during hyperthermia treatments to be studied in closed form and also provide an improved basis for verification of numerical codes. Accordingly, the main contribution of this work is to employ the classical integral transform technique to establish an analytical solution to the two dimensional transient bioheat transfer equation subjected to convective boundary conditions. Following the solution, the influence of blood perfusion on transient heat transfer in several human tissues subjected to a heat source is discussed, leading to conclusions that may aid the planning of hyperthermia treatment. Moreover, this straightforward methodology (Azevedo, 2004; Presgrave, 2005; Presgrave et al., 2005) provides benchmark results for the numerical investigator interested in developing and validating bioheat transfer software.

2. Mathematical formulation

The following heat transfer problem for a rectangular perfused organic tissue is considered in accordance to Pennes (1948) model:

$$\begin{cases} k_t\left(\dfrac{\partial^2 T}{\partial x^2}+\dfrac{\partial^2 T}{\partial y^2}\right)-w_b c_b (T-T_a)+g=\rho_t c_t \dfrac{\partial T}{\partial t} & 0<x<L,\quad 0<y<l,\quad t>0 \\ \dfrac{\partial T}{\partial x}=0 & x=0,\quad t>0 \\ \dfrac{\partial T}{\partial x}=0 & x=L,\quad t>0 \\ -k\dfrac{\partial T}{\partial y}+hT=hT_\infty & y=0,\quad t>0 \\ T=T_p & y=l,\quad t>0 \\ T=T_0 & 0\le x\le L,\quad 0\le y\le l,\quad t=0 \end{cases} \tag{1}$$

The second term on the left hand side of the bioheat transfer equation is a sink term due to the convective effect of capilar vascularization in living tissues while the third one is a source term representing a combined effect of both the internal metabolic heat generation and the external irradiation. This mathematical model aims to predict the temperature levels in a perfused tissue subjected to a hyperthermic treatment based on an external heating device.

The boundary conditions are taken as prescribed constant temperature at the top and convective heat transfer with an external medium at the bottom. This latter boundary condition attempts to simulate the heat transfer between the tissue and an adjoint large blood vessel. Initial temperature is considered constant.

By introducing the following dimensionless variables:

$$\theta=\frac{T-T_p}{g_0\dfrac{L^2}{k_t}},\quad G=\frac{g}{g_0},\quad A=\frac{l}{L},\quad X=\frac{x}{L},\quad Y=\frac{y}{L},\quad \tau=\frac{\alpha_t\, t}{L^2},\quad Pf=\frac{w_b c_b L^2}{k_t},\quad Bi=\frac{hL}{k_t}\ . \tag{2}$$

Problem (1) is given in dimensionless form as:

$$\frac{\partial^2\theta}{\partial X^2}+\frac{\partial^2\theta}{\partial Y^2}-Pf\,\theta+G=\frac{\partial\theta}{\partial\tau} \qquad 0<X<1,\quad 0<Y<A,\quad \tau>0 \tag{3.a}$$

$$\frac{\partial\theta}{\partial X}=0 \qquad X=0,\quad \tau>0 \tag{3.b}$$

$$\frac{\partial\theta}{\partial X}=0 \qquad X=1,\quad \tau>0 \tag{3.c}$$

$$-\frac{\partial\theta}{\partial Y}+Bi\theta=Bi\theta_\infty \qquad Y=0,\quad \tau>0 \tag{3.d}$$

$$\theta=0 \qquad Y=A,\quad \tau>0 \tag{3.e}$$

$$\theta=T_0 \qquad 0\le X\le 1,\quad 0\le Y\le A,\quad \tau=0 \tag{3.f}$$

This is a particular case of the so-called class I problem (Mikhailov and Özisik, 1984), and may be solved by the classical Integral Transform Technique (Özisik, 1980) as described in the next section. Dimensionless time τ is also referred as Fourier number (Fo) in the literature. However, for the sake of conciseness, the symbol τ shall be employed here.

3. Solution

The temperature field is expressed in the form of an expansion in terms of eigenfunctions :

$$\theta(X,Y,\tau)=\sum_{i=1}^{\infty}\sum_{j=1}^{\infty} C_{ij}(\tau)\,\psi_i(X)\,\lambda_j(Y) \tag{4}$$

where eigenfunctions $\psi_i(X)$ and $\lambda_j(Y)$ are solutions to eigenvalues problems in the X and Y directions, respectively, obtained as follows:

First, in order to extract the desired Sturm-Liouville problems basic to eq. (4), the homogeneous version of problem (3) is considered:

$$\frac{\partial^2\theta}{\partial X^2}+\frac{\partial^2\theta}{\partial Y^2}-\mathrm{Pf}\theta+=\frac{\partial\theta}{\partial\tau} \qquad 0<X<1,\quad 0<Y<A,\quad \tau>0 \tag{5.a}$$

$$\frac{\partial\theta}{\partial X}=0 \qquad X=0,\quad \tau>0 \tag{5.b}$$

$$\frac{\partial\theta}{\partial X}=0 \qquad X=1,\quad \tau>0 \tag{5.c}$$

$$-\frac{\partial\theta}{\partial Y}+\mathrm{Bi}\theta=0 \qquad Y=0,\quad \tau>0 \tag{5.d}$$

$$\theta=0 \qquad Y=A,\quad \tau>0 \tag{5.e}$$

$$\theta=T_0 \qquad 0\le X\le 1,\quad 0\le Y\le A,\quad \tau=0 \tag{5.f}$$

Then, by applying the method of separation of variables in problem (5), two eigenvalues problems are obtained. The first one is an eigenvalue problem in the X direction,

$$\frac{d^2\psi_i}{dX^2}+\mu_i^2\psi_i(X)=0 \qquad 0<X<1 \tag{6.a}$$

$$\left.\frac{d\psi_i}{dX}\right|_{X=0}=0 \tag{6.b}$$

$$\left.\frac{d\psi_i}{dX}\right|_{X=1}=0 \tag{6.c}$$

the eigenfunction of the above problem is found to be:

$$\psi_i(X)=\cos\mu_i X \tag{7}$$

where,

$$\mu_i=(i-1)\pi \qquad i=1,2,3,4,...$$

and the norm is

$$N_i=\int_0^1\psi_i^2(X)dX=2 \tag{8}$$

Moreover, due to the boundary condition of the second type at both x extremes, $\mu_0=0$ is also a solution to problem (6) and the corresponding eigenfunction and norm are:

$$\psi_0(X)=1 \tag{9}$$

and

$$N_0=1 \tag{10}$$

The second eigenvalue problem is:

$$\frac{d^2\lambda_j}{dY^2} + (\gamma_j^2 - Pf)\lambda_j(Y) = 0 \qquad 0 < Y < A \tag{11a}$$

$$-\frac{d\lambda}{dY} + Bi\lambda_j(Y) = 0 \qquad Y = 0 \tag{11b}$$

$$\lambda_j(Y) = 0 \qquad Y = A \ . \tag{11c}$$

By considering

$$\gamma_j^2 - Pf = \beta_j^2 \tag{12}$$

the solution to problem (11) above is:

$\lambda_j(Y) = \operatorname{sen}\beta_j(A-Y)$, where β_j are the positive roots of the following transcendental equation

$$\beta_j \cot\beta_j A = -Bi \tag{13}$$

and the norm M_j is given by $\int_0^A \lambda_j^2(Y)dY$, i.e.,

$$M_j = \frac{A(B_j^2 + Bi^2) + Bi}{2(B_j^2 + Bi^2)} \qquad j = 1,2,3,4... \tag{14}$$

Transcendental equation (13) may be solved by the Bissection Method or by well-established mathematical routines such as DZEBREN/IMSL (1999).

Next, the eigenvalues problems obtained above are used to yield the transformations in the X and Y directions and its respectives inversions.

Thus, eq. (4) is operated on by $\int_0^1 \psi_m(X)\ dX$:

$$\int_0^1 \theta(X,Y,\tau)\ \psi_m(X)dX = \sum_{i=1}^{\infty}\sum_{j=1}^{\infty} C_{ij}(\tau)\lambda_j(Y)\int_0^1 \psi_m(X)\psi_i(X)\ dX \tag{15}$$

Recalling the orthogonality property of the eigenfunctions $\psi_m(X)$, which is written as:

$$\int_0^{As} \psi_i(X)\psi_m(X)\ dX = \begin{cases} 0, & \text{if} \quad i \neq m \\ M_j, & \text{if} \quad i = m \end{cases} \tag{16}$$

Equation (15) results in,

$$\int_0^1 \theta(X,Y,\tau)\ \psi_m(X)dX = \sum_{j=1}^{\infty} C_{mj}(\tau)\lambda_j(Y)N_m \tag{17}$$

Now, eq. (17) is operated on with $\int_0^A \lambda_n(Y)\ dY$:

$$\int_0^A \int_0^1 \theta(X,Y,\tau)\ \psi_m(X)\lambda_n(Y)dXdY = \sum_{j=1}^{\infty} C_{mj}(\tau)N_m \int_0^A \lambda_j(Y)\lambda_n(Y)dY \tag{18}$$

Again, by the orthogonality property of the eigenfunctions $\lambda_n(Y)$:

$$\int_0^A \int_0^1 \theta(X,Y,\tau)\ \psi_m(X)\lambda_n(Y)dXdY = C_{mn}(\tau)N_m M_n \tag{19}$$

and therefore $C_{mn}(\tau)$ is obtained as

$$C_{mn}(\tau) = \frac{1}{N_m M_n} \int_0^A \int_0^1 \theta(X,Y,\tau)\ \psi_m(X)\lambda_n(Y)dXdY \tag{20}$$

Upon substitution of $C_{mn}(\tau)$ into Eq. (4), it is obtained:

$$\theta(X,Y,\tau) = \sum_{i=1}^{\infty}\sum_{j=1}^{\infty} \frac{\psi_i(X)}{N_i}\frac{\lambda_j(Y)}{M_j} \int_0^A \int_0^1 \theta(X,Y,\tau)\ \psi_i(X)\lambda_j(Y)dXdY \tag{21}$$

Now, let

$$\overline{\theta_i}(Y,\tau) = \int_0^1 \psi_i(X)\ \theta(X,Y,\tau)\ dX \tag{22}$$

This integral represents the transform of temperature distribution $\theta(X,Y,\tau)$ in the X direction, resulting into a transformed potential $\overline{\theta_i}(Y,\tau)$.

The substitution of eq. (22) into eq. (21) yields:

$$\theta(X,Y,\tau) = \sum_{i=1}^{\infty}\sum_{j=1}^{\infty} \frac{\psi_i(X)}{N_i}\frac{\lambda_j(Y)}{M_j} \int_0^A \overline{\theta_i}(Y,\tau)\ \lambda_j(Y)dY \tag{23}$$

The above equation is the inversion for the transform, which takes the transformed temperature $\overline{\theta_i}(Y,\tau)$ back to its original form $\theta(X,Y,\tau)$. Now, let :

$$\overline{\overline{\theta_{ij}}}(\tau) = \int_0^A \lambda_j(Y)\ \overline{\theta_i}(Y,\tau)dy \tag{24}$$

This integral is the transform of $\overline{\theta_i}(Y,\tau)$ in the Y direction, resulting in a second transform $\overline{\overline{\theta}}_{ij}(\tau)$, now a function of dimensionless time only.

Upon substitution of eq. (24) into eq. (23), a recovery formulae for the original temperature $\theta(X,Y,\tau)$ is obtained, which performs the inversion of the transformed potentials into the X and Y directions, $\overline{\overline{\theta}}_{ij}(\tau)$:

$$\theta(X,Y,\tau) = \sum_{i=1}^{\infty}\sum_{j=1}^{\infty} \frac{\psi_i(X)}{N_i}\frac{\lambda_j(Y)}{M_j}\ \overline{\overline{\theta_{ij}}}(\tau) \tag{25}$$

Having established the desired integral-transform pair for problem (3), the next step is to rewrite the original formulation in terms of $\overline{\overline{\theta}}_{ij}(\tau)$. Thus, eq. (3a) is multiplied by $\psi_i(X)$ and integration from X = 0 to X = 1 is performed, giving:

$$\int_0^1 \psi_i(X)\frac{\partial^2\theta}{\partial X^2}dX + \int_0^1 \psi_i(X)\frac{\partial^2\theta}{\partial Y^2}dX - \int_0^1 \psi_i(X)\ \mathrm{Pf}\ \theta\ dX + \int_0^1 \psi_i(X)\ G\ dX = \int_0^1 \psi_i(X)\frac{\partial\theta}{\partial\tau}dX \tag{26}$$

By making use of eq. (22), this expression is rewritten as:

$$\int_0^1 \psi_i(X)\frac{\partial^2\theta}{\partial X^2}dX + \frac{\partial^2\overline{\theta_i}}{\partial Y^2} - \mathrm{Pf}\,\overline{\theta_i} + \overline{G_i} = \frac{\partial\overline{\theta_i}}{\partial\tau} \tag{27}$$

where it is defined,

$$\overline{G_i} = \int_0^1 \psi_i(X)\ G\ dX \tag{28}$$

By solving the integral in eq. (27) by parts, one obtains:

$$\left[\psi_i(X)\frac{\partial\theta}{\partial X}-\theta\frac{d\psi_i}{dX}\right]_0^1+\int_0^1\theta\frac{d^2\psi_i(X)}{dX^2}dX+\frac{\partial^2\overline{\theta_i}}{\partial Y^2}-Pf\,\overline{\theta_i}+\overline{G_i}=\frac{\partial\overline{\theta_i}}{\partial\tau} \tag{29}$$

The first term of this equation is evaluated by multiplying boundary condition eq. (5b) by $\psi_i(0)$:

$$\psi_i(0)\left.\frac{\partial\theta}{\partial X}\right|_{X=0}=0 \tag{30}$$

and boundary condition eq. (6b) by $\theta(0,Y,\tau)$:

$$\left.\frac{d\psi_i(X)}{dX}\right|_{X=0}\theta(0,Y,\tau)=0 \tag{31}$$

and subtracting eq. (30) from eq. (31) to give:

$$\psi_i(0)\left.\frac{\partial\theta}{\partial X}\right|_{X=0}-\left.\frac{d\psi_i(X)}{dX}\right|_{X=0}\theta(0,Y,\tau)=0 \tag{32}$$

Analogously, by using boundary conditions at X = 1 from eq. (5) and eq. (6), the following relation is established:

$$\psi_i(1)\left.\frac{\partial\theta}{\partial X}\right|_{X=1}-\left.\frac{d\psi_i(X)}{dX}\right|_{X=1}\theta(1,Y,\tau)=0 \tag{33}$$

Next, eq. (32) and eq. (33) are substituted into eq. (29) resulting in:

$$0+\int_0^1\theta\frac{d^2\psi_i(X)}{dX^2}dX+\frac{\partial^2\overline{\theta_i}}{\partial Y^2}-Pf\,\overline{\theta_i}+\overline{G_i}=\frac{\partial\overline{\theta_i}}{\partial\tau} \tag{34}$$

Now, the integral in eq. (34) above is evaluated by operating on eq. (6a) with $\int_0^1\theta_i dX$ and making use of transform eq. (22):

$$\int_0^1\theta_i\frac{d^2\psi_i(X)}{dX^2}dX=-\mu_i^2\int_0^1\theta_i\,\psi_i(X)dX=-\mu_i^2\overline{\theta_i} \tag{35}$$

Next, eq. (35) is substituted into eq. (34) resulting in:

$$-\mu_i^2\overline{\theta_i}+\frac{\partial^2\overline{\theta_i}}{\partial Y^2}-Pf\,\overline{\theta_i}+\overline{G_i}=\frac{\partial\overline{\theta_i}}{\partial\tau} \tag{36}$$

Equation (36) is a partial differential equation in Y and τ . In order to transform the problem in the Y direction, eq. (36) is multiplied by $\lambda_j(Y)$ and integration from Y = 0 to Y = A is performed, resulting in:

$$-\mu_i^2\int_0^A\lambda_j(Y)\overline{\theta_i}dY+\int_0^A\lambda_j(Y)\frac{\partial^2\overline{\theta_i}}{\partial Y^2}dY-Pf\int_0^A\lambda_j(Y)\overline{\theta_i}dY+\int_0^A\lambda_j(Y)\,\overline{G_i}dY=\int_0^A\lambda_j(Y)\frac{\partial\overline{\theta_i}}{\partial\tau}dY \tag{37}$$

By utilizing transform eq. (24) and by defining $\overline{\overline{G_{ij}}}=\int_0^A\lambda_j(Y)\,\overline{G_i}dY$, it is obtained:

$$-\mu_i^2 \overline{\overline{\theta_{ij}}}(\tau) + \int_0^A \lambda_j(Y) \frac{\partial^2 \overline{\theta_i}}{\partial Y^2} dY - Pf\, \overline{\overline{\theta_{ij}}}(\tau) + \overline{\overline{G_{ij}}} = \frac{d\overline{\overline{\theta_{ij}}}(\tau)}{d\tau} \tag{38}$$

Equation (38) is integrated by parts to yield :

$$-\mu_i^2 \overline{\overline{\theta_{ij}}}(\tau) + \left[\lambda_j(Y) \frac{\partial \overline{\theta_i}}{\partial Y} - \overline{\theta_i} \frac{d\lambda_j}{dY} \right]_0^A + \int_0^A \overline{\theta_i} \frac{d^2 \lambda_j}{dY^2} dY - Pf\, \overline{\overline{\theta_{ij}}}(\tau) + \overline{\overline{G_{ij}}} = \frac{d\overline{\overline{\theta_{ij}}}(\tau)}{d\tau} \tag{39}$$

The third term of this equation is evaluated with the aid of the eigenvalue problem in the Y direction. Equation (11) is operated on with $\int_0^A \overline{\theta_i}\, dY$ and the transform eq. (24) is used to give:

$$\int_0^A \overline{\theta_i} \frac{d^2 \lambda_j}{dY^2} dY = -\beta_j^2 \int_0^A \overline{\theta_i} \lambda_j(Y) dY = -\beta_j^2 \overline{\overline{\theta_{ij}}}(\tau) \tag{40}$$

After substituting eq. (40) above into eq. (39), it is found that:

$$-\mu_i^2 \overline{\overline{\theta_{ij}}}(\tau) + \left[\lambda_j(Y) \frac{\partial \overline{\theta_i}}{\partial Y} - \overline{\theta_i} \frac{d\lambda_j}{dY} \right]_0^A - \beta_j^2 \overline{\overline{\theta_{ij}}}(\tau) - Pf\, \overline{\overline{\theta_{ij}}}(\tau) + \overline{\overline{G_{ij}}} = \frac{d\overline{\overline{\theta_{ij}}}(\tau)}{d\tau} \tag{41}$$

The second term of eq. (41) above is evaluated by multiplying the boundary condition at Y = 0 for problem (11) by $\overline{\theta_i}(0,\tau)$:

$$-\overline{\theta_i}(0,\tau) \left. \frac{d\lambda_j}{dY} \right|_{Y=0} + Bi\, \overline{\theta_i}(0,\tau)\, \lambda_j(0) = 0 \tag{42}$$

and the boundary condition at Y = 0 for problem (3) by $\lambda_j(0)$:

$$-\lambda_j(0) \left. \frac{\partial \theta}{\partial Y} \right|_{Y=0} + Bi\, \theta\, \lambda_j(0) = Bi \theta_\infty \lambda_j(0) \tag{43}$$

Next, the X direction transform is applied to give:

$$\lambda_j(0) \left. \frac{\partial \overline{\theta_i}}{\partial Y} \right|_{Y=0} - Bi\, \lambda_j(0) \overline{\theta_i} = -Bi\, \theta_\infty \lambda_j(0) \int_0^1 \psi_i dX \tag{44}$$

By substituting, now, eq. (42) into eq. (44), the following expression at Y = 0 is obtained:

$$\lambda_j(0) \left. \frac{\partial \overline{\theta_i}}{\partial Y} \right|_{Y=0} - \overline{\theta_i}(0,\tau) \left. \frac{d\lambda_j}{dY} \right|_{Y=0} = -Bi\, \theta_\infty \lambda_j(0) \int_0^1 \psi_i dX \tag{45}$$

By multiplying eq. (11c) by $\left. \frac{\partial \overline{\theta_i}}{\partial Y} \right|_{Y=A}$ and eq. (3e) by $\frac{d\lambda_j(A)}{dY}$ results in, respectively:

$$\lambda_j(A) \left. \frac{\partial \overline{\theta_i}}{\partial Y} \right|_{Y=A} = 0 \tag{46}$$

and

$$\theta(X,A,\tau) \frac{d\lambda_j(A)}{dY} = 0 \tag{47}$$

The X direction transform is applied in eq. (47) above furnishing:

$$\int_0^1 \psi_i \theta(X, A, \tau) \frac{d\lambda_j(A)}{dY} dX = 0 \tag{48}$$

or,

$$\left.\frac{d\lambda_j}{dY}\right|_{Y=A} \overline{\theta_i}(A, \tau) = 0 \tag{49}$$

By subtracting eq. (46) from eq. (49), the following expression at Y = A results:

$$\lambda_j(A) \left.\frac{\partial \overline{\theta_i}}{\partial Y}\right|_{Y=A} - \left.\frac{d\lambda_j}{dY}\right|_{Y=A} \overline{\theta_i}(A, \tau) = 0 \tag{50}$$

Finally, substituting eq. (45) and eq. (50) into eq. (41),

$$-\mu_i^2 \overline{\overline{\theta_{ij}}}(\tau) - \beta_j^2 \overline{\overline{\theta_{ij}}}(\tau) + Bi\theta_\infty \lambda_j(0) \int_0^1 \psi_i(X) dX - Pf\, \overline{\overline{\theta_{ij}}}(\tau) + \overline{\overline{G_{ij}}} = \frac{d\overline{\overline{\theta_{ij}}}(\tau)}{d\tau} \tag{51}$$

and making use of definition eq. (12):

$$-\mu_i^2 \overline{\overline{\theta_{ij}}}(\tau) - \beta_j^2 \overline{\overline{\theta_{ij}}}(\tau) + Bi\theta_\infty \lambda_j(0) \int_0^1 \psi_i(X) dX - \gamma_j^2 \overline{\overline{\theta_{ij}}}(\tau) + \beta_j^2 \overline{\overline{\theta_{ij}}}(\tau) + \overline{\overline{G_{ij}}} = \frac{d\overline{\overline{\theta_{ij}}}(\tau)}{d\tau} \tag{52}$$

Therefore, a system of ordinary differential equations as a function of τ results, for the determination of the transformed original problem. This system is rewritten in the following form:

$$\frac{d\overline{\overline{\theta_{ij}}}(\tau)}{d\tau} + (\mu_i^2 + \gamma_j^2)\, \overline{\overline{\theta_{ij}}}(\tau) = \overline{\overline{P_{ij}}} \tag{53}$$

where,

$$\overline{\overline{P_{ij}}} = Bi\ \theta_\infty\ \lambda_j(0) \int_0^1 \psi_i(X) dX + \int_0^A \int_0^1 \lambda_j(y) \psi_i(X)\, G\, dX\, dY \tag{54}$$

The transformed initial condition is given by :

$$\overline{\overline{\theta_{ij}}}(0) = \int_0^A \int_0^1 \lambda_j(y)\, \psi_i(X)\, \theta(X, Y, 0)\, dX\, dY \tag{55}$$

The exact solution for this decoupled system of ordinary differential equations is:

$$\overline{\overline{\theta_{ij}}}(\tau) = \frac{\overline{\overline{P_{ij}}}}{\mu^2{}_i + \gamma_j^2} - \frac{e^{-(\mu_i^2+\gamma_j^2)\tau}}{\mu^2{}_i + \gamma_j^2} \overline{\overline{P_{ij}}} + e^{-(\mu_i^2+\gamma_j^2)\tau}\, \overline{\overline{\theta_{ij}}}(0) \tag{56}$$

Now, the original temperature field $\theta(X, Y, \tau)$ is recast by successive application of inversion in the X and Y directions, eq.(29) and eq. (27), resulting in:

$$\theta(X, Y, \tau) = \sum_{i=1}^{\infty} \sum_{j=1}^{\infty} \frac{\psi_i(X)}{N_i} \frac{\lambda_j(Y)}{M_j} \left[\frac{\overline{\overline{P_{ij}}}}{\mu^2{}_i + \gamma_j^2} - \frac{e^{-(\mu_i^2+\gamma_j^2)\tau}}{\mu^2{}_i + \gamma_j^2} \overline{\overline{P_{ij}}} + e^{-(\mu_i^2+\gamma_j^2)\tau}\, \overline{\overline{\theta_{ij}}}(0) \right] \tag{57}$$

4. Results and discussion

In this section, numerical simulations are presented in order to analyze the effects of the perfusion term on Pennes equation for several tissues subjected to external heating and metabolic generation. According to the dimensionless variables employed here, the initial (θ_0) and ambient (θ_∞) temperatures are functions of both tissue and heat generation. In every case studied, the characteristic dimension L is 0.03 m and T_a = 36.5 °C. The adopted value for the external heat source is 50,000 W/m^3 and metabolic heat generation rate is 33,800 W/m^3, (Deng and Liu, 2002). As a result, g = 83,800 W/m^3 in all computations performed in this section. Perfusion is regarded as constant and its value varies with the tissue being considered. Thermophysical properties of blood and tissues are also considered constant. Accordingly, blood density and specific heat are taken as ρ_b = 1060 kg/m^3 and c_b = 3720 J/kgK, respectively, (Brix et al., 2002), while perfusion and thermal conductivity for several tissues are listed in Tab. (1).

Table 1. Thermophysical properties for several tissues (subscript t)

Reference	Blood perfusion w_b $[m_b^3 s^{-1} m_t^{-3}]$	Density ρ_t $[kgm^{-3}]$	Specific heat c_t $[Jkg^{-1}k^{-1}]$	Thermal conductivity k_t $[Wm^{-1}k^{-1}]$	Pf Eq.(2)
Chan (1992) - ficticious tissue	0.00001	1000	4185	0.50	0.1
Brix et al. (2002) – adipose tissue	0.00050	950	3100	0.27	5
Jiang et al.(2002) – inner tissue	0.00125	1000	4000	0.50	10
Jiang et al.(2002) – subcutaneous tissue	0.00125	1000	2500	0.19	15
Brix et al. (2002) – liver	0.01500	1060	3600	0.52	100
Brix et al. (2002) – kidney	0.06100	1050	3700	0.54	400

For the sake of computations, dimensionless perfusion (Pf) values computed with above data are rounded to the figures indicated in the table.

Dimensionless temperature distributions are obtained from Eq. (57) upon truncation of the infinite sums to a sufficiently large order that ensures a converged result of at least three significant digits. Convergence is found to be fast and typically no more than 30 terms are needed in the summations. A complete discussion regarding the convergence behavior of the infinite series is found in Azevedo (2004).

Figures (1) - (3) show dimensionless temperature distributions at the center of the tissue as a function of dimensionless time and dimensionless perfusion for the situation of Bi = 5, G = 1, θ_0 = 0.003 and θ_∞ = 0.001, and three different aspect ratios, namely, 0.25, 0.50 and 1.

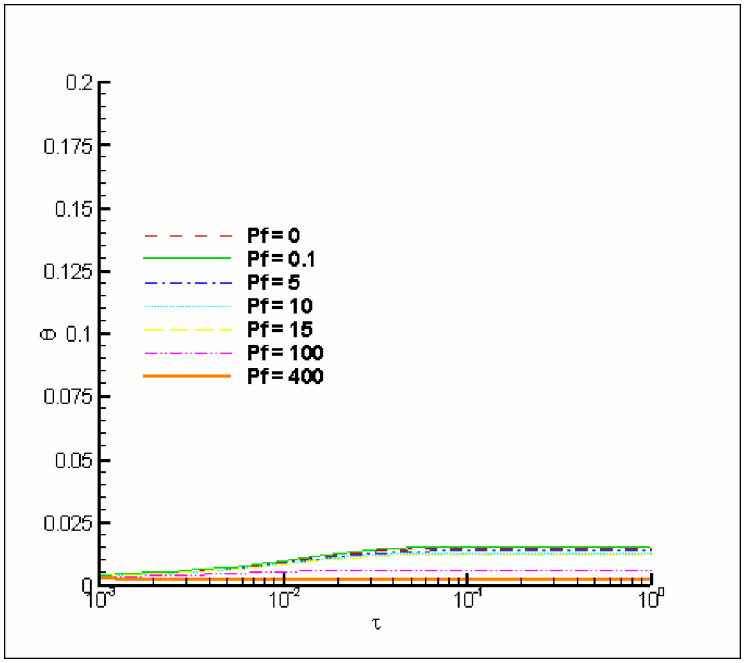

Figure 1. Dimensionless temperature distribution: Bi = 5, G = 1, θ_0 = 0.003 , θ_∞ = 0.001, A = 0.25.

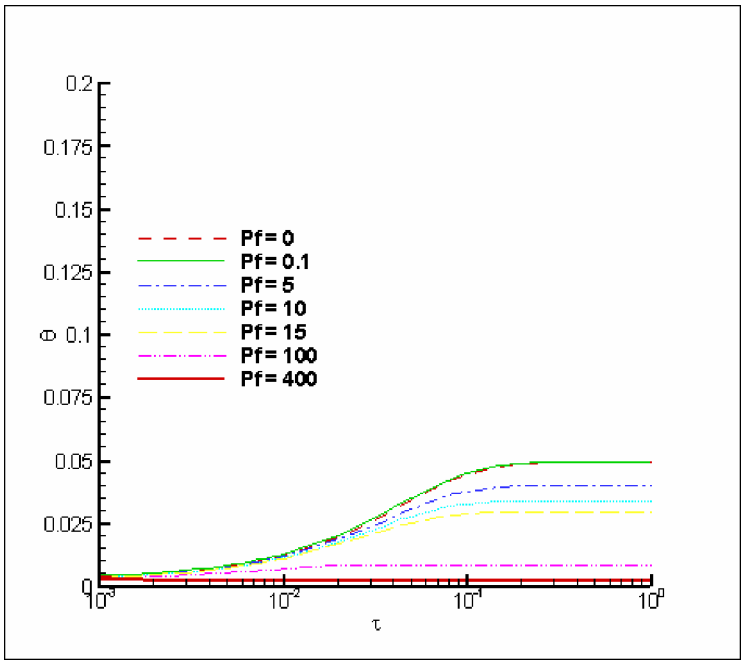

Figure 2. Dimensionless temperature distribution: Bi = 5, G = 1, θ_0 = 0.003 , θ_∞ =0.001, A = 0.50.

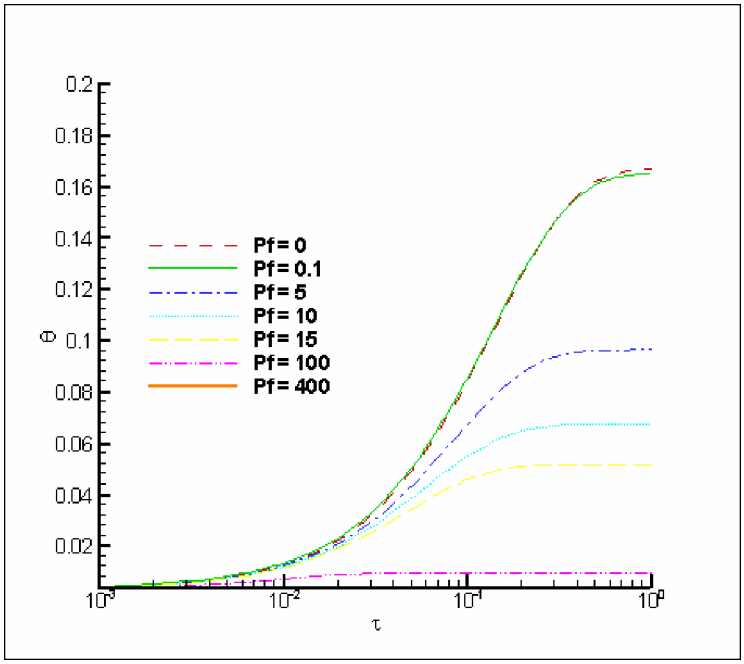

Figure 3. Dimensionless temperature distribution: Bi = 5, G = 1, θ_0 = 0.003 , θ_∞ =0.001, A = 1.0.

An inspection of the above graphs reveal certain interesting trends regarding the transient temperature distributions in an applied situation such as a hyperthermia treatment of a cancerous tissue. As already mentioned earlier, in such situations, it is desired to achieve a certain degree of temperature, usually around 44 °C, in order to destroy the malignant cells. Figure (1) shows that the temperature distributions are only slightly above its initial condition for the case of a low aspect ratio tissue such as A = 0.25 for all the simulated perfusion coefficients suggesting that the desired threshold for hyperthermia is not being achieved. On the other hand, for aspect ratios greater than 0.25, temperature levels are significantly detached from their initial conditions. In fact, Fig. (2) and Fig. (3) illustrate this tendency when dimensionless times greater than 0.01 are considered. Also, the role of the perfusion coefficient in the temperature

distribution can be inferred from these figures. Consistent with its role as a sink term, a high perfusion rate results in a severe temperature decrease. This behavior can be better observed in Fig. (3) by analyzing the curves related to $P_f = 0.0$ and 400, which simulate a situation without any perfusion effects and another one in which an extreme heat sink due to blood flow is considered. For the steady-state situation, despite the action of the external heat source, the $P_f = 400$ curve is slightly above the initial condition whereas the $P_f = 0$ situation achieves a dimensionless temperature of around 0.16. Also worth mentioning is the fact that for dimensionless times less than 0.01, the temperature in the center of the targeted area does not seem to be strongly influenced by the perfusion coefficient. If high temperatures are desired, as in the case of hyperthemia, certainly the exposure time should be much greater than 0.01.

Next, we present some results in dimensional form in order to obtain a better physical perception of the role of the various above mentioned quantities, in the temperature fields related to the bioheat transfer problem in question. Table (2) shows the dimensional initial temperature together with its steady-state value in the geometrical center of the targeted area for three aspect ratios and for several tissues as described in Tab. (1). Despite the variation of the thermophysical properties, an analysis of Tab. (2) suggests that it is a good assumption to consider the same initial condition and external temperature for all the cases reported. On the other hand, a fixed Biot number does not imply in the same convective heat transfer since here, the thermal conductivity of a certain tissue may be quite different from another one. For a fixed perfusion coefficient, temperature levels monotonically increases for increasingly aspect ratios. A closer observation shows that for liver and kidney, steady state temperature distributions remain very close to their initial levels for the external heat source of 50,000 W/m^3. This observation suggest that the hypertermia treatment for these tissues is inefficient for the value of external heating adopted here as the results obtained in the simulations indicate that the temperature is below 44 °C. Also, target areas with an aspect ratio of 0.25 show steady state temperature below the 44 °C threshold. As a result, with such perfusion coefficients, hyperthemia will only be an effective treatment for situations which involve tissues with aspects ratios greater or equal to 0.5. In addition, an inspection of this table shows the role of the combined effects of the perfusion, conduction and convection in the bioheat transfer process. For instance, although the perfusion coefficient for the adipose tissue is 50 times greater than the one reported by Chan (1992), its steady state temperature is actually about 2 °C higher for the A=0.25 situation. This apparent contradiction is better understood by noticing that the thermal conductivity of the adipose tissue and the convective coefficient are considerably smaller than those reported by Chan (1992) implying that the convection and conduction effects for this situation are not dominant, resulting in a low heat transfer rate to the external environment. Therefore, the energy balance indicates that the source term combined with the low convection and poor conduction dominates over the perfusion heat sink. On the other hand, a comparison between the results reported by Chan (1992) and our simulations regarding the inner tissue show that for this case the temperature levels decrease as expected since the thermal conductivity, initial and environmental temperatures and convective coefficients are the same in both cases. Since the only difference is in the perfusion coefficient, it is naturally expected that the inner tissue should present a smaller steady-state temperature.

Table2 - Initial and steady-state temperatures for Bi = 5.0; G = 1.0; $\theta_0 = 0.003$; $\theta_\infty = 0.001$.

Reference	T_0 [^{0}C]	T_∞ [^{0}C]	h [W m^{-2} K^{-1}]	$T_{\frac{1}{2}f}$ [^{0}C] A = 0.25	$T_{\frac{1}{2}f}$ [^{0}C] A = 0.50	$T_{\frac{1}{2}f}$ [^{0}C] A = 1.00
Chan (1992) - ficticious tissue	36.95	36.65	83.3	38.76	43.92	61.32
Brix et al. (2002) – adipose tissue	37.34	36.78	45.0	40.43	47.81	63.51
Jiang et al. (2002) – inner tissue	36.95	36.65	83.3	38.49	41.67	46.71
Jiang et al. (2002) – subcutaneous tissue	37.69	36.90	31.7	41.43	48.29	57.08
Brix et al. (2002) – liver	36.94	36.65	86.7	37.41	37.79	37.94
Brix et al. (2002) – kidney	36.92	36.64	90.0	36.82	36.85	36.85

Finally, Table (3) shows the equivalent dimensional times for $\tau = 0.1$ together with the respective central point temperatures for the high aspect ratio situation reported in this contribution. Once again, an inspection of these values indicate that the hyperthermia threshold is not achieved for the liver and kidney tissues. However, for the other biological tissues considered in our analysis, temperature levels are indeed above 44 °C in a time frame greater than 10 and less than 20 minutes for the external heat source mentioned earlier. Such results are believed to be relevant for the planning of a successful treatment of malignant tumors by hyperthermia.

Table 3 . Equivalent dimensional times for τ = 0.1 and respective temperatures at the center of the tissue. Bi = 5.0; G = 1.0; θ_0 = 0.003; θ_∞ =0.001; A = 1.0

Reference	Time	$T_{\frac{1}{2}f}\,[^0C]$
Chan (1992) - ficticious tissue	10min 54sec	49.24
Brix et al. (2002) – adipose tissue	16min 21sec	55.48
Jiang et al. (2002) – inner tissue	12min	44.88
Jiang et al. (2002) – subcutaneous tissue	19min 44sec	54.86
Brix et al. (2002) – liver	11min	37.94
Brix et al. (2002) – kidney	10min 47sec	36.85

5. Conclusions

In conclusion, a straightforward methodology based on the classical integral transform technique is devised to aid physicians throughout the decision making process regarding the use of high energy sources for the destruction of cancerous cells located in various parts of the human body. Although the methodology here reported was only tested in the cartesian system, our research points out that more elaborate geometries can also be successful tackled by the same approach with equal mathematical simplicity. For example, the same solution procedure was successfully applied to the temperature distribution in a human limb subjected to a skin burn and also to the selective cooling of the human brain which is a medical procedure designed to aid patients in the immediate moments following an ischemic trauma (Presgrave, 2005).

6. References

Azevedo, M. D. B., 2004, "Analytical Numerical Simulation of the Bioheat Transfer in Organic Tissues" (in Portuguese), M.Sc. Dissertation, IME, Rio de Janeiro, Brazil, 252 p.

Brix, G., Seebass, M., Hellwig, G. and Griebel, J., 2002, "Estimation of Heat Transfer and Temperature Rise in Partial-Body Regions During MR Procedures: An Analytical Approach With Respect to Safety Considerations", Magnetic Resonance Imaging, Vol. 20, pp. 65-76.

Chan, C.L., 1992, "Boundary Element Method Analysis for the Bioheat Transfer Equation", Journal of Biomedical Engineering, Vol. 114, pp. 358-365.

Chato, J.C., 1980, "Heat Transfer to blood Vessels", Journal of Biomechanical Engineering, Vol. 102, pp. 110-118.

Deng, Z. S. and Liu, J., 2002, "Analytical Study on Bioheat Transfer Problems with Spatial or Transient Heating on Skin Surface or Inside Biological Bodies", Journal of Biomedical Engineering, Vol. 124, pp. 638-649.

Huang, H. W., Chan, C. L. and Roemer, R. B., 1994, "Analytical Solutions of Pennes Bioheat Transfer Equation with a Blood Vessel", Journal of Biomechanical Engineering, Vol. 116, pp. 208-212.

IMSL Library, Visual Numerics, Inc., Houston, Texas, 1999.

Jiang, S.C., Ma, N., Li, H. J. and Zhang, X. X., 2002, "Effects of Thermal Properties and Geometrical Dimensions on Skin Burn Injuries", Burns, Vol. 28, pp. 713-717.

Mikhailov, M. D. and Özisik, M. N., 1984, "Unified Analysis and Solutions of Heat and Mass Diffusion", Dover Publications, New York, 458 p.

O'Brien, K. T. and Mekkaoui, A. M., 1993, "Numerical Simulation of the Thermal Fields Ocurring in the Treatment of Malignant Tumors by Local Hyperthermia", Journal of Biomechanical Engineering, Vol. 115, pp. 247-253.

Ozisik, M. N., 1980, "Heat Conduction", Wiley Interscience, , p.686.

Pennes, H.H., 1948, "Analysis of Tissue and Arterial Blood Temperatures in the Resting Human Forearm", Journal of Applied Physiology, Vol. 1, pp. 93-122.

Presgrave, A. V., 2005, "Modelling and Simulation of Blood Perfusion Effects in Bioheat Transfer Problems" (in Portuguese), M.Sc. Dissertation, IME, Rio de Janeiro, Brazil, 205 p.

Presgrave, A. V., Guedes, R. O. C. and Scofano Neto, F., 2005, "Hybrid Analytical-Numerical Solution to the Bioheat Transfer Equation ", Proceedings of the 18 th. International Congress of Mechanical Engineering, Ouro Preto, Brazil.

Rawnsley, R. J. , Roemer, R. B. and Dutton, A. W., 1994, " The Simulation of Discrete Vessel Effects in Experimental Hyperthermia", Journal of Biomechanical Engineering, Vol.116, pp. 256-262.

7. Copyright Notice

Proceedings of the 11th Brazilian Congress of Thermal Sciences and Engineering -- ENCIT 2006
Braz. Soc. of Mechanical Sciences and Engineering -- ABCM, Curitiba, Brazil, Dec. 5-8, 2006

Paper CIT06-705

ANÁLISE DO ALONGAMENTO MUSCULAR DE ISQUITIBIAIS UTILIZANDO O MÉTODO CONVENCIONAL PASSIVO E ASSOCIADO A CALOR SUPERFICIAL E PROFUNDO

Bárbara Maria Camilotti
Pontifícia Universidade Católica do Paraná (PUCPR). Avenida Iguaçu, 1325 ap 408 A, Rebouças, Curitiba, Paraná, Brasil. CEP: 80250-190
ba.camilotti@gmail.com

Cássio Preis
Pontifícia Universidade Católica do Paraná (PUCPR). Rua Imaculada Conceição, 1155, Prado Velho, Curitiba, Paraná CEP: 80215-901.
cássio.preis@pucpr.br

Vera Lúcia Israel
Universidade Federal do Paraná-campus Litoral (UFPR). Rua Oyapok, 99 ap 1401, Curitiba, Paraná CEP: 80050-450.
veraisrael@terra.com.br

Caroline Leitão Riella
Pontifícia Universidade Católica do Paraná (PUCPR). Rua Padre germano Mayer, 99 ap 702, Curitiba, Paraná, Brasil. CEP: 80.050-270
carollis_riella@yahoo.com.br

Resumo. Recursos térmicos são freqüentemente utilizados associados ao alongamento muscular (AM). Este estudo objetiva analisar alterações no torque e comprimento muscular dos isquiotibiais em resposta a AM estático passivo e associado a recursos térmicos. Participaram 12 voluntárias divididas em 3 grupos. O grupo alongamento (GA) recebeu AM, o grupo calor profundo (GCP) recebeu 30 minutos de diatermia por ondas curtas contínuo e AM, e o grupo calor superficial (GCS) recebeu 30 minutos de calor, por bolsas de água aquecida, e AM. Foram realizadas quatro séries de AM de 45 segundos, com intervalo de 45 segundos entre as mesmas. A avaliação e reavaliação (após 10 sessões) constaram dos testes sentar-alcançar, retração de isquiotibiais e dinamometria isocinética. Houve incremento na flexibilidade em todos os grupos (GA 32% e 33,6%; GCP 29,2% e 19,4% e GCS 21,3 e 15,1%, teste de retração de isquiotibiais e sentar e alcançar respectivamente), acréscimo no pico de torque da flexão concêntrica de joelho a 60º/s (GA 6,9%, GCP 9,6% e GCS 3,24) e no torque, nos primeiros graus de flexão e nos últimos graus de extensão de joelho em todos os grupos. Pode-se concluir que o uso de termoterapia não teve influência percentual importante no ganho de flexibilidade.

Palavras chave: alongamento muscular, força muscular, recursos térmicos, Fisioterapia.

1. Introdução

Recursos térmicos são constantemente utilizados em procedimentos fisioterapêuticos, porém existem muitas controvérsias a respeito de seus efeitos no alongamento muscular. Existem ainda dúvidas a respeito dos efeitos do alongamento muscular, associado ou não a recursos térmicos, na performance muscular.

De acordo com knight et al. (2001), o alongamento muscular é utilizado em programas de reabilitação e atividades físicas e Fisioterapia devido a sua influência positiva na performance e prevenção de danos.

Os músculos esqueléticos de homens e mulheres contêm elementos contráteis e usam de mecanismos fisiológicos similares para produzir força durante os movimentos (Willems e Stauber, 2001).

Embora os exercícios de alongamento muscular melhorem a flexibilidade, Nelson et al. (2001), Marek et al. (2005) e Robertson et al. (2005) sugerem que o alongamento antes do exercício pode temporariamente comprometer a habilidade do músculo em produzir força, afetando negativamente a performance de atividades relacionadas com força máxima.

Exercícios de alongamento são freqüentemente combinados com aplicação de agentes térmicos, conforme relata Burke et al. (2001). O calor é amplamente utilizado em aplicações clínicas envolvendo Fisioterapia e especialmente relevante na resolução de problemas musculoesqueléticos. Os efeitos do calor superficial têm sido documentados, por Hecox (1994) e Lin (2003), como responsáveis pelo aumento da temperatura local dos tecidos e do tecido conjuntivo frouxo circunvizinho, o qual é responsável pela amplitude de movimento das articulações.

O calor profundo diminui a sensibilidade nervosa, aumenta o fluxo sangüíneo e o metabolismo tecidual, diminui a sensibilidade muscular ao alongamento, causa relaxamento muscular, reduz o espasmo muscular, aumenta a flexibilidade tecidual e aumenta o limiar da dor (Lentell et al., 1992, Cameron, 1999 e Shields et al., 2002). É

geralmente aceito que, os efeitos fisiológicos maiores da diatermia por ondas curtas, modo contínuo, estão relacionados com a indução do aumento do calor na temperatura tecidual (Shields et al., 2002).

A mobilidade articular é aumentada pela diminuição da viscosidade tecidual, aumento da extensibilidade do tecido conectivo e redução da dor através do calor. Em investigações prévias tem sido demonstrado que a temperatura influencia significativamente a propriedade mecânica dos tecidos moles. Especificamente, com o aumento da temperatura tecidual, a força do tecido conectivo diminui e a extensibilidade aumenta. Rigby et al. (1959) concluiu que o stress de relaxamento viscoso do tecido colágeno ocorre em associação com a condução de calor na microestrutura do colágeno. No entanto, Lehmann et al. (1970), Sluka et al. (1999), Burke et al. (2001) e Laufer et al. (2005) notaram que a deformação plástica ocorre com a extensibilidade tecidual.

2. Objetivo

Analisar as alterações na força e no comprimento muscular dos músculos isquiotibiais em resposta ao alongamento muscular utilizando o método convencional passivo e associado aos recursos térmicos.

3. Metodologia

3.1 Sujeitos

A amostra constituiu-se de 12 sujeitos do sexo feminino, hígidas, sedentárias, faixa etária de 18 a 25 anos.

Foram excluídos da pesquisa indivíduos que apresentassem qualquer patologia osteomusculoarticular, comprometimento da sensibilidade, gestantes, portadores de prótese metálica, marcapasso, dispositivo intra-uterino, tumor, processo inflamatório local, insuficiência circulatória e edema ou ulceração.

As participantes assinaram voluntariamente um termo de consentimento e foi respeitada a Resolução 156/96, com aprovação do Comitê de Ética e Pesquisa sob parecer número 319.

As participantes foram divididas aleatoriamente em três grupos: O grupo alongamento (GA) recebeu 10 sessões de alongamento muscular, o grupo calor (GCP) recebeu 10 sessões de alongamento muscular precedidas da aplicação de 30 minutos de calor profundo, por meio da diatermia por ondas curtas e o grupo calor superficial (GCS) recebeu 10 sessões de alongamento muscular precedidas de 30 minutos de calor superficial por meio de bolsas de água aquecida.

3.2 Pré e pós-teste

No dia anterior ao início e posterior ao término do procedimento foram realizados, no Centro de Dinamometria Isocinética da PUCPR, os testes sentar e alcançar, retração de isquiotibiais e dinamometria isocinética.

Foram avaliados o membro dominante e não dominante, porém utilizou-se apenas os dados obtidos do membro dominante. Para análise foi realizada uma média dos resultados obtidos.

No teste sentar e alcançar, foi utilizado um Banco de Well´s, no qual a voluntária sentou com seus pés apoiados na parte inferior do banco e, mantendo os joelhos estendidos, realizou uma flexão anterior do tronco, a fim de alcançar a extremidade do membro inferior. Numa fita métrica fixada na parte superior do banco obteve-se a medida alcançada pela extremidade do dedo médio (fig.1).

Figura 1: Teste sentar e alcançar

A retração de isquiotibiais foi obtida com a utilização de um goniômetro. A participante permaneceu em decúbito dorsal, com o membro inferior esquerdo estendido e o membro inferior direito com flexão de 90º de quadril e joelho, o avaliador estendeu gradualmente o joelho direito até encontrar resistência ao movimento, neste momento mensurou o ângulo obtido. O braço fixo do goniômetro foi posicionado na linha média lateral da coxa e o braço móvel na direção da fíbula da voluntária, o eixo foi posicionado na linha articular do joelho (fig.2).

Figura 2: Teste de retração de isquitibiais

A articulação do joelho foi avaliada por meio da dinamometria isocinética (Cybex Norm 7000), na posição sentada, onde foram executados, após aquecimento específico, três repetições a 60º/s (fig 3).

Figura 3: Dinamometria Isocinética

3.3 Protocolo dos recursos térmicos

A diatermia por meio de ondas curtas (Carci, Brasil; freqüência 27,12MHz, intensidade de saída 180W, eletrodo borracha de silicone 12x17 cm) foi aplicada por 30 minutos da forma contínua. A voluntária permaneceu em decúbito dorsal com os membros inferiores estendidos (fig.4). Os eletrodos foram posicionados da forma coplanar, sendo um deles posicionado na região glútea ao nível do tubérculo isquiático e o outro abaixo da fossa poplítea (fig. 4 e 5). A sensação térmica foi de um calor forte, porém tolerável.

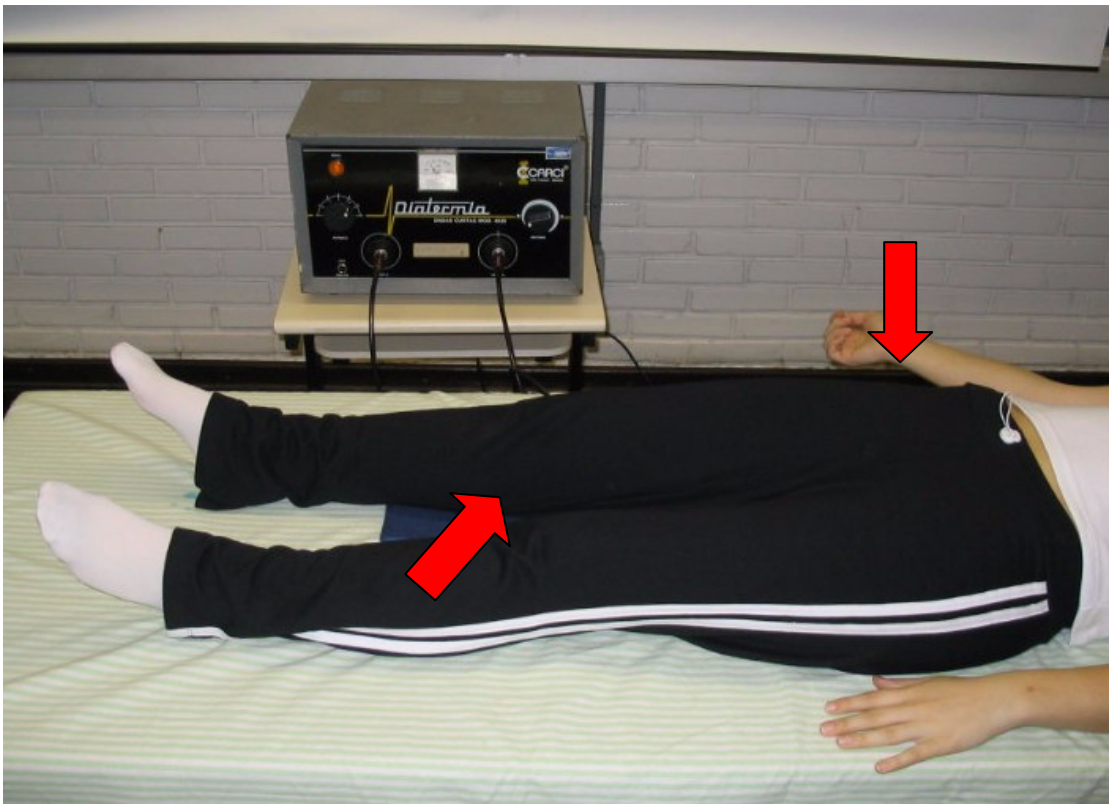

Figura 4: Diatermia por ondas curtas

Figura 5: Posicionamento dos eletrodos

As bolsas de água aquecida foram aplicadas por 30 minutos, na região compreendida entre o tubérculo isquiático e a fossa poplítea, numa temperatura de aproximadamente 44ºC. A voluntária permaneceu em decúbito ventral com os membros inferiores estendidos e os pés posicionados para fora da maca (fig. 6).

Figura 6: Bolsas de água aquecida

3.4 Protocolo de alongamento muscular

O alongamento muscular foi realizado da forma convencional passiva, onde a voluntária permaneceu em decúbito dorsal com os membros inferiores estendidos. O pesquisador flexionou gradualmente o membro inferior direito da voluntária, mantendo o joelho em extensão, a voluntária informou ao pesquisador o limite doloroso do alongamento (fig.7). Foram realizadas 4 séries de 45 segundo com um intervalo de 45 segundos entre cada série.

Nos grupos que receberam aplicação de agentes térmicos, o alongamento muscular foi realizado imediatamente após o término da aplicação.

Figura 7: Alongamento Muscular

4. Resultados

Observou-se, em todos os grupos de pesquisa, um incremento na flexibilidade, testes sentar e alcançar e retração de isquiotibiais (fig. 8 e 9 respectivamente). Pode-se observar que o GA foi o que apresentou maior destaque sob os demais grupos, os quais sofreram influência dos recursos térmicos.

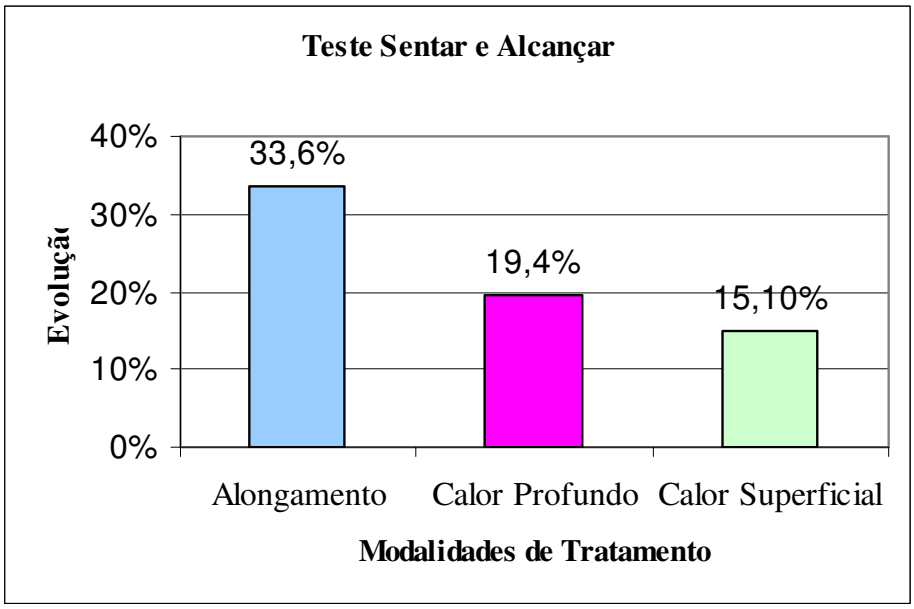

Figura 8: Evolução do Teste Sentar e Alcançar

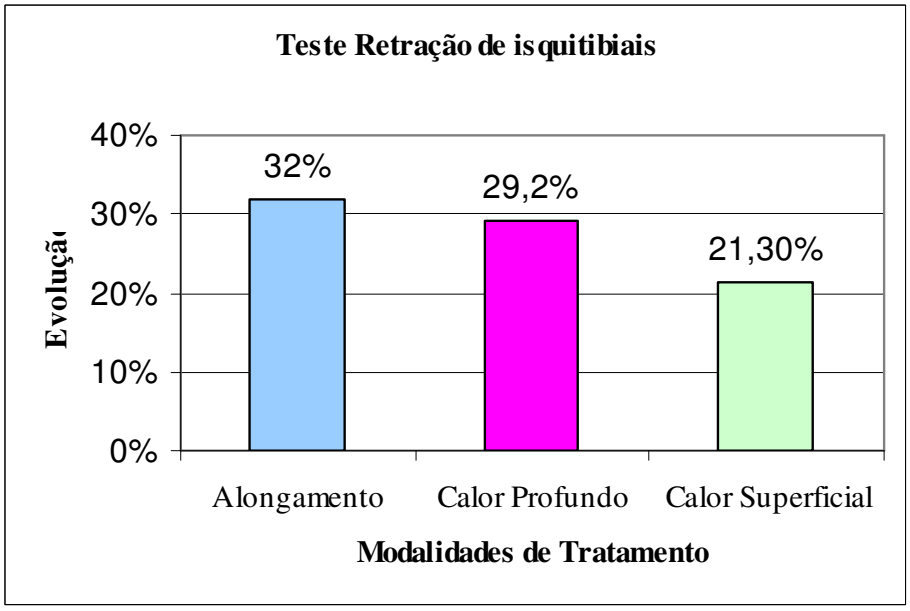

Figura 9: Evolução do Teste Retração de Isquiotibiais

Houve um acréscimo na força muscular após as 10 sessões de alongamento muscular, evidenciado pelo progresso no pico de torque da flexão concêntrica de joelho (fig.10).

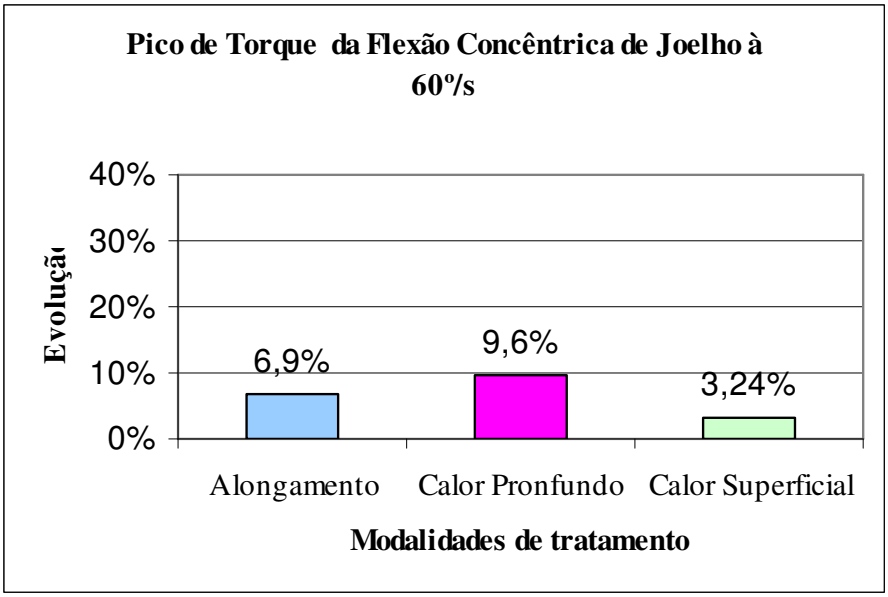

Figura 10: Evolução do Pico de Torque da Flexão concêntrica de Joelho à 60º/s

O incremento no torque nos 15 primeiros graus de flexão concêntrica de joelho e nos últimos 15 graus de extensão concêntrica de joelho (Tab. 1) foi observado em todos dos grupos de pesquisa.

Tabela 1: Progresso do Torque a 60º/s nos primeiros 5º, 10º e 15º de flexão concêntrica de joelho e nos últimos 5º, 10º e 15º de extensão concêntrica de joelho

Progresso do Torque a 60º/s nas angulações 5º, 10º e 15º em Flexão e Extensão Concêntrica de Joelho						
Grupo	5º flexão	10º flexão	15º Flexão	5º Extensão	10º Extensão	15º Extensão
A	221,75%	40,50%	22%	13,75%	29%	27%
CP	77,25%	32%	20,75%	5%	11,75%	4,75%
CS	198%	57%	28,75%	29,50%	29,75%	21,50%

5. Discussão

Em estudos realizados por Burke et al. (2001), Cornelius et al. (1992), Rosemberg et al. (1990) e Draper et al. (2002) não foi observada a influência dos recursos térmicos na efetividade do alongamento muscular, porém knight et al. (2001), Peres et al. (2002), Pinfild et al. (2004) e Taylor et al. (1984) observaram melhora na flexibilidade com a aplicação de calor.

O contraste existente entre as duas teorias está na maneira em que o calor contribui e/ou interfere na extensibilidade dos tecidos colágenos. Uma importante diferença está na interferência do calor em atingir não somente os tecidos conectivos, mas também os músculos e nervos que acarretam o aumento da extensibilidade, onde os resultados na força mecânica do tecido muscular e as mudanças nas atividades das fibras do nervo aferente pelo calor, ou a combinação desses fatores podem permitir diferentes resultados.

Segundo Rigby et al. (1959) e Rigby (1964) em temperaturas maiores que 37º C as propriedades dos tendões mudam sob stress mecânico. Com o aumento da temperatura ocorrem mudanças na microestrutura do colágeno as quais permitem deformações plásticas do tecido, sugerindo então, que no presente estudo, ocorreu apenas uma deformação elástica (não permanente).

Os poucos efeitos referentes ao calor superficial sugerem que a contribuição de resposta tenha se limitado à pele, ou o reflexo de vasodilatação associado ao calor na pele tenha sido mínimo, para que criasse suficiente resposta no músculo.

Houve um acréscimo na força muscular após as 10 sessões de alongamento muscular, evidenciado pelo progresso no pico de torque da flexão concêntrica de joelho. Kokkonenn et al. (1998), Fowles et al. (2000), Behm et al. (2001) e Marek et al. (2005) observaram redução na força muscular, porém estes resultados são referentes a alongamento agudo.

O incremento no torque nos primeiros graus de flexão concêntrica de joelho e nos últimos graus de extensão concêntrica de joelho observado em todos dos grupos de pesquisa, pode ter ocorrido em resposta ao alongamento muscular. Segundo Hamil e Knutzen (1999), no final de um movimento articular, o músculo fica fraco e incapaz de gerar grandes quantidades de força, devido seu comprimento encurtado e a conseqüente sobreposição dos filamentos de actina e miosina. Além disso, Wilson et al. (1994) sugere que a unidade músculo tendinosa, quando forte, permite que esta força, gerada por um componente contrátil do músculo, seja transmitida para o sistema esquelético muito mais eficientemente que uma unidade alongada.

6. Conclusão

Os resultados obtidos neste estudo permitem avaliar que a flexibilidade e força muscular aumentam estando associada ou não a recursos térmicos, porém o aumento da flexibilidade em decorrência do uso de termoterapia não teve um percentual de diferença importante.

Este estudo é importante e acrescenta conhecimento à base de dados da performance muscular. A limitação do estudo envolve o pequeno número do universo amostral e a diferenças em relação à metodologia utilizada no alongamento pelos demais autores.

7. Referências

Behm, DG.; Button DC.; Butt., JC., 2001, "Factors affecting force loss with prolonged stretching", Can J of Appl Phys, vol.26, no. 262-272.

Burke DG, Holt LE, Rasmussen R, MacKinnon NC, Vossen JF, Pelhamt T.W., 2001, "Effects of Hot or Cold Water Immersion and Modified Propioceptive Flexibility Exercise on Hamstring Length", Journal of Athel Train, vol.36, no.1, pp.16.

Burke, DG.; Holt, LE.; Rasmussen, R.; Mackinnon, N.C.; Vossen, J. F.; Pelham T.W., 2001, "Effects of hot and cold water immersion and modified proprioceptive neuromuscular facilitation flexibility exercise on hamstring length", Journal of Athl Train, vol.36, no.1, pp.16-19.

Cameron MH., 1999, "Physical agents in rehabilitation from research to practice", Philadelphia:WB Saunders.

Cornelius WL.; Ebraim, K.; Watson J.; Hill, D., 1992, "The effects of cold application and modified PNF stretching techniques on hip joint flexibility in college males", Resear Quart for Exerc and Sport, vol.63, no.3, pp.311-314.

Draper DO, Miner L, Knight KL, Ricard MD., 2002, "The Carry-Over Effects of Diathermy and Stretching in Developing Hamstring Flexibility", Journal of Athel Trainers´Assoc, vol.37, no.1, pp.37-42.

Fowles JR.; Sale, DG.; Macdougall, JD., 2000, "Reduced strength after passive stretch of the human plantarflexors", Journal of Appl Phys, vol.89, pp.1179-1188.

Hamil, J; Knutzen, K. M., 1999, "Bases biomecânicas do movimento humano", São Paulo: Manole. 532p.

Hecox B., 1994, "Clinical effects of thermal modalities", Physical agents, Norwalk, CT: Appleton & Lange, pp. 94-123.

Knight CA, Rutledge CR, Cox ME, Acosta M, Hall S., 2001, "Effect of Superficial Heat, Deep Heat, and Active Exercise Warm-up on the Extensibility of the Plantar Flexors", Phys Ther, vol. 81, pp. 1207-1214.

Kokkonen J, Nelson AB, Cornewell, 1998, "Acute Muscle Stretching Inhibts Maximal Strengh Performance", Research Quarterly for Exercise and Sport, vol.69, no.4, p.141.

Laufer Y, Zilberman R, Porat R, Nahir AM., 2005, "Effect of pulsed short-wave diathermy on pain and function of subjects osteoarthrits oh the knee: a comparison placebo controlled double-blind clinical trial", Clin Rehabil, vol.19, pp.255-263

Lehmann J, Masock A, Warren C., 1970, "Effect of Therapeutic temperatures on tendon extensibility", Arch Phys Med Rehabil, vol.51, pp.481-487.

Lentell G, Heatherington T, Eagan L, Morgan M., 1992, "The use of thermal agents to influence the effectiveness of a low-load prolonged stretch", Journal Orthop Sports Phys Ther, vol.16, pp.200–207.

Lin YH., 2003, "Effects of thermal therapy in improving the passive range of knee motion: comparison of cold and superficial heat applications", Clin Rehabilb, vol.17, pp.618-623.

Marek SM, Cramer JT, Fincher AL, Massey LL, Dangelmaier SM, Purkayastha S, Fitz KA, Culberston JY., 2005, "Acute Effects of Static and Proprioceptive Neuromuscular Facilitation Stretching on Muscle and Power Output", Journal of Athl Trainers´Ássoc, vol.40, no.2, pp.94-103.

Nelson, AG.; Allen, JD.; Cornwell, A; Kokkonem, J., 2001, "Inhibition of maximal voluntary isometric torque production by acute stretching is joint angle specific", Research quarterly for exercise and sport, vol.72, no.1, pp. 68-70.

Peres, S.E.; Draper, D.O.; Knight K.L.; Ricard M.D., 2002, "Pulsed Shortwave Diathermy and Prolonged Long-Duration Stretching Increase Dorsiflexion Range of Motion More Than Identical Stretching Without Diathermy", Journal of Athl Train, vol.37, no.1, pp.43–50.

Pinfild, C E; Prado, R P; Liebano, R E., "Efeito do alongamento estático após diatermia de ondas curtas versus alongamento estático nos músculos isquiotibiais em mulheres sedentárias", Fisioterapia Brasil, vol.5, no. 2, pp.119-130.

Rigby B, Hirai N, Spikes JD, Eyring H., 1964, "The mechanical properties of rat tail tension", Journal Gen Phys, vol.43, pp. 265-283.

Rigby B., 1964, "The effect of mechanical extension upon the thermal stability of collagen", Biochim Biophys Acta, vol.79, pp.634-636.

Robertson VJ, Ward, AR, Jung P., 2005, "The effect of Heat on Tissue Extensibility: A Comparison of Deep and Superficial Heating", Arch Phys Med Rehabil, vol.86, pp.819-823.

Rosemberg BS, Cornelius, WL.; Jackson, A.W., 1990, "The effects of cryotherapy and PNF stretching techniques on hip extensor flexibility on elderly females", Journal of Phys Education and Sport Science, vol.2, no.2, pp.31-36.

Shields N, Gormely J O´Hare N., 2002, "Short Wave diathermy: current clinical and safety practices", Physiother Res Int., vol.7, pp.191-202.

Sluka KA, Christy MR, Rudd SL, Troy SM., 1999, "Reduction of pain-related behaviors with either cold or heat in an animal model of acute arthritis", Arch Phys Med Rehabil, vol.80, pp.313-317.

Taylor B, Waring C, Brashear T., 1984, "The effects of therapeutic application of heat or cold followed by static stretch on hamstring flexibility", Journal Orthop Sports Phys Ther, vol.6, pp.110-115.

Willems MET, Stauber WT., 2001, "Force deficits after repeated stretches of activated skeletal muscles in female and male rats", Acta Physiol Scand , vol.172, pp. 63-67.

Wilson GJ, Murphy AJ, & Pryor JF., 1994, "Musculo-tendinous stiffness: is relationship to eccentric, isometric, and concentric performance", Journal of Appl Phys, vol.76, pp. 2714-2719.

ANALYSIS OF THE MUSCULAR STRETCH OF HAMSTRINGS USING THE CONVENCIONAL PASSIVE METHOD AND IN ASSOCIATION WITH SUPERFICIAL AND DEEP HEAT

Bárbara Maria Camilotti
Pontifícia Universidade Católica do Paraná (PUCPR). Iguaçu Avenue, 1325 ap 408 A, Rebouças, Curitiba, Paraná, Brazil. ZIP: 80250-190
ba.camilotti@gmail.com

Cássio Preis
Pontifícia Universidade Católica do Paraná (PUCPR). Imaculada Conceição Street, 1155, Prado Velho, Curitiba, Paraná ZIP: 80215-901.
cássio.preis@pucpr.br

Vera Lúcia Israel
Universidade Federal do Paraná-Litoral (UFPR). Oyapok Street, 99 ap 1401, Curitiba, Paraná ZIP: 80050-450.
veraisrael@terra.com.br

Caroline Leitão Riella
Pontifícia Universidade Católica do Paraná (PUCPR). Padre germano Mayer Street, 99 ap 702, Curitiba, Paraná, ZIP: 80.050-270
carollis_riella@yahoo.com.br

Abstract
Thermal resources are often used in association with muscular stretch (MS). These study aim to analyses the alteration on torque and muscular length of hamstrings as a response to static passive MS and in association with thermal resources. Participate twelve female volunteers, divided into 3 groups. The stretch group (SG) received MS, the deep heat group (DHG) received 30 minutes of continuous diathermy by short wave and MS, and the superficial heat group (SHG) received 30 minutes of heat by purses of warm water and MS. It was realized 4 series of MS of 45 seconds each, with intervals of 45 seconds between each. The evaluation e reevaluation (after 10 sessions), consisted of seat and reach and hamstrings contraction tests and isokinetic dynamometry. There was increase in the flexibility (SG 32% and 33,6%; DHG 29,2% and 19,4% and SHG 21,3 e 15,1%, in seat and reach and hamstrings contraction respectively), augment in the peak of torque at 60º/s (SG 6,9%, DHG 9,6% e SHG 3,24) and in torque, on the first degrees of flexion and last degrees of extension in all groups. It was possible to conclude that the use o thermotherapy don't have percentual influence in the gain of flexibility.

Key words: Muscular Stretch, Muscular Strength, Thermal Resources and Physiotherapy.

Paper CIT06-0782

DEVELOPMENT OF AN AIR HEATING AND HUMIDIFYING SYSTEM FOR MECHANICAL VENTILATION OF INTENSIVE CARE UNIT PATIENTS

Eliana Leal Ferreira
Programa de Pós-Graduação em Engenharia Mecânica, PGMEC, Universidade Federal do Paraná, C.P. 19011, Curitiba, PR 81531-990, Brazil
elianalealf@yahoo.com.br

José Viriato Coelho Vargas
Programa de Pós-Graduação em Engenharia Mecânica, PGMEC, Universidade Federal do Paraná, C.P. 19011, Curitiba, PR 81531-990, Brazil
jvargas@demec.ufpr.br

Marcos Carvalho Campos
Departamento de Engenharia Mecânica, PGMEC, Universidade Federal do Paraná, C.P. 19011, Curitiba, PR 81531-990, Brazil
mccampos@demec.ufpr.br

Fernando Gallego Dias
Programa de Pós-Graduação em Engenharia, PIPE, Universidade Federal do Paraná, C.P. 19011, Curitiba, PR 81531-990, Brazil
gallego@ufpr.br

Juan Carlos Ordonez
Department of Mechanical Engineering and Center for Advanced Power Systems, Florida State University, Tallahassee, Florida, 32310, USA
ordonez@caps.fsu.edu

Marcos Leal Brioschi
Clínica Brioschi, Rua da Paz, 195, cj 118, Curitiba, PR 80060-160, Brazil
termometria@yahoo.com.br

Abstract. *The mechanical ventilators, also named artificial ventilators, are devices used in Intensive Care Units (ICU) for clinically critical patients. The equipment provides artificial breathing for the patient, creating favorable conditions for the patient recovery. It works as a system that is connected to the electric grid and two other networks, one supplies compressed air and the other supplies pure oxygen. Inside the equipment the gases are mixed, and then warmed up and humidified to be finally delivered to the patient. The existing system for treatment of the mixture is not effective, since it delivers the breathing air to the patient out of the normal physiology recommended range, i.e., temperature ~ 32-34°C and relative humidity ~ 80-95%. The objective of this work was to develop a new air heating and humidifying system for mechanical ventilation. First, it was built an air feeding system, composed by a compressor and an electronically controlled valve to simulate an actual mechanical ventilation system in the laboratory. A device for conditioning the air (temperature and humidity) was conceived and built for treating the air feeding system output air. The results of the laboratory measurements show that the developed equipment was capable of making the breathing air to reach the recommended ranges by the normal physiology.*

Keywords*. Mechanical ventilation, humidifiers, air filter, barrier filter, air relative humidity, temperature*

1. Introduction

It has long been considered desirable to provide warm and humid inspired gas to mechanically ventilated patients, and various methods to achieve this have been proposed (Chalon et al., 1972; Stone et al., 1981 and Hedley and Allt-Graham, 1994). An artificial air inlet (endotracheal intubation or tracheostomy) associated with mechanical ventilation does not allow the normal physiologic air heating and humidifying process of inspired gases through the upper airway to happen. As a result, in mechanically ventilated patients, a continuous loss of heat and moisture occurs, which predisposes patients to serious airway damage (Chalon et al., 1972; Stone et al., 1981; Hedley and Allt-Graham, 1994; Chalon et al., 1979; Forbes, 1973; Forbes, 1974 and Noguchi et al., 1973). In addition, medical gases are dried to avoid condensation damage to valves and regulators in the distribution network.

The mechanical ventilators, also called artificial breathing machines, are instruments built to aid clinically unstable patients or that do not have conditions to breath by themselves. So, there are means to aid the health recovery of those

patients. The functioning of most of these machines can basically be described as a system that connects to the power line to two gas lines, which are: I) compressed air – which is responsible for keeping the pressure flow of the machine to the respiratory system of the patient, and II) oxygen – responsible for keeping the oxygenation of the organs and tissues of the patient. Inside of this machine it occurs the mixture of the gases in the blender, which are then passed to the patient, after the gases are treated by another system coupled to the machine. This coupled system works on heating and humidification of the inspired air, or technically speaking, the insufflated air fraction to the patient's lung interior. The insufflated air fraction depends on the ventilatory mode: i) VCV – volume controlled ventilation; ii) VCAV – volume controlled assisted ventilation; iii) PCV – pressure controlled ventilation; iv) PCAV – pressure controlled assisted ventilation; v) SIMV – synchronized intermittent mandatory ventilation; vi) VCV – pressure supported ventilation; vii) PAV – proportionally assisted ventilation. Those systems basically differ from one another on the type of utilized mechanism to create the air mass flow rate to the patient's lungs. After that, an inspiratory valve triggers and cycles the flow. The final stage is the insufflated air heating and humidification which is performed by humidifiers coupled to the mechanical ventilator. This is accomplished in a pre-determined time, according to the pathology being treated. It's specifically about this system of treatment of the insufflated air in the patient that this article analyzes and develops a study, since the existing systems feed air with low temperature (~ 22°C) and low relative humidity (under 60%).

Some systems are available in the market that have been created with the purpose of heating the air, or filter it of germs and bacteria (general impurities). Nevertheless, none of them show a reading system capable of informing the amount of water in the insufflated air (relative humidity), the value of the internal temperature and the heat that is being lost to the environment. So, there is a necessity of a specific thermodynamic study for this system, which allows, after applying the energy balance (first law of thermodynamics), the development and improvement of the system of conditioning of the insufflated air that comes out of the mechanical ventilation system.

This work has the following objectives: i) to develop an equipment capable of improving the current mechanical ventilation systems, and ii) to insure the air supply in the conditions established by the medical protocol: 32 ºC to 34ºC of temperature, and 80% to 95% of relative humidity. The new equipment to be coupled to the mechanical ventilation system is expected to meet the required air conditions for the intubated patient.

2. Materials and Methods

In the period between January 2005 and December 2005, measurements were performed of temperature and relative humidity of the input and output air of a test lung, during procedures of simulation and mechanical ventilation which normally is made on patients on ICU. To do this simulation, first it was built in the laboratory an air feeding system, composed by one compressor and one valve for opening and closing the insufflating air flow, which was electronically controlled to simulate an actual ventilation system.

A prototype of an equipment for conditioning the air to be insufflated in patients (temperature and humidity) was idealized and built for air treatment in the output of the air feeding system. The criteria of selection of the materials idealized for the composition of the experimental prototype were the following:

I – selection of the adequate instrumentation which makes possible the adequate registration and controlling of the temperature and air relative humidity;

II – availability of an air compressor, for air flow generation, with pressure and flow enough to expand-fill the test lung, of the same model used in the calibration of the mechanical ventilators used in the ICU;

III – availability of a data acquisition system, which makes possible the generation of a data bank, for the numerical and graphical evaluation of the acquired data;

IV – utilization of acrylic transparent material for the manufacturing of the system, with the purpose of visualization of the process and to provide the necessary rigidity;

V – utilization of thermistors of high precision, of the type YSI4404 (2250 Ω @25 º C) made by the company YSI Incorporated, USA, for the measurement of temperature;

VI – utilization of relative humidity sensors of the type SC-500, made by the company Ohmic Instruments Co., USA, for the measurement of the air relative humidity;

VII – utilization of a regular thermostat with a scale of 0 to 40 ºC, for controlling of a resistance for air heating;

VIII – utilization of a mechanical hygrostat, made by the company Lufft, Germany, for the control of a water jet pump for the humidification of the air, and

IX - utilization of a system for air heating and humidification, interconnected, with simultaneous control, to reach the values established by medical protocol.

For all the equipments tests were made for calibration, until the final configuration of the equipment was achieved. The experiments were conducted integrally at the Hydraulic Machines Laboratory, at the Department of Mechanical Engineering of Universidade Federal do Paraná, UFPR.

3. Results and Discussion

The following graphs present the experimental measurements made in the laboratory, using the data acquisition system. The measured data was converted in numerical values of temperature and relative humidity of the air in the input and output of the system.

Two tests were performed in this work. The graphs show the behavior of the temperature and air relative humidity in three points of the system. The first selected point was the air input of the new system, which corresponds to the air output of the traditional mechanical ventilator. The second selected point was the air output of the new system, i.e., after the air was treated by the new system. The ambient temperature was also measured. The main objective was to verify if the proposed system is capable of producing the desirable effects, i.e., conditioning the air insufflated to the patient within the levels recommended by medical protocol. Both tests were conducted in the period of 3600 seconds (1 hour).

The graphs for test 01 (Figs. 1 and 2) show that the input temperature of the system was at 23 ºC and the relative humidity was at 40%, in the beginning of the experiment. Figure 1 shows that it took 1800 seconds (30 minutes) for the air to reach the temperature of 34 ºC in the output of the system (which is the lower point in the range established by the medical protocol). The system response for the relative humidity is quite faster, since that right in the beginning of the experiment it reached 66% as shown in Fig. 2. After 3600 seconds (1 hour), the air in the output of the system, which is delivered to the patient, was at 34 ºC, and the relative humidity at 77%. The ambient temperature remained at 21ºC during the experiment.

Test 02 was performed in the following day of test 01. The results of Figs. 3 and 4 are quite similar to test 01. The idea of performing several tests is to demonstrate that the system repeats its results under different conditions. For test 02, the input temperature in the system was 24 ºC and the relative humidity was 46% in the beginning of the experiment. Similarly to the first test, the air took about 1800 seconds (30 minutes) to reach the conditions established by medical protocol, i.e., 34 ºC in the system output. The response of the relative humidity was quite faster again, i.e., in the beginning of the experiment it reached 69%. After 3600 seconds (1 hour), the air in the output of the system, which is delivered to the patient, was at 35 ºC, and the relative humidity at 80%. The ambient temperature remained at 21ºC during the experiment.

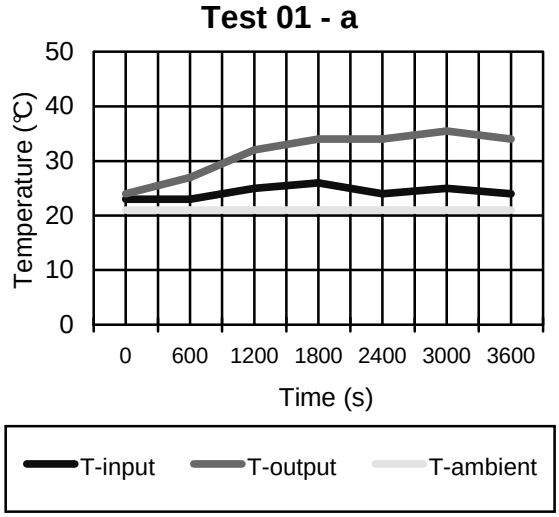

Figure 1. The three temperatures behavior during test 01.

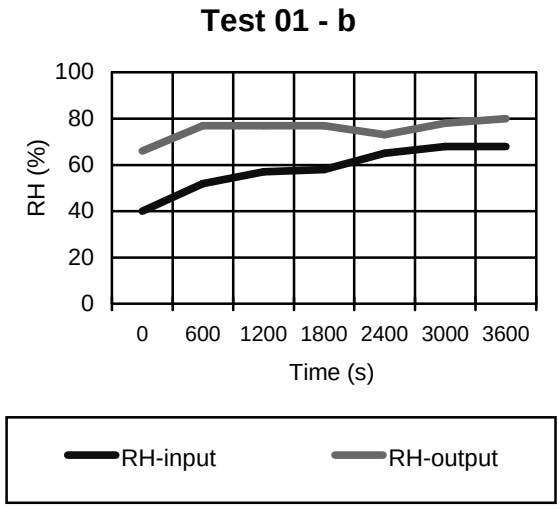

Figure 2. The two relative humidities (RH) behavior during test 01.

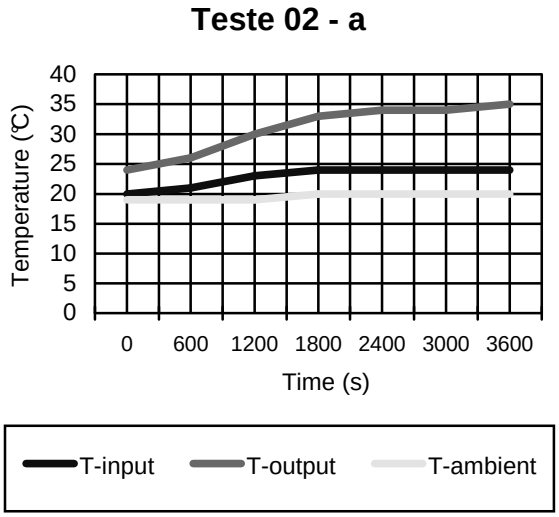

Figure 3. The three temperatures behavior during test 02.

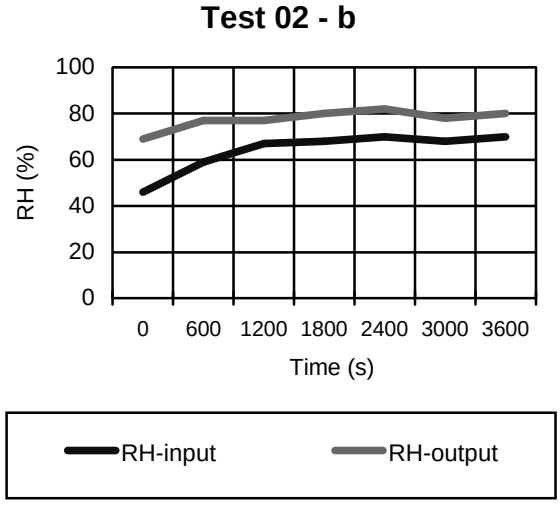

Figure 4. The two relative humidities (RH) behavior during test 02.

4. Conclusions

In this research, a new system for conditioning the output air of mechanical ventilators was developed and a prototype was built and patented (Ferreira et al., 2006), with the main objective of minimizing the problems caused to the intubated patients in the ICU by the existing systems, such as hypothermia, hyperthermia and water condensation in the system. This leads to great proliferation of germs and bacteria, and delays the treatment of the critical ICU patient.

According to the results presented in this paper, it is possible to minimize the effects on the respiratory system of intubated patients in the ICU by controlling the temperature and relative humidity of the air in the input of endotracheal tube that conducts the air to the patient. This was demonstrated by connecting a new equipment to the output of a mechanical ventilator, of simple conception, considered in this work, to condition the air to be insufflated to the intubated patient. It is interesting to point out that the new equipment does not take too long to reach the desired temperature and relative humidity conditions, i.e., approximately 30 minutes in the tests performed in this study, mainly if it is considered that without the equipment, the patient would have to breath air out of the recommended conditions by the medical protocol.

Finally, it is important to point out that the need to demonstrate the effectiveness of the new equipment through studies in human beings is crucial, under the ethical and legal points of view. Only after performing such experiments, it will be demonstrated the viability and applicability of the system in human beings.

5. References

Chalon, J., Loew, D. and Malebranche, J., 1972, “Effect of Dry Anesthetic Gases on Tracheobronchial Ciliated Epithelium”, Anesthesiology, Vol. 37, pp. 338-343.

Chalon, J., Patel, C., Ali, M., Turndorf, H. and Fischgrund, G. K., 1979, “Humidity and the Anesthetized Patient”. Anesthesiology, Vol. 50, pp. 195-198.

Ferreira, E. L., Vargas, J. V. C., Campos, M. C., Brioschi, M. L., Alves, J. L. and Ordonez, J. C., 2006, “Sistema De Aquecimento e Umidificação de Ar para Ventilação Mecânica de Pacientes de Unidade de Terapia Intensiva”, Patente: Privilégio e Inovação. Nr. PI06010687, 31 de Mar (Depósito).

Forbes, A. R., 1973, “Humidification and Mucus Flow in the Intubated Trachea”, Br J Anaesth Vol. 45, pp. 874-878.

Forbes, A. R., 1974, “Temperature, Humidity and Mucus Flow in the Intubated Trachea”, Br J Anaesth, Vol. 46, pp. 29-34.

Hedley, R. M. and Allt-Graham, J., 1994, “Heat and Moisture Exchangers and Breathing Filters”, Br J Anaesth, Vol. 73, pp. 227-236.

Noguchi, H., Takumi, Y. and Aochi, O., 1973, “A Study of Humidification in Tracheostomized Dogs”, Br J Anaesth, Vol. 45, pp. 844-848.

Stone, D. R., Downs, J. B., Paul, W. L. and Perkins, H. M., 1981, “Adult Body Temperature and Heated Humidification of Anesthetic Gases during General Anesthesia”, Anesth Analg, Vol. 60, pp. 736-741.

6. Copyright Notice

Proceedings of the 11th Brazilian Congress of Thermal Sciences and Engineering -- ENCIT 2006
Braz. Soc. of Mechanical Sciences and Engineering -- ABCM, Curitiba, Brazil,- Dec. 5-8, 2006

Paper CIT06-811

AN APPARATUS FOR TESTING EXTERNAL SHUNTS UTILIZED IN HYDROCEPHALUS SURGERY TREATMENT

José Ricardo Camilo
Ventura Biomédica, São José do Rio Preto,SP, Brazil.
camilo@venturaneuro.com.br

Angelo L. Maset
INNEURO - Instituto de Neurocirurgia e Neurociências do Oeste Paulista, São José do Rio Preto, Brazil,
maset@venturaneuro.com.br

Kleber Paiva Duarte
INNEURO - Instituto de Neurocirurgia e Neurociências do Oeste Paulista, São José do Rio Preto, Brazil,
Brazil, kleberduarte@uol.com.br

Sérgio Said Mansur
Unesp – Faculdade de Engenharia de Ilha Solteira, Ilha Solteira, SP, Brazil.
mansur@dem.feis.unesp.br

Edson Del Rio Vieira
Unesp – Faculdade de Engenharia de Ilha Solteira, Ilha Solteira, SP, Brazil.
delrio@dem.feis.unesp.br

Abstract. *The watery solution continually produced inside the brain in the choroid plexus tissues is named cerebrospinal fluid (CSF). Humans are estimated to produce about 0.5 ml/kg per hour, or about 500 ml or more of CSF each day. A discrepancy in CSF production and absorption cumulates an excess of fluid in the brain. Elevated levels of CSF are associated with traumatic brain injury, meninge infections (meningitis) and a pediatric disease known as hydrocephalus. In all of these cases, an increasing fluid pressure (intracranial pressure), resulting in permanent brain injury and death, can be observed. Following the diagnosis of hydrocephalus, there are few options other than surgery for treatment. Most surgeons use various types of systems called shunts to channel the fluid from the ventricles to other sites in the body such as the abdominal cavity (internal shunts). Liquor can also be drained towards an external reservoir (external shunts). In the present work an apparatus operating as bench test has been developed for testing external shunts. Utilizing automated control and data acquisition system, in order to realize the experiments, hydrodynamics characteristics of several shunts parts can be rapidly obtained. Some first results from a first prototipe of an anti-siphon valve are included.*

Keywords. *External shunt, cerebrospinal fluid, hydrocephalus, neurosurgical devices.*

1. Introduction

The watery solution continually produced internal the brain in choroid plexus tissues is named, in medical literature, liquor or cerebrospinal fluid (CSF). The CSF flows through a series of cavities (ventricles) out of the brain and down along the spinal cord. The brain and spinal cord float in a sea of cerebrospinal fluid within the skull and spine. Additionally, brain and spinal cord are covered by a series of membranes called meninges.

Humans are estimated to produce continually about 0.5 ml/kg per hour, or approximately 500 ml or more of liquor each day. In an adult, in normal conditions, 150 ml of CSF have been estimated at any given time located in the brain ventricles. A discrepancy in CSF production and absorption cumulates an excess of fluid in the brain. Elevated levels of CSF are associated with traumatic brain injury, meninge infections (meningitis) and a pediatric disease known as hydrocephalus. In all of these cases, an increase fluid pressure (intracranial pressure – ICP) can be observed resulting in permanent brain injury and death.

If diagnosis of hydrocephalus has been obtained there are rarely options other than surgery for treatment. If a definable mass is causing the obstruction of flow it may be possible, if not essential, to remove the mass and allow for normal flow and resolution of the hydrocephalus. More often then not however, the blockage can not be removed and the fluid needs to bypass the normal circulation. Most surgeons use various types of systems called shunts to channel the fluid from the ventricles to other sites in the body such as the abdominal cavity (internal shunts). Liquor drainage can be realized also for an external reservoir (external shunts). In accord to Sesay *et al.* (2002), the external drainage of CSF has been realized only in emergency situations and frequently external drainage is a provisory condition after the surgery to implant semi permanent internal drainage device. A sketch of an external device for CSF drainage has been shown in Fig. 1. External reservoir is submitted to atmospheric pressure (Patm) and the height H should be carefully determined by surgeon. ICP should overpass the height H to produce drain effect. If height H is very small or negative

over-drainage occurs after shunting. Over-drainage of cerebrospinal fluid can occur with relative high frequency and after few seconds in this adverse condition unavoidable non reversible cerebral damage occurs. Over-drainage of gravitational external shunts studies have been intensely realized by Camilo *et al.* (2005) and Maset *et al.* (2005). Over drainage of the ventricles can result in collapse of the brain away from the inner surface of the skull with a resultant risk of bleeding with compression of the brain. Long term over drainage can result in headaches of a very debilitating degree.

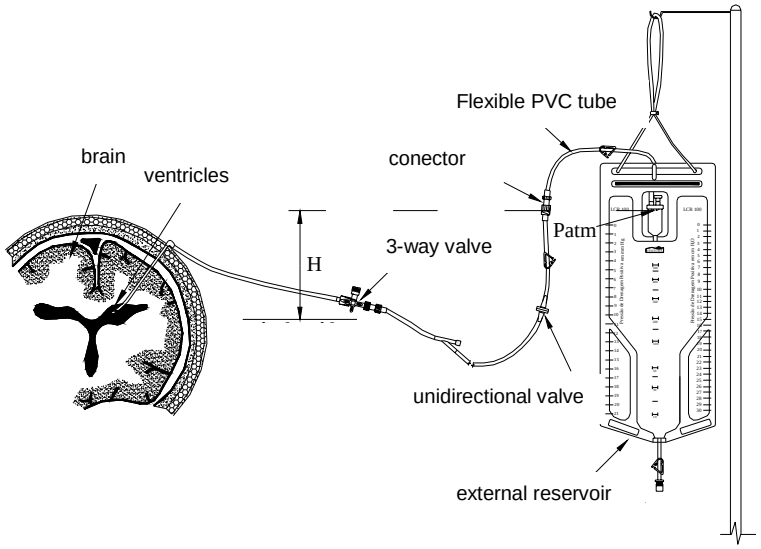

Figure 1. Neurosurgical external gravitational shunt sketch.

In 1999, Aschoff *et al.* (1999) show 127 different types of neurological valves commercially available since 1949 and more than others 70 models in different developing phases. All of these valves have been developed for application exclusively in internal shunts. Internal shunts for drainage CSF utilize a neurological valve to stabilize the ICP controlling the flow rate. Unfortunately, even at present day, the drainage characteristics of neurological valves are far from ideal. In this viewpoint, many effort of research are realized to improve of neurological valves. In addition the use of internal shunts has created problems of shunt dependence with frequent shunt revisions being the rule for most hydrocephalic children. Because of this inconvenient, internal shunt problems assume a major amount of all neurosurgeon's efforts and the more target of research. In the other side, few efforts have been realized in research in external shunts. The use of external shunts is an important provisory procedure in a first phase of hydrocephalus treatment, before the implantation of internal shunts. In this work of research an apparatus for testing external shunts utilized in hydrocephalus surgery treatment has been proposed in order to obtain hydraulic characteristics of external shunts parts. This test device permits measurements of differential pressure in function of flow rate for individual shunt parts or in testing complete external shunts. Additionally, results of a first prototype of an anti-siphon valve for external shunts have been showed.

2. Intracraneal pressure (ICP)

Hydrocephalus is caused by an increase in the production rate of CSF (very rare) or, more frequently, by disturbing in CSF absorption. Production/absorption imbalance of CSF causes a sensible increase of ICP. Second Puget (2005), congenital hydrocephalus can to occur one time in each 2 000 births. The incidence of acquired hydrocephalus is not known. The peak ages for the development of hydrocephalus are in infancy, between four and eight years, and in early adulthood. Normal pressure hydrocephalus generally occurs in patients over the age of 60.

In accord to Gusmão *et al*. (2000), in an adult laing, the intracranial pressure changes from 50 to 200 mm of water. Frequently, in several works utilize 150 mm of water column as a reference value. In this situation, the ICP is same into ventricles and around all spinal cord. In standing up position, measured in hydrocephalus patient, ICP shows small values near atmospheric pressure. In children, ICP shows a medium value around 45 mm of water in standing up position and near zero in lay down position.

Measurement, involving 80 patients, performed by Kajimoto *et al.* (2000) show ICP value in lay position of 4.6 ± 3 mm of Hg and for standing up of -14.2 ± 6.3 mm of Hg. Negative values of ICP have been observed because different measurement procedures. Utilizing an adequate referential of pressure, ICP in standing up position can be corrected utilizing an adequate referential.

Kajimoto *et al.* (2000) also studied the ICP variation in function of changes in postural position Sudden alteration in postural position provokes rapid alteration, less than 30 seconds, in ICP values.

ICP monitoring studies are now being used more frequently in younger patients and older patients with possible low grade hydrocephalus – Pople (2002). ICP monitoring may reveal "B waves" either at night time alone or throughout the day and night. An ICP above 15 mm Hg at frequent intervals during the night or day while asleep or resting is abnormal, and patients with functioning shunts should normally have an ICP below or near to zero while 45° head up in bed. CSF infusion tests measure CSF outflow resistance, which in simple terms represents the overall compliance of the intracranial and spinal CSF compartment. During this test saline or artificial CSF is constantly infused via a lumbar puncture needle or catheter, and the subsequent gradient of rise in the ICP with time is recorded. A low outflow resistance corresponds to high cerebral compliance and vice versa. Normal values are 5–10 mm Hg/ml/minute and a value > 18 mm Hg/ml/minute appears to be the approximate cut off point for diagnosing active hydrocephalus in the elderly. Other compliance monitors have recently been developed that are placed as bolts through small twist drill holes in the skull. These tests can be used to guide treatment of patients with newly diagnosed ventricular enlargement they can also be useful in patients with possible blockage of their shunts or delayed occlusion of their third ventriculostomy site.

3. External shunts

Figure 1 shows a typical external system of cerebrospinal fluid drainage. This apparatus consists of a proximal (ventricular) end that is inserted through the skull (via a small hole), through the brain substance, and into the cerebral ventricles. This catheter is connected to a small diameter flexible tube. A typical flexible tube made in PVC is depicted in the Fig. 2. The three-way taps were utilized in external CSF drainage in order to connect devices for monitoring ICP, to provide a rapid means of drugs infusion (antibiotics for CSF infection or chemotherapy medication for tumors) and to gather samples of CSF to be examined for bacteria, cancer cells, blood or protein, depending on the cause of hydrocephalus. In post-subarachnoid and post-meningitic hydrocephalus, CSF samples are useful for cell counts, protein concentration, and to exclude residual infection. A protein concentration greater than 4 g/l will clog up most ventriculo-peritoneal internal shunt valves. Recently, optimized design of three-way taps for external shunts attracted attention of researchers – Camilo *et al.* (2006).

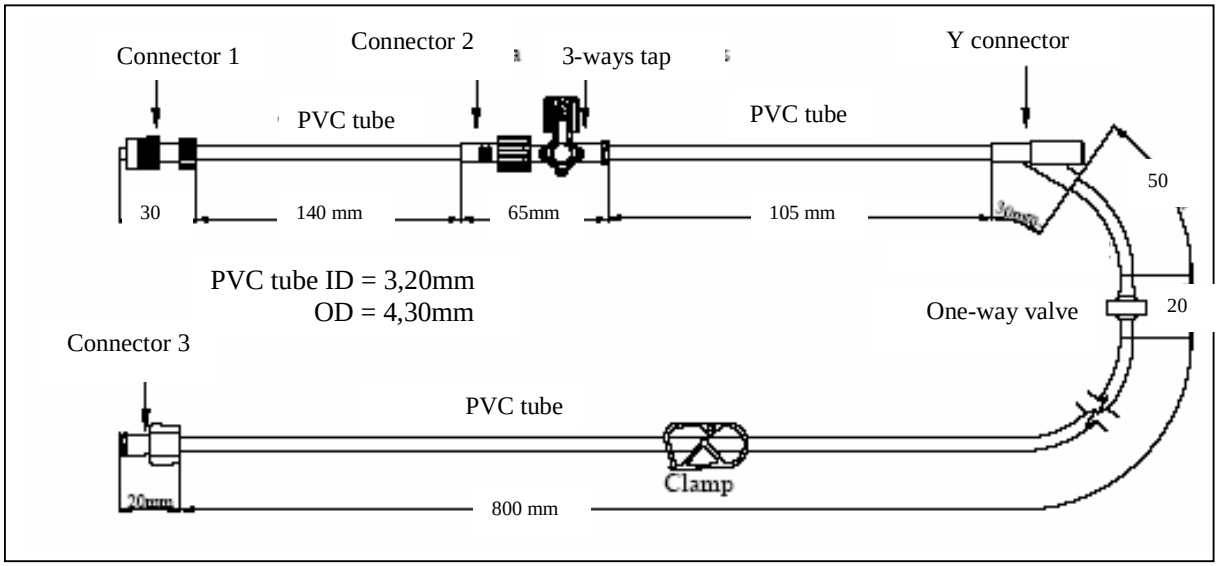

Figure 2. Ventura Biomédica mod. LCR - 500 neurosurgical external tube sketch.

The main function of Y connector is to remove the CSF sample for analysis. One-way valve is a smart device to prevent CSF reverse flow if differential pressure to assume negative or near zero values. Finally, a simple plastic clamp permits a complete flow blockage, if necessary. After the flexible tube, a bag operating as an external reservoir receives the CSF flow drained. All of these shunts components represent a pressure loss. In an external shunt can to occur over-drainage of CSF due to the siphoning effect if differential pressure assume high values. The hydrostatic pressure (25–75 cm of water), caused by the weight of the column of CSF, leads to fluid being sucked out of the ventricles in the upright position. Siphoning effect may lead to excessive CSF drainage from the ventricles with irreversible consequences for unlucky patients. Recently, Ventura Biomédica developing an ingenious anti-siphoning device to prevent with success the over-drainage of CSF in external shunt in relative high pressure gradient.

4. Experimental procedure

All efforts in this present work have been geared to design and construct a test apparatus for external CSF shunts. A CSF drainage system works by communicating vase principle and essentially is constituted of a ventricular catheter, flexible tube and bag reservoir. Two opposite conditions can be observed in relation the height H. The first one is related in Fig. 1 showing positive values for height H, i.e., the reservoir bag is positioned above the head of the patient. In opposition, if the reservoir bag is positioned below the head of the patient, height H assumes negative relative values facilitating over-drainage. The present apparatus for shunt testing is able to operate under positive, near null and negative values of H.

Apparatus for testing of anti-siphoning valves of internal shunts can be found in technical literature. Drake & Sainte-Rose (1994) show several conceptions of devices to performing test in valves shunts involving cheap and others more sophisticated apparatus utilizing infusion pumps and electronic measurements of pressure and volumetric flow. In many other works, the construction details of test devices of valves for CSF drainage are not available, such example, Horton & Pollay (1990), Sood *et al*. (1998) and Kremer *et al*. (1994).

In the present work, a device for testing complete external shunts or parts of shunts has been designed and constructed in order to measure the behavior of the flow rate as function of loss of pressure. Inlet the reservoir bag the pressure is exactly the value of the local atmospheric pressure. ICP should be sufficient to win the hydrostatic barrier of the height H (regarding H positive). For different height H a value of flow rate is observed for each individual shunt tested. Fig. 3 depicts a sketch of the test device proposed.

A –Elevator mechanism
B –Pass motor
C –Microcomputer
D –Discharge reservoir
E –Drain
F –Electronic balance
G –Mariotte bottle
H –Height
I –Bi-distillated water
J –Hole for catheter
K –Air tube
L –Shunt
M –Flexible PVC tube
N –Rigid supports

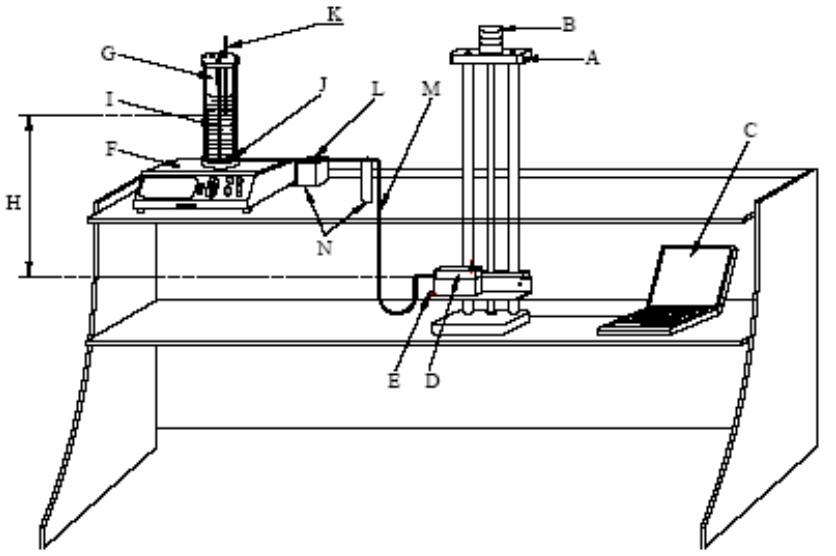

Figure 3 Device of hydrodynamic simulation of external CSF shunts.

The test device, Fig. 3, is composed by an elevating mechanism (A), to apply vertical movement to a platform with controlled velocity by means a pass motor (B) interlinked to a micro computer (C). The flow is drained to a reservoir of discharge (D) localized in the platform. A drain (E) permits to evacuate the reservoir previously to begin of the test. A digital balance (F) - Mars Balanças model AS 2000 - with ±0,005 g of measured accuracy equipped with a RS232C interface permits a continuum record the mass drained with the time of the reservoir (G). The reservoir (G) is a well know Mariotte bottle, an ingenious device able to keep the pressure output constant independent of the liquid level inside the bottle. The Mariotte bottle supplies the liquid flow dependent only of the loss of pressure determined by the height H and by hydraulic resistance of the shunt tested. Constructive details about Mariotte bottle can be found on the work of Camilo (2005).

The physical characteristics of CSF, especially the density, are near to ultra centrifuged plasma. Several researchers utilize bi-distilled water in ambient temperature in test of neurological valves of internal shunts, Horton & Pollay (1990), Kremeer *et al*. (19940 and Sood *et al*. (1998). In the present work is also employed bi-distilled water (I). In the bottom of the Mariotte bottle has a small hole (J) for introducing the catheter of drainage. The height H is determined by vertical distance between the low end of the air tube (K) and the entrance of the reservoir (D) installed on the platform of vertical displacement. The shunt (L) is installed following the catheter and the flexible PVC tube (M) finishes the connection with the discharge reservoir (D). Because the vertical movement of the platform executed by means of the elevating mechanism (A), the flexible tube movement can produce interference in the weigh measured in the balance. In order to prevent interference in the weigh measured, two rigid supports (N) fix the shunt tube.

The test device has been designed to operate according to some steps. First of all, the Mariotte bottle is filled partially with bi-distilled water. The shunt or part of the shunt to be tested is connected to Mariotte bottle and to the discharge reservoir. The platform is positioned at the the top of the elevating mechanism. The pass motor is adequately adjusted by means of a digital control and the platform moves in a descends in a controlled constant velocity. The vertical position of the platform and the water mass in the Mariote bottle are continually registered in a digital data acquisition system. These data can be processed and the mass temporal difference can be converted in mass flow and the vertical position of the platform converted in equivalent differential pressure. If the vertical velocity of the platform is sufficiently small the data obtained can be considered equal to data obtained in a static test.

The present device permits to obtain reliable measurements of the mass flow internal to the shunt in function of the differential pressure and data acquisition is automatically realized. This automated test permits to obtain rapid and precise results.

4.1. Test device characterization

The flow inlet a shunt can be considered one-dimensional without significant loss of precision. The Reynolds number maximum (based in the internal diameter of the tube) is less than 600. In this situation, without shadows of doubts, the flow field can be considered laminar. Small effects of superficial stress can be observed in the test without meaningful interference in the results.

A small perturbation in the internal pressure of the Mariotte bottle has been produced introducing 2 ml of bi-distilled water by means of an infusion pump. This introduction of small water mass produces a light rise in the flow mass. Extensive measurements of the time needed to stabilize the flow after small perturbations have been made and presented very small. In all of cases tested the test apparatus shows a quick time necessary to stabilize small perturbations.

In literature consulted, all of testes realized in all devices proposed, were static, i.e., a differential pressure was created and the flow is generated and the measurements are obtained only after the assurance the flow stabilization. In this procedure, few points of measurements can be obtained only after a large time period. In the other side, the present proposed device of shunts test permits to obtain a quasi-continuous curve in an automated process in a relative small time of work.

A comparative test utilizing several descendent velocities for the platform is showed in Fig. 4. This test permits to visualize the adequate velocity of the platform. Static measurements, i.e., for the platform velocity equal to zero, is considered the reference value (vref). Three other velocity values are showed. Under very small velocity (v1), values of flow lower than the reference value are showed, probably due to surface stress effects. For a platform velocity (v2) equal to 1.07 m/h the volumetric flow measured is close to reference values. For velocity (v3) the flow values shows a large discrepancy. In this present work all of tests have been realized utilizing a platform velocity (v2).

In this present quasi-continuous process of measurements an important question should be attacked, related to the flow measurement. The balance utilized in the test have a RS 232C interface with a sample frequency of 4.21 Hz. In other words, 253 measurement points can be recorded per minute. This frequency is adequate for the present application. The mass flow can be obtained utilizing Eq. (1).

$$Q_{aver} = \frac{m_1 - m_2}{t_2 - t_1} \tag{1}$$

were, (Q_{aver}) is a average mass flow measured in a time interval determined by ($t_2 - t_1$) and ($m_1 - m_2$) is the mass difference registered in the same time interval.

In this present work, a time interval of 4.439 s (equivalent to 57 points of weight measurements) has been adequate to flow measurements. A platform velocity of (v2) equal to 1.07 m/h represents only 4.0 mm of platform displacement.

Finalizing, Table 1 shows an estimate values of uncertainty for several variables utilized in this work. The uncertainty of the volumetric flow and height H, in accord to Moffat (1998), can be calculated equal to 0.1 and 1% respectively.

4.2. Test of a anti-siphon valve.

The external shunt is implanted only in emergency situations, if the height H shows values very close to zero or negative, the flow rise and in a small time interval serious injuries can happen to the patients. This situation can be observed if the patient suddenly stands up or in case of the external reservoir fall of their pedestal. Camilo (2005) describes several prototypes of anti-siphon valves to be utilized in external shunts. Fig. 5 shows typical results of the flow in function of the height H for a first prototype of anti-siphon valve in several velocities of the platform.

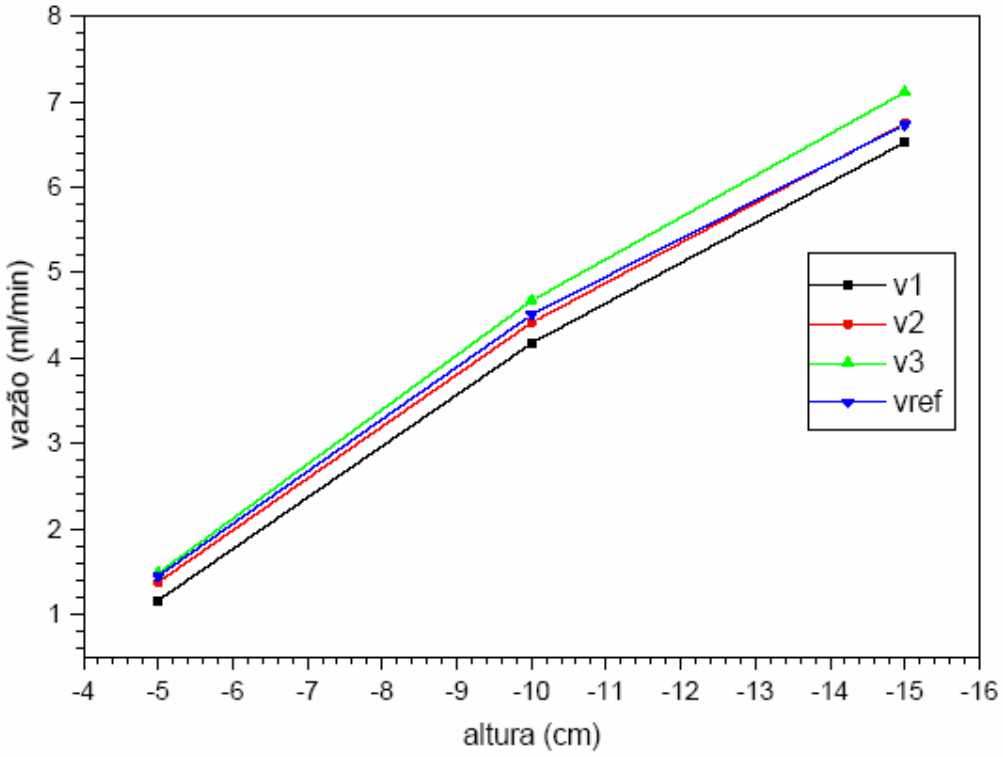

Figure 4 Experimental values of the flow [ml/min] for different values of platform velocities.

Table 1 – Uncertainty associated to shunt test apparatus

Variable measured	Sistematic error	Statistical error	Total error
Weight	<0.123%	$<10^{-3}$ %	<0.12 %
Sample frequency	$<10^{-4}$	$<10^{-4}$	$<10^{-4}$
Plataform displacment	$<10^{-2}$ mm	<0.04 mm	<0.05 mm
Time interval	$<10^{-3}$	-	$<10^{-3}$

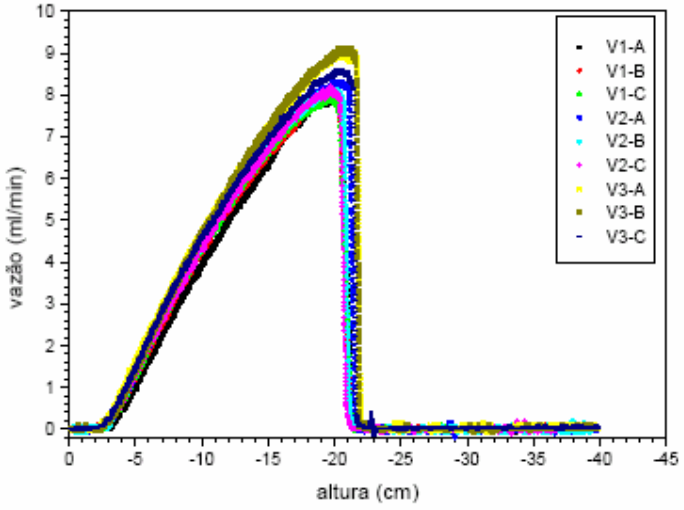

Figure 5 Volumetric flow in function of the height H for a anti-siphon prototype valve.

5. Conclusions

The use of shunting for hydrocephalus has a long history of improvements made through basic science, as well as clinical innovations and biomedical products. Shunting has dramatically changed the outlook of children with hydrocephalus, with many of them having normal life expectancies and attaining normal intelligence.

Modern trends in surgical treatment of hydrocephalus are moving towards the greater use of minimally invasive endoscopic procedures and away from routine shunting wherever feasible. Patients with isolated hydrocephalus should have a normal life expectancy, as long as prompt detection and treatment of complications is provided through maintaining appropriate arrangements for long term follow up.

The cerebrospinal fluid shunt is one of the most common surgical procedures in encephalic neurosurgery. Nevertheless, an important rate of failure (mechanical, infectious or functional) can occur in this procedure. In the engineering viewpoint, mechanical failures should be availed in details. Several engineering criterion of design should be found in order to obtain an optimized shunt operation.

Internal shunts, more precisely, peritoneal shunts have been intensively studied after the sixties and numerous internal shunt valves have been developed to provide an effective flow control. In other side, external shunt remains a procedure necessary to several neurosurgical activities and, apparently, few efforts of research have been devoted to establish optimized external shunting.

In the present work, an apparatus for testing of shunting has been proposed and extensively tested in order to study the flow behavior as function of differential pressure of shunts. Flow mass measurements have been performed utilizing an electronic balance with a digital interface and an adequate data processing. This innovating approach permits a cheap and reliable flow measurement when compared to much related expensive digital precise flow measurement devices. Other important point is relative to the use of a Mariotte bottle, permitting a continuous pressure independently of the internal level of fluid.

Utilizing a pass motor, digitally controlled, platform velocity is maintained precisely constant. In this situation, the testes have been developed in a quasi-continuous mode permitting to obtain consistent data in a short time period.

The present shunt test device is adequate for engineering of shunts investigation and permits rapid developing of parts of shunts. Additionally, preliminary results of a first prototype of a valve developed to use in external shunts impeding siphoning have been showed. Independently of statistics, siphoning is a constant source of mechanical failure in external shunt implants. Prevention of siphon effects in external shunt is a notable advance in neurosurgical procedures.

6. Acknowledgement

VENTURA BIOMÉDICA supplied all materials to manufacturing the test apparatus for external shunts and provides funding for this work. Thanks to Prof. Emanuel Rocha Woiski for proofreading the manuscripts.

7. References

Aschoff, A.; Kremer, P.; Hashemi, B. and Kunze, S., 1999, "The Scientific History of Hydrocephalus and its treatment", Neurosurgical Review, vol. 22, pp. 67 – 93.

Camilo, J. R, 2005 , "Simulação Hidrodinâmica e Caracterização Experimental de Mecanismos Anti-sifão em Sistemas de Drenagem Externa de Líquido Cefalorraquidiano", Dissertação de Mestrado, Unesp de Ilha Solteira, 91 p.

Camilo, J. R.; Maset, A. L.; Duarte, K. P.; Vieira, D. G. S. D. R.; Perini, E. A. and Vieira, E. D. R., 2006, "Mechanical Testes of Three-Way Valves of External Neurosurgical Shunts", DINCON 2006 - Brazilian Conference on Dynamics, Control and Their Applications, Guaratinguetá, SP.

Drake, J. M. and Sainte-Rose, C., 1994, The Shunt book", Blackwell Science, 228 p.

Gusmão, S., Silveira, R. H., Cabral filho, G. and Arantes, A., 2000, "Aplicações Clínicas da Hidrodinâmica na Derivação Ventrículo-peritonial", Arquivos Brasileiro de Neurocirurgia, vol. 14, no. 4, pp.179-183.

Horton, H. & Pollay, M. P., 1990, "Fluid flow performance of a new siphon-control device for ventricular shunts". Journal of Neurosurgical, vol. 72, pp.926-932.

Kajimoto, Y.; Ohta, T.; Miyake, H., Matsukawa, M. Ogawa, D.; Nagao, K. and Kuroiwa, T., 2000, "Posture-related changes in the pressure environment of the ventriculoperitoneal Shunt System", Journal of Neurosurgical, vol. 93, pp. 614-617.

Kremeer, P., Aschoff, A & Kunze, S., 1994, "Risks of Using Siphon-reducting Devices", Child's Nerv. Syst., vol 10, pp. 231-235.

Maset, A. L, Camilo, J. R. & Vieira, E. D. R., 2005, "Considerações Hidrodinâmicas sobre a Derivação Liquórica Parte II: O Efeito Sifão em Sistemas de Drenagem Externa" Arquivos Brasileiros de Neurocirurgia da Sociedade Brasileira de Neurocirurgia, vol. 24, n. 2, pp. 45-51.

Moffat, R. J., 1998, "DEscribing the Uncertainties in Experimental Results, Experimental Thermal and Fluids Science, vol.1, pp.3-17.

Pople, I. K., 2002, "Hydrocephalus and Shunts: What the Neurologist Should Know", Journal of Neurology, Neurosurgery, and Psychiatry, vol. 73, pp. 17i - 22i.

Puget, S. 2005, "Les Dérivations de Liquide Cerebrospinal", Archives de Pédiatrie, vol. 12, pp. 224-227.

Sesay M., Tentillier, M., Mehsen, M., Marguinaud, E., Stöckle, M., Crozat, P., Dubicq, J., Boulard, G., and Maurette, P., 2002 "Les dérivations du Liquide Céphalorachidien: Particularités Anesthésiques", Ann. Fr. Anesth. Réanim., pp. 78-83, vol. 21.

Sood, S.; Canady, A. I. and Ham, A. D., 1998, "Adjustable Antisiphon Shunt", Child's Nerv. System, pp. 246-249.